# Observation of the stress distribution in crushed glass with applications to soil reinforcement

*Submitted for the degree of Doctor of Philosophy from the University of Oxford*

M.R. Dyer
Magdalen College
Michaelmas Term 1985

To Fiona

CONTENTS


| | | Page |
|---|---|---|
| 1. | INTRODUCTION | |
| 1.1 | Background of the dissertation | 1.1 |
| 1.2 | Soil reinforcement techniques | 1.4 |
| | 1.2.a Insitu soil reinforcement | 1.5 |
| | 1.2.b Reinforcing fill material | 1.7 |
| 1.3 | Outline of dissertation | 1.11 |
| 2. | DETERMINING PRINCIPAL TRAJECTORIES IN A GRANULAR SOIL USING PHOTOELASTICITY | |
| 2.1 | Nature of light | 2.1 |
| 2.2 | Reflection and refraction of light | 2.1 |
| 2.3 | Plane polariscope | 2.2 |
| 2.4 | Circular polariscope | 2.5 |
| 2.5 | Analysis of a transparent plate subjected to plane stress in a plane polariscope | 2.6 |
| 2.6 | Determining the stress distribution in an assembly of crushed glass using photoelasticity | 2.8 |
| 3. | APPARATUS AND EXPERIMENTAL TECHNIQUE | |
| 3.1 | Crushed glass and matching liquid | |
| | 3.1.a Type of glass and matching liquid | 3.1 |
| | 3.1.b Method of crushing glass | 3.3 |
| 3.2 | Types of reinforcement | 3.5 |
| 3.3 | Shear box and pull-out test apparatus | 3.6 |
| | 3.3.a Shear box | 3.7 |
| | 3.3.b Pull-out test apparatus | 3.7 |
| | 3.3.c Glass side walls | 3.8 |
| | 3.3.d Measurement of boundary displacement and forces | 3.9 |
| | 3.3.e Perspex tank | 3.9 |

| | | Page |
|---|---|---|
| 3.4 | Polariscope | |
| | 3.4.a Polariscope frame and polarising filters | 3.10 |
| | 3.4.b Light source | 3.11 |
| | 3.4.c Assembly of plane polariscope | 3.11 |
| | 3.4.d Assembly of circular polariscope | 3.11 |
| 3.5 | Sample preparation and test procedure | |
| | 3.5.a Immersing crushed glass in liquid paraffin | 3.12 |
| | 3.5.b Attaching reference markers to the glass sidewall | 3.13 |
| | 3.5.c Direct shear tests on crushed glass with and without reinforcement | 3.13 |
| | 3.5.d Direct sliding of crushed glass over reinforcement | 3.15 |
| | 3.5.e Pull-out test | 3.16 |
| 3.6 | Photographing the light stripes and grid of steel balls in the crushed glass | 3.16 |
| 3.7 | Strain analysis using the grid of steel balls in the crushed glass | 3.17 |
| 3.8 | Alternative methods for crushing glass and sample preparation | 3.18 |
| 4. | DIRECT SHEAR TESTS ON CRUSHED GLASS | |
| 4.1 | Boundary measurements | 4.1 |
| 4.2 | Patterns of light stripes visible in crushed glass | 4.3 |
| 4.3 | Combining boundary forces with patterns of light stripes at maximum shear load | 4.6 |
| 4.4 | Strains within the crushed glass | 4.7 |
| | 4.4.a Strains before maximum shear load | 4.8 |
| | 4.4.b Strain increments after maximum shear load | 4.8 |
| | 4.4.c Orientation of the rupture band | 4.9 |
| 4.5 | Comparison of directions of principal stress and strain increment | 4.11 |
| 4.6 | Conclusions | 4.13 |
| 4.7 | Suggestions for future work | 4.15 |

Page

5. THE INTERACTION OF CRUSHED GLASS WITH FLEXIBLE AND RIGID REINFORCEMENTS PLACED AT DIFFERENT ORIENTATIONS IN THE SHEAR BOX

5.1 Introduction 5.1

5.2 Boundary measurements 5.1

5.3 40° Orientation 5.2

5.4 -45° Orientation 5.3

5.5 0° Orientation 5.4

5.6 Discussion and conclusions 5.8

5.7 Suggestions for future work 5.11

6. THE TRANSFER OF STRESSES FROM CRUSHED GLASS TO REINFORCEMENTS WITH OPENINGS

6.1 Introduction 6.1

6.1.a Tests used for examining soil-reinforcement interaction 6.2

6.1.b Some previous observations on the pull-out test 6.3

6.1.c Photoelastic tests performed 6.5

Part A - Transfer of Stresses from Crushed Glass to Grid and Perforated Sheet for Reinforcing, Direct Sliding and Pull-Out

6.2 Transfer of stresses to the reinforcements when strengthening crushed glass 6.5

6.2.a Transfer of stresses to the grid reinforcement 6.5

6.2.b Transfer of stresses to the perforated sheet reinforcement 6.6

6.2.c Relative performance of the two reinforcements 6.7

6.2.d Patterns of strain in the crushed glass 6.7

6.3 Direct sliding resistance of crushed glass over the reinforcements 6.8

6.3.a Introduction 6.8

6.3.b Boundary measurements 6.9

6.3.c Pattern of stresses for direct sliding over the grid 6.9

| | | | Page |
|---|---|---|---|
| | 6.3.d | Pattern of stresses for direct sliding over the perforated sheet | 6.11 |
| | 6.3.e | Different mechanisms for direct sliding resistance of soil over grid reinforcement | 6.11 |
| 6.4 | Pull-out tests on lengths of grid and perforated sheet | | 6.13 |
| | 6.4.a | Boundary measurements | 6.13 |
| | 6.4.b | Pattern of stresses for pull-out of the grid | 6.14 |
| | 6.4.c | Patterns of stresses for pull-out of the perforated sheet | 6.15 |
| 6.5 | Discussion and conclusions on the transfer of stresses crushed glass to the grid and perforated sheet for reinforcing, direct sliding and pull-out | | 6.17 |
| | 6.5.a | Transfer of stresses for reinforcing | 6.17 |
| | 6.5.b | Transfer of stresses for direct sliding | 6.17 |
| | 6.5.c | Transfer of stresses for pull-out | 6.18 |
| | 6.5.d | Comparison of the transfer of stresses to the grid in the different tests | 6.19 |
| | 6.5.e | Comparison of the transfer of stresses to the perforated sheet in the different tests | 6.19 |
| | 6.5.f | Average apparent coefficient of bond from pull-out tests | 6.20 |
| Part B - Interference Between Transverse Members of the Grid | | | |
| 6.6. | Pull-out tests on single and pairs of transverse members | | 6.21 |
| | 6.6.a | Boundary measurements | |
| | 6.6.b | Pattern of stresses and strains for pull-out of single transverse members | 6.22 |
| | 6.6.c | Pattern of stresses for pull-out of pairs of transverse members | 6.24 |
| | 6.6.d | A comparison between the pull-out resistance against individual transverse members at different spacings with the corresponding bond for a grid | 6.26 |
| | 6.6.e | Conclusions on interference between transverse members of the grid | 6.28 |
| 6.7 | Suggestions for future work | | |


(223 pages including figures)

# 1. INTRODUCTION.

## 1.1. Background of the dissertation.

The research described in this dissertation follows on from the study made by Jewell (1980) into the effects of tensile reinforcement on the mechanical behaviour of sand. For this study Jewell used the direct shear test with reinforcement placed about the central plane as shown in fig.1.1. The direct shear test was chosen for the following reasons.

(1) The reinforcement variables could be better controlled and examined in a unit cell test than in model or field studies of soil reinforcement systems.

(2) The pattern of deformation is similar to that experienced by soil in which a rupture band develops, with the principal axes of stress, strain and strain increment free to rotate as is the case in model and field structures.

(3) The overall shear strength of the sample is measured directly at the boundaries of the apparatus.

The direct shear tests were monitored by boundary measurements and internal measurements using a radiographic technique. The findings are outlined below with reference made to relevant observations by other researchers.

1) The optimum orientation for a relatively flexible steel grid was found to be approximately along the direction of principal tensile strains in the unreinforced sand, see fig.1.2. This indicated that the reinforcement functioned by limiting tensile strains in the sand. McGown et al. (1978) obtained a similar result for plane strain cell tests on

sand containing a single layer of flexible reinforcement. However in both studies the reinforcement was observed to weaken the sand. Jewell recognized weakening to occur when the steel grid was placed along the direction of principal compressive strains in the unreinforced sand. This was attributed to a reduction in vertical effective stress. McGown et al. observed weakening of the sand when the reinforcement orientation approached the rupture band which developed in the sand alone. This was recognized to be the direction of zero-extension in the unreinforced sand. The weakening was linked to a lower bond between soil and reinforcement than soil alone.

2) Internal strains determined by Jewell showed the tensile reinforcement modified strains in the sand over a well defined zone, see fig.1.3. This resulted in a significant rotation of principal axes of strain increment, with the band of major strains which developed across the centre of the box in the unreinforced sand being prohibited from forming. This agreed with boundary measurements, indicating the reinforcement functioned by limiting tensile strains in the sand. Consequently a less favourable mode of failure took place. The limit of rotation of principal axes of strain increment was understood to be the alignment of a direction of zero-extension in the sand with the reinforcement. These findings agree with the ideas expressed by Basset and Last (1978) on the mode of action of tensile reinforcement, which in particular was related to the effect of tensile reinforcement on the strain field in a reinforced earth wall as shown in fig.1.4.

3) For efficient use of tensile reinforcement it was demonstrated that the bond with sand should be as high as possible. This could be achieved by roughening the surface. Alternatively, the bond was improved by introducing openings or apertures in the reinforcement, changing the shape

to a grid. It appeared that the bond for a suitably proportioned grid could be as high as for a fully roughened surface.

4) The longitudinal stiffness of tensile reinforcement was observed to affect the magnitude and rate of increase in strength in the direct shear tests. The rupture strain of tensile reinforcement relative to maximum tensile strains of the soil, under the same operational stress conditions, have also been observed to influence the reinforcing effect in terms of its limiting behaviour, i.e. whether brittle or ductile failure (McGown, et al. 1978). With regards to the performance of reinforced earth walls, Al-Hussaini and Perry (1976) observed that steel reinforced strips produced a stiffer and stronger structure than a more extensible fabric reinforcement, even through surface roughess was less. The importance of reinforcement tensile stiffness is recognized in limit equilibrium designs for tensile reinforced soil structures by limiting the available reinforcement force to the tensile strains that can develop in the soil (e.g. Jewell 1985).

For highly structured non-woven and composite geotextiles, McGown et al.(1982) demonstrated that the stress-strain behaviour can be significantly affected by soil confinement. Testing wider strips in isolation was not found to replicate the effects of soil confinement.
Another factor which needs to be considered when assessing the tensile property of a polymer reinforcement is creep. McGown et al. (1984) illustrated an appropriate method of interpreting creep data using isochronous curves, which enable long term laboratory test data to be extrapolated to the design life of the soil structure.

5) The strain and hence stress fields in the reinforced direct shear tests have been shown to be complex and non-uniform. However Jewell successfully modelled the variation of reinforcing effect for tensile

reinforcement at different orientations by using a simple limit equilibrium analysis, see fig.1.5. The effect of the tensile reinforcement force was represented as:

- an increase in the normal effective stress acting on the central plane of the box due to the normal component of the force and
- a reduction in the applied shear stress due to the parallel component of the force to the central plane.

Subsequently this analysis has been applied to limit equilibrium design methods for reinforcing soil retaining walls and embankements, Jewell et al. 1984b, and Jewell 1982 respectively.

6) A reduction in the reinforcing effect for individual reinforcement due to the presence of other reinforcement was observed in the shear box. This loss of efficiency of individual reinforcement was termed interference. Interference between tensile reinforcement has also been studied by Guilloux et al. (1979) for the pull-out resistance from soil. However interference between reinforcement has yet to be introduced into a limit equilibrium design method.

## 1.2. Soil reinforcement techniques.

The common feature of soil reinforcement techniques is understood to be that soil transfers loads to the reinforcement and not the converse. General descriptions of the available soil reinforcement techniques are provided by Mitchell (1981), Schlosser et al. (1983) and Eggestad (1983). These techniques can be divided into two broad categories: (1) in situ reinforcement to improve bearing capacity or stabilise a slope or steep excavation and (2): reinforcing fill material for constructing retaining

walls, embankments, unpaved roads etc. The tensile reinforcement of soil studied by Jewell was primarily related to the second category. To put Jewell's research and the research presented later in this dissertation in context, brief descriptions of the soil reinforcement techniques available are given as follows.

## 1.2.a. Insitu soil reinforcement.

### (1) Dowel Piles

Creeping slopes in clay have been stabilized using substantial steel or reinforced concrete piles of up to 3 m diameter (Sommer, 1979; Gudehus and Schwarz, 1985), see fig.1.6. The dowel piles transmit the stabilizing force from the stratum below the slip surface by resisting shear and bending loads. A classical method for estimating the yield soil pressures on a large dowel pile is the Brinch-Hansen dowel theory (1960). Figure 1.6 shows a comparison of the measured soil pressures exerted against a 3 m diameter dowel pile compared with the Brinch-Hansen dowel theory. Gudehus and Schwarz describe an alternative method being developed for modelling the dowelling effect by treating the soil as a viscous fluid. The authors suggest the optimum diameter for a dowel pile is approximately five percent of the depth to the slip surface. The piles should also be spaced to prevent soil from flowing between then.

(2) Micropiles

These are 100 to 200 mm diameter steel reinforced grouted piles which are mainly used for improving bearing capacity and slope stability. The micropiles are understood to function by supporting tension or compression with a limited capacity to support bending. A major user of micropiles is the construction technique known as Pali Radice (Lizzi, 1983). This technique deploys the micropiles in a network as shown in fig.1.7, with the objective of creating a monolith structure to improve stability. This group effort is recognised to be of fundamental importance. The action of micropiles is not fully understood when used in this way. Hence analysis is mostly intuitive, where the system is understood to behave like reinforced concrete with the micropile providing resistance against tensile stresses. The use of micropiles to improve bearing capacity in Pali Radice system does not strictly satisfy the definition given for soil reinforcement because the micropiles can be attached to the base of a foundation and so would be subjected directly to an external load.

(3) Soil nailing

Soil nailing generally refers to stabilising steeply inclined or vertical excavations by driving or boring and grouting small steel sections into the remaining soil mass as the excavation proceeds, see fig.1.8. For example, Cartier and Gigan (1983) used 50x50x3 'L' sections and Shen et al. (1981) 25 mm diameter bars. The steel sections are usually inclined downwards by typically 20°. The surface of the excavation is covered by shotcrete reinforced with steel mesh. The reinforcing bars are understood to primarily function in tension and to a lesser degree by resisting shear and bending (Guilloux et al. 1983). Maximum tension has been observed to develop in the reinforcing

bars at some distance behind the face of the excavation with the locus of points of maximum tension curving upwards in the excavation as shown in fig.1.8. This distribution of tensile force in the reinforcements is similar to a reinforced earth retaining wall as will be shown. The reinforcement dowel action is understood to occur at the point of maximum axial tension, which indicates the potential failure surface in the soil.

The term soil nailing has also been confusingly used to describe stabilising slopes by using dowel piles of steel sections encased in concrete (Cartier and Gigan loc. cit.).

### 1.2.b. Reinforcing fill material.

This generally involves using flexible reinforcement that can only support tensile loads. Reinforcements in use for example are: galvanised steel strips and grid, polymer fabrics and grids. Modern interest in using flexible tensile reinforcement largely stems from the construction technique introduced by Vidal for building inclined or vertical faced retaining walls known as Reinforced Earth (Schlosser and Vidal 1969). This consists of placing flexible galvanised steel strips in horizontal layers in a granular backfill and attaching them to a flexible wall face as shown in fig.1.9a. Initially, the cladding was in the form of horizontal rows of elliptical metal sheets. Later cruciform shaped concrete slabs with compressive joints were adopted. Compressible joints are necessary because the backfill settles and so the reinforcing strips pull the facing units downwards.

A particular feature of a reinforced earth wall is that maximum tensions develop in the reinforcing elements at some distance behind the wall face (Bolton et al. 1978; Schlosser and Elias, 1978), see fig.1.10.

Additionally the locus of points of maximum tension in the reinforcing elements, which represents the potential failure surface, is observed to vary between curving upwards in the wall to being approximately vertical. Basset and Last (1978) attributed this steepening of the failure surface in a reinforced earth wall, compared with the classical active condition, to the reorientation of zero-extension characteristics in the soil caused by the reinforcing elements. The shape and location of the failure surface in a reinforced earth wall has also been shown in model tests by Smith and Wroth (1978) to depend on the quantity and geometry of the reinforcement.

Well documented field studies of reinforced earth retaining walls are provided by Chang and Forsyth (1976), Al-Hussaini and Perry (1976), Finlay (1978) and John et al. (1983). A notable study on the collapse limit states of reinforced earth walls is provided by Bolton and Pang (1982) from a series of well instrumented model tests in the geotechnical centrifuge. This covers collapse by internal slippage or tensile rupture of the reinforcing elements. In particular, the authors observed the redistribution of stresses amongst reinforcing elements when ultimate tensile strength was approached. This was observed to provide a possible increase in strength of the walls of up to fifty percent. However the authors noted that conditions given by the Institution of Structural Engineers on structural safety prohibit a single reinforcing element from reaching its ultimate tensile strength under any forseeable conditions. Therefore for checking tensile stability of reinforcing elements, the authors did not recommend upper bound calculations using general collapse mechanisms which automatically invoke plastic redistribution of forces. Instead the simple anchor concept was recommended, where an individual reinforcing element balances lateral earth pressures within its vertical spacing panel. Information on the lateral earth pressures in reinforced earth

walls is provided in these model tests and the field studies referenced.

Since Vidal's introduction of reinforced earth a number of alternative methods for constructing reinforced soil walls have been introduced. Some of these are as follows:

(1) York Method (Jones, 1978). Reinforcing strips are permitted to slide relative to the wall face along vertical poles.

(2) Anchored Earth (Jones et al., 1985). Metal rods attached to concrete facing panels are anchored into the backfill primarily by generating passive restraint at the end of the rod which is formed into a triangle.

(3) Polymer Fabrics and Grids. These are usually termed geotextile and geogrids respectively and have been used for reinforcement in walls (geotextile - Holtz and Broms 1977, Al-Hussaini and Perry, geogrid - Pigg and McCafferty 1984). These reinforcing elements are sometimes wrapped around the face of the wall to provide wall facing.

A general guide to the nature of polymer reinforcements is given by Christopher and Holtz (1985). Additional uses of polymer reinforcements for soil reinforcement are as follows, see fig. 1.9.

1) Construction of embankments over very soft soils has been aided by building on a geotextile (Olivera, 1982; Rowe et al. 1984; Rathamyer and Korhonen, 1985 and Fowler, 1985). This has been observed to reduce the intrusion of fill into the subgrade by 50% to 80% (Olivera and Fowler respectively) and to assist construction by providing a working platform. Geotextiles have also been placed under embankments

on marginal ground with the aim of increasing the safety factor (Williams and Sanders, 1985). In these situations the geotextiles are recognized to function as a combination of separator, filter, membrane and reinforcement. The reinforcing effect is understood to limit lateral spreading of the fill material. Rowe et al. observed that variation of the longitudinal profile of the soft ground can also mobilise significant longitudinal strains in the geotextile. In addition the authors observed that substantial compression of a soft subgrade can be expected before significant strains are developed in the geotextile.

2) To minimize land requirement the slopes of an embankment on competent ground can be steepened by incorporating horizontal layers of geotextile similar to a reinforced earth retaining wall (Jewell, Paine and Woods, 1984).

3) Reinstating failed slopes (Murray, 1984).

4) Andrawes et al. (1982) demonstrated that the load-displacement behaviour of cohesionless soil subject to surfacing loading can be improved with the appropriate location of a horizontal geotextile in the soil. This has applications to the reinforcement of road sub-base, airfield pavement and railway ballast.

5) The performance of unpaved roads of parking areas on soft ground can be improved by placing geotextile between the granular fill and subgrade (geotextile - Gourc et al. 1983, geogrid - Milligan and Love 1984, design method - Giroud et al. 1984).

Generally granular fills have been used although cohesive fills and mine waste may be more available and so less expensive. However fine grained and cohesive soils have been generally considered

unsuitable for reinforced soil construction for the following reasons (Jewell and Jones 1979):

(1) Short term stability, the bond between cohesive soil and reinforcement is poor and subjected to reduction if positive pore water pressure is developed.

(2) Corrosion, fine grained cohesive soils are significantly more aggressive than cohesionless soil.

(3) Post construction movements due to consolidation of the cohesive fill.

The feasibility of using cohesive fill for constructing reinforced earth walls has been demonstrated in full-scale tests by Murray and Boden (1979) and Balletino (1983). In both cases a layer of granular fill was placed at the front face of the cohesive fill to aid drainage of excess pore water pressure.

Jewell (1980) demonstrated in direct shear tests on kaolin that the shear strength of cohesive fill could be improved by grid reinforcement in both short (undrained) and long (drained) term. Reinforcement of clay has also been examined in the direct shear box and model walls by Ingold (1981).

## 1.3. Outline of dissertation.

New scope was given to Jewell's line of research by using a photoelastic technique which displayed the distribution of stresses within a granular medium. This meant using crushed glass instead of sand. The theory for this photoelastic technique is explained in Chapter 2. Experimental details involved in the technique are described in Chapter 3. Consequently the transfer of load from a granular medium to reinforcement could be observed. This was examined as outlined below.

Using Jewell's test arrangement of a single reinforcing element placed about the central place of the shear box, the transfer of stresses to a flexible sheet reinforcement was observed for different orientations. In addition the performance of a very rigid reinforcement at the vertical orientation was examined. The results are presented in Chapter 5 and related to the use of flexible and rigid reinforcements in fill material and insitu.

Secondly the mechanism for transfering stresses to tensile reinforcements with openings was examined. The reinforcements were a perforated sheet with openings approximately the same size as the crushed glass and a grid with aperture length and width approximately ten and five times greater than the average particle size of crushed glass. These findings were compared with the transfer of stresses to the reinforcements in tests used in practice for measuring soil/reinforcement bond, i.e. the direct sliding of the soil over the reinforcement and the pull-out of reinforcement from soil. The results are presented in Chapter 6.

Prior to these studies on soil reinforcement, the results for direct shear tests solely on crushed glass are presented in Chapter 4. The photoelastic results illustrate the orientation of principal stress trajectories in the shear box. These are compared with the strain field providing information on the relative orientation of directions of principal stress and strain increment.

The photoelastic results were recorded on slide film. These were difficult to reproduce as good quality prints or slides. So both forms are presented. The slides are stored at the rear of the dissertation with captions given in appendix B. The prints are contained amongst the other figures.

# 2. DETERMINING PRINCIPAL STRESS TRAJECTORIES IN A GRANULAR SOIL USING PHOTOELASTICITY.

## 2.1. Nature of light.

For the purpose of explaining photoelasticity it is sufficient to define the nature of light using Maxwell's theory that light is an electromagnetic disturbance, where the disturbance is expressed as a light vector normal to the direction of propagation. Typically the amplitude of the light vector is described by a simple harmonic transverse wave as shown in fig. 2.1. The wavelength $\lambda$, velocity of propagation v and frequency f are related by $\lambda.f=v$. The frequency is independent of the medium being transversed. The wave's transverse displacements can be represented by the vertical displacements of an arm rotating uniformly with radial velocity $\omega$, where one complete rotation $2\pi$ corresponds to one wavelength as in fig. 2.2. Hence $2\pi/\omega=\lambda/v$ and so $\omega=2\pi v/\lambda$ . $\omega$ will be used later in this chapter to describe the transverse motion of a light wave in a photoelastic test.

## 2.2. Reflection and refraction of light.

The velocity of light in any transparent medium is always less than the velocity of light in vacuo. The ratio of the velocity in vacuo to the velocity in a transparent medium is a property known as the refractive index $\mu$, which is greater than unity. In optically isotropic materials the refractive index is the same in all directions. When a beam of light strikes the surface between two optically isotropic materials with different refractive indices, it divides into reflected and refracted rays. These rays lie in a plane defined by the

incident ray and normal to the surface, which is known as the plane of incidence as shown in fig. 2.3.

However when a beam of light is directed at oblique incidence onto the surface of certain crystalline materials, such as calcite and quartz, it usually divides into one reflected and two refracted rays. This behaviour is termed double refraction and the material is said to be birefringent. Some transparent materials that are optically isotropic when unstressed become doubly refracting when stressed eg. glass. This change of a material's optical properties when stressed is the basis of photoelasticity and is observed using a polariscope. There are two types of polariscope, plane and circular. The names derive from the types of polarised light used in their operation. Plane polarised light is obtained by restricting the light vector to vibrate in a single plane known as the plane of polarisation as shown in fig. 2. 4. Circular polarised light is obtained when the tip of the light vector describes a circular helix as the light propogates, also shown in figure 2.4. Descriptions of both types of polariscope follow.

## 2.3. Plane polariscope.

The plane polariscope consists of two linear polarisers and a light source as shown in fig. 2.5. The first linear polariser, known as the polariser, is used to plane polarise light emitting from a light source. The second linear polariser is known as the

analyser and its axis of polarisation is crossed with the polariser's axis. Therefore without any disturbance of the plane polarised light between the polariser and analyser no light is transmitted through the analyser and so the optical system produces a dark field.

The plane polariscope is used by inserting a photoelastic specimen between the polariser and analyser and then viewing through the analyser. If the photoelastic specimen is stressed it becomes temporarily doubly refracting as already mentioned. In the case of a photoelastic plate subjected to plane stress, a beam of polarised light striking the plate at normal incidence can be considered to resolve into two orthogonal polarised components. These vibrate parallel to the directions of the principal stresses $\sigma_1$ and $\sigma_2$ ($\sigma_3 = 0$) as shown in fig. 2.6. The velocity of propagation of these components through the plate is proportional to the magnitude of the principal stress ie. $v_1 \propto \sigma_1$, $v_2 \propto \sigma_2$. On emerging from the plate the two components have suffered a relative change of phase or retardation $\delta$. The relative retardation is proportional to $(v_1 - v_2) \cdot d$, where d is the length of the light path through the plate. This would be the thickness of the plate for normal incidence of light. Since $(v_1 - v_2) \propto (\sigma_1 - \sigma_2)$ the relative retardation $\delta$ can be expressed as $\delta = c.d.(\sigma_1 - \sigma_2)$, where c is the stress optic constant for a given material at a particular temperature.

Only components of light emerging from a photoelastic specimen that are parallel to the analyser's axis can pass through the analyser. There are two conditions of extinction for polarised light passing through the photoelastic specimen and analyser.

1) Everywhere in the photoelastic specimen where principal stress trajectories align with the polariscope's axes, extinction occurs irrespective of the particular wavelength of light. A black fringe will link points on the photoelastic specimen where this condition of extinction occurs. The fringe is called an isoclinic. The principal stress trajectories at a point on the photoelastic specimen can be found by rotating the crossed polariser and analyser until an isoclinic fringe appears at that point.

2) Extinction also occurs when the relative retardation between two component vibrations emerging from the photoelastic specimen is an integral number of wavelengths. This produces a fringe called an isochromatic which links points on a photoelastic specimen where the same relative retardation occurs ie. same principal stress difference. If white light is used in the polariscope, isochromatic fringes will be in the form of various colour bands, where the relative retardations produce extinction of particular wavelengths of light. For example when the relative retardation extinquishes the green wavelength, the complementary colour red appears as the isochromatic fringe. In monochromatic light the isochromatic fringe is black. Isochromatic fringes are ordered according to the integral number of wavelengths of relative retardation which produce them ie. $1^{st}$ order, $2^{nd}$ order for $\delta = \lambda, 2\lambda$ respectively. Isochromatics are used for measuring principal stress difference.

After an explaination of the circular polariscope, these conditions of extinction will be proved mathematically for a plane polariscope.

## 2.4. Circular polariscope.

In a plane polariscope isoclinic and isochromatic fringes are superimposed on the photoelastic specimen. For stress measurements using the isochromatics the isoclinics can get in the way. One method of eliminating isoclinics would be to rotate the crossed polariser and analyser fast enough to obscure the isoclinics. Isoclinics can also be eliminated optically by rotating the plane polarised light so that the light vector describes a circular helix as the light propagates. This is how a circular polariscope functions, eliminating isoclinics but retaining isochromatics.

In a circular polariscope the plane polarised light is converted to circularly polarised light using a quarter wave plate ($\lambda/4$). The conversion process is as follows. The $\lambda/4$ plate is double refracting, so there are two axes of polarisation. The $\lambda/4$ plate is installed with its axes inclined at 45° to the polariser's axis, so that the plane polarised light is resolved into two orthogonal polarised components of equal amplitude as shown in fig. 2.7. The components propagate through the $\lambda/4$ plate at different velocities. The faster component is transmitted along the "fast" axis, whilst the slower component is transmitted along the "slow" axis of the $\lambda/4$ plate. On emerging from the $\lambda/4$ plate the components have suffered a relative retardation. The $\lambda/4$ plate is so called because it is designed to produce a relative retardation of $\lambda/4$ for a particular wavelength of light. Vectorial addition of two orthogonal waves of equal amplitude and $\lambda/4$ out of phase gives a resultant light vector of constant amplitude which rotates through $2\pi$ in one wavelength as shown in fig. 2.8.

In a circular polariscope a second $\lambda/4$ plate is used to convert the circularly polarised light back to plane polarised light. This is achieved by aligning the fast axis of the second $\lambda/4$ plate with the slow axis of the first $\lambda/4$ plate as shown in fig. 2.9. Hence the relative retardation produced by the first $\lambda/4$ plate is cancelled out by the second $\lambda/4$ plate. Vectorial addition of the two components emerging from the second $\lambda/4$ plate results in plane polarised light. This arrangement of crossed linear polarisers and crossed $\lambda/4$ plates produces a dark field of circularly polarised light for a particular wavelength of light. For other wavelengths the resultant trace is an ellipse giving elliptically polarised light. The only condition of extinction of light from a photoelastic effect in a dark field of circularly polarised light is an isochromatic fringe.

## 2.5. Analysis of a transparent plate subjected to plane stress in a plane polariscope.

The effects produced on a beam of monochromatic, plane polarised light passing through a photoelastic specimen and analyser can be analysed as follows.

Assuming the polariser's axis of polarisation is vertical the initially polarised light can be defined by:

$$U_p = a \cdot \cos \omega t$$

as shown in fig. 2.10, where $U_p$ is the light wave's transverse displacement at time t.

On entering the photoelastic plate, the light wave can be considered to resolve into two components along the principal stress directions 01 and 02 as shown in fig. 2.10 giving:

$$U_1 = a.\cos\alpha.\cos\omega t$$

$$U_2 = a.\sin\alpha.\cos\omega t$$

These light waves travel through the plate, thickness d, with velocities $v_1$ and $v_2$ and emerge as:

$$U_1' = a.\cos\alpha.\cos\omega.(t-d/v_1)$$

$$U_2' = a.\sin\alpha.\cos\omega.(t-d/v_2)$$

Only components of these waves parallel with the analyser's axis of polarisation OA finally emerge from the polariscope, giving:

$$U_a = -U_1' \sin\alpha + U_2' \cos\alpha$$

$$U_a = -a.\sin\alpha.\cos\alpha. \left|\cos\omega.(t-d/v_1)-\cos\omega.(t-d/v_2)\right|$$

Using the expressions:

$$2\sin A.\cos A = \sin 2A$$

$$\cos D - \cos C = 2\sin\left(\frac{C+D}{2}\right) . \sin\left(\frac{C-D}{2}\right)$$

the expression for $U_a$ can be rewritten as:

$$U_a = -a.\sin 2\alpha. \left|\sin\omega.(t-d/2v_1-d/2v_1).\sin\omega.(d/2v_1-d/2v_2)\right|$$

This is in the form $U_a = A.\sin(\omega t-B)$, where A is the amplitude function and B is the phase angle. The transmitted intensity of light emerging from the analyser is proportional to $A^2$ or

$$\sin^2 2\alpha.\sin^2\omega.(d/2v_1-d/2v_2)$$

where $\omega = 2\pi v_o/\lambda_o$. There are two conditions for extinction of the emerging light.

1) $\sin 2\alpha = 0$ when $\alpha = 0°$ or $90°$. This condition of extinction depends on the orientation of the plane polariscope's axes and produces an isoclinic fringe.

2) $2\pi v_o/\lambda_o.(d/2v_1-d/2v_2) = 0$ or $i\pi$ $(i=1, 2, 3, \ldots)$. This can be rewritten as $\pi d/\lambda_o.(v_o/v_1 - v_o/v_2) = 0$ or $i\pi$. From the definition of

refractive index $\mu$, this expression can be rewritten as $\pi d/\lambda.(\mu_1-\mu_2)=0$ or $i\pi$ . $d(\mu_1-\mu_2)$ is the relative retardation $\delta$ between the two component vibrations. Hence:

$$\pi\delta/\lambda_o = 0 \text{ or } i\pi$$

This condition of extinction occurs when the relative retardation is zero or an integral number of wavelengths and produces an isochromatic fringe.

A similar type of analysis can be performed for a transparent plate subjected to plane stress in a dark field of circularly polarised light (Holister, 1967). In this case the only condition for extinction is an isochromatic fringe.

## 2.6. Determining the stress distribution in an assembly of crushed glass using photoelasticity.

An opaque assembly of crushed glass, which could resemble very angular sand or gravel, can be made transparent by filling the pores with a liquid of the same refractive index. Wakabayashi (1957, 1959) and Dantu (1957) observed that when such a transparent assembly of crushed glass is contained between parallel glass sides, sufficiently stressed in plane strain and viewed through a dark field of circularly polarised light, an orthogonal network of light stripes appears with one family of light stripes being much more pronounced than the other.

Wakabayashi also reported light stripes observed in a plane polariscope. The direction and intensity of these light stripes depended on the inclination of the polariscope axes, varying from dimmest to brightest by a 45° rotation of the polariscope. A light stripe observed through

the circular polariscope was dimmest in a plane polariscope when one of the polariscope axes was aligned with the light stripe.

Similar behaviour has been observed in a direct shear test on crushed glass containing a flexible reinforcement inclined at approximately 45° to the vertical. The pattern of light stripes observed through a circular polariscope is shown in fig. 5.11 (slide 1). The corresponding pattern of light stripes observed through a plane polariscope with axes inclined at 45° to the vertical is shown in fig.5.12 (slide 2). These results show that the light stripes inclined at approximately 45° in a circular polariscope were virtually extinguished when viewed through a plane polariscope. Whereas, the vertical and horizontal light stripes observed through the circular polariscope were well lit in the plane polariscope. In comparison, the light stripes observed through a plane polariscope with vertical and horizontal axes are shown in fig. 5.13 (slide 3). In this case the vertical light stripes previously observed through the circular polariscope were virtually extinguished in the plane polariscope. Whilst the light stripes inclined at 45° were well lit.

To understand the light stripes visible in plane and circularly polarised light, Wakabayashi examined the light pattern for a glass disc loaded along a diameter in plane and circularly polarised light. The light pattern observed in a dark field of circularly polarised light for a glass disc crudely loaded along a diameter is shown in fig. 2.14. The loaded diameter is along the height of the photograph. The result is a broad band of light along the loaded diameter, which bulges at the centre of the disc. There are two overall directions of brightness, a major direction along the loaded diameter and a minor direction across the bulge. The light band is due to a relative retardation which is not

an integral number of wavelengths of visible light. The small black circles at the base of the disc are isochromatic fringes. When viewed in a plane polariscope with the polariscope's axes inclined at 45° to the loaded diameter a similarly shaped light band is observed but with a more pronounced bulge as shown in fig. 2.15. However when one of the plane polariscope's axes is aligned with the loaded diameter an isoclinic fringe mostly masks the previously observed light band, fig.2.16. The isoclinic fringe indicates where principal stress trajectories are parallel and perpendicular to the loaded diameter. A further 20° rotation of the plane polariscope results in the isoclinic fringe appearing away from the loaded diameter, see fig. 2.17, and so exposing more of the central light band. However the overall direction of this exposed light band differs from that observed in the circular polariscope.

The change of intensity and direction of the light band for the loaded glass disc in a plane polariscope is similar to that observed for light stripes in crushed glass. The intensity varies from dimmest to brightest by a 45° rotation of the plane polariscope. Dimmest intensity occurs when one of the plane polariscope axes is aligned with the direction of brightness seen in the circular polariscope. This indicates that a light stripe observed in crushed glass is due to a highly loaded column of particles, analogous to a column of glass discs. The higher interparticle forces along such columns cause the individual particles to light up in circularly polarised light. The average effect along such a column is a light stripe.

Additional evidence of a discrete distribution of forces through a granular material by means of highly loaded columns is given by Drescher and De Josselin de Jong (1972) for tests on an assembly of discs constituting a two dimensional analogue of a granular material. The

discs were made from a photoelastic material and stacked between glass plates to prevent them from buckling. The system employed for loading the disc assembly is shown in fig. 2.18. The assembly of discs was viewed in a dark field of circularly polarised light to observe isochromatic fringes inside the discs and so determine the magnitude and direction of contact forces between discs. Isochromatics observed in an area ABCDO for an anticlockwise rotation of the hinged beam are shown in fig. 2.19. The corresponding network of contact forces is shown in fig. 2.20. The thickness of line is proportional to the magnitude of contact force. The network indicates a discrete distribition of forces through the assembly, resulting in forces concentrated along columns of discs spaced several discs apart. A clockwise rotation of the hinged beam produced highly loaded columns of discs that were approximately vertical.

Drescher and De Josselin de Jong proposed that these highly loaded columns were created because contact forces along them were aligned and so provided a greater rigidity than surrounding particle groups. Drescher extended this observation to light stripes observed in crushed glass through a circular polariscope. Hence it was argued that the light stripes coincided, although irregularly, with principal stress trajectories in the crushed glass.

In an assembly of crushed glass the initially circularly polarised light undergoes several resolutions and relative retardations whilst propagating through the assembly before emerging. In most cases the polarised light entering the glass particle will have already undergone resolution by passing through previous glass particles. Wood (1984) and Allersma (1982a) have shown that this optical averaging of stresses on different planes in the granular medium is in good agreement with

volumetric averaging using vectorial addition of polar vectors. Hence the polarised light emerging from the sample, displayed as light stripes, should be a good representation of the average stress field existing through the thickness of the sample.

To conclude, the light stripes observed in crushed glass through a circular polariscope under a plane strain condition represent highly loaded columns of crushed glass. These are understood to coincide, although irregularly, with principal stress trajectories.

# 3. APPARATUS AND EXPERIMENTAL TECHNIQUE.

This chapter describes the practical details involved with using the photoelastic technique described in the last chapter. The suppliers of equipment and materials for the photoelastic tests are listed in appendix A. Also explained are the mechanical details of performing direct shear and pull-out tests and a procedure for estimating strains in the crushed glass by monitoring the movement of a grid of steel balls. Less laborious methods for crushing glass and sample preparation are suggested at the end.

## 3.1. Crushed glass and matching liquid.

### 3.1.a. Type of glass and matching liquid.

For safety and convenience the possibility of using glass ballotini instead of crushed glass was investigated. Glass ballotini were found to be manufactured in soda and lead glass with refractive indices of approximately 1.51 and 1.60 respectively. Appropriate mixtures of α-bromonaphthalene and colourless liquid paraffin (light grade) were used to match these refractive indices. The refractive indices of α-bromonaphthalene and colourless liquid paraffin (light grade) are 1.659 and between 1.461 to 1.467 respectively. Mixtures of these liquids are commonly used in photoelasticity to provide a liquid with a similar refractive index as the photoelastic specimen. When immersed in suitable mixtures of these liquids, both types of ballotini were observed to have a crazed appearance. This is unacceptable for the photoelastic technique which requires the mass of crushed glass to be made transparent so that polarised light can pass through.

Epoxy resins are much more sensitive photoelastic materials than glass i.e. a similar photoelastic effect can be produced at lower stresses. Hence the possibility of using an epoxy resin called Araldite CT200 was investigated. A suitable mixture of α-bromonaphthalene and colourless liquid paraffin was used to provide a matching liquid. The Araldite proved to be unsuitable by floating in the liquid. A less dense matching liquid could not be found.

Attention was returned to using crushed glass. Drescher (1976) used the combination of crushed pyrex glass immersed in castor oil. Refractive indices of pyrex glass and castor oil are 1.474 and 1.479 respectively. The slight differences between refractive indices renders the glass particles faintly visible. Castor oil has quite a high viscosity (0.65 $Ns/m^2$). This makes it difficult to avoid trapping air bubbles when immersing the crushed glass. Air bubbles appear opaque in the oil and so reduce the quality of light stripes. Hence a search was made for a less viscous liquid with a refractive index sufficiently close to that of soda or pyrex glass to avoid the inconvenience of mixing with another liquid. The liquid also needed to be: 1) non toxic, 2) non flammable and 3) relatively inexpensive as about 50 litres were used in a test. Only colourless liquid paraffin (heavy grade) was found to satisfy these requirements and to match the refractive index of pyrex glass reasonably well. The refractive index of colourless liquid paraffin (heavy grade) is between 1.475 and 1.482.

Therefore the combination of pyrex glass and colourless liquid paraffin (heavy grade) was used. Corning Ltd. very kindly supplied sufficient pyrex glass free of charge. One unexpected problem encountered with the liquid paraffin was that different batches reacted when mixed,

turning opaque. Therefore a sufficient quantity of paraffin from one batch was required for a series of tests. Otherwise it would have been necessary to throughly clean the test apparatus between batches of paraffin.

### 3.1.b. Method of crushing glass.

The suitability of 1) bottle crusher, 2) ball mill and 3) mortar and pestle to produce crushed glass which reasonably resembled sand or gravel was investigated. The bottle crusher produced glass splinters which were totally unsuitable. The ball mill and mortar and pestle proved to be more suitable, producing glass particles which were not too dissimilar to a very angular sand or gravel. However the glass particles were significantly platey so that samples of the crushed glass could be expected to behave differently when sheared in different directions relative to the direction of deposition. A motor driven mortar and pestle was already available in the laboratory, so it was used to crush the glass. A sample of the crushed glass produced by the mortar and pestle is shown in fig. 3.1.

The pyrex glass was supplied as bowls. These were broken under water with a steel rod into suitable sizes for crushing with the mortar and pestle. The mortar and pestle was used in a fume cupboard, so that glass dust could be extracted, and run for about three minutes to crush a sample of glass. The crushed glass was then sieved to obtain particle sizes between 2.00 and 3.35 mm., washed and air dried. This yielded about 50 grams of crushed glass at a time. This range of particle size was chosen because 2 mm was about the finest particle size that could be conveniently used for sample preparation.

Crushing glass was very laborious, so the same sample of crushed glass was used for all tests. During these tests the crushed glass experienced some particle crushing with the corners of the very angular glass particles being chipped off. This could be detected by the fine gritty feel of the sample after testing. Some indication of the change in particle size was given by a sieve analysis after eight direct shear tests. Flushing the crushed glass through a 2 mm sieve with paraffin, less than 1% of weight was found to pass through the sieve. However very fine glass particles could have stayed in suspension. The messy nature of the paraffin coated crushed glass made it very difficult to accurately quantify changes in particle size and shape.

The effect of repeated testing of the crushed glass on its mechanical behaviour was examined by performing three unreinforced direct shear tests amongst a series of reinforced tests. The boundary and photoelastic results for these unreinforced direct shear tests are given in the next chapter. No significant difference was found between these tests. In any case the photoelastic results were largely used to identify qualitatively the type of loading mechanism which took place. However precise measurement of the photoelastic results were made for the unreinforced direct shear tests to compare principal axes of stress and strain increment, and estimate the orientation of the plane of maximum stress obliquity.

To avoid any portion of the crushed glass being repeatedly placed in a highly stressed zone, where there was a greater susceptibility to crushing, the crushed glass was mixed well before being placed in the shear box.

## 3.2. Types of reinforcement.

The photoelastic technique is only useful under plane strain conditions. Therefore the reinforcement needed a plane form. However the observations should apply at least qualitatively to reinforcement in a linear form. The three types of reinforcement used were:

1) Perforated brass sheet;

2) Galvanised steel grid;

3) Mild steel plate.

The width of reinforcement used in tests was 45 mm. This meant the grid was three apertures wide, and the perforated sheet eleven perforations wide. The length of reinforcement in direct shear tests was 125 mm.

The perforated brass sheet was 0.55 mm thick with 3.5 mm diameter perforations, see fig. 3.2. Load-extension curves for two widths of perforated sheet, when loading along the same direction as experienced in shearbox and pull-out tests, are shown in fig. 3.2. The curve for the width of five perforations was measured using a manually operated extensometer. The curve for the width of eleven perforations was extrapolated. The curve for the wider strip, as used in shear box and pull-out tests, indicates a yield strain and load of approximately 1% and 1150 N respectively and a failure strain and load of 25% and 2400N respectively.

The galvanised steel grid was made from 1.65 mm diameter wire (19 SWG) with 12.5 mm apertures. An illustration of the grid is shown in fig. 3.3. In this dissertion the grid is considered to consist of two sets of members 1) transverse members which are perpendicular to the direction of shear and pull-out and so span the width of the grid and

2) longitudinal members that are parallel to the direction of shear and pull-out and so span the length of the grid. Load-extension curves for grids with two and four longitudinal members are given in fig. 3.3. The curve for the grid with two longitudinal members was measured using a manually operated extensometer. The curve for the grid with four longitudinal members, as used in shear box and pull-out tests, was extrapolated. The curve for four longitudinal members indicates a yield strain and load of approximately 1.4% and 2350 N respectively and failure strain and load of 14% and 2950 N. Yield strain for mild steel is 0.115% (Howatson, Lund and Todd), an order of magnitude less than the value obtained using the extensometer. This difference suggests that the longitudinal members slipped inside the extensometer clamps. Although strain measurements appear suspect, the extensometer tests were still valuable for identifying yield and failure loads. These were particularly useful when interpreting pull-out tests.

Finally, the mild steel plate was 3.1 mm thick. Its sides were made rough by glueing a layer of glass particles.

## 3.3. Shear box and pull-out test apparatus.

The shear box and pull-out test apparatus were modifications of the shear box used by Jewell (1980). Sample dimensions were: length 204 mm, width 52 mm and height 150 mm. Glass side walls were fitted for the photoelastic technique. To contain the paraffin, the shear and pull-out box were surrounded by a perspex tank.

### 3.3.a. Shear box.

A schematic diagram of the shear box is given in fig. 3.4. The halves of the box were sheared apart by displacing the lower half relative to the upper half which reacted against a deflector bar via a roller bearing. The lower half was displaced at 0.08 mm/min by a displacement controlled device. These horizontal forces were applied to the box at mid height of the sample. The lower half of the box ran along two tracks of crossed roller bearings. Metal clamps were fitted to the box to hold the glass side walls in place.

### 3.3.b. Pull-out test apparatus.

A schematic diagram of the pull-out apparatus is given in fig. 3.5. This involved the two halves of the shear box being firmly clamped together at all four corners to provide a rigid box suitable for pull-out tests. Reinforcement was pulled out of the box, at mid height of the sample through a 3.5 mm deep slot in the end wall. A pull-out force was applied to the reinforcement by attaching it to the deflector bar. The box was then steadily pulled away from the deflector bar at 0.08 mm/min by a displacement controlled device. The arrangement devised for attaching the reinforcement to the deflector bar is shown in fig. 3.6. The reinforcement was clamped between steel plates, through which a circular steel bar was inserted. This bar was then bolted to the deflector bar. A lip on the circular steel bar supported the sandwiched reinforcement so that the bar was loaded at its midspan. The main concern for this arrangement was preventing the reinforcement from slipping between the steel plates. Therefore in addition to tightly bolting grid reinforcement between the steel plates,

a transverse member was placed against the back face of the lower steel plate. For the perforated sheet araldite was liberally used between the steel clamping plates.

### 3.3.c. Glass side walls.

19 mm thick float glass was used for the side walls. Float glass (or soda glass) was preferred to pyrex glass because it contained less residual stresses when bought from the manufacturer. This meant that when viewed in a circular polariscope the pyrex glass displayed isoclinic and isochromatic fringes across the whole surface, whereas the float glass only displayed stresses along the edges due to machine cutting. Annealing surprisingly failed to remove stresses from the pyrex glass. Annealing of the float glass was not attempted, because it would have taken too long (approximately 3 months) and have been too expensive. Stress free optical glass was also too expensive.

For shear box tests separate plates of glass were required for upper and lower halves of each side wall. For pull-out tests a single plate of glass could be used for each side wall because the box remained as a whole during tests. Consequently, when the shear box was viewed in the circular polariscope residual stresses were visible across the midheight of the box as shown in fig. 5.7 (slide 4). Whereas in the pull-out test residual stresses were only visible along the base of the box. In addition to edge stresses, lateral pressures generated in the sample during a test would have induced stresses in the side walls. However stresses in the side walls did not disrupt the continuity of the pattern of light stripes. This suggests that the direction of light stripes was unaffected by stresses in the sidewall. However the intensity of light stripes may have been effected.

0.75 mm thick cardboard stripes were used to accomodate any unevenness between the glass side wall and the metal clamp. The glass plates were installed in a circular polariscope to ensure that clamping did not induce stresses in the sidewalls. When the two halves of the box were clamped together for the pull-out test, metal plates were used as sidewalls to ensure the upper and lower clamps were aligned. Afterwards glass sidewalls were installed.

### 3.3.d. Measurement of boundary displacement and forces.

A vertical load was applied to the sample through a rigid loading platen which rested freely on the top surface of the sample. The load was provided by a load hanger with lead weights and applied to the platen through a ball joint. Horizontal movement of the shear/pull-out box and vertical movement of both ends of the loading platen were measured by dial gauges to an accuracy of 0.01 mm. The shear force and pull-out force reactions on the deflector bar were measured by a dial gauge to an accuracy of 3 N.

### 3.3.e. Perspex tank.

To contain the liquid paraffin, the shear box and pull-out apparatus was surrounded by perspex walls. These were lightly bolted to the metal table on which the shear box rested and the base sealed with a silicon sealant.

## 3.4. Polariscope.

### 3.4.a. Polariscope frame and polarising filters.

To view most of the shear box side wall, where light stripes were observed, a 250 mm diameter polariscope was built. This consisted of two dural circular frames as shown in fig. 3.8. Each contained a linear polariser and quarter plate. Lines were inscribed on the faces of the frames at 45° intervals to help install the filters at the correct orientations. Linear polariser and analyser filters were provided by a Polaroid butyrate-laminated linear polarising filter, grade HN 32 and 0.08 mm (0.03") thick. Quarter wave plates were provided by a Polaroid retardation plate, 0.08 mm (0.03") thick with a retarding wavelength of 140 nm. These filters were cut to shape and edged with 1.5 mm thick dural rings. The filters were installed in the circular polariscope frames, which were held rigidly on either side of the shear box by clamping them to horizontal beams overhead as shown in fig. 3.9.

To avoid photoelastic effects from the perspex tank surrounding the shear box, the polariscope was placed inside the tank. This meant submerging the filters in liquid paraffin. This was possible because the filters did not react with the paraffin. To install the filters in paraffin, the paraffin needed to be able to flow freely between the linear polariser and quarter wave plate mounted in each frame. Hence a gap was incorporated between the halves of the frames.

### 3.4.b. Light source.

The polariscope was evenly lit by diffusing light from a 250 watt mercury arc lamp through a sheet of flashed opal perspex as shown in fig. 3.9. The quarter wave plates produced circularly polarised light for a wavelength of 560 nm, which is a yellowish green light. To isolate a narrow band of wavelengths of light around 560 nm, the white light emerging from the circular polariscope was viewed through Kodak wratten filters nos 15 and 58. Light transmission charts for the two colour filters are given in fig. 3.10. The filters were framed with Kodak mounts and supported in a Kodak filter carrier which was attached to the camera used to record the light stripes. However no difference was noticed between the direction of light stripes visible in white light compared with monochromatic light. The light stripes shown in this dissertation are those visible in monochromatic light. This is because better quality copies of slides and prints could be made for light stripes recorded in monochromatic rather than white light.

### 3.4.c. Assembly of plane polariscope.

Having installed the polariser and analyser filters in opposite frames, the analyser was rotated to obtain maximum extinction of light. The linear polarisers were then crossed, as shown in fig.3.11.a.

### 3.4.d. Assembly of circular polariscope.

Having assembled the plane polariscope, the first quarter-wave plate was installed in the same frame as the polariser filter. To convert the plane polarised light to circularly polarised light the quarter-wave plate axes of polarisation needed to be inclined at 45°

to the polariser axis of polarisation. This would result in a maximum transmission of light through the analyser, which was difficult to judge. Instead the quarter-wave plate was rotated to produce maximum extinction of light, which was much easier to judge. This condition occurred when one of the quarter-wave plates axes was aligned with the polariser axis as shown in fig. 3.11.b. This continued to provide plane polarised light. The quarter-wave plate was then rotated at 45° to transmit circularly polarised light, as shown in fig. 3.11.c. The second quarter-wave plate was then installed in the same frame as the analyser filter and rotated to produce maximum extinction of light through the analyser. This occurred when the fast axis, of the second quarter-wave plate was aligned with the slow axis of the first quarter-wave plate as shown in fig.3.11.d. So the circularly polarised light was converted to plane polarised light . This arrangement of crossed linear polarisers and crossed quarter-wave plates produced a dark field of circularly polarised light.

## 3.5. Sample preparation and test procedure.

### 3.5.a. Immersing crushed glass in liquid paraffin.

The objective was to fill the pores of crushed glass with liquid paraffin without trapping air bubbles. This was done by firstly filling the shear or pull-out box with paraffin without generating bubbles. Crushed glass was then slowly slid down a ramp into the paraffin as shown in fig. 3.12, having already been coated in paraffin. Coating the particles in paraffin prior to immersion minimized the trapping of air bubbles. The settled glass was tamped in layers of 10 to 15 mm. to obtain a denser packing. An intial void ratio of approximately 0.60 was achieved.

As the fill operation proceeded a grid of 3 mm diameter steel balls, approximately 15 mm apart, was incorporated in a vertical plane in the sample. This was 15 mm behind the side wall of the box observed through the polariscope. The grid was prepared by filling just above each proposed level of the grid and then positioning the steel balls by dropping then down a tube. The tube was held in place by spacing bars which were supported above the box as shown in fig. 3.13. Photographs were taken of the steel balls at various stages of a test to determine strains within the crushed glass.

### 3.5.b. Attaching reference markers to the glass sidewall.

Before installation, the glass side walls were cleaned and reference markers attached to the front face of the side wall to be observed through the polariscope. The reference markers were used for: 1) providing a reference grid when performing strain analysis of the grid of steel balls and 2) superimposing patterns of stresses on strains. The co-ordinates of the reference markers were measured to an accuracy of 0.01 mm using a travelling microscope. This was done before installing the glass side wall in the box and again after immersion in paraffin during a series of tests. No movement of the reference markers was detected after immersion in paraffin.

### 3.5.c. Direct shear tests on crushed glass with and without reinforcement.

0.8 mm diameter metal rollers were placed between the end walls of the upper and lower halves of the shear box. This provided relatively free movement between the halves of the shear box, but was primarily intended to prevent the glass side walls of the upper and lower halves

from touching. If the edges of the glass sidewalls had touched any uneveness would have created a stress concentration and so caused a photoelastic effect. The halves of the box were then locked rigidly together using external catches at diagonally opposite corners.

For tests without reinforcement the shear box was simple flooded with paraffin and then filled with crushed glass in the manner already described. When reinforcement was to be incorporated in the crushed glass, the reinforcement was firstly suspended in the empty shearbox using a network of threads as shown in fig. 3.14.

The parallel lines shown in this figure alongside the grid reinforcement were drawn on perspex sheets placed against the shear box.These acted as a guide for the desired orientation of the reinforcement. The shear box was then flooded with paraffin. After checking that the reinforcement was still in the required position, the box was filled with crushed glass around the reinforcement. The threads were cut before the crushed glass reached the level at which they were attached to the reinforcement. The top surface of the sample was levelled by sighting along the underside of the support frames of the upper half of the shear box.

The rigid platen for applying vertical load to the sample was slowly lowered onto the sample, taking care not to disturb the sample unduly by displacing paraffin too quickly. The platen was levelled and a gap left between it and the walls of the shear box. A vertical load of 2030 N, corresponding to 191.4* $k/N/m^2$, was applied by means of a hanger and lead weights. The crushed glass settled under this load as shown in fig. 3.16. External catches were next removed allowing the halves of the box to be sheared apart.

---

(*) This vertical stress produced good quality light stripes at maximum shear load with faintly visible light stripes before shearing.

### 3.5.d. Direct sliding of crushed glass over reinforcement.

These tests were carried out to investigate the direct sliding of crushed glass in the upper half of the shear box over reinforcement placed along the top of the lower half of the box. This was performed for the steel grid and perforated brass sheet placed on a polished steel block in the lower half of the box and also for the steel grid placed directly on crushed glass.

(1) For reinforcement placed on highly polished steel

A steel block was placed in the lower half of the shear box. By packing with crushed glass it was positioned so that the top surface of the reinforcement lying on top of it was flush with the top of the lower half of the box. The perforated sheet was kept in place during the test by glueing a 10 mm end strip to the steel block. The grid was kept in place by hooking a transverse member over a set of teeth milled out of the end wall of the lower half of the box, as shown in fig. 3.15. The two halves of the box were then locked rigidly together using external clamps and the box flooded with paraffin. The upper half of the box was then filled with crushed glass.

(2) For grid reinforcement placed directly on crushed glass.

The two halves of the box were locked together and then flooded with paraffin. The lower half of the box was filled with crushed glass. The paraffin was then drained from the box down to a level just above the surface of the crushed glass. The upper half of the box was removed and the grid reinforcement placed along the central plane of the box. The upper half of the box was replaced and locked rigidly together with the lower half. After reflooding, the upper half of the box was filled with crushed glass. After sample preparation, vertical load was applied and direct sliding performed.

### 3.5.e. Pull-out test.

The pull-out box was flooded with paraffin and the lower half of the box filled with crushed glass up to the proposed level of the reinforcement. The paraffin was then drained from the box down to a level just above the surface of the crushed glass. Reinforcement was inserted into the box through the opening in the end wall. Its free end had already been clamped between steel plates, as described in 3.3.b. and illustrated in fig. 3.6. The deflector bar was then bolted to its stand near the end of the pull-out box. A cylindrical steel reaction bar was inserted through a hole in the steel plates clamping the reinforcement and bolted to the deflector bar. The box was flooded with paraffin and the upper half filled with crushed glass. Vertical load was next applied and pull-out performed.

## 3.6. Photographing the light stripes and grid of steel balls in the crushed glass.

A 35 mm SLR camera was used to photograph the light stripes and grid of steel balls at different stages during a test. The light stripes could obscure the steel balls. So to photograph them separately the pattern of light stripes was replaced by a plain background of white light by removing the analyser filter from the polariscope. The camera was fitted with a 135 mm lens to reduce the perspective visible in the shear box. Using a long focus length lens meant the camera had to be placed as close as possible to the shear box so that as much film exposure as possible was filled with the image of the shear or pull-out box. This was a distance of 1.5 m. Placing the camera so close minimised the depth of field. For the light stripes, steel balls and reference markers to be in focus a depth of field of approximately 75 mm was needed. This required a lens aperture size of f8 or smaller. This was

obtained using a 400 ASA film speed and 1 second exposure time. The film type used was Kodak Ektachrome, which produces colour slides. The light stripes recorded are shown in this dissertation in black and white prints and colour slides, captions for slides are given in appendix B. During each test the camera was firmly clamped to a rigid stand. The camera was positioned to minimise distortion on film of the shear or pull-out box. For obtaining good photographs, the tests were performed in a black out shelter.

## 3.7. Strain analysis using the grid of steel balls in the crushed glass.

Strains which developed within the crushed glass during a test were estimated by determining the strains undergone by the grid of steel balls incorporated in the crushed glass. This was done by recording the position of the steel balls along with reference markers, attached to the side wall of the box, at various stages of a test on slide film. Their relative positions were later measured by projecting the slide film onto a digitising pad using a photographic enlarger and then spotting with a cursor. Co-ordinates could be measured to an accuracy of 0.15 mm. These were stored in a computer and assigned to particular steel balls or reference markers using a program called 'POINTS' (Houlsby, 1984). The actual movements of steel balls between different stages of a test and the corresponding uniform strains undergone by triangles of steel balls were determined using a programme called 'STRAIN' (Houlsby). These could then be plotted at the centroid of each triangle of steel balls. The accuracy of this strain analysis is discussed in the next chapter when considering the first set of results.

## 3.8 Alternative methods for crushing glass and sample preparation

Crushing glass can be automated using a ball mill with a perforated drum (Allersma 1982c). The result being that glass particles pass out of the perforations when crushed down to that size. To control glass dust when crushing, the drum should be partly immersed in water.

After immersing the glass particles in paraffin by sliding them down a ramp as described in 3.5a, sample preparation can be speeded up by keeping the glass submerged in paraffin.

# 4. DIRECT SHEAR TESTS ON CRUSHED GLASS

Three direct shear tests were performed on crushed glass i.e. tests nos. 23, 30 and 39. By performing three tests the consistency of the experimental technique and the effect of repeated loading of the same sample of crushed glass were examined. Photoelastic results were obtained which illustrate the transfer of shear load into the crushed glass. The internal stress observations were combined with the boundary stresses using Mohr's circle of stress. This indicated the orientation of planes of maximum stress obliquity. Additionally the principal stress trajectories were compared with principal strain and strain increment directions before and after maximum shear load.

The sign conventions and use of Mohr's circle of stress and strain increment are illustrated in figs. 4.1 and 4.2 respsectively.

## 4.1. Boundary measurements.

Fig. 4.3 shows plots for all three tests of both shear load and central vertical displacement of the loading platen against shear displacement. Experimental scatter is at most 5% which indicates a reasonably consistent experimental technique. The slight peak of shear load accompanied by dilation of the crushed glass after an initial contraction indicates the sample was medium dense. It is difficult to decide at what shear displacement maximum shear load is mobilised, but it took place at approx. 4 mm. displacement. The ratio of maximum shear and vertical load gives a mobilised angle of friction along the central plane of the box $\phi_m = 36°$. The maximum gradient of central vertical displacement

against shear displacement is approximately 10°. If the direction of zero-extension in the crushed glass was aligned with the central plane of the box, this gradient would approximately correspond to the maximum angle of dilation in the crushed glass. This mechanical behaviour is not dissimilar from a medium dense sand.

However, some difference between the mechanical behaviour of crushed glass and sand was noticed. For instance, there was evidence of particle crushing. This was indicated by crushing noises during the tests and after evidence of slight particle degradation. This did not however seem to affect the mechanical behaviour of the crushed glass during repeated use according to the boundary measurements and patterns of light stripes as will be shown later. If particle crushing was significant then the energy required for crushing would need to be considered in addition to mobilised friction and dilation. The second difference was that the dilation of the crushed glass was continuing strongly at the end of test. This may have been influenced by the test arrangement which resulted in the loading platen tilting longitudinally, as will be illustrated later. Wood (1984) observed similar behaviour for direct shear tests on dry crushed glass and attributed it to particle crushing. Thirdly, it was noted in an earlier chapter that the glass particles were significantly platey so that a sample of crushed glass could be expected to behave differently when sheared in different directions relative to the direction of deposition. This predicted anisotropy due to sample preparation of crushed glass should be more pronounced than a similarly prepared sample of sand with a rounded particle shape.

Figure 4.4 compares the vertical displacements at both ends of the loading platen with that at the centre. The plot shows that the platen tilted longitudinally, rising highest at the end of the box which reacted against the deflector bar. The pattern of stresses observed in these tests, as will be discussed later, show a concentration of stress in the upper half of the box at the end wall which reacted against the deflector bar. This could explain the longitudinal tilting. The platen did not tilt transversely.

## 4.2. Patterns of light stripes visible in the crushed glass.

Rather than describe in detail the patterns of light stripes visible throughout each test, since they are similar, only those visible during test no. 30 are described in detail. The patterns of light stripes visible at maximum shear load for all three are then compared to illustrate the extent of agreement between tests. Fig. 4.5 shows at what stages during test no. 30 the patterns of light stripes to be discussed were observed.

(1) Only vertical load applied.

The application of vertical load at the start of test no. 30 produced the faint light stripes shown in fig. 4.6 (slide 5). The light stripes were generally vertical which indicated that the vertical stress was the major principal stress in most of the sample at the start of the test. Skin friction on the end walls of the box is understood to have caused the inclination of light stripes nearby. The dark band visible across the centre of the box was due to residual stresses along the edges of upper and lower halves of the glass sidewalls.

(2) After 0.56 mm shear displacement.

Figure 4.7 (slide 6) shows the effect which 0.56 shear displacement had on the initially vertical light stripe. Although light stripes were still faint, it is clear that the shear displacement produced a counter clockwise rotation of light stripes about the central plane of the box.

(3) At maximum shear load.

By maximum shear load light stripes were brighter and better defined, as shown in fig. 4.8 (slide 7). The increase of light intensity signified that the magnitude of principal stresses in the crushed glass had increased. The bright zones at the ends of the box show that external load was transferred into the crushed glass by passive pressures at the ends of the box. Away from the ends of the box, the combination of horizontal and vertical loads produced a reasonably uniform inclination of light stripes about the central plane. Although upper and lower boundaries were made ideally rough by coating with glass particles, shear stresses do not appear to have been generated along them.

A sketch of the major principal stress trajectories indicated by these light stripes is shown in fig. 12.a. This was produced by projecting an image of the light stripes onto a sheet of paper with the reference markers already drawn on by the computer. The reference markers ensured the projection of light stripes was reasonably accurate. From individual distinct light stripes, the overall pattern of light stripes was drawn to within an accuracy of approximately 5°. This figure indicates that the major principal stress trajectories were inclined at approximately 37° to the central plane of the box at maximum shear load. The central plane was located from reference markers attached to the lower sidewall.

(4) After 7.33 mm shear displacement.

The effect of shearing beyond maximum shear load is shown in fig. 4.9 (slide 8). This appeared to concentrate light stripes more to the centre of the box. However the sketch of major principal stress trajectories shown in fig. 4.12b indicates the same inclination to the central plane as at maximum shear load.

(5) At maximum shear load in the other tests.

Light stripes visible at maximum shear load for test nos. 23 and 30 are shown in fig. 4.10 and 4.11 (slides 9 and 10) respectively. The patterns are similar as for test no.30. Sketches of major principal stress trajectories from these light stripes are shown in fig. 4.13. These indicate an inclination of principal stress trajectories to the central plane of the box of approximately 38°.
This agrees very well with the inclination measured in test no.30, even though the crushed glass was tested eight times during these tests.

Some additional features of the pattern of stresses worth noting are as follows:

(1) Resistance to shear load appeared to be limited to a band about the centre of the box of approximately thirty average particle sizes in height. This gave an effective sample height to length ratio for resisting shearing of approximately 1 to 2.7.

(2) There was no single state of stress in the box. At the ends of the box where the shear load was transmitted into the crushed glass there were highly stressed zones of passive pressure. Whilst on the opposite side of the central plane there was a dark region of low stress, which may have been in an active state. Away from the end

walls, there was a reasonably uniform inclination of light stripes that could be represented by shear and normal stresses along that part of the central plane. Hence a Mohr's circle of stress does not represent completely the stress state in the shear box. However it should provide a reasonable approximation of stress state along most of the central plane.

(3) During each test individual light stripes were seen to extinguish. This was due to the highly loaded columns of particles becoming unstable and collapsing. Therefore individual light stripes did not rotate as the crushed glass was sheared, but extinguished while new ones formed at a different orientation.

(4) There was a concentration of light stripes towards the middle of the rigid upper and lower boundaries of the box. A greater uneven distribution of stress at these boundaries took place for the reinforced direct shear tests. This could have been avoided by installing a flexible inner surface, such as a paraffin filled rubber bag. However priority was given to investigating other problems.

## 4.3. Combining boundary forces with patterns of light stripes at maximum shear load.

To combine boundary measurements with the orientation of light stripes, which are understood to represent major principal stress trajectories, external shear and vertical loads are assumed to act uniformly across the central plane of the box. The pattern of light stripes indicates this is a reasonable assumption. The corresponding normal and shear stresses ($\sigma_y$, $\tau_{yx}$) acting on the central plane can be combined as shown in fig. 4.14. Average values from test nos. 23, 30

and 39 for each of these parameters at maximum shear load are plotted in this manner in fig. 4.15. This analysis indicates that both planes of maximum obliquity were inclined to the central plane of the box, with the closest inclined at approximately 14°. Hence the internal angle of friction in the crushed glass is shown to be approximately $\phi = 40°$. This is greater than the maximum mobilised angle of friction along the central plane of the box $\phi_m = 36°$, given by the ratio of vertical and maximum shear loads. This result conflicts with findings by Arthur et al. (1977) which show good agreement between the maximum mobilised angle of friction for sand along the central plane of direct shear box with the value for internal angle of friction obtained from a simple shear apparatus.

## 4.4. Strains within the crushed glass.

The results of strain analyses for test nos. 23 and 30 before and after maximum shear load, i.e. stages A to B and C to D respectively as shown in fig. 4.16 and 4.17, are plotted in fig. 4.18 to 4.21. In all cases major strains developed in a band across the centre of the box, with strains slightly greater at the end of the box. Away from the ends of the box, there is a reasonably uniform inclination of principal axes within a range of approximately 5° for each analysis. A similar strain pattern was observed by Jewell (1980) when testing dense sand in the same box but with a wider sample.

The strain analysis presented in this dissertation was made assuming uniform strain within the triangle of steel balls. This provided a simple approximation of the strain field within the crushed glass but one which was certainly invalid if a rupture band developed through a triangle of steel balls. This may have ocurred across the

centre of the box, where the band of major strains indicates a rupture layer in the crushed glass. The repeatability of the strain analysis is illustrated in fig. 4.22. This compares the analyses performed between identical stages of test no. 30, with the position of the steel balls for the earlier stage measured from different slides. The maximum difference between the direction of strain is approximately 5°. Gaps in the plot of strains occur where co-ordinates of steel balls could not be measured.

### 4.4.a. Strains before maximum shear load.

Strains wich developed before maximum shear load, i.e. between stages A and B as indicated in fig. 4.16 and 4.17, are shown in fig.4.18 and 4.20 for test nos. 23 and 30 respectively. Generally the magnitudes of principle compressive and tensile strains are equal. This indicates that no volume change took place between these stages. This agrees with boundary displacement measurements which show an initial contraction was matched by dilation. The inclination of principal compressive strains to the central plane of the box are shown in these figures to be approximately between 40° to 45° in tests nos. 23 and 30.
Taking into account the accuracy of the strain analysis, this strain data suggests that the direction of zero-extension in the crushed glass approximately lay along the central plane of the box. This observation agrees with observations by Jewell (1980) for dense sand in the shear box.

### 4.4.b. Strain increments after maximum shear load.

Strain increments which developed after maximum shear load between stages C and D are shown in fig. 4.19 and 4.21, for test nos. 23 and 30 respectively. Away from the ends of the box the average magnitudes of

principal strain increments are approximately $\dot{\varepsilon}_1$ = 6%, $\dot{\varepsilon}_3$ = -9% for test no.23 and $\dot{\varepsilon}_1$ = 4.7%, $\dot{\varepsilon}_3$ = -7.6% for test n. 30. This difference in the magnitudes of minor and major principal strains confirms the sample dilated. The inclination of major principal strain to the central plane of the box is shown to generally lie between 37° to 42° for test no. 23 and 37° to 40° for test no. 30. Average values for inclination and magnitudes of principal strains are plotted in Mohr's circles in fig. 4.23. These suggests the direction of zero-extension still lay along the central plane of the box. The average value for the angle of dilation from these internal measurements are shown in the Mohr's circles to be 11.5° and 13.5° for test nos. 23 and 30 respectively. In comparison, the estimated angle of dilation from boundary measurements is 10°.

### 4.4.c. Orientation of the rupture band.

The major strains which developed across the centre of the box appear to represent a single rupture band. However the rupture band may have divided into subdivisions as observed by Scarpelli and Wood (1982) but the strain analysis was not sensitive enough to detect this. Hence within the accuracy of the strain analysis it seems that the rupture band developed along a direction of zero-extension in the crushed glass, i.e. velocity characteristic. In comparison the Mohr's circle analysis of stress data indicated that the rupture band did not coincide with the plane of maximum stress obliquity, i.e. stress characteristic, which appears to have been inclined at approximately 14° to the central plane of the box.

It is understood in the literature that this result is not a unique orientation for a rupture band relative to the stress and strain fields in a granular medium, but depends on the constraints imposed on the medium (Scarpelli and Wood, Arthur et al.). The two basic orientations suggested for a rupture band in a sand mass are along: (1) planes of maximum stress obliquity based on statical requirements provided by the Mohr-Coloumb failure criterion, or (2) zero-extension directions (Roscoe, 1970). For the former suggestion the rupture band in a cohesiveless soil would be inclined at $(45-\phi'/2)$ to the major principal stress trajectory as shown in fig. 4.24.a. Whilst for the latter suggestion, if coaxility of principal axes of stress and strain increment is assumed,as is usually done, then the rupture band in a cohesionless soil would be inclined at $(45-\nu/2)$ to the major principle stress trajectory, as shown in fig. 4.24.b. A further possibility is to regard the formation of a rupture band as a combination of these two basic cases, which depends on the degree of constraints imposed on the sand mass (Arthur et al., Vardoulakis, 1982). From radiographic observations of direct shear tests on long thin samples of sand, Scarpelli and Wood suggested that when the sand has freedom of movement, it may satisfy these combined solutions. However, where imposed constraints are greater the soil may have no choice but to develop along a zero-extension direction and satisfy Roscoe's solution. The latter case presumably took place in direct shear tests on crushed glass.

## 4.5. Comparison of directions of principal stress and strain increment.

The plastic behaviour of an ideal elastic-plastic material can be specified by a yield surface, flow and hardening law (Atkinson and Bransby, 1978). Drescher (1976) noted that the various flow rules proposed for soils could be divided into two categories according to whether or not principal axes of stress and strain increment are considered to coincide. The author reported discrepancies between tests on sand as to whether or not principal axes coincide. This was attributed to the assumptions made about the distribution of stresses in the sand masses. Hence Drescher examined the stress distribution in crushed glass through a circular polariscope. The glass was loaded in a double shear apparatus. The displacement field in the crushed was also measured using a stereo-photogrammetric method. A comparison of principal stress and strain increment directions indicated coincidence in the upper part of the shear box but deviation in the lower part near the end walls, see fig. 4.25a. The maximum deviation was 20°, which was greater than assumed degree of accuracy of $\pm$ 5° for each principal direction. By observing changes in the brightness of the light stripes, the author concluded that deviation of principal axes occurred when the crushed glass was close to or beyond the peak stress.

A comparison of principal stress and strain increment directions in crushed glass has also been made by Allersma(1982b). This involved a more sophisticated optical system which enabled principal stress magnitudes as well as directions to be determined. The author observed in simple shear tests that principal axes may deviate in the limit state of stress, see fig. 4.25b.

Comparison of principal stress and strain increment directions before and after maximum shear load are shown in fig.4.26 and 4.29 for test nos. 23 and 30. The principal stress trajectories (i.e. light stripes) were those observed at the end of each strain increment. This was done because the strains were plotted with respect to the reference marker positions at the end of the strain increment, i.e. the grid of reference markers for upper and lower halves of the box having moved apart. The projection of stresses on the plot of strain was aligned using the reference markers. The continuous lines for principal stress trajectories were drawn from distinct individual light stripes. This was considered to be done within an ~~of~~ accuracy of approximately 5°. It should be noted when comparing these principal directions that during the strain increment before maximum shear load the light stripes rotated from vertical to the inclination shown. Whereas during the strain increment after maximum shear load the inclination of light stripes was reasonably constant.

Figures 4.26 and 4.27 relating to test no. 23, suggest that principal directions coincided before and after maximum shear load. In comparison, figures 4.28 and 4.29 relating to test no. 30 suggest principal directions deviated before maximum shear load but coincided after. Given the rapid rotation of light stripes during the first strain increment and the discrepancies between tests, it is not clear whether principal directions coincided before maximum shear load. However, after maximum shear load it appears within the acccuracy of the analysis that principal directions coincided.

This coincidence of principal directions can be shown to be in good agreement with the earlier Mohr's circle analysis of stress and

strain data. For coincidence of principal directions the angle between the plane of maximum stress obliquity and direction of zero-extension is $(\phi - \nu)/2$ . Analysis of strain indicated that the direction of zero-extension lay approximately along the central plane of the box. Analysis of stress data at maximum shear band indicated the plane of maximum stress obliquity was inclined to the central plane, and so the direction of zero-extension, by 14°. The internal angle of friction given by this stress analysis is $\phi = 40°$. This was accompanied by an average value for the angle of dilation of $\nu = 12.5°$ from internal measurements. These values give $(\phi - \nu)/2 = 13.7°$. This agrees very well with the angle of 14° between the plane of maximum stress obliquity and direction of zero-extension given by Mohr's circle analyses. This further indicates that principal directions concided at maximum shear load.

## 4.6. Conclusions.

1) The pattern of stresses showed shear load was transferred into the crushed glass by passive pressures at the end walls. Away from the end walls there was a reasonably uniform inclination of light stripes. The resistance of shear load appeared to be limited to a band about the central plane of the box of approximately thirty particle size in height. This gave an effective sample height to length ratio for resisting shearing of approximately 1 to 2.7. Shear stresses were not observed along the upper and lower boundaries of the box, even though the surfaces were made fully rough by coating with crushed glass.

2) It appeared that directions of principal stress and strain increment coincided at and beyond maximum shear load. It was less clear whether coincidence took place before maximum shear load. In contrast Drescher (1976) and Allersma (1982b) observed principal directions to deviate in crushed glass at a limit state of stress.

3) There was no single state of stress in the shear box as already mentioned. However Mohr's circle analyses of stress and strain data was in good agreement with the coincidence of principal axes observed by direct comparison of principal trajectories. This indicated it was acceptable to combine boundary forces with principal stress trajectories using Mohr's circle.

4) A single rupture band across the centre of the box appeared to coincide with the direction of zero-extension and not the plane of maximum stress obliquity. Combined with the coincidence of principal directions, this result indicated that the value of internal angle of friction for the crushed glass depended on the angle of dilation, see fig. 4.30. It can be shown for this situation that:

$$\sin \phi = \frac{\tan \phi_m}{\cos \nu + \tan \phi_m - \sin \nu}$$

$\phi_m$ is the mobilised angle of friction across the central plane of the box given by the average shear and normal stresses. However it is shown in the literature that this is not a unique orientation for a rupture band relative to the stress and strain fields in a granular medium, but dependent on the constraints imposed (eg. Scarpelli and Wood, 1982).

5) The internal angle of friction for crushed glass estimated from Mohr's circle analysis was $\phi$ = 40°. The mobilised angle of friction along the central plane of the box was $\phi_m$ = 36°. In comparison Allersma (1982b) observed a maximum mobilised angle of friction in crushed glass under simple shear of 36° with no volume change.

6) The angle of dilation estimated from boundary measurements, assuming the direction of zero-extension coincided with the central plane of the box, was close to internal measurements i.e. 10° compared with an average of 12.5°.

## 4.7. Suggestions for future work.

1) Boundary measurements indicated that the mechanical behaviour of crushed glass was not too dissimilar from a cohesionless soil. However the effects of particle crushing and the platey particle shape need close examination to really gauge how relevant the photoelastic results are to the mechanical behaviour of a cohesionless soil.

2) The slight difference in refractive indices between the crushed glass and liquid paraffin rendered the glass particles faintly visible. A stereo-photogrammetric method could therefore be used for future work to measure displacements in the crushed glass (Butterfield et al. 1979, Drescher, 1976). This should provide a more accurate measurement of displacements than obtained from the grid of markers, i.e. an accuracy of 0.01 mm. is possible. Additionally the whole displacement field would be measured instead of at discrete points as for a grid of markers.

This should enable a more detailed examination to be made of areas of high displacement gradients than possible from the grid of markers. In which case a more accurate study could be made of the relative orientation of a rupture band to stress and strain fields in the crushed glass. It may be possible to identify sub-divisions of rupture bands as for example studied by Scarpelli and Wood (1982). The comparison of principal strain directions with principal stress trajectories could also be made more accurate.

3) The accuracy of comparing principal directions could also be improved by uniformly shearing a larger volume of crushed glass. This, for example, could be achieved by installing single plates at the ends of the existing shear box to convert to a simple shear apparatus.

4) The orientation of the rupture band through the centre of the shear box appeared to be constrained to develop along a direction of zero-extension and not a plane of maximum stress obliquity. The relative orientation of a rupture layer, stress and strain field in crushed glass could be examined for a greater freedom of movement.

5) The photoelastic results presented only involved examining the directions of principal stress. However a more complex optical system has recently been developed (Allersma 1982a) to measure the intensity of polarised light passing through crushed glass in order to determine principal stress magnitudes as well as directions. This alternative technique requires automatic readings in an x-y plane, so it would be quite costly to install. However it is a possible technique for use in future work if funds and time are available.

# 5. THE INTERACTION OF CRUSHED GLASS WITH FLEXIBLE AND RIGID REINFORCEMENTS PLACED AT DIFFERENT ORIENTATIONS IN THE SHEAR BOX

## 5.1. Introduction

Having identified the stress and strain fields in direct shear tests on crushed glass alone, the effect of including a single reinforcing element was examined. This followed on from research by Jewell (1980). Three orientations of reinforcement were considered, i.e. $\theta$=40°, 0° and -45° as shown in fig. 5.1. These showed reinforcement loaded in tension, compression, shear and bending. This was for a flexible perforated brass sheet at the three orientations. At the vertical orientation, where the flexible sheet was loaded in tension and shear, the performance of a rigid reinforcement was also investigated.

The result is a series of tests which illustrate the relative performance of flexible and rigid reinforcements at different orientations. These results are related to the use of flexible and rigid reinforcement in the field.

## 5.2 Boundary measurements.

Boundary measurements taken when the perforated brass sheet was used as reinforcement are given in fig. 5.2. These indicate that the ability of the sheet reinforcement to strengthen the crushed glass depended on its orientation. However prior to a shear displacemnt of approximately 2 mm. the sheet reinforcement had a negligible effect. Similar behaviour has been observed by Jewell (1980) when testing with dense sand in the shear box.

The marginal differences between unreinforced and reinforced tests before 2 mm. shear displacement are: (1) a slightly stiffer response when the sheet was orientated at $\theta = 40°$ and $-45°$ and (2) a slight weakening of the sample when the sheet reinforcement was orientated at $\theta = 0°$. The differences are just outside the range of experimental scatter.

From the patterns of stresses and strains determined in the crushed glass explanations for the different reinforcing effects are given in the following sections.

## 5.3. 40° Orientation

40° orientation approximately placed the flexible sheet reinforcement along the direction of principal tensile strain in the unreinforced crushed glass as shown in fig. 5.3. Light stripes in fig. 5.4 (slide 11) show that this orientation resulted in the crushed glass transferring a considerable amount of the shear load to the reinforcement, putting it in tension. This is represented by a fairly even distribution of light stripes inclined along the sheet. The remaining shear load resisted by the crushed glass passed almost orthogonally through the middle of the reinforcement. Hence the reinforcement provided an additional means for the crushed glass to resist loading. A simple representation of how crushed glass and reinforcement resisted loading is given in fig. 5.6a. This was the optimum orientation examined for the flexible sheet reinforcement, which agreed with findings by Jewell (1980) and McGown et al. (1978).

Strains which developed in the crushed glass between 1.87 and 8.60 mm. shear displacement are shown in fig. 5.7. Strains are absent from underneath the reinforcement because it was too difficult to form a grid of steel balls there. The data show the reinforcement influenced the development of strains in the crushed glass and so inhibited a band of major strains from forming along the centre of the box. Instead major strains developed in the crushed glass along arcs from the end walls of the box towards the ends of the reinforcement. This is a less favourable mode of failure. Similar behaviour was observed by Jewell (1980) as reported in chapter 1. Hence the tensile reinforcement functioned by limiting tensile strains in the crushed glass. Rotation of principal axes in the crushed glass is understood to be limited by alignment of a direction of zero-extension with the tensile reinforcement.

## 5.4 -45° Orientation

-45° orientation approximately placed the sheet reinforcement along the direction of principl compressive strain increment in the unreinforced crushed glass, as shown in fig. 5.3. This resulted as shown in fig. 5.5 (slide 12) in the crushed glass transferring a large amount of shear load to the reinforcement putting it in compression. This is represented by light stripes inclined along the reinforcement and bearing on the ends. The crushed glass presumably transferred stresses to the reinforcement because the reinforcement was more rigid. Consequently this produced the slightly stiffer initial response to loading. The transfer of stresses to the reinforcement resulted in a considerable reduction of stress in the crushed glass across the central plane of the box. Therefore the reinfocement provided an alterna-

tive path of resistance across the central plane rather than an additional one as when loaded in tension at $\theta = 40°$. Not surprisingly negligible benefit was gained from the reinforcement. This is therefore an inefficient orientation at which to install reinforcement.

Note that the slender reinforcement was able to carry large compressive loads without buckling due to lateral support from the crushed glass. Buckling only occurred when shear displacement had caused excessive misalignement of the two halves of the sheet reinforcement, thus weakening the sample. A simple representation of how reinforcement and crushed glass resisted shearing is given in fig. 5.6b.

Strains which developed in crushed glass between 2.71 and 7.00 mm. shear displacement are given in fig. 5.8. Again strains are absent from underneath the reinforcement. This shows that the reinforcement slightly modified strains in the crushed glass. However the overall pattern still contains a band of major strains across the centre of the box as in the unreinforced test.

## 5.5. 0° Orientation

Placing the flexible sheet reinforcement at $\theta = 0°$ produced a significant reinforcing effect but not as great as when working in tension at the orientation $\theta = 40°$. Light stripes observed at 8.98 mm. shear displacement are shown in fig. 5.10 (slide 14). The intensity of light stripes indicates the main resistance to loading across the central plane of the box was due to a concentration of stresses at the middle of the sheet reinforcement. The reinfocement

was too flexible to support bending and shear loads except close to its middle. The reinforcing effect produced is understood to be due to the sheet supporting shear load at its middle in dowel action.

In addition the crushed glass is shown to have put the reinforcement in tension by an inclination of light stripes along its ends. This is understood to be because the crushed glass dilated in the unreinforced test. Consequently the vertical orientation still lay within range of tensile strains in the unreinforced crushed glass.

The effect of using a rigid reinforcement at the vertical orientation was investigated using a 3 mm. thick steel plate. This produced a much greater reinforcing effect as shown in fig. 5.11. After 6 mm. shear displacement, the reinforcing effect was greater than that produced by the flexible sheet reinforcing when placed along the optimum orientation at $\theta = 40°$. The loading mechanism which produced this greater reinforcing effect is illustrated by light stripes in fig. 5.13 (slide 16). This shows the reinforcement was able to support passive pressures well away from its middle and rotated as a rigid body generating passive pressure at its ends.

Simple interpretations of the passive pressures acting on the rigid and flexible reinforcements are given in fig. 5.14. For the rigid reinforcement this is a combination of the dowel action which took place at the middle of the flexible sheet reinforcement (portrayed by force R) and the moments of two couples i.e. ($2\ Q\ Y_z$ and $2\ P\ y_1$). For rotational equilibrium $Q.Y_z = P.y_1$. The arms of the couples differ, so Q is greater than P. The difference between these forces gives a

shear force (Q-P) at the middle of the reinforcement. This resisted the shear load in addition to the dowel action at the middle. In this case the limiting condition appears to be the ability of the crushed glass to support rotational equilibrium of the reinforcement. For a more flexible reinforcement the passive pressures P and Q would be less and closer to the middle of the reinforcement.

The reinforcing effect provided by reinforcement supporting passive soil pressures has also been investigated by Juran et al. (1981). The authors used a row of reinforcing bars orientated at $\theta = 0°$ which were rigidly fixed in the base of the box as shown in fig. 5.15. The interaction of crushed glass with the rigid reinforcement indicates that rigidly fixed reinforcement should relieve to some degree, if not totally depending on the flexural stiffness of the reinforcement, the need for soil to support rotational equilibrium of the reinforcement. Hence rigidly fixing reinforcement does not model the interaction of reinforcement with soil when equally stiff either side of the failure surface. However it could model the condition when soil is very much stiffer on one side. The extreme condition of the latter situation is reinforcement embedded in rock with soil sliding over the rock face.

Although flexible and rigid reinforcements significantly strengthened the crushed glass, initially a slight weakening was observed. This was accompanied as shown in figs. 5.9 and 5.12 (slides 13 and 15) by the reinforcements supporting some vertical load. This began with the application of vertical load at the start of the test and not because of sample contraction during the initial stages of shearing. The transfer of vertical load to the reinforcements indicated a reduction of vertical effective stress which would have weakened the sample. However it may not have

been the only cause of weakening because the rigid reinforcement supported much more vertical load than the flexible reinforcement, yet the weakening effect was similar. Another possible reason for weakening could be the discontinuity to resistance caused by the reinforcement across the central plane of the box. However when reinforcing effects were registered the reinforcements no longer supported the vertical load. Juran et al. also observed reinforcement at $\theta = 0°$ weakening soil, but to a much greater extent than in these direct shear tests on crushed glass. This could have been due to the type of soil used, which was a clayey silt.

Strains which developed in the crushed glass when strengthened by the flexible reinforcement are shown in fig. 5.16. The reinforcement had a negligible effect on the strains except to marginally reduce the magnitudes about its middle. Yet the flexible reinforcement had significantly strengthened the crushed glass towards the end of this strain increment. The strains which developed in the crushed glass when strengthened by the rigid reinforcement are given in fig. 5.17. The rigid reinforcement clearly had a much greater effect on the development of strains. Major strains were inhibited from developing through the centre, but instead diverted to the ends of the reinforcement. This is similar to the mechanism for reinforcement working in tension. However the rigid reinforcement does not appear to have affected the strains to the same extent as a tensile reinforcement, even though a greater reinforcing effect was produced.

## 5.6. Discussion and conclusions.

1) Orientation of flexible tensile reinforcement. In agreement with McGown et al. (1978) and Jewell (1980), the optimum orientation for a single flexible reinforcement in a plane strain unit cell test on cohesionless soil is indicated to be the direction of principal tensile strains in the unreinforced soil. At this orientation, the flexible reinforcement acts in tension and provides an additional means for the soil to resist loading as a result of limiting tensile strains in the soil.

In practice however, the orientation of tensile sheet and strip reinforcement in soil structures depends on:

- practical limitations of construction and
- additional uses such as a separator between soft ground and fill material for embankments and unpaved roads.

This typically means a horizontal placement in walls, embankments, unpaved roads, etc.

When compared with the direction of principal tensile strains for a classical active condition behind a conventional retaining wall, the horizontal direction for reinforcement in a reinforced earth wall appears to be an optimum orientation (Basset and Last 1978). However model studies indicate instead an optimum orientation of 10° to 15° inclined downwards (Smith and Birgisson 1979). But this would be impractical to construct.

Altough the direction of the tensile reinforcement may be pre-determined in a soil structure, model tests on embankments by McGown et al . (1981) illustrate that the strain field for the soil fill is

still a variable which depends on the filling procedure. These model tests show that firstly constructing mounds at the edge of the embankment generally reduced strains in the fill and avoided significant inclination of principal stress trajectories at the toe compared with a straightforward horizontal filling sequence as shown in fig. 5.18. Hence the former filling sequence generates strains more favourable to a horizontal orientation of reinforcement under the embankment base, besides generally limiting strains in the fill. In practice though reinforcemnt under an embankment is unlikely to remain horizontal during the filling operation because of large displacements in the soft ground.

2) Reinforcement with a limited bending capacity used for in situ applications. The direct shear test results show the flexible sheet reinforcement was most effective working in tension. The magnitude of the reinforcing effect produced by the flexible reinforcement in tension was equalled by the very rigid reinforcement resisting shear and bending, but only after a greater shear displacement. These findings suggest that the more robust reinforcements needed for in situ applications are most effective in cohesionless soil working in tension even though a limited bending capacity exists. This suggestion is particularly relevant to the use of small steel sections for stabilising steep excavations in the technique known as soil nailing.

This suggestion is supported by results for numerical modelling of a soil nailed excavation in sand by Juran et al. (1985). The authors observed that resistance of shear stresses by 50 mm. diameter steel bars placed horizontally in the excavation had practically no effect on the behaviour of the soil nailed structure under working conditions. The authors also observed that horizontal placement of the steel bars was

more effective than 30° inclination downwards. In comparison, Shen et al. (1978) also observed numerically an optimum orientation for parallel reinforcing bars of 20 ± 5° inclined downwards in an excavation in cohesive-frictional soil. In this case the effect of reinforcement rigidity on the results was not indicated, i.e. whether purely tensile reinforcement would have given the same result.

3) Reinforcement in compression. It is observed that when reinforcement is required to work in compression it will be ineffective unless stiffer than the soil and even then it will only remove load from the soil rather than strengthen the soil itself. This finding can for example be related to a typical network of micropiles that would be used to stabilise a slope, as shown in fig. 5.19. The micropiles that could be expected to work in compression are identified by a broken line. These it appears would provide an alternative path for load across the sliding surface in the slope rather than strengthen the soil. However this reinforcing system is not that straightforward because micropiles are usually employed to work as a group and create a monolith structure. However the remarks about the compressive piles should have some merit.

4) Dowel reinforcement. To calculate shear force and bending moments for a dowel pile an estimate is needed of the distribution of stresses along the pile. The photoelastic results for the flexible sheet and rigid plate reinforcements at $\theta = 0°$ show such stress distributions for two extreme cases of flexibility for a dowel pile. The stress distribution for the rigid reinforcement is a similar pattern as for the Brinch-Hansen dowel theory (1960). Further tests could be performed to observe the change in stress distribution along a dowel pile for varying degrees of flexibility between these extreme cases.

5) Relative effects on stress and strain fields. The effects on stress and strain fields in the crushed glass by reinforcement supporting tension compared with bending and shear suggest that the latter category strengthened primarily by modifying stresses in the crushed glass, whilst the converse applied to the former category.

## 5.7 Suggestions for future work.

1) Interference between tensile reinforcement. It was reported in the first chapter that the performance of tensile reinforcement can be weakened by interference from adjacent reinforcement. The photoelastic technique with crushed glass is well suited for identifying interference between reinforcement.

2) Larger shear box. Using a larger shear box, it would be interesting to investigate whether the different reinforcing effects observed for flexible and rigid reinforcements at various orientations are similar when magnified.

3) Soil nailing. It has been recommended from the direct shear tests that the reinforcing bars used for soil nailing and excavation are most effective in cohesionless soil working in tension. However in practice excavations stabilised by soil nailing have been in sand with some fines (e.g. Shen et al. 1981 - clay and silty sand, Cartier and Gigan 1983 - silty sand, Guilloux et al. 1983 - moraine mostly of sand and gravel). Direct shear tests could be performed to examine whether the reinforcing bars used for soil nailing are still most effective working in tension when placed in silty sand.

There is very limited information on the optimum orientation of steel bars for soil nailing of excavations. Yet such an insitu technique provides a greater freedom for the orientation of reinforcement than when strengthening fill material. It could be very rewarding to carry out such an investigation. Following the numerical studies made by Shen et al. (1978) and Juran et al. (1985) it seems the greatest contribution could be made by initiating field studies. This is a relatively new soil reinforcement with much potential for providing temporary support of deep excavations. However it has received relatively little attention to date.

# 6. THE TRANSFER OF STRESSES FROM CRUSHED GLASS TO REINFORCEMENTS WITH OPENINGS.

## 6.1. Introduction.

This chapter is concerned with the bond that developes between granular soil and tensile reinforcement compared with the interaction that takes place in the tests used to measure the potential bond. In particular the interaction with reinforcements which have openings or apertures is considered. In practice this covers fabrics, nets and grids, with the apertures in the grids being much the larger. An example of aperture sizes for a commercially available polymer net and grid is given in fig. 6.1. In this study two types of reinforcement were used. These were a perforated brass sheet and a steel grid. The transfer of stresses to the perforated sheet was shown in the previous chapter when examining the performance of a flexible reinforcement at different orientations in the shear box. Specifications for these reinforcements are given in Chapter 3. For this study the important feature of the reinforcements is the different aperture or opening size. For the sheet, perforations were a similar size to the glass particles, whereas the grid aperture length and width were approximately ten and five times greater than the average particle size.

In practice these proportions could represent the following combinations:

a) for the steel grid:
   - polymer grid with sand or gravel;
   - polymer net with fine to medium sand;

b) for the perforated sheet:
   - polymer grid with crushed rock or brick;
   - polymer net with gravel;

- polymer fabric with fine to medium sand.

There is little experimental data published on the mechanism of soil - reinforcement interaction. This reflects the difficulty of identifying the detailed behaviour of the soil at the interface with reinforcement, e.g. using radiographic or stereo-photogrammetic method for measuring internal displacements or by interpreting boundary measurements. The photoelastic technique with crushed glass provided a means of identifying this interaction. Before presenting the photoelastic results obtained, the types of tests used for examining soil - reinforcement interaction and the findings by previous researchers are described.

## 6.1.a. Tests used for examining soil - reinforcement interaction.

There are two basic tests used for examining soil - reinforcement interaction. These involve measuring:

- direct sliding resistance of soil over reinforcement, and
- pull-out resistance of reinforcement from soil.

The former is usually measured in a shear box. The reinforcement is laid flush across the top of the lower half of the box, whilst mounted on soil or a rigid block (Ingold, 1984). Soil in the upper half of the box is sheared over the reinforcement, which is held stationary to either one end of the lower half of the box or to the rigid mount if used. Within the accuracy of the test, direct sliding resistance has been found not to exceed the shearing resistance of the soil, i.e. tan $\phi'$ and to be generally independent of the stress level (Myles, 1982; Ingold, 1984).

Examples of the typical configurations and boundary conditions which have been adopted for measuring pull-out resistance are shown in fig. 6.2. This is a more complex type of test which has attracted lots of discussion. Some of the arguments expressed and results obtained are

described below.

## 6.1.b. Some previous observations on the pull-out test.

One of the potential failure modes in a tensile reinforced soil structure is understood to be the pull-out of reinforcement from the restraining zone of soil, see fig. 6.4. The pull-out test is considered by some to model this condition (Schlosser and Juran, 1979).

Ingold (1984) recommended the pull-out test, even with only a qualitative interpretation, because faults in the structure of a geotextile can be detected.

McGown (1979) opposed the pull-out because the stress transfer mechanism was consider different from that operating in a soil reinforcement system. The reason being that in the pull-out test external stresses are applied directly to the reinforcement, whereas in a soil reinforcement system stresses are transferred to the reinforcement by the soil through limiting tensile strains.

Actual experimental observations of the behaviour of a pull-out test compared with a soil reinforcement system have been provided by Jewell (1979, 1980). The author determined strains in sand and reinforcement for:

- sand reinforced in a shear box, and
- a pull-out test on the reinforcement from sand

as shown in fig. 6.4. A difference was observed between the strain pattern in the sand and the mobilisation of the reinforcement force for the two test arrangements. Hence Jewell concluded that there was a difference between the pull-out test and the action of tensile reinforcement when strengthening sand.

McGown (1979) also argued against the pull-out test because a very non-uniform strain distribution can be developed along the reinfor-

cement, particularly for the more extensible polymer fabrics, see fig. 6.5. This makes it difficult to back analyse for a measure of soil-reinforcement interaction. However a practical solution for measuring the strain distribution along reinforcement in a pull-out test has been demonstrated by Holtz (1977) using magnets.

The usual approach for interpreting the pull-out test is to determine an average apparent bond for the whole embedded length. This has resulted in apparent bond values dependent on stress level and reinforcement geometry (Schlosser and Elias 1979; Ingold 1983 and 1984). In many cases apparent bond values have exceeded tan $\phi'$, particularly for stiff polymer grids and steel strip reinforcement, see fig. 6.6. This conflicts with fundamental soil mechanics, because the bond should be limited by the shear resistance of the soil. For steel strip reinforcement, high apparent bond values have been attributed to a local increase in stress due to confined dilation of the soil (Guilloux et al. 1979). This does not apply to sheet reinforcement since the whole plan area is covered. High apparent bond values have also been attributed to boundary effects (Jewell, 1980).

The variation of apparent bond with stress level for pull-out of steel strips has been attributed to a suppression of soil dilation at higher stress levels (Schlosser and Elias, 1978). For the more extensible fabric reinforcement, a variation of apparent bond with stress level can be attributed to a restriction of pull-out resistance to a small proportion of its length because it is too extensible. This should explain very low apparent bond values for fabrics at high stress levels (Ingold, 1984).

Geometry of steel strips has also been observed to influence apparent bond values (Schlosser and Elias, 1978).

To conclude, direct sliding resistance is easier to measure and results are more consistent than pull-out resistance. Hence direct sliding resistance has generally been recommended to provide design

values for soil-reinforcement bond (Department of Transport 1978; Christopher and Holtz, 1985; Netlon, 1984).

### 6.1.c. Photoelastic tests performed.

The photoelastic results presented in this chapter illustrated the transfer of stresses from crushed glass to the perforated sheet and grid for:

- crushed glass strengthened by tensile reinforcement in the shear box,
- direct sliding of crushed glass over the reinforcements, and
- pull-out of the reinforcements from crushed glass.

Pull-out tests were also performed on single and pairs of transverse members of the grid at different spacings to investigate interference between the transverse members. The types of pull-out tests performed are shown in fig. 6.7.

## PART A - TRANSFER OF STRESSES FROM CRUSHED GLASS TO GRID AND PERFORATED SHEET FOR REINFORCING, DIRECT SLIDING AND PULL-OUT.

## 6.2. Transfer of stresses to the reinforcements when strengthening crushed glass.

### 6.2.a. Transfer of stresses to the grid reinforcement.

Figs.6.9 and 6.10 (slide 17 and 18) are two examples of the transfer of stresses from crushed glass to the steel grid when used as tensile reinforcement in the shear box. Both photographs were taken when most of the possible reinforcing effect had been produced, as indicated in fig.6.8, and show good agreement.

These results show that outside of the concentration of stresses that passed through the middle of the grid, the transfer of stresses to the grid putting it in tension primarily dependend on a concentration of stresses against the transverse members. This was most pronounced at the top end of the grid. The transfer of stresses at the ends of the grid should represent the soil bond with such a grid in a full scale soil structure. The concentration of stresses which passed through a large proportion of the grid in the shearbox should be limited to a very short length of the grid in a full scale structure at the intercept of a potential failure surface, i.e. position of maximum tension in the reinforcement. Therefore to measure this soil - grid bond a similar concentration of stresses at the transverse members needs to be generated.

## 6.2.b. Transfer of stresses to the perforated sheet reinforcement.

Fig. 6.11 (slide 11) shows the transfer of stresses to the perforated sheet when used as tensile reinforcement in the shear box. Again, the photograph was taken when most of the possible reinforcing effect had been produced, as indicated in fig. 6.8. For this reinforcement the apertures (or perforations) are a similar size as the glass particles and occur more frequently than for the grid. Consequently the transfer of stresses to the perforated sheet was more frequent compared with the grid, producing a reasonably continuous distribution of stresses along the end lengths. The transfer of stresses to the perforated sheet is understood to depend on one or two glass particles lodging in each perforation.

The maximum inclination of light stripes to the sheet is shown in fig. 6.12a to have ranged between approximately 50° to 60°. This was less than the inclination of the light stripes observed along the central

plane of the shear box for the direct shear of crushed glass alone, see fig. 6.12b. In which case, it appears the mobilised bond along the perforated sheet was considerably less than the angle of friction $\phi'$ for the crushed glass. This observation lends support to a back analysis performed by Jewell (1980) for a similar direct shear test where a steel grid reinforced dense sand. This indicated a very low equivalent mobilised angle of friction along the grid of approximately 10° compared with $\phi' \cong 55°$ for the dense sand. The high $\phi'$ value was due to a low vertical effective stress of 30 kPa.

### 6.2.c. Relative performance of the two reinforcements.

Boundary measurements given in fig. 6.8 for the two tests performed with steel grid as tensile reinforcement indicate an experimental scatter of approximately 5%. Outside this range of scatter the steel grid provided approximately 25% greater reinforcing effect than the perforated sheet by the end of the tests. Neither reinforcement showed signs of being loaded beyond the elastic tensile range. In which case, both behaved as very stiff in the tests. Hence it seems that the different reinforcing effect was due to a higher bond developed with the steel grid. This might have been influenced by the short length of reinforcement used. Because there appears a greater transfer of stresses at the ends of the grid than for the perforated sheet. This could have had a significant effect for such a short length of reinforcement.

### 6.2.d. Patterns of strains in the crushed glass.

The patterns of strains that developed in the shear box are illustrated in fig. 6.13. The results show that both reinforcements limited tensile strains in the soil and so modified the surrounding strain field,

as already described in the previous chapter. However the patterns of strains do not distinguish between the different mechanisms for interacting with the reinforcements as shown in the patterns of stresses.

## 6.3. Direct sliding resistance of crushed glass over the reinforcements.

### 6.3.a. Introduction.

The test procedure used for examining the direct sliding resistance of crushed glass over the reinforcements is described in detail in Chapter 3. In brief, crushed glass in the upper half of the shear box was sheared over the reinforcement, which lay flush across the top of the lower half of the box and held stationary with respect to the lower half of the box.

The apertures of the perforated sheet were a similar size as the glass particles. So the particles above the sheet could not readily penetrate through the apertures to interact with the surface underneath. Hence direct sliding of crushed glass over the perforated sheet was only investigated with the sheet mounted on a steel block. In contrast, the glass particles penetrated through the apertures of the steel grid and interacted with the surface underneath. Hence direct sliding of crushed glass over the grid was investigated for the grid mounted on crushed glass and on a steel block. The steel block was used to investigate whether minimizing the skin friction underneath the grid would concentrate sliding resistance at the transverse members of the grid, as observed when used as tensile reinforcement. The alternative arrangement of mounting the grid on the granular medium has been recommended in the literature for measuring soil/grid bond (Netlon, 1984).

### 6.3.b. Boundary measurements.

Boundary load and displacement measurements for the direct sliding resistance of crushed glass over the grid and perforated sheet are shown in fig. 6.14. Also shown are one result for direct shear resistance of crushed glass itself and the direct sliding resistance over the polished steel used to support the reinforcements.

There are only marginal differences between the direct sliding resistance over the reinforcements compared with the direct shear resistance of crushed glass. For example, the direct sliding over the reinforcements produced a slightly stiffer initial response, particularly for the grid mounted on polished steel. This was combined with a greater reduction in resistance after peak. But overall the shapes of the loading curves, peak resistance and displacement required to mobilise peak resistance are very similar. In contrast direct sliding resistance over the polished steel was considerably lower than the shear resistance of crushed glass, approximately 55% less, with the displacement required to mobilise peak resistance only 0.5 mm. The perforated sheet also felt smooth, having small perforations that curved inwards. So, it was surprising to find the direct sliding resistance over the perforated sheet was the maximum possible and not closer to the skin friction of the parent material. This is understood to have been influenced by the high angularity of the crushed glass which assisted the particles to lodge in the perforations.

### 6.3.c. Pattern of stresses for direct sliding over the grid.

The pattern of stresses generated by the direct sliding of crushed glass over the grid when mounted on (a) polished steel, and (b) crushed glass are shown in fig. 6.15 and 6.16 (slides 20 an 21), respectively. For both arrangements the resistance to direct sliding was represented by a continuous distribution of light stripes above the grid, without

any concentration of stresses at the transverse members. The inclination of light stripes to the grid when mounted on polished steel is shown in fig.6.18a to have been approximately 37°. The light stripes were similarly inclined to the grid when mounted on crushed glass. This is in good agreement with the inclination of light stripes to the central plane of the shear box for the direct shear resistance of crushed glass, as shown in fig.6.18c.

The continuous distribution of light stripes across the grid is understood to have been caused by glass particles lodging in the apertures of the grid. This was accompanied by a similar inclination of light stripes and boundary measurements as for the direct shear resistance of crushed glass itself. Hence it appears the rupture zone was forced away from the surface of the grid and fully into the crushed glass. This is a different mechanism from the transfer of stresses to the grid when used as tensile reinforcement. Then the transfer of stresses to the grid primarily depended on a concentration of stresses against the transverse member.

Underneath the longitudinal members of the grid there appears some concentration of stress at the transverse members, but compared with resistance mobilised across the top of the grid it is negligible.

When the grid is laid on crushed glass, fig.6.16 (slide 21) shows the only significant transfer of sliding resistance into the bottom half of the box took place at the tail end of the grid. This is indicated by the continuity of light stripes from above to below the grid at the tail end. Hence it appears that not all of the sliding resistance was transfered into the grid.

### 6.3.d. Pattern of stresses for direct sliding over the perforated sheet.

The pattern of stresses produced by direct sliding of crushed glass over the perforated sheet when mounted on a steel block is illustrated in fig. 6.17 (slide 19). This shows a similar continuous distribution and inclination of light stripes across the top of the perforated sheet as across the grid (see fig. 6.18b). Hence it appears that the sliding resistance across the perforated sheet was again influenced by glass particles lodging in the apertures. As mentioned in the earlier section on boundary measurements, it is thought that the ability of glass particles to lodge in these similarly sized perforations was assisted by the high particle angularity.

The transfer of stresses to the perforated sheet for direct sliding resistance appears similar to when the perforated sheet is used as tensile reinforcement. However for direct sliding stresses were transferred to only one side of the sheet as opposed to both sides for reinforcing. For such a thin sheet, the lodging of glass particles on one side of a perforation could limit the ability of glass particles to lodge in the perforation on the other side. This suggests the maximum bond for the perforated sheet could be less than direct sliding resistance.

### 6.3.e. Different mechanisms for direct sliding resistance of soil over grid reinforcement.

The photoelastic results indicate the resistance to direct sliding over the grid and perforated sheet was influenced by glass particles lodging in the grid apertures and sheet perforations. The similarity of boundary measurements and inclination of light stripes for direct sliding resistance with the direct shear resistance of crushed glass itself indicates the rupture zone developed fully in the crushed glass.

Jewell et al. (1984b) propose that the type of mechanism observed with crushed glass is one of four main mechanism for direct sliding over a grid, which depend on the relative size of soil particles to grid apertures, see fig. 6.19. The three additional mechanisms identified are A, B and D. These mechanisms were used to interpret results from a series of tests performed to investigate the influence of soil particle size on the direct sliding resistance over polymer grids. The characteristics given for these additiononal mechanisms for direct sliding over a polymer grid are as follow.

Mechanism A. Fine sand and silt are understood to have sufficient kinematic freedom to take full advantage of shearing over the relatively smooth longitudinal and transverse members of the polymer grid.

Mechanism B. A coarser sand can only take advantage of shearing over the top surface of the transverse members of the polymer grid.

Mechanism D. Soil particles are too large to penetrate the grid apertures. In the extreme case this could result in the resistance to direct sliding being reduced to that over a plane sheet of the reinforcement material.

From these mechanisms Jewell et al. developed a general expression for direct sliding resistance in terms of two contributions of shear from between soil and the plane surfaces of the grid and between the soil itself in the grid apertures. Values from the expression bound the experimental data well for direct sliding resistance of soils with different grading curves over polymer grids, see fig. 6.20.

Direct sliding resistance of crushed glass over the steel grid agrees approximately with both sets of data by Jewell et al., see fig. 6.20. However direct sliding resistance over the perforated sheet agrees with the results for soil F but not soil G. Both soil F and crushed glass

indicate a maximum direct sliding resistance for an aperture grid/average soil particle size ratio of one, i.e. provided by soil particles lodging in the grid apertures. However it is thought that the high direct sliding resistance over the perforated sheet depended on the high angularity of the glass particles enabling particles to lodge in the perforatins. The discrepancy of results by Jewell et al. for soils F and G could be explained by the following.

1) The average particle size for soils F and G were similar, but soil F contained 25% of sand size particles. Whereas soil G only contained medium gravel size particles. The sand size particles in soil F could have enabled soil particles to lodge in the grid apertures at a narrower aperture width than soil G. Hence the maximum direct sliding resistance was mobilised at a smaller ratio of aperture width to average particle size.

2) Grid aperture length as well as width should influence the ability of soil particles to lodge in the grid apertures. In these tests by Jewell et al. a different polymer grid was used for the two sets of data. However there is no indication whether the aperture lengths were similar.

## 6.4. Pull-out tests on lengths of grid and perforated sheet.

### 6.4.a. Boundary measurements.

Load-displacement curves for pull-out tests on two lengths of grid and a 100 mm embedded length of perforated sheet are shown in fig. 6.21. The displacements are of the relative movement between the pull-out box and the deflector bar, to which the reinforcement was attached. Hence the displacements include the extension of the reinforcement outside the crushed glass between the deflector bar and box.

Comparison of these pull-out curves with the tensile load-extension curves for the reinforcements, see fig. 3.2 and 3.3, show that yielding in the pull-out tests coincided with the yield loads for the respective reinforcements. Hence after yielding took place in the pull-out tests, the displacements were mostly due to the plastic extension of the reinforcements. This was exaggerated by the relatively long length of reinforcement between the box and deflector bar. For example, the plastic extension incurred by the perforated sheet at the end of test is indicated in fig. 6.21. When this is taken into account the pull-out loading curve for the perforated sheet coincides with the loading curve for the grid.

The grid was ruptured in only one test. In the other test, which was the first performed, the grid gradually slipped out of the connector with the deflector bar. However pull-out load-displacement values were obtained for this latter test by measuring the movement of the grid in the slides using a digitising pad. These internally measured values agree very well with the boundary measurements obtained for the other test, prior to yielding.

### 6.4.b. Pattern of stresses for pull-out of the grid.

The transfer of stresses from crushed glass to the two lengths of steel grid are shown in figs. 6.22 and 6.23 (slides 22 and 23). Fig.6.22 is for the longer length of grid with seven transverse members, which slipped out of the connector with the deflector bar. Fig. 6.23 is for the shorter grid with only six transverse members and at a higher pull-out load. Hence the pattern of light stripes is more developed in this latter figure. These patterns of light stripes indicate the following.

- Pull-out was resisted by a concentration of stresses bearing against the transverse members. This was accompanied by a dark zone behind the transverse member. This is understood to represent a reduction in stress behind the transverse member due to the concentration of stresses in front. The light stripes radiated from the transverse members in a wedge shape on either side of the direction of pull-out, separated by the dark zone generated by the transverse member in front.

- There was a higher pull-out resistance at the front of the grid due to the crushed glass reacting against the end wall of the box. This end wall effect extended to two transverse members in these results, but earlier in the tests it only appeared to extend to one transverse member.

- At the free end of the grid, there was an abrupt reduction in pull-out resistance. This could have been caused by the absence of a concentration of stresses behind the end transverse member. Because elsewhere along the grid the wedge shaped concentration of stresses against transverse members could have provided mutual confinement on the crushed glass, which would have enhanced pull-out resistance at these members.

- Between the ends of the grid, there appeared to be a reasonably constant pull-out resistance against the transverse members. If the end effects could be removed or quantified, a good estimate of soil-grid pull-out resistance could be obtained from this intermediate zone.

- The distribution of pull-out load along the grid did not appear to change significantly during the tests. So the transfer of stresses is only shown for one stage of each test.

### 6.4.c. Patterns of stresses for pull-out of the perforated sheet.

The transfer of stresses from crushed glass to a 100 mm embedded length of perforated sheet are shown in fig. 6.24 and 6.25 (slides 24

and 25) for two stages during pull-out. These pattern of light stripes indicate the following:

- The relative magnitude of stresses on either side of the sheet changed during the test. In the earlier stage, see fig. 6.24, considerably more stresses were transferred to the underside of the sheet than above. Further pull-out reduced the difference, see fig. 6.25. This difference could have been due to the sample preparation, which firstly put the sheet in contact with the crushed glass underneath. Hence this could have caused the glass particles underneath to initially lodge in the perforations of the sheet in preference to the crushed glass above the sheet This would have resulted initially in more stresses being transfered to the underside of the grid until pull-out evened out the situation, as observed.

- Changes in pull-out resistance along the sheet were similar to those observed along the grid. This involved: a greater pull-out resistance near the end wall, an abrupt reduction in pull-out resistance at the free end of the sheet and in between a reasonably uniform transfer of stresses to the sheet. The extent of these different zones along the sheet are judged to be approximately:

. 40 mm for the end wall effect;

. 45 mm for reasonably uniform transfer of stresses, and

. 15 mm for an abrupt reduction in resistance at the free end.

- The orientation of light stripes shown for the latter stage of pull-out are given in fig.6.26. Away from the influence of the end wall effects, the inclination of light stripes to the sheet is approximately 45°. Compared with direct sliding resistance, this is closer to the inclination of light stripes to the sheet when reinforcing crushed glass in the box. However this does not mean the pull-out test is more appro-

priate for measuring the bond between crushed glass and the sheet. Firstly, it is not known what proportion of maximum pull-out resistance was mobilised because the test was ended due to excessive extension of the sheet. Secondly, the mobilized bond in the shear box appears to have been low.

- The mechanism for transfering stresses to the sheet is again understood to involve one or two glass particles interlocking with each perforations. This would produce the series of light stripes along the sheet.

## 6.5. Discussion and conclusions on the transfer of stresses from crushed glass to the grid and perforated sheet for reinforcing, direct sliding and pull-out.

### 6.5.a. Transfer of stresses for reinforcing.

Crushed glass transfered stresses to the grid reinforcement putting it in tension primarily by a concentration of stresses at the transverse members. Transfer of stresses to the perforated sheet reinforcement involved a relatively continuous distribution of light stripes along its end lengths. This was understood to depend on one or two glass particles interlocking with a perforation.

### 6.5.b. Transfer of stresses for direct sliding.

Resistance to direct sliding of crushed glass over the grid and perforated sheet was affected by glass particles lodging in the apertures and perforations. This produced a relatively continuous distribution of light stripes over both reinforcements, without a concentration of stresses at the transverse members of the grid. The inclination of light stripes and boundary measurements were similar to the direct shear resistance of

crushed glass itself, indicating that rupture developed fully in the crushed glass. Jewell et al. 1984 have observed the mechanism for direct sliding resistance over a grid to depend on the relative size of soil particles to grid aperture. The authors suggested three other main mechanisms for direct sliding over a grid in addition to the mechanism observed with crushed glass.

### 6.5.c. Transfer of stresses for pull-out.

Pull-out of the grid from crushed glass was resisted by a concentration of stresses at the transverse members. This confirms the interpretation of boundary measurements for past pull-out tests of grids from soil (Chang et al., 1977; Ingold, 1983). The result is also similar to the photoelastic result obtained by Peterson (1980) for pull-out of a steel mesh from gelatine.

Pull-out of the perforated sheet was resisted by a distribution of inclined light stripes along its length, in a similar manner to reinforcing and direct sliding.

Pull-out resistance was non-uniform along both reinforcements, with a higher resistance at the end wall from which pull-out took place and an abrupt reduction in resistance towards the free end of the reinforcement. It should be possible to remove the end wall effect by sufficiently distancing the start of pull-out resistance against the reinforcement. This could be done by sleeving the front of the reinforcement or for grids by removing a number of transverse members. The photoelastic results indicated the influence of the end wall extended to approximately 50 mm. With regards the abrupt reduction of resistance at the free end, it could be quantified if practically constant for different lengths of reinforcement. This appeared to be the case for the grid with a change in length from seven to six transverse members.

### 6.5.d. Comparison of the transfer of stresses to the grid in the different tests.

The transfer of stresses to the grid for both reinforcing and pull-out depended on a concentration of stresses against the transverse member. However for direct sliding there was a reasonably continuous distribution of stresses across the top of the grid. Hence it appears that stresses concentrated at the transverse members when there was relative movement between the crushed glass and grid on both sides, but not when relative movement only took place on one side as for direct sliding. This was presumably caused by different constraints imposed on the crushed glass.

To conclude, it appears that pull-out and not direct sliding was appropriate for simulating the transfer of stresses to the grid reinforcement. This should also apply for a similar and at least greater relative size of grid aperture to average particle size ratios, i.e. 5 or greater, and may be smaller.

Direct sliding resistance over the grid would instead be useful for examining the possible failure mode in a reinforced soil structure of gross outward sliding over the grid reinforcement, e.g. in a reinforced earth retaining wall (Jewell et al., 1984) and along a base reinforcing layer in an embankment (Jewell, 1982).

### 6.5.e. Comparison of the transfer of stresses to the perforated sheet in the different tests.

For the perforated sheet, with a ratio of average glass particle size to perforation of approximately one, the transfer of stresses for direct sliding, pull-out and reinforcing was understood to depend on one or two glass particles lodging in a perforation. A comparison of the

inclination of light stripes to the sheet for the different loading schemes was inconclusive for deciding whether direct sliding or pull-out better simulated the transfer of stress to the sheet reinforcement. However the ability of the glass particles to lodge in perforations may have differed when stresses were transferred to both sides (as for reinforcing and pull-out) compared with only one side (as for direct sliding). In which case pull-out would better simulate the transfer of stresses to the sheet reinforcement.

### 6.5.f. Average apparent coefficient of bond from pull-out tests.

As noted in the introduction to this chapter, the usual approach for analysing the pull-out test is to calculate an average apparent bond for the whole emebedded length. For the pull-out tests on crushed glass the average apparent coefficient of bond is approximately 1.05 for both the grid and perforated sheet. In common with other pull-out test results for stiff reinforcement, this apparent coefficient of bond exceeds the coefficient of friction for the crushed glass i.e. $\tan \phi' = 0.87$ for $\phi' = 41°$. The photoelastic results show that this apparent conflict with fundamental soil mechanics was mainly due to a concentration of stresses against the end wall of the box. Patterns of stresses also show that the vertical stresses were concentrated towards the front end of the box. This may be remedied by using a stress controlled upper and lower boundary.

PART B - INTERFERENCE BETWEEN TRANSVERSE MEMBERS OF THE GRID.

## 6.6. Pull-out tests on single and pairs of transverse members.

To investigate interference between transverse members of the grid, pull-out tests where performed on single transverse members and pairs of transverse members spaced 25, 50 and 75 mm apart, see fig. 6.7. These spacing were multiples of the 25 mm spacings from which the grid was made. The single and pairs of members were prepared from a length of grid by clipping unwanted transverse members and grinding the previous joints with the longitudinal members smooth. Spacings were varied by altering the position of the forward transverse member. This kept the length of longitudinal members constant and the position of the rear of transverse member. The closest a forward transverse member was placed to the end wall was 70 mm. Pull-out tests on the lengths of grid and perforated sheet indicated this should be outside the influence of the end wall. Two tests were performed on single transverse members to check the experimental technique. In the latter test steel balls were embedded in the crushed glass to determine strains.

### 6.6.a. Boundary measurements.

Boundary measurements for the pull-out of single transverse members and pairs of transverse members at 25 and 50 mm spacings are shown in fig. 6.27. The pull-out loads were less than the combined yield load for the longitudinal members so the relative displacement between the pull-out box and deflector bar was practically all due to the pull-out displacement of the transverse members.

Pull-out resistance is shown to have steadily increased up to a level where resistance fluctuated slightly. In both tests on pairs and for

one test on a single transverse members, this period of relatively stable resistance was followed by a further increase in resistance. This further increase in resistance is not understood.

Tests on single transverse members differ in several ways. Only test no.45 exhibited the further increase in resistance towards the end of the test. Test no.45 also showed a slight peak of resistance at 4 mm displacement which was absent in test no.49. Resistance was more stable for test no.49. However the tests agreed reasonably well on 1) a displacement of approximately 4 mm to reach a level of relatively stable resistance and 2) the level of that resistance.

The addition of a second transverse member to form a pair increased the pull-out resistance, depending on the spacing.

The pattern of light stripes which accompanied these changes in boundary measurements are shown as indicated in figures 6.27.

Boundary measurements for 75 mm spacing of transverse members is shown in fig. 6.28, with those for 25 and 50 mm spacings. Data for 75 mm spacing was ommitted from the previous figure because the resistance was very unstable after about 4 mm displacement, which confuses the other data. The variation in resistance for 75 mm spacing was between the resistances for 50 and 25 mm spacing.

A discussion of the pattern of light stripes observed for these tests follows.

### 6.6.b. Pattern of stresses and strains for pull-out of single transverse members.

The patterns of light stripes observed after approximately 6 mm pull-out displacement of single transverse members are shown in figs. 6.29 and 6.30 (slides 26 and 27). The black dots in the latter figure represent

steel balls embedded in the crushed glass to determine strains. These results illustrate the patterns of stresses which developed against the pull-out of a transverse member without interference from other transverse members. It can now be seen in figs.6.22 and 6.23 that the pattern of stresses for individual transverse members spaced 25 mm along the lengths of grid were considerably restricted by accompanying transverse members.

The light stripes for a single transverse member radiated approximately 60 mm around the front of the member. This was accompanied by a dark zone behind which extended approximately 40 mm. Hence it appears the minimum spacing to avoid interference between this type of transverse members was approximately 100 mm. To generalize the result for other grids, the actual spacing can be divided by the section height of the transverse member against which the granular medium reacts (Jewell et al. 1984). This dimension should influence the size of the zone of soil affected by the movement of the transverse member and hence the minimum spacing to avoid interference. The transverse member used in these tests had a circular cross-section. The light stripes radiated from it over approximately 180°. Compared with an equivalent rectangular section it is difficult to judge the effective section height for this circular section. However an indication can be obtained by considering the diameter and half the circumference of the circular section. According to these dimensions the normalized spacing to avoid interference between transverse members is approximately 40 to 60 respectively.

The light stripes for a single transverse member curved towards the horizontal boundaries of the box. This was accompanied by the pattern of stresses appearing brighter on either side of the direction of pull-out. This may be caused by one or both of the following reasons:

- Upper and lower boundaries of the box were closer than the end wall and hence could have imposed a greater constraint on the crushed glass.

- The crushed glass resisted a combination of vertical and horizontal loads which required an inclined resultant.

The strains which developed in the crushed glass between 0.00 and 9.20 mm. pull-out displacement of a single transverse member are illustrated in fig. 6.31. These are small and without a distinct pattern. The area in which strains are shown also appears small compared with the corresponding pattern of stresses. The strain data may be limited because the method for determining strains was too crude.

## 6.6.c. Pattern of stresses for pull-out of pairs of transverse members.

(i) 25 mmm spaced transverse members Fig. 6.32 (slide 28) shows the effect of placing another transverse member 25 mm in front of where previously only the single transverse member had been. This resulted in a pattern of stresses for the rear member similar to the 25 mm spaced transverse members along the length of grid as shown in figs. 6.22 and 6.23. In contrast the pattern of stresses for the forward transverse member was similar to the single transverse member. Except in this figure, it appears slightly brighter and move evenly lit. However this is difficult to judge accurately because the exposures for the photographic films were not necessarily the same. To conclude, the test indicates that interference between transverse members causing a reduction in pull-out resistance is due to the pattern of stresses for the transverse member in front.

Eventhough the pattern of stresses for the rear transverse member was considerably smaller than for a single transverse member, the pull-out resistance was approximately fourty five percent greater than for a single transverse member, see fig. 6.27. As already mentioned, this increase in resistance may have been partly due to an enhanced resistance against the forward transverse member compared with a single transverse

member. However it seems likely that most of increase was due to the rear transverse member.

(ii) 50 mm spaced transverse members Fig. 6.33 (slide 29) shows the effect of moving the forward transverse member to 50 mm from the rear transverse member. This considerably enlarged the pattern of stresses for the rear transverse member. However it was still clearly restricted by the pattern of stresses for the forward transverse member, which again was similar to that for the single member. The difference in pull-out resistance for this pattern of stresses above that for a single member was approximately seventy five percent. Assuming the resistance against the forward transverse members for 25 and 50 mm spacings did not change significantly, this represented aproximately fifty percent increase in resistance against the rear member. However the increase in size of the pattern of stresses suggests a greater difference in resistance.

(iii) 75 mm spacing of transverse members Fig. 6.34 (slide 30) shows the pattern of stresses for 75 mm spacing of transverse members at approximately the same pull-out load and displacement corresponding to the patterns of stresses for 50 mm spacing shownin fig. 6.33 (slide 29). Increasing the spacing slightly enlarged the pattern of stresses for the rear member, while still keeping the same shape. Again the pattern of stresses for the forward transverse member was similar to that for a single transverse member. Additionally, a noticeable gap appeared between the boundaries of light stripes from the rear and forward transverse members. This concided with practically no change in pull-out resistance compared with that for 50 mm. spacing.

Presumably increasing the spacing of transverse members further would eventually avoid interference from the forward transverse member and so result in the pattern of stresses for the rear transverse member being the same as the forward transverse member. However results for 50 mm.

and 75 mm spacing suggest that an intermediate range of spacings exist where the pattern of stresses for the rear transverse member does not change significantly, but mainly moves away from the forward transverse member. Hence negligible, if any, change in pull-out resistance for the rear member appeared to takes places.

Fig. 6.34 (slide 31) shows the pattern of stresses after an abrupt reduction in pull-out load had taken place for the 75 mm spaced transverse members. The difference between the pattern of stresses in figs. 6.34 and 6.35 (slide 30 and 31) suggests the reduction in pull-out resistance primarily took place at the forward transverse member. The difference between this test and others, which might explain the less stable pull-out resistance, is the closer proximity of the forward transverse member to the end wall. However this would be expected to have strengthened rather than weakened resistance.

### 6.6.d. A comparison between the pull-out resistance against individual transverse members at different spacings with the corresponding bond for a grid.

The pattern of stresses indicated that the pull-out resistance against the forward transverse members of the pairs of transverse members were approximately the same as a single transverse member. If this is accepted, the pull-out resistance against the rear transverse members can be determined from the boundary measurements. Hence the interference suffered by the rear transverse members at different spacings can be quantified. This is shown in Fig. 6.36a, where the pull-out resistances of the rear transverse members are given as a ratio of the pull-out resistance of single transverse member and termed efficiency, i.e. 100% efficient represents no interference from other transverse members. The

corresponding spacings are also shown normalized with respect to the diameter and half the circumference of the transverse member, which should bracket the effective section height of the member. The average resistance against the single transverse members is plotted as one hundred percent efficient, for a spacing corresponding to the size of the pattern of stresses i.e. approximately 100 mm. The peculiar feature of this plot is the apparent interruption of increase in pull-out resistance for an increase in spacing between 50 to 75 mm. This has already been commented on.

From the pull-out resistance against rear transverse members at different spacings the corresponding pull-out bond for a length of grid with similarily spaced transverse members can be estimated. This has been done in terms of an equivalent coefficient of friction between the crushed glass and grid, as illustrated in fig. 6.37. This allows the relative performance of the predicted bond between crushed glass and grid to be expressed as a multiple of $\tan \phi'$ for the crushed glass which defines a fully rough bond, as shown in fig. 6.36b.

A comparison of the relationships obtained for the efficiency of individual transverse members at different spacings with the corresponding bond indicates that minimising or avoiding interference between individual transverse members would not improve bond. On the contrary the highest bond is predicted for the closest spacing examined of 25 mm, where the individual transverse members are estimated to operate at 45% efficiency. The results indicated that reducing the spacing further should improve grid bond. However extension of the curve for bond falls short of the upper limit corresponding to $\tan \phi'$. This is surely wrong, being caused by the inaccuracy of the test. No change in bond is predicted between 75 to 150 mm spacing. This indicates that the reduction of effi-

ciency for individual members was in proportion to the reduction in spacing within this range.

Upper and lower estimates of grid geometry for a fully rough bond, i.e. tan $\phi'$, have been provided by Jewell et al. (1984) as shown in fig. 6.38. These were derived from estimates of the ratio of the maximum effective bearing stress against a transverse member to the vertical effective stress. For crushed glass with an estimated $\phi' = 40°$, Jewell et al. indicate the ratio of transverse member spacing to section height for a maximum grid bond lies between $8 < (S/B)_\theta < 40$. Results for single and pairs of transverse members in crushed glass indicate $(S/B)_\theta \leq 10 \div 15$. One criticism of Jewell et al's approach is the use of a value for bearing stress without taking into account interference between transverse members. Patterns of light stripes indicate that interference between transverse members reduces the limiting bearing stress.

## 6.6.e. Conclusions on interference between transverse members of the grid.

1) Interference between transverse members resulting in an reduction of pull-out resistance was caused by the pattern of stresses for the transverse member in front.

2) Minimising or avoiding interference between transverse members was not observed to improve the overall soil-grid bond. On the contrary, the highest bond was predicted for the closest spacing examined of 25 mm, where the transverse members were estimated to operate at an efficiency of 45%.

## 6.7. Suggestions for future work.

1) An attempt has been made to investigate the optimum grid geometry for a fully rough bond. This could be continued with a series of pull-out tests in real soils with different grid geometry. As with direct sliding resistance, the optimum grid geometry should be influence by the soil particle size. There are apparently no test data on the influence of soil particle size on bond strength for a grid (Jewell et al., 1984). When performing the pull-out tests, the end wall effect as observed in crushed glass should be considered as suggested in 6.5.c.

2) The pattern of stresses observed for a single transverse member moving through crushed glass could be compared with existing models for this problem, e.g. stress characteristics fields (Jewell et al., 1984).

3) Having observed interference between transverse members, interference generally between rigid members pulled in series through soil could be quantified more accurately. This could be done in terms of the variation in bearing stress with spacing between the members. The results could be normalised by vertical effective stress and section height of the members respectively. For ease of calculating bearing stress the members should be flat faced and very rigid to obtain a uniform distribution of bearing stresses. The results may not be particularily relevant for estimating the bond of a grid reinforcement because the distribution of stresses along the relatively flexible transverse member is likely to be very non-uniform with a concentration of stresses at the joint with the longitudinal members (Peterson, 1981). Instead, the results could be more useful for design of a series of anchor plates.

AKNOWLEDGEMENTS.

The work reported here was carried out whilst I was a member of the soil mechanics group at the Engineering Science Department, Oxford University. It is part of a programme investigating the reinforcement of soil. I am grateful for the help and encouragement I received from members of the soil mechanics group and would particularly like to thank Dr. G. Milligan, my supervisor, Dr. G. Houlsby who made some useful suggestions and was always willing to help and Mr. R. Earl who assisted in modifying and building the equipment described.

I am also indebted to Studio Geotecnico Italiano, in particular Professor Jamiolkowski who allowed me access to office facilities and some time during office hours in which I was able to complete the dissertation.

I am grateful to Corning Ltd. for supplying pyrex glass free of charge.

Financial support was provided by the Science and Engineering Research Council.

## REFERENCES

AL-HUSSAINI, M. and PERRY, E. 1976 Effect of horizontal reinforcement on stability of earth masses. Technical report No. S-76-11, U.S.Army Engineer, Waterways Experiment Station, Vicksburg

ALLERSMA, H.G.B. 1982a Determination of the stress distribution in assemblies of photoelastic particles: theoretical and experimental description of the application of the photoelasticity model to three dimensional assemblies of glass particles. Experimental mechanics 22, 9, pp. 336-341.

ALLERSMA, H.G.B. 1982b Photoelastic stress analysis and strains in simple shear. Proc. IUTAM Symp. on deformation and failure of granular materials, Delft, pp. 345-353.

ALLERSMA, H.G.B. 1982c Personal communication

ANDRAWES, K.Z., McGOWN, A. and WILSON-FAHMI, R.F. 1983 The behaviour of a geotextile reinforced sand loaded by strip footing. Proc. 8th ECSMFE, Vol. 2, Helsinki, pp. 329-334.

ARTHUR, J.R.F., DUNSTAN, T., AL-ANI, Q.A.J.L. and ASADI, A. 1977 Plastic deformation and failure in granular media. Geotechnique, 27 (1) pp. 53-74.

BALLETINO, D. 1983 Some experience in reinforced cohesive earth. Proc. 8th ECSMFE, Helsinki, Vol. 2, pp. 463-468.

BASSET, R.H. and LAST, N.C. 1978 Reinforced earth below footing and embankment. ASCE Symp. on earth reinforcement, Pittsburgh.

BOLTON, M.D., CHOUDHURY, S.P. and PANG, P.L.R. 1978 Modelling reinforced earth. ASCE Symp. on earth reinforcement, Pittsburgh.

BOLTON, M.D. and PANG, P.L.R. 1982 Collapse limit states of reinforced earth retaining walls. Geotechnique 32 (4), pp.349-367.

BUTTERFIELD, R., HARKNESS, R.M. and ANDRAWES, K.Z. 1970 A Stereo-photogrammetric method for measuring displacement fields. Geotechnique 20 (3), pp. 308-314.

CARTIER, G. and GIGAN, J.P. 1983 Experiments and observations on soil nailing structures. Proc. 8th ECSMFE, Helsinki, Vol. 2, pp. 473-476.

CHANG, J.C. and FORSYTH, R.A. 1977 Design and field behaviour of reinforced earth wall. J. Geotech. Div. ASCE, July, pp. 677-692.

CHANG, J.C., HANNON, J.B. and FORSYTH, R.A. 1977 Pull-out resistance and interaction of earth reinforcement and soil. Transport Research Record No. 640, Washington D.C.

CHRISTOPHER, B.R. and HOLTZ, R.D. 1985 Geotextile engineering manual. Federal Highway Administration report, Washington D.C.

DALLY, J.W. and RILEY, W.F. 1978 Experimental stress analysis. McGraw Hill.

DANTU, P. 1957 Contribution à l'etude mécanique et geometrique des milieux pulverulents. Proc. 4th ICSMFE, London, pp. 144-148

DEPARTMENT OF TRANSPORT 1978 Reinforced earth retaining walls and bridge abutements for embankments. Technical Memorandum (Bridges), BE3/78.

DRESCHER, A. 1976 An experimental investigation of flow rules for granular materials using optically sensitive glass particles. Geotechnique 26 (4), pp. 591-601.

DRESCHER, A. and DE JOSSELIN DE JONG, G. 1972 Photoelastic verification of a mechanical model for the flow of a granula material. J. Mech. Phys. Solids 20, pp. 337-351.

EGGSTAD, A 1983 State of the art report on improvement of cohesive soils. Proc. 8th ECSMFE, Helsinki, Vol. 3.

FINLAY, T.W. 1978 Performance of a reinforced earth structure at Granton. Ground Engineering, October

FOWLER, J. 1985 Building on muck. Civil Engineering, Vol.55 (5), ASCE.

GOURC, J.P., PERRIER, H. and RIONDY, G. 1983 Unsurfaced roads on soft subgrade: mechanism of geotextile reinforcement. Proc. 8th ECSMFE, Helsinki, Vol. 2, pp. 495-498

GUILLOUX, A., SCHLOSSER, F. and LONG, N.T. 1979 Laboratory investigation of sand-strip friction. Int.Conf. on Soil Reinforcement, Paris, Vol. 1, pp. 35-40.

GUILLOUX, A., NOTTE G., and GONIN, H. 1983 Experiences on a retaining structure by nailing in morraine soils. Proc. 8th ECSMFE, Helsinki, Vol. 2, pp.499-502.

GUDHEUS, G. and SCHWARTZ, W. 1985 Stabilization of creeping slopes by dowels. Proc. 11th ICSMFE, San Francisco, Vol. 3, pp.1697-1700.

HOLISTER, G.S. 1967 Experimental stress analysis. Cambridge University Press.

HOLTZ, R.D. 1977 Laboratory studies of reinforced earth using a woven polyester fabric. Int.Conf. on the use of fabrics in geotechnics, Paris Vol.3, pp. 149-154.

HOLTZ, R.D. and BROMS, B.B. 1977 Walls reinforced by fabrics - results of model tests. Int.Conf. on the use of fabrics in geotechnics, Paris

HOULSBY, G.T. 1984 A program for calculating displacement and strain from a photograph of marker points. O.U.E.C. report No. 1519/84, Dept. Eng. Science, University of Oxford.

HOWATSON, A.M., LUND, P.G. and TODD, J.D. 1972 Engineering tables and data. Chapman and Hall, p. 43.

INGOLD, T.S. 1981 A laboratory simulation of reinforced clay walls. Geotechnique 31 (3), pp. 399-412.

INGOLD, T.S. 1983 Laboratory pull-out testing of grid reinforcements in sand. Geotechnical Testing Journal, Vol.6 (3), Sept., pp.101-111.

INGOLD, T.S. 1984 A laboratory investigation of soil-geotextile friction. Ground Engineering, Vol.17, Nov., pp.21-28.

JEWELL, R.A. 1979 Contribution to discussion on reinforced earth. Proc. 7th ECSMFE, Brighton, Vol. 4, pp.287-289.

JEWELL, R.A. 1980 Some effects of reinforcement on the mechanical behaviour of soils. Ph.D. Thesis, University of Cambridge.

JEWELL, R.A. and JONES, C.J.F.P. 1981 Reinforcement of clay soils and waste materials using grids. Proc. 10th ICSMFE, Stockholm, Vol.3 pp. 701-706.

JEWELL, R.A. 1982 A limit equilibrium design method for reinforced earth embankments on soft foundations . 2nd Int. Conf. on geotextiles, Las Vegas, Vol.3, pp.671-676.

JEWELL, R.A., PAINE, N. and WOODS, R.I. 1984a Design methods for steep reinforced embankments. Symp. on polymer grid reinforcement in civil engineering, London.

JEWELL, R.S., MILLIGAN, G.W.E., SARSBY, R.W. and DUBOIS, D. 1984b Interaction between soil and geogrids. Symp. on polymer grid reinforcement in civil engineering, London.

JEWELL, R.A., 1985. LImit equilibrium analysis of reinforced soil walls. Proc. 11th ICSMFE, San Francisco, Vol.3, pp.1705-1708.

JOHN, N.W., RITSON, R., JOHNSON, P.B. and PETLEY, D.J. 1983 Instrumentation of reinforced soil walls. Proc. 8th ECSMFE, Helsinki, Vol. 2, pp. 509-512.

JONES, C.J.F.P. 1978 The York method of reinforced earth construction. ASCE Symp. on earth reinforcement, Pittsburgh.

JONES, C.J.F.P., MURRAY, R.T., TEMPORAL, J. and MAIR, R.J. 1985 First application of anchored earth. Proc. 11th ICSMFE, San Francisco, Vol. 3, pp. 1709-1712.

JURAN, I., SCHLOSSER, F., KERMOA, M., ECKMANN, B. and LOUIS, C. 1981 Le renforcement des sols par barres passives. Proc. 10th ICSMFE, Stockholm, Vol. 3, pp. 713-716.

JURAN, I., SHAFIE, S. and SCHLOSSER, F. 1985 Numerical study of nailed soil retaining structure. Proc. 11th ICSMFE, San Francisco, Vol. 3, pp. 1713-1716.

KAYE, G.W.C. and LABY, T.H. 1973 Tables of physical and chemical constants, p. 95, 'Refractive indices of liquids' Longman Group, London

KODAK WRATTEN FILTERS, Fouth edition, Kodak Ltd., London

LIZZI, F. 1983 Reticulated root piles for the improvement of soil resistance. Proc. 8th ECSMFE, Helsinki, Vol.2, pp. 521-524.

McGOWN, A., ANDRAWES, K.Z. and AL-HASANI, M.M. 1978 Effects of inclusion properties on the behaviour of sand. Gotechnique 28 (3), pp. 327-346.

McGOWN, A. 1979 Contribution to discussion on reinforced earth. Proc. 7th ECSMFE, Brighton, Vol. 4, pp. 285-287.

McGOWN, A., ANDRAWES, K.Z., MASHHOUR, M.M. and MYLES, B. 1981 Strain behaviour of soil-fabric model embankment. Proc. 10th ICSMFE, Srockholm, Vol.3, pp. 739-744.

McGOWN, A. ANDRAWES, K.Z. and KABIR, M.H. 1982 Load extension testing of geotextiles confined in soil. 2nd Int. conf.on geotextiles, Las Vegas, Vol. 3, pp. 793-798.

McGOWN, A. ANDRAWES, K.Z., YEO, K.C. and DUBOIS, D. 1984 The load-strain-time behaviour of tensar geogrids. Symp. on polymer reinforcement in civil engineering, London.

MILLIGAN, G.W.E. 1974 The behaviour of rigid and flexible retaining walls in sand. Ph.D. Thesis, University of Cambridge.

MILLIGAN, G.W.E. and LOVE, J.P. 1984 Model tests of geogrids under an aggregate layer on soft ground. Symp. on polymer grid reinforcement in civil engineering, London.

MITCHELL, J. 1981 General report on soil improvement. Proc. 10th ICSMFE, Stockholm, Vol. 4.

MURRAY, R.J. and BODEN, J.B. 1979 Reinforced earth wall constructed with cohesive fill. Int.Conf. on soil reinforcement, Paris, Vol.3, pp.569-577.

MURRAY, R.I., CARDER, D.R. and KRAWCZYK, J.V. 1979 Pull-out tests on reinforcements embedded in uniformely graded sand subject to vibration. Proc. 7th ECSMFE, Brighton, Vol.3, pp.115-120.

MURRAY, R. 1984 Reinforcement techniques in repairing slope failures. Symp. on polymer grid reinforcement in civil engineering, London.

MYLES, B. 1982 Assessment of soil fabric friction by means of shear. 2nd Int. Conf. on geotextiles, Las Vegas, Vol.3, pp. 787-791.

NETLON Limited 1984 Test methods and physical properties of tensar geogrids. Technical guidelines.

OLIVERA, A. 1982 Use of non-woven geotextiles to construct a deep highway embankment over swamp soil. 2nd Int. Conf. on geotextiles, Las Vegas, Vol. 3, pp.625-630.

PETERSON, L.M. 1980 Pull-out resistance of welded wire mesh embedded in soil. M.Sc. Thesis, Utah State University.

PIGG, D.R. and McCAFFERTY, W.R. 1984 The design and construction of a reinforced soil retaining wall at Low Southwick. Symp. on polymer grid reinforcement in civil engineering, London.

RATHMAYER, H.G. and KORHONEN, O.E. 1985 Geotextile reinforced land reclamation in the bay of river Vantaa, Helsinki. Proc. 11th ICSMFE, Helsinki, Vol. 3, pp. 1795-1800.

ROSCOE, K.H. 1970 The influence of strains in soil mechanics. Geotechnique, 20 (2), pp. 129-170.

ROWE, R.K., MacLEAN, M.D. and BARSVARY, A.K. 1984 The observed behaviour of a geotextile reinforced embankment constructed on peat. Canadian geotechnical Journal, May, pp. 289-304.

SCARPELLI, G. and WOOD, D.M. 1982 Experimental observations of shear band patterns in direct shear tests. Proc. IUTAM Symp. on deformation and failure of granular materials, Delft, pp. 473-484.

SCHLOSSER, F. and VIDAL, H. 1969 Reinforced earth. Bulletin de Liaison des Laboratoires Routiers, Ponts et Chaussées, No. 41, Nov.

SCHLOSSER, F. and ELIAS, V. 1978 Friction in reinforced earth. ASCE Symp. on earth reinforcement, Pittsburgh.

SCHLOSSER, F. and GUILLOUX, A. 1979 Friction between soil and strips in reinforced earth structures. Int. Conf. on soil reinforcement, Paris, Vol. 1, pp. 151-156.

SCHLOSSER, F. and JURAN, I. 1979 General report on soil reinforcement. Proc. 7th ECSMFE, Brighton, Vol. 5, pp. 200-203.

SCHLOSSER, F. JACOBSEN, H.M. and JURAN, I. 1983 General report on soil reinforcement. Proc. 8th ECSMFE, Helsinki, Vol.3.

SHEN, C.K., BANG, S., HERRMANN, L.R. and ROMSTAD, K.L. 1978 A reinforced lateral earth support system. ASCE Symp. on earth reinforcement, Pittsburgh, pp. 764-791.

SHEN, C.K., BANG, S., ROMSTAD, K.M., KULCHIN, L. and DE NATALE, J.S. 1981 Field measurements of an earth support system. J. Geotech. Eng. Div. ASCE, Vol. 107, No. GT12, Dec.

SMITH, A.K.C. and WROTH, C.P. 1978 The failure of model reinforced earth walls. ASCE Symp. on earth reinforcement, Pittsburgh.

SMITH, G.N. and BIRGISSON, G.I. 1979 Inclined strips in reinforced earth walls. Civil Engineering, June, pp. 62-63.

SOMMER, H. 1979 Stabilization of a creeping slope in clay with stiff elements. Proc. 7th ECSMFE, Brighton, Vol. 3, pp. 269-274.

VARDOULAKIS, I. 1980 Shear band inclination and shear band modulus of sand in biaxial tests. Int. J. for Num.and Analytical Methods in Geomechanics, 4, pp. 103-119.

WAKABAYASHI, T. 1957 Photoeleastic method for determination of stress in powdered mass. Proc. 7th Jap.Nat.Conf.App.Mech., pp. 153-158.

WILLIAMS, C.H. and SANDERS, R.L. 1985 Design of reinforced emabnkments for Great Yarmouth bypass. Proc. 11th ICSMFE, San Francisco, Vol. 3, pp. 1811-1814.

WOOD, D.M. 1984 Experiments with crushed glass. Int. report No. CUED/D-Soils/TR161, Cambridge University.

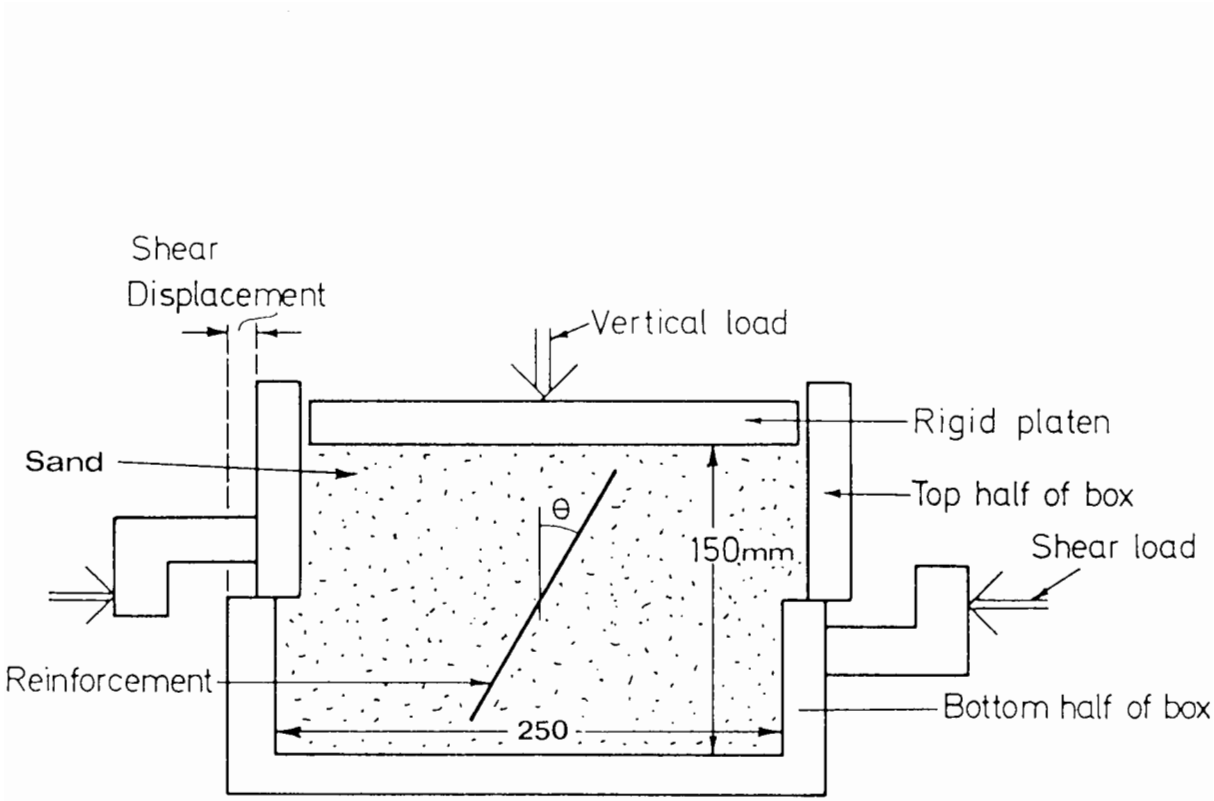


Fig. 1.1 Schematic diagram of test arrangement used by Jewell (1980) for examining the effect of tensile reinforcement on the mechanical behaviour of sand

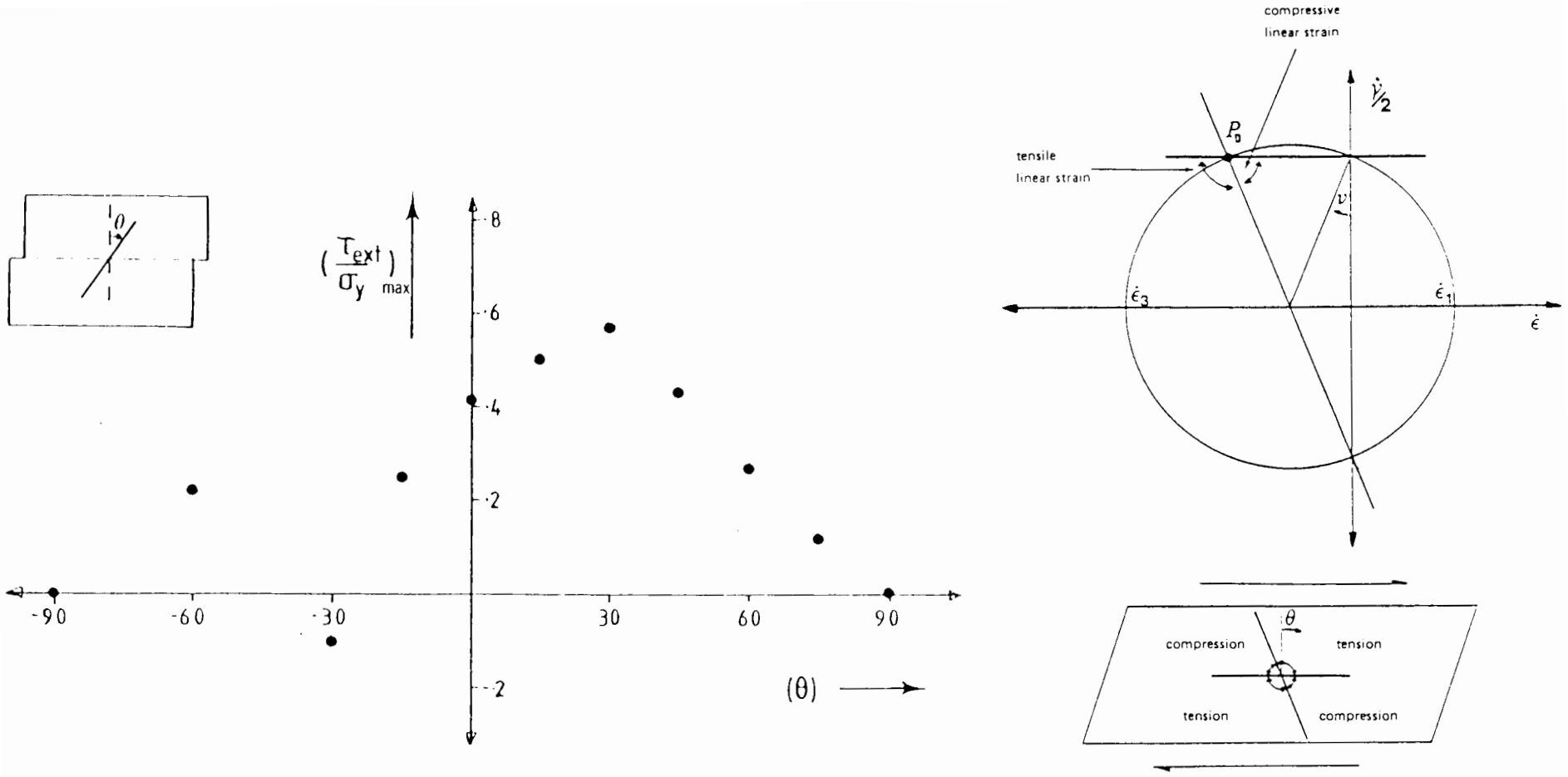


Fig. 1.2 a) Relationship between the maximum increase in shear strength of sand $(\tau_{ext} / \sigma_v)_{max}$ and the orientation (θ) of a single grid reinforcement observed by Jewell (1980) and b) related to the strain field in the unreinforced sand

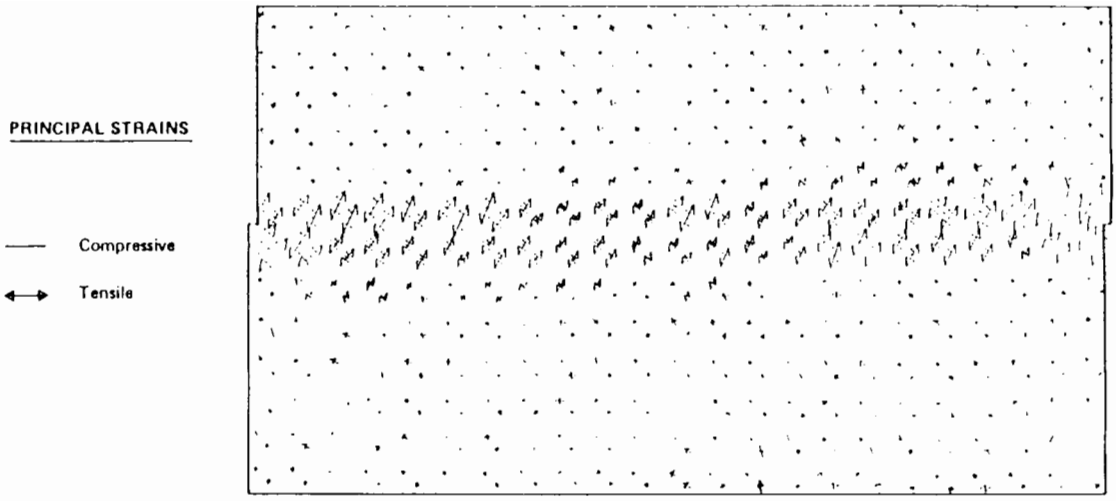


a) Unreinforced test - principal strains

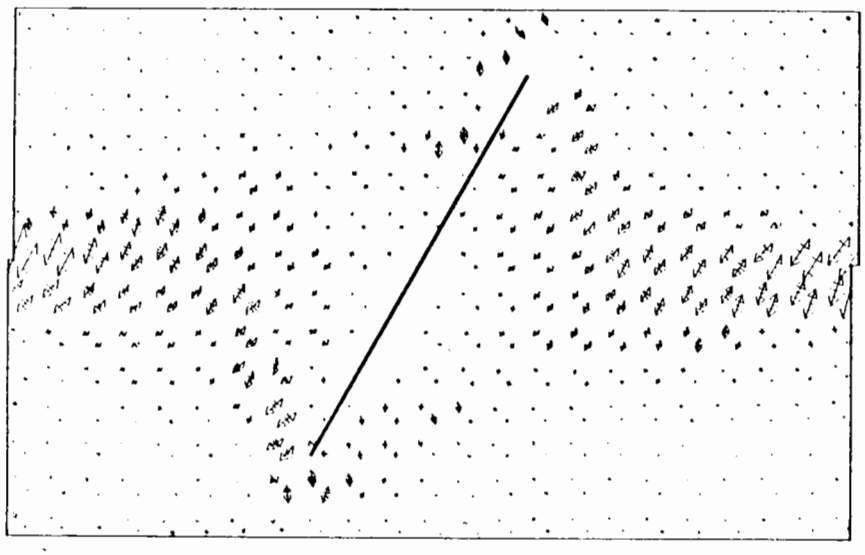

b) Reinforced test - principal strains

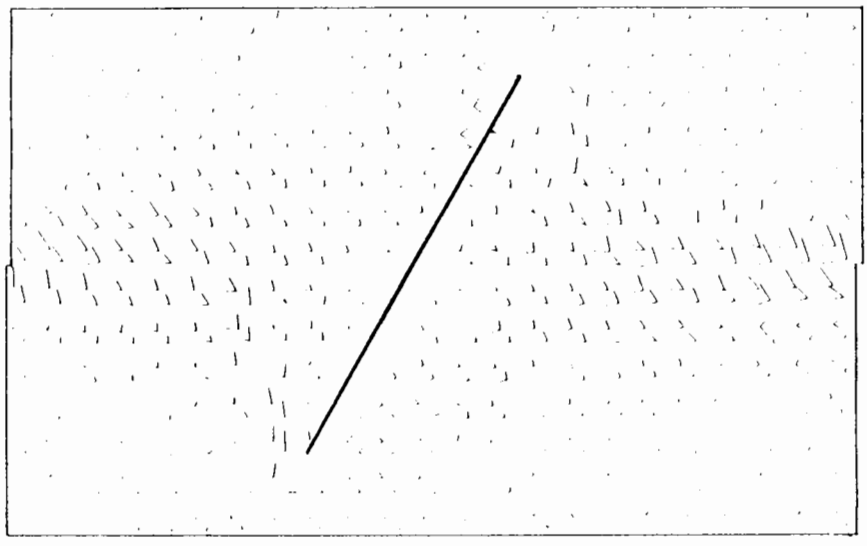

c) Reinforced test - zero-extension directions

Fig. 1.3 Modifications to the strain field in sand by tensile reinforcement during a direct shear test observed by Jewell (1980)

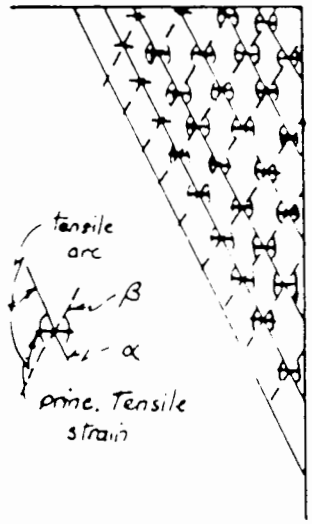


(a) Zero extension directions (α and β) for classical active condition in soil behind a retaining wall (from Milligan 1974)

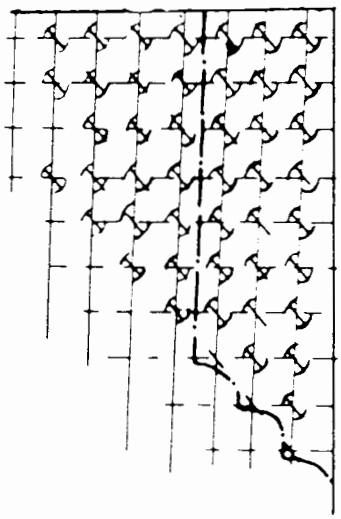

(b) Idealised zero extension directions for a reinforced earth wall, i.e. β direction aligned with the stiff horizontal reinforcement

Fig. 1.4 Effect of tensile reinforcement on the strain field in a reinforced earth wall proposed by Bassett and Last (1978)

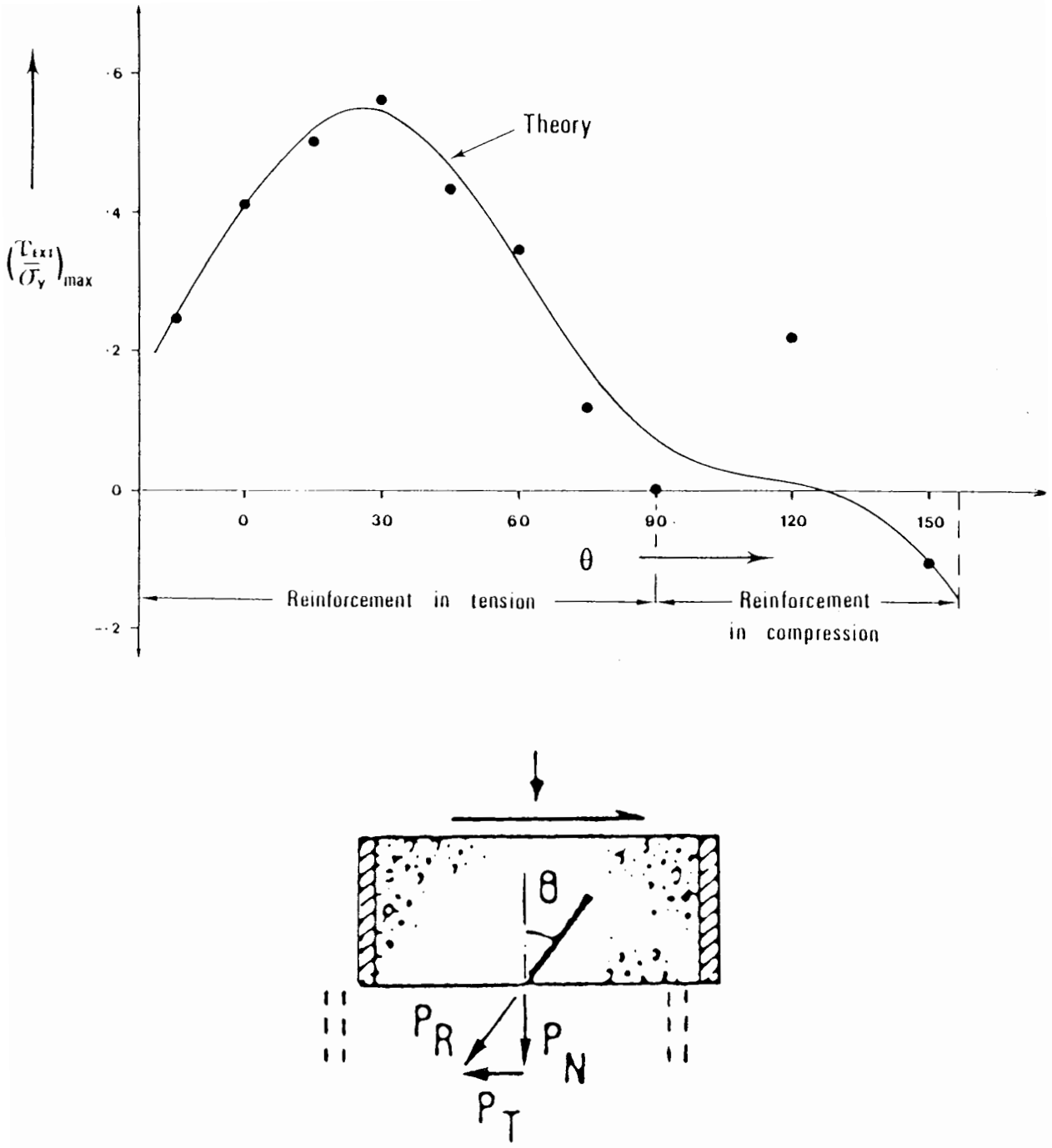


Fig. 1. 5 a) Comparison of experimental results and theoretical prediction for the relationship between the increase in shear strength of sand $(\tau_{ext}/\sigma_y)_{max}$ and the orientation of $(\theta)$ of reinforcement in the shearbox by Jewell (1980), where b) effect of the reinforcement force $P_r$ was represented by:

i) $P_n$ increasing normal effective stress

ii) $P_t$ reducing applied shear stress

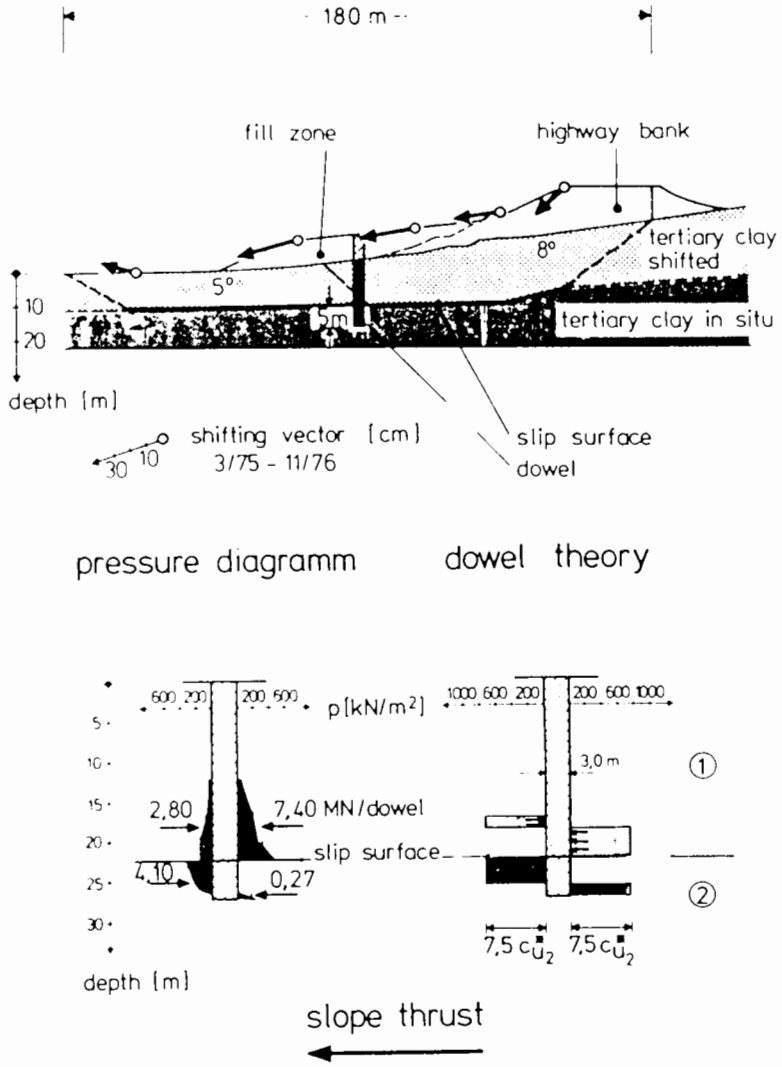


Fig. 1.6 Creeping slopes in clay stabilized by dowel piles with theoretical and measured pressures on a large dowel pile shown (from Sommer 1979)

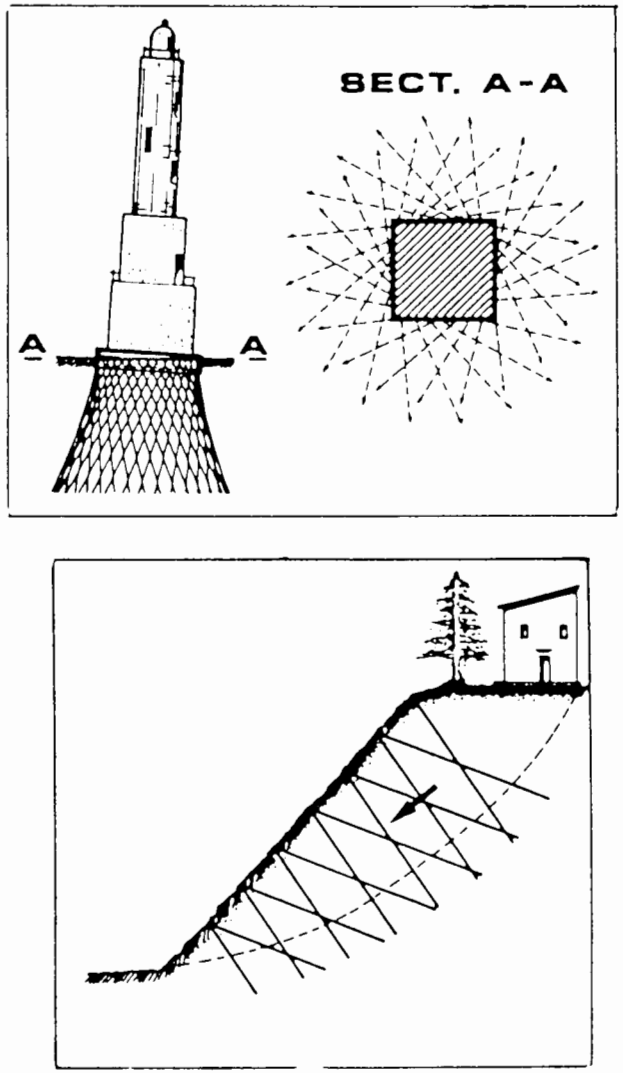


Fig. 1.7 Use of micropiles for stabilising slopes and improve bearing capacity (from Lizzi 1983)

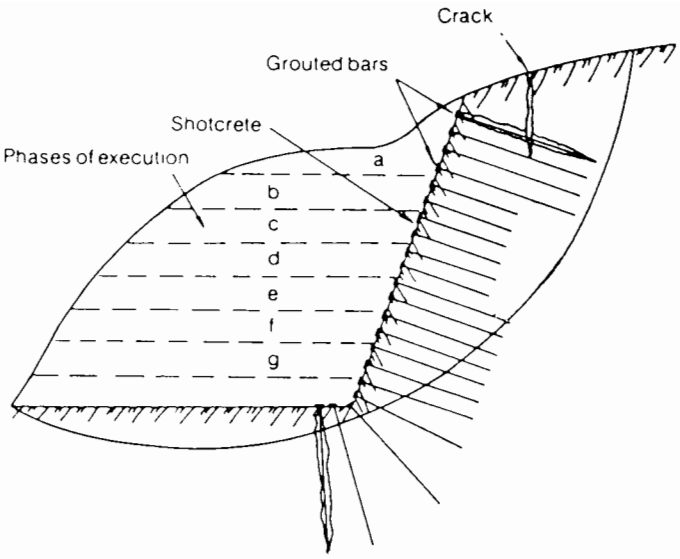


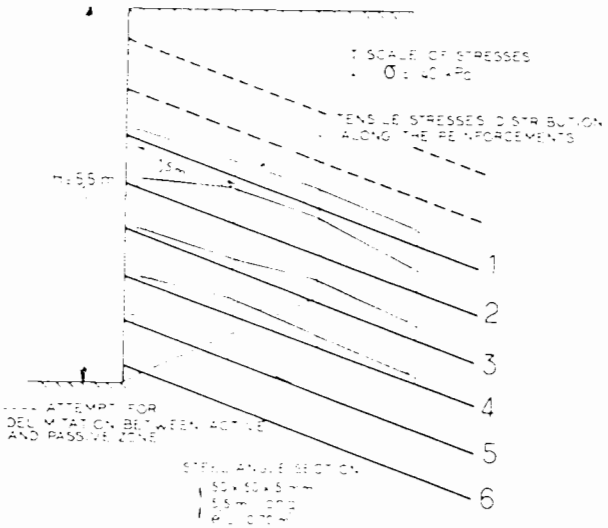


from Cartier and Gigan (1983)

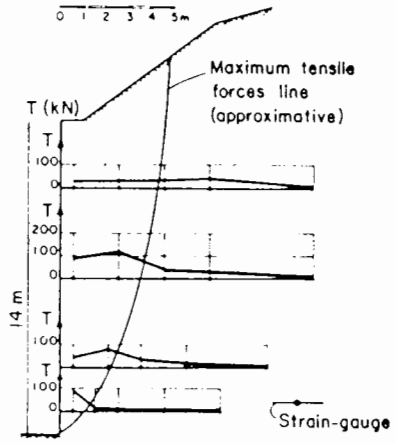


from Guilloux et al. (1983)

Fig. 1.8 a) Steep excavations stabilised by soil nailing (from Schlosser and Juran 1979) and b) distribution of measured tensile force in steel bars used for nailing (from Cartier and Gigan 1983, and Guilloux et al. 1983)

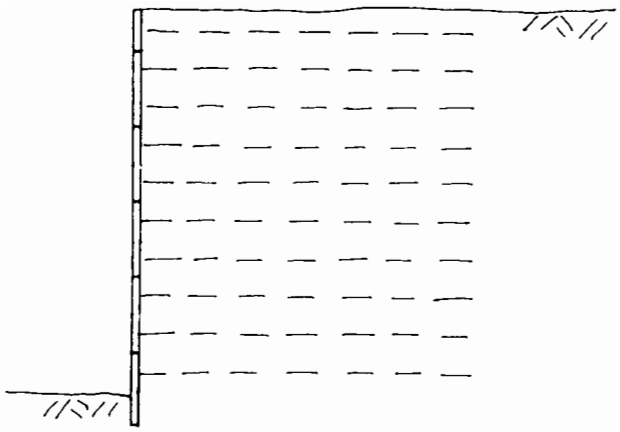

a) Reinforced earth retaining wall

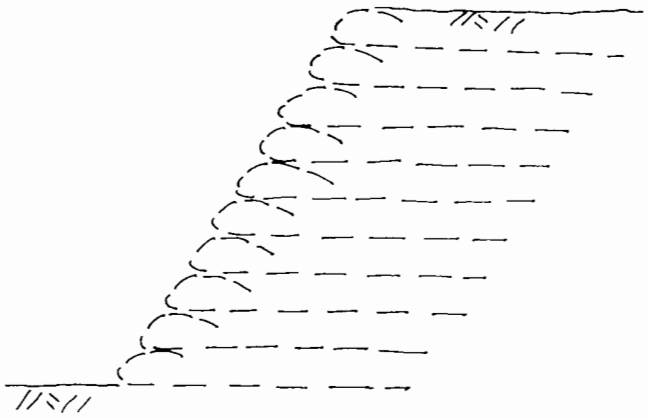

b) Steep sided embankment

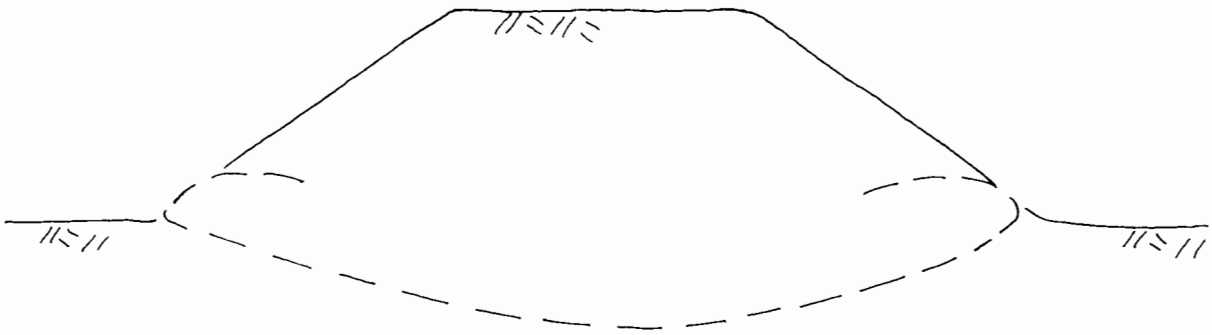

c) Reinforced embankment on soft ground

Fig. 1.9 Examples of tensile reinforcement of fill material

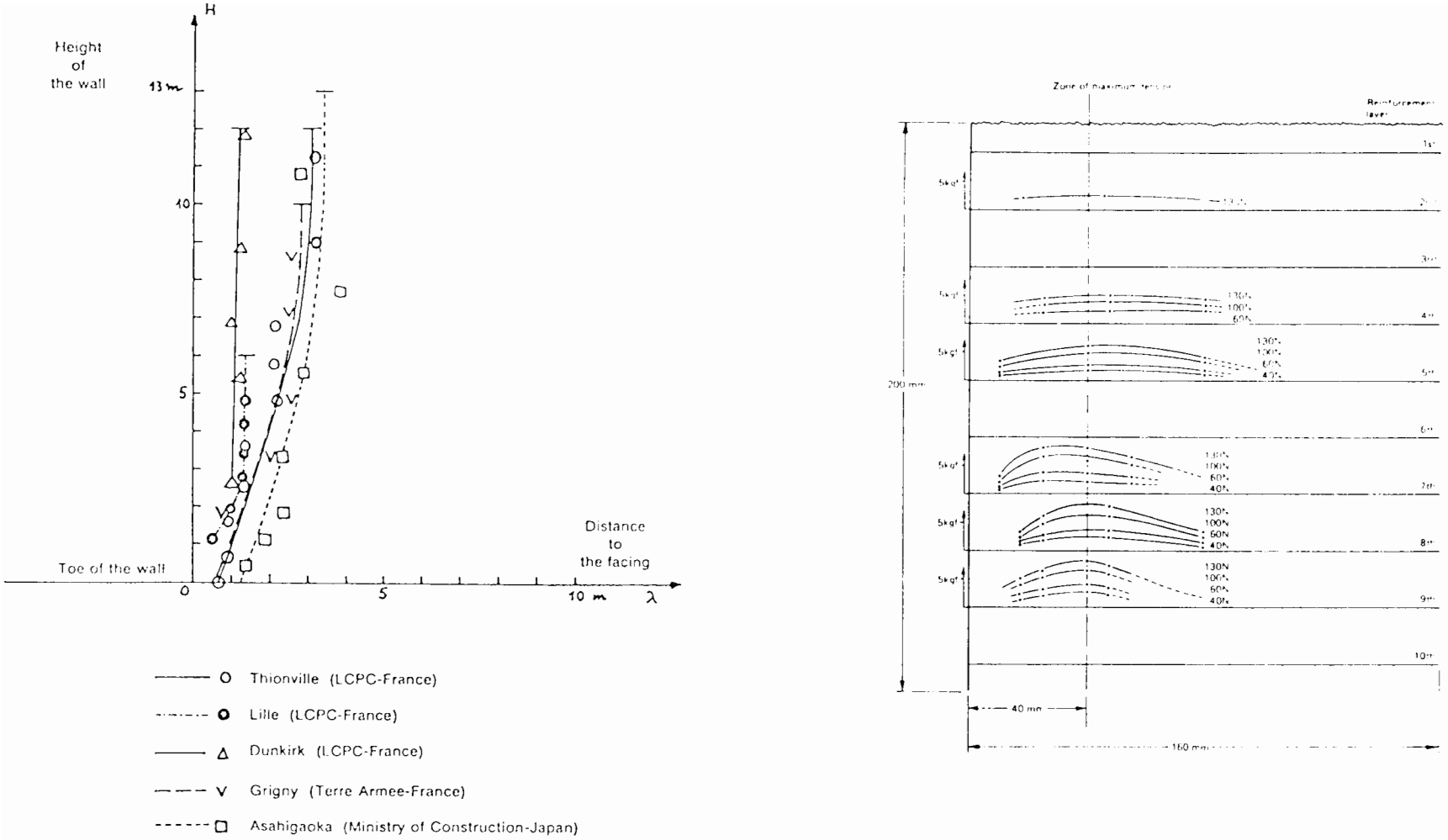


Fig. 1.10 Location of maximum tension for reinforcing elements in reinforced earth retaining walls a) at full scale (from Schlosser and Elias 1978), and b) in model tests in the geotechnical centrifuge at N gravities (from Bolton et al. 1978)

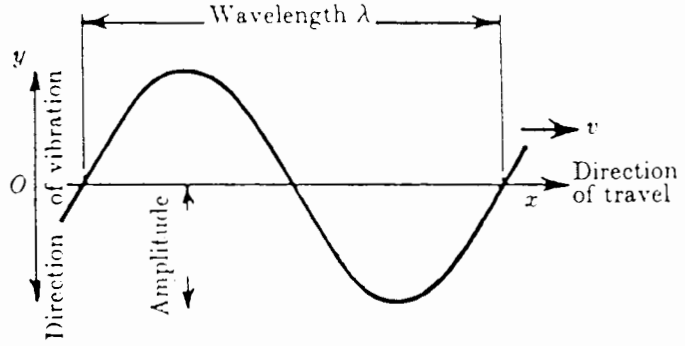


Fig. 2.1 Light wave shown diagrammatically (from Holister (1967)

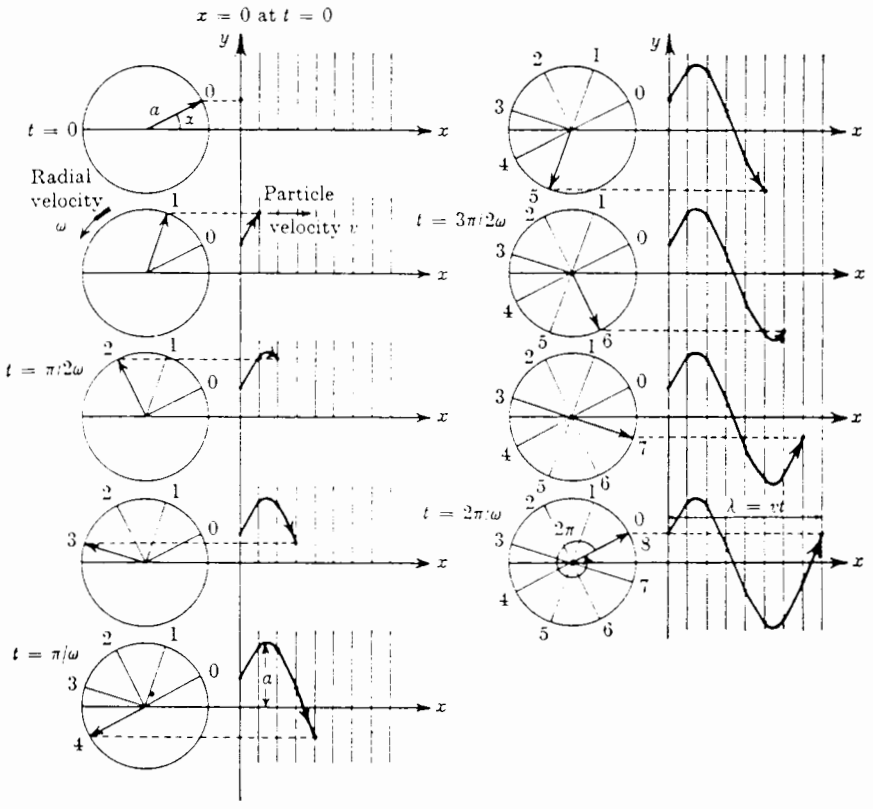


Fig. 2.2 Generation of a simple harmonic wave by a periodic vibration of period $2\pi/\omega$ with a uniform velocity v in the x-direction (from Holister 1967)

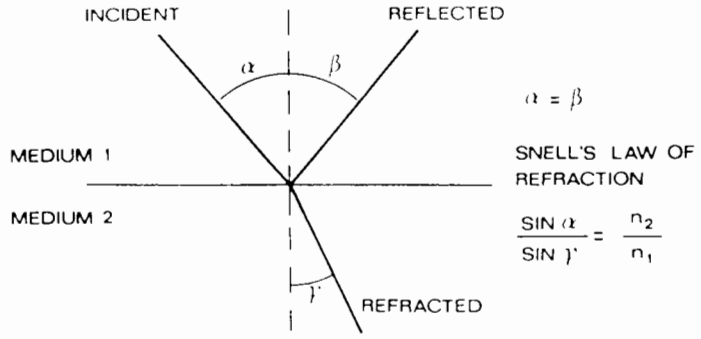


Fig. 2.3 Refraction and reflection of an incident ray of light for optically isotropic medium

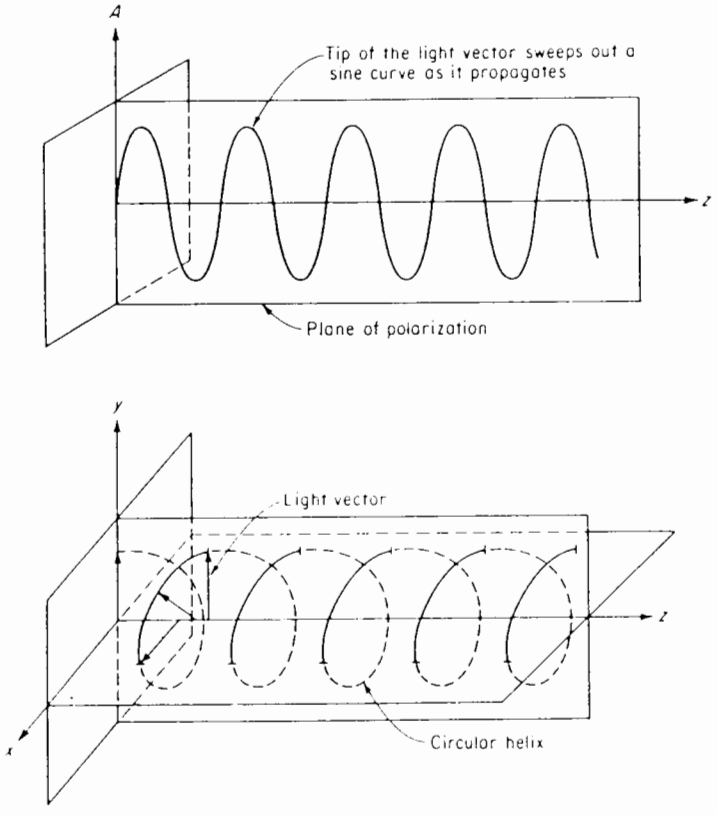


Fig. 2.4 Plane and circular polarised light (from Dally and Riley 1978)

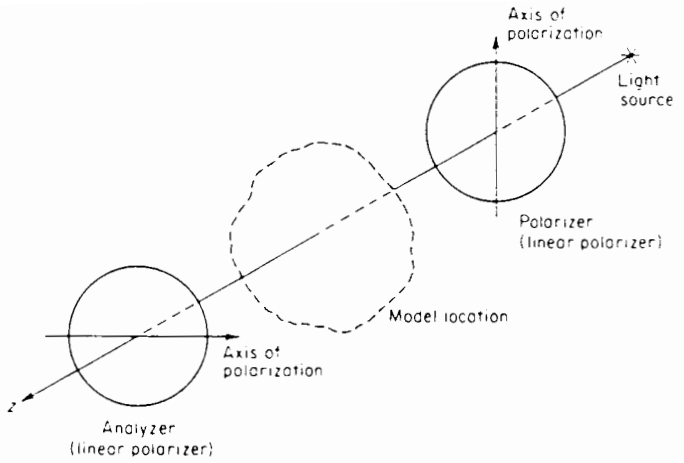


Fig. 2.5 Arrangement of optical elements in a plane polariscope (from Dally and Riley 1978)

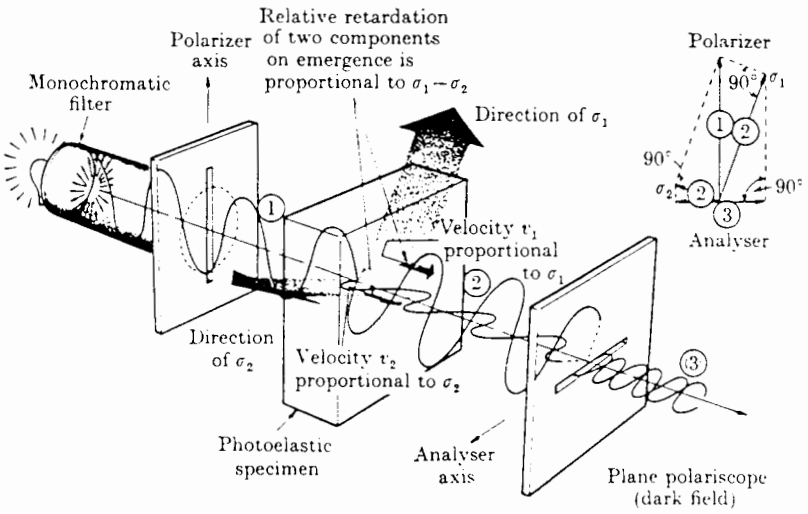


Fig. 2.6 Photoelastic effect in a plane polariscope (from Holister 1967)

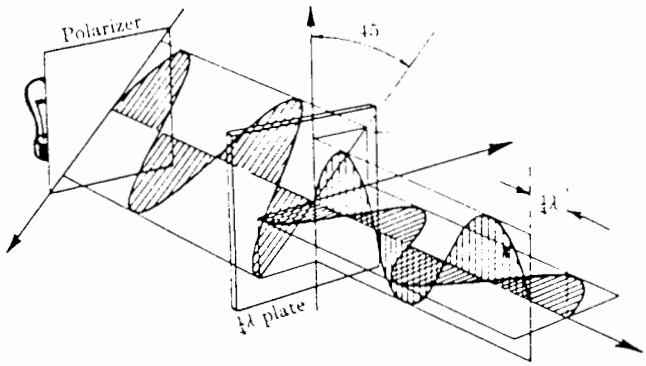


Fig. 2.7 Plane polarised light passing through a quarter-wave plate (from Holister 1967)

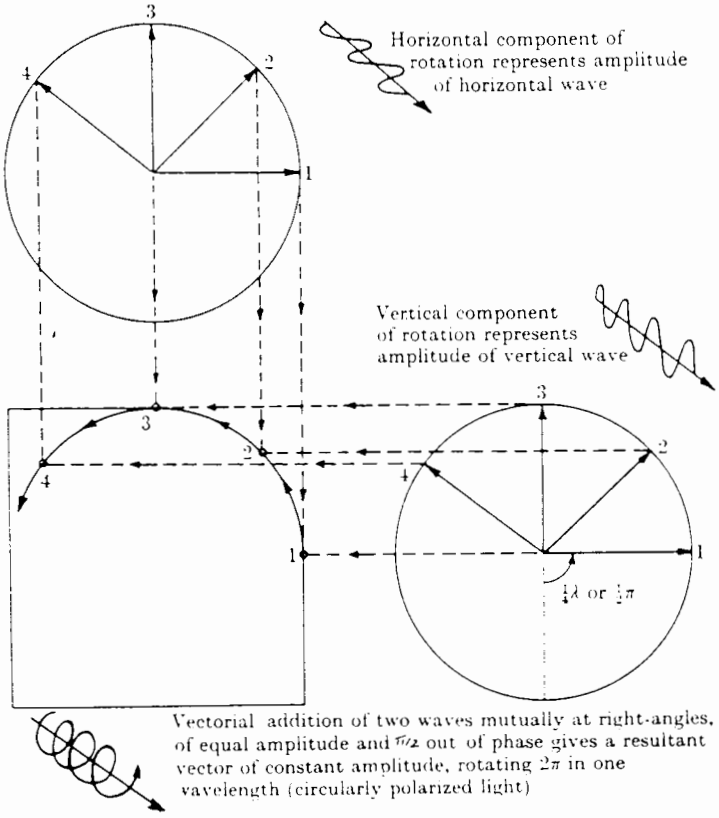


Fig. 2.8 Addition of two light waves to give circularly polarised light (from Holister 1967)

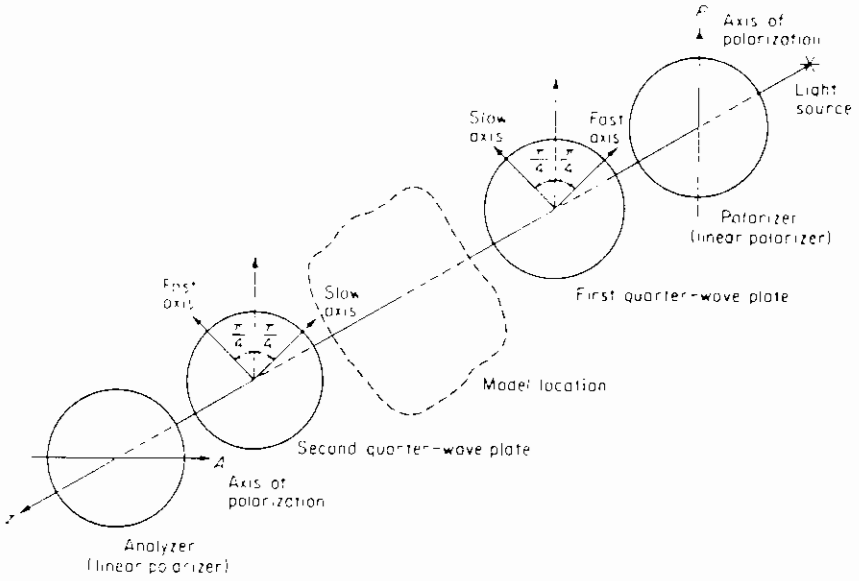


Fig. 2.9 Arrangement of optical elements in a circular polariscope with a dark field (from Dally and Riley 1978)

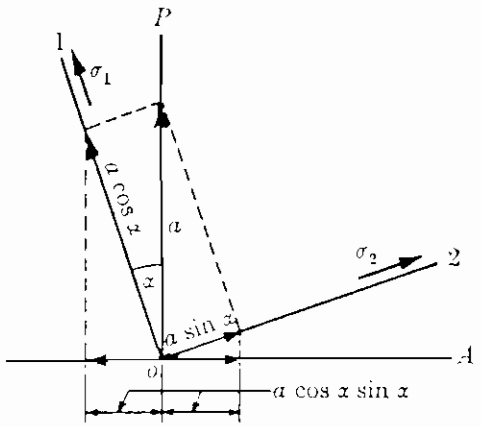


Fig. 2.10 Effect produced on a beam of monochromatic plane polarised light (P) passing through a photoelastic specimen ($\sigma_1$, $\sigma_2$) and analyser (A) (from Holister 1967)

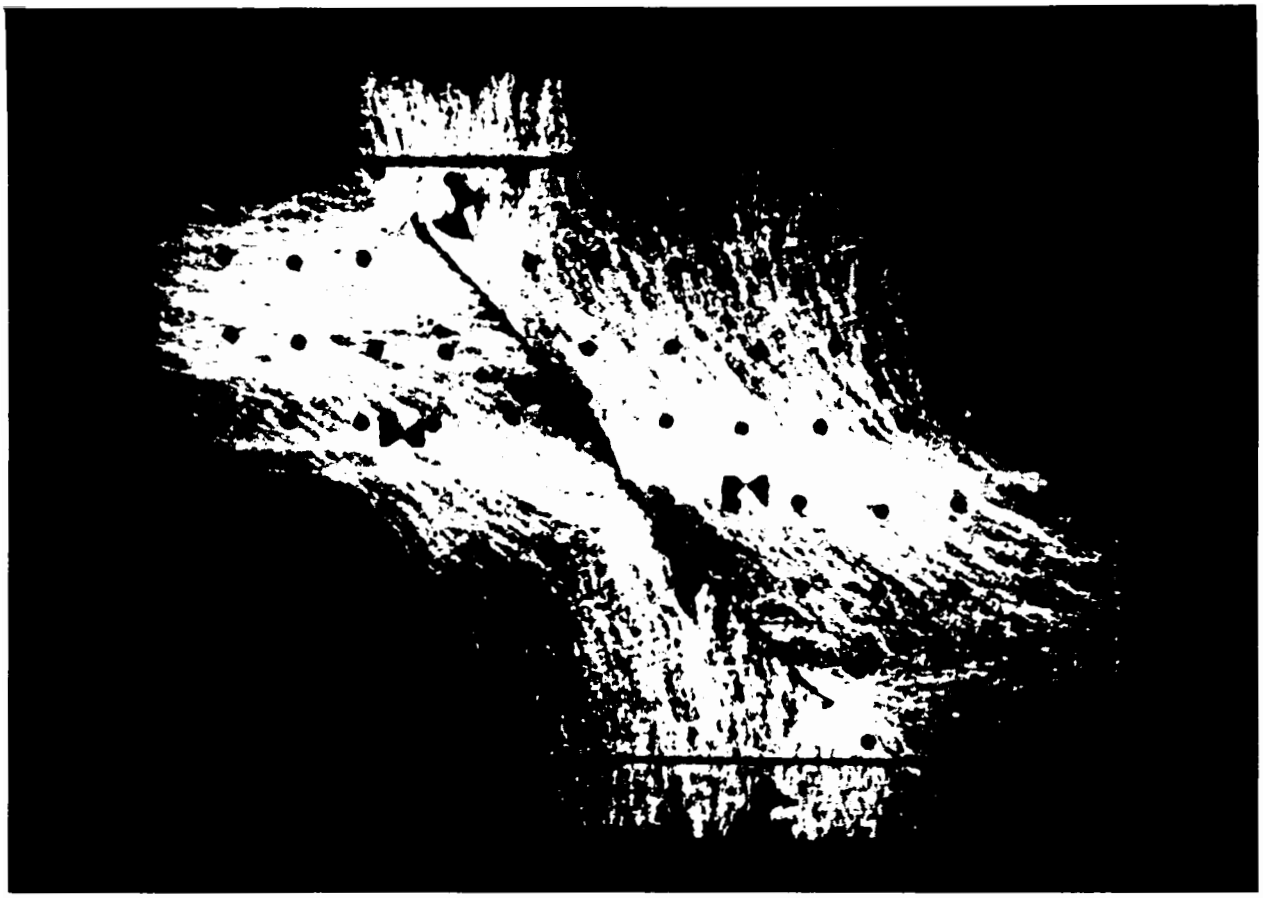

Fig. 2.11 Light stripes observed through a circular polariscope with a dark field for a direct shear test on crushed glass containing a flexible sheet reinforcement orientated at $\theta = -45°$

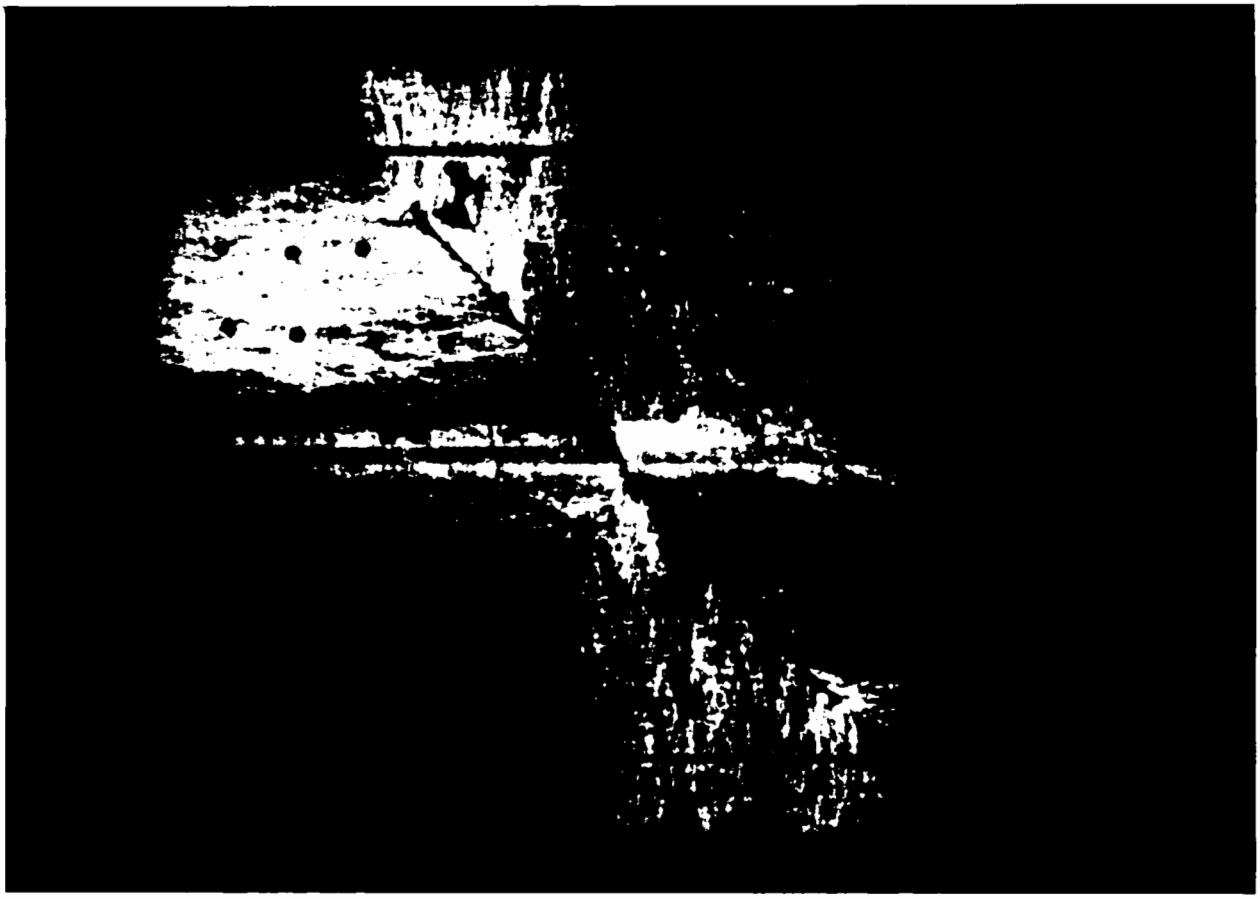

Fig. 2.12 Light stripes observed in the same direct shear test as in fig. 2.11 but through a plane polariscope with axes inclined at 45° on either side of vertical

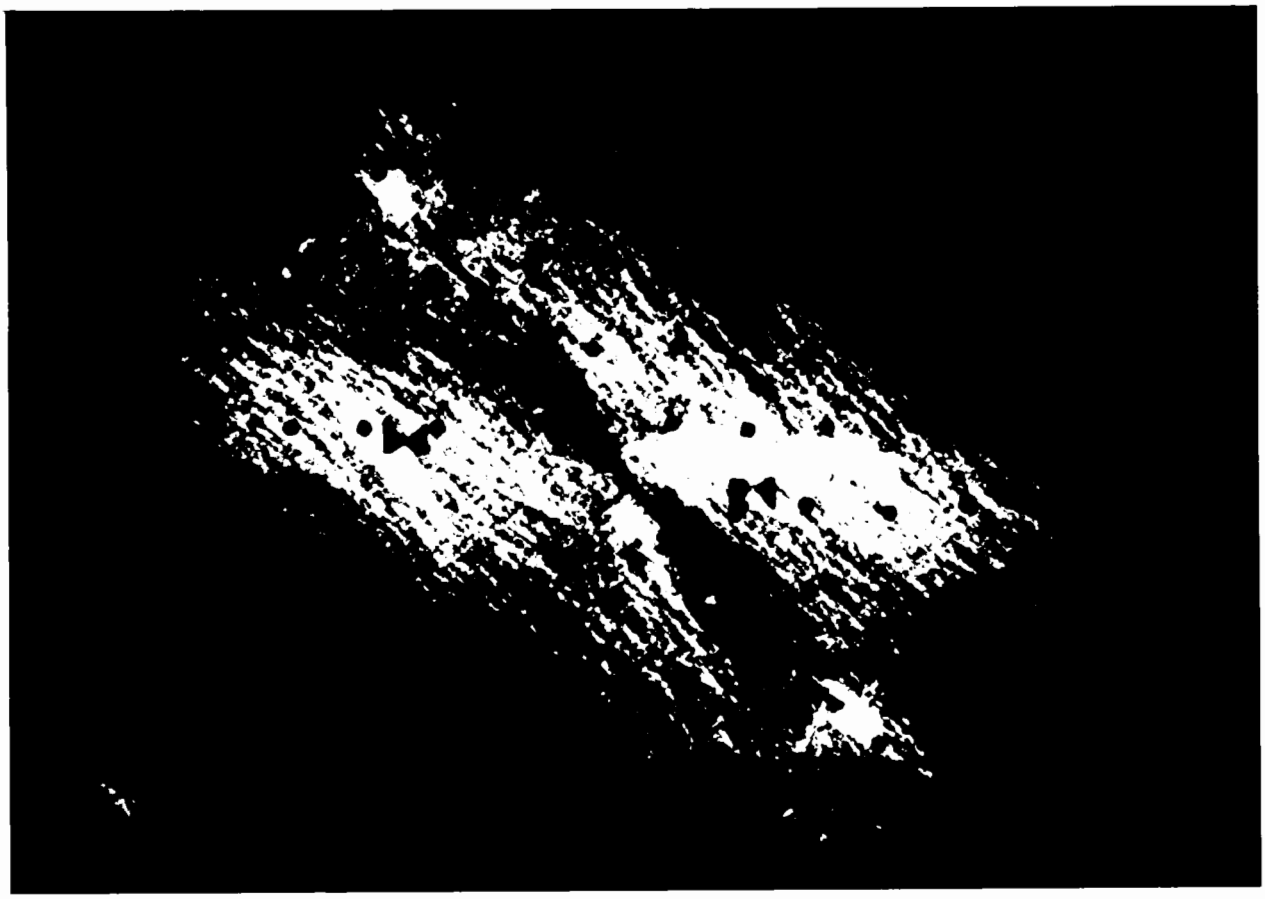

Fig. 2.13 Light stripes observed in the same direct shear tests as in fig. 2.11 but through a plane polariscope with axes vertical and horizontal

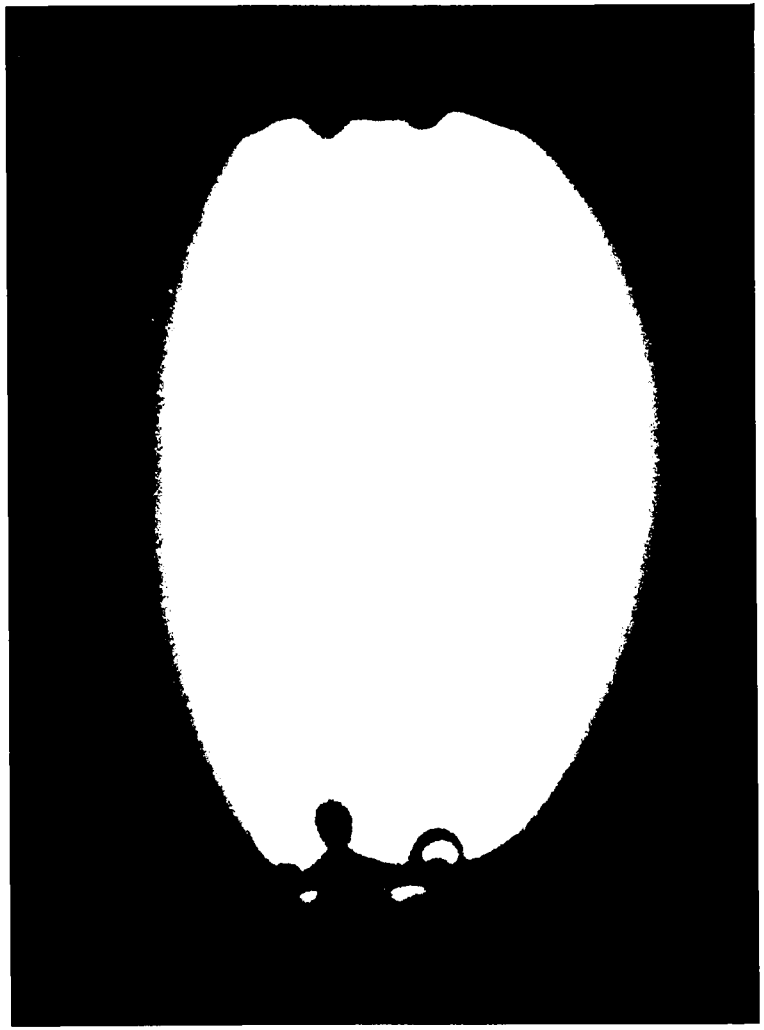

Fig. 2.14 Light pattern observed through a circular polariscope with a dark field for a glass disc loaded along the diameter from top to bottom in the photograph

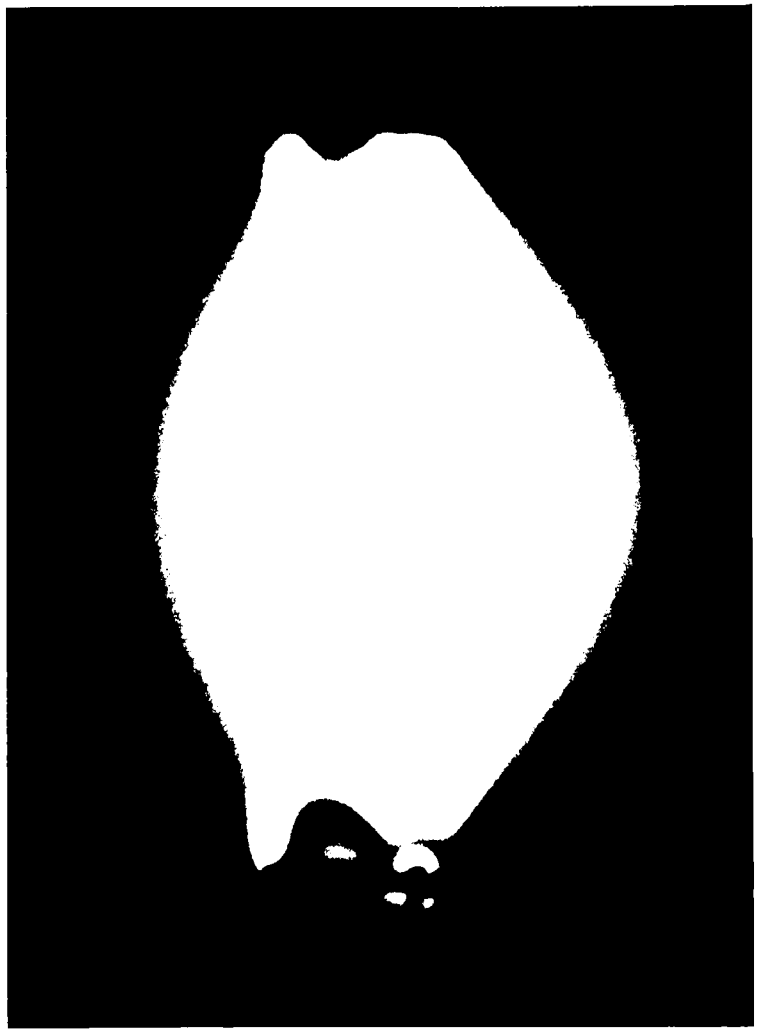

Fig. 2.15 Light pattern observed for the same loaded glass disc as in fig. 2.14 but through a plane polariscope with axes inclined at 45° to the loaded diameter

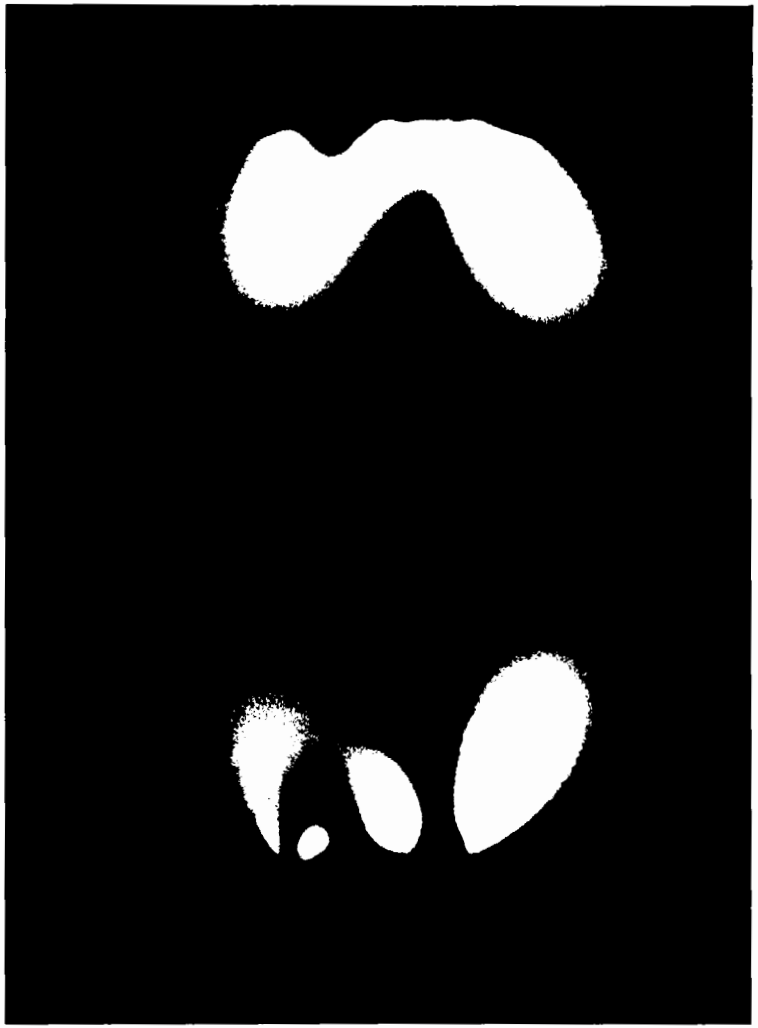

Fig. 2.16 Light pattern observed for the same loaded glass disc as in fig. 2.14 but through a plane polariscope with axes aligned and perpendicular to the loaded diameter

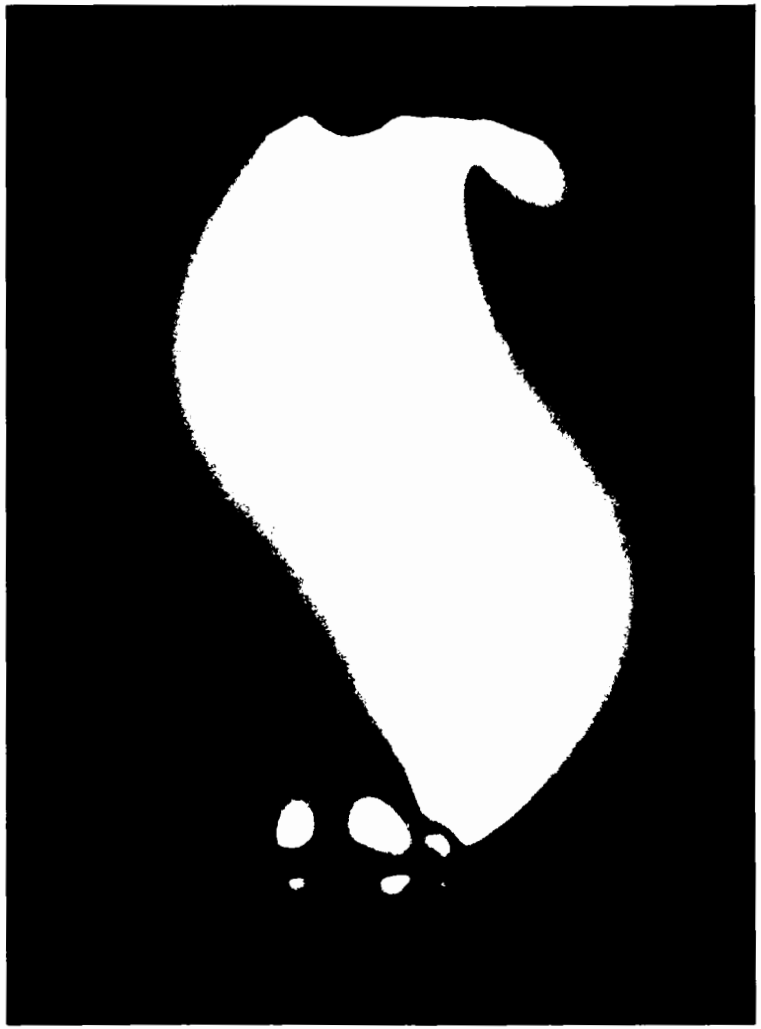

Fig. 2.17 Light pattern observed for the same loaded glass disc as in fig. 2.14 but through a plane polariscope with axes rotated 20° from the loaded diameter

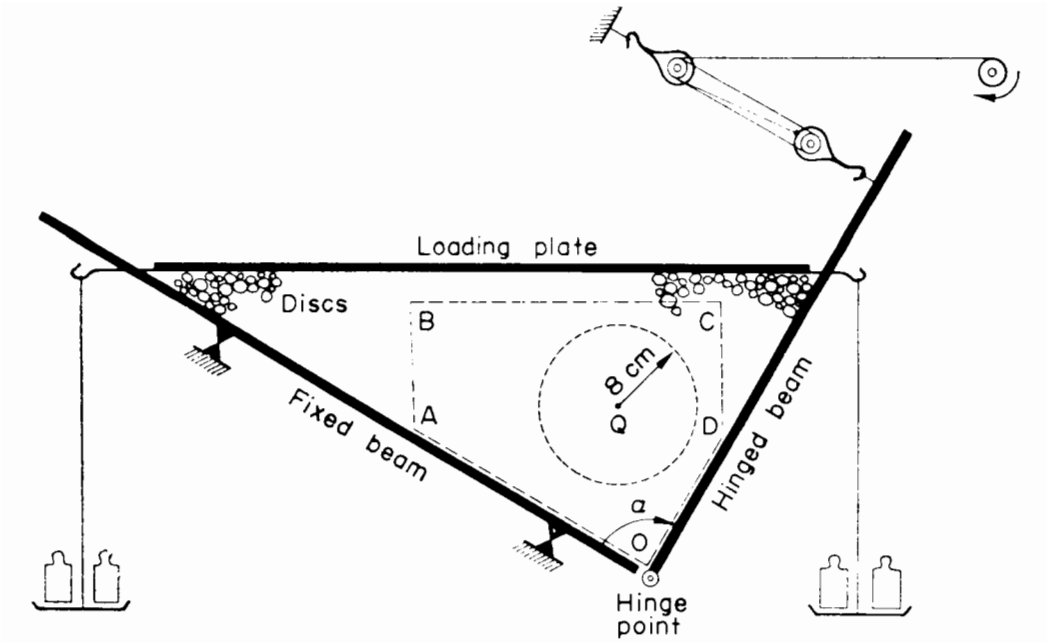


Scheme of loading system.

Fig 2.18 Loading scheme employed by Drescher and De Josselin de Jong (1972) on an assembly of discs

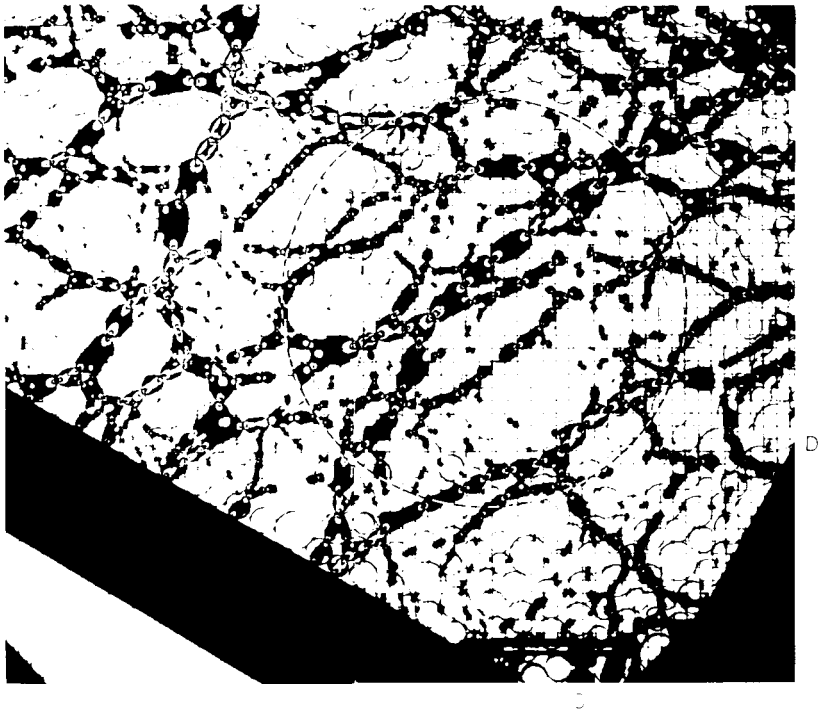


Fig. 2.19 Isochromatic fringes observed in an assembly of discs through a circular polariscope by Drescher and De Josselin de Jong

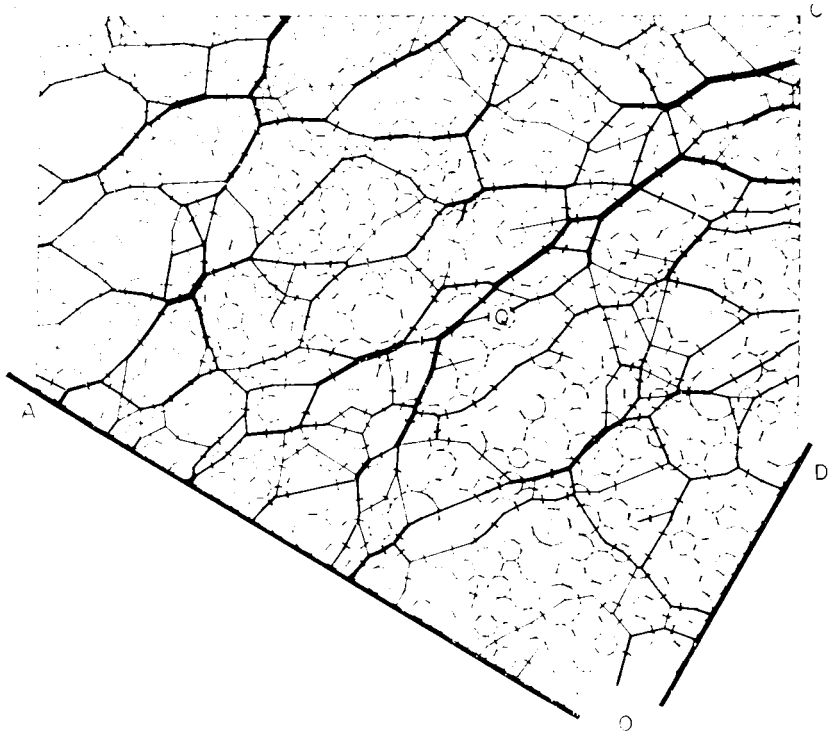


Fig. 2.20 Network of contact forces in an assembly of discs determined from isochromatic fringes by Drescher and De Josselin de Jong

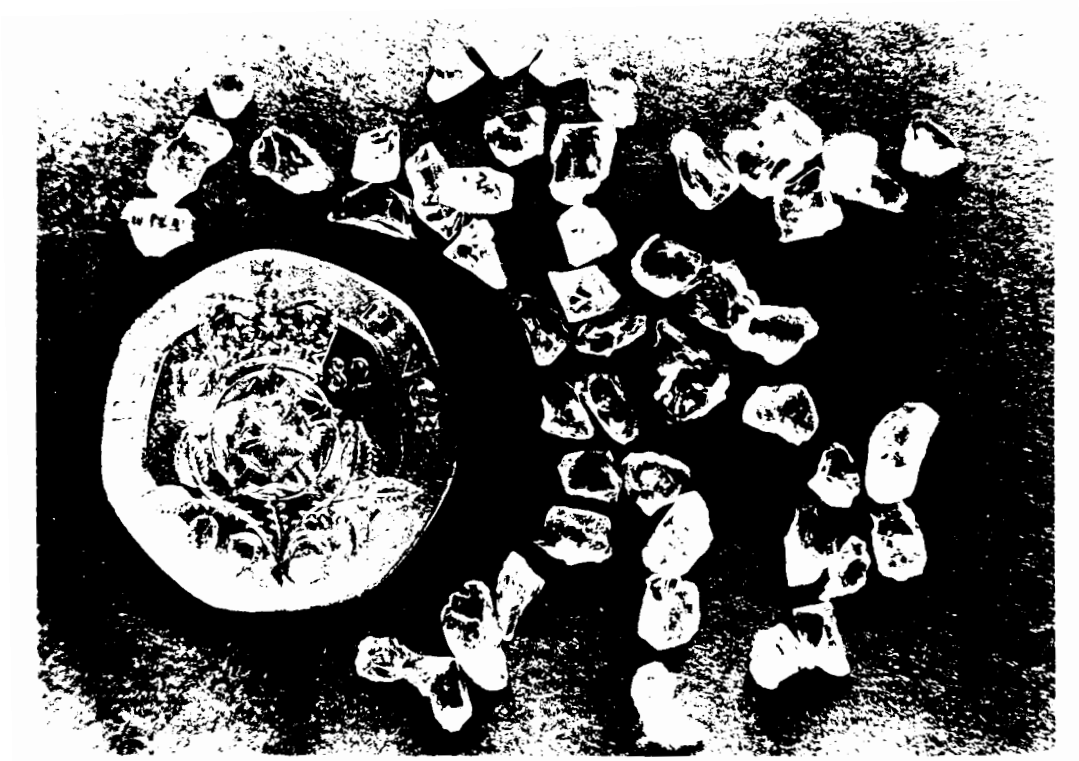

Fig. 3.1 Sample of crushed glass used in the photoelastic tests

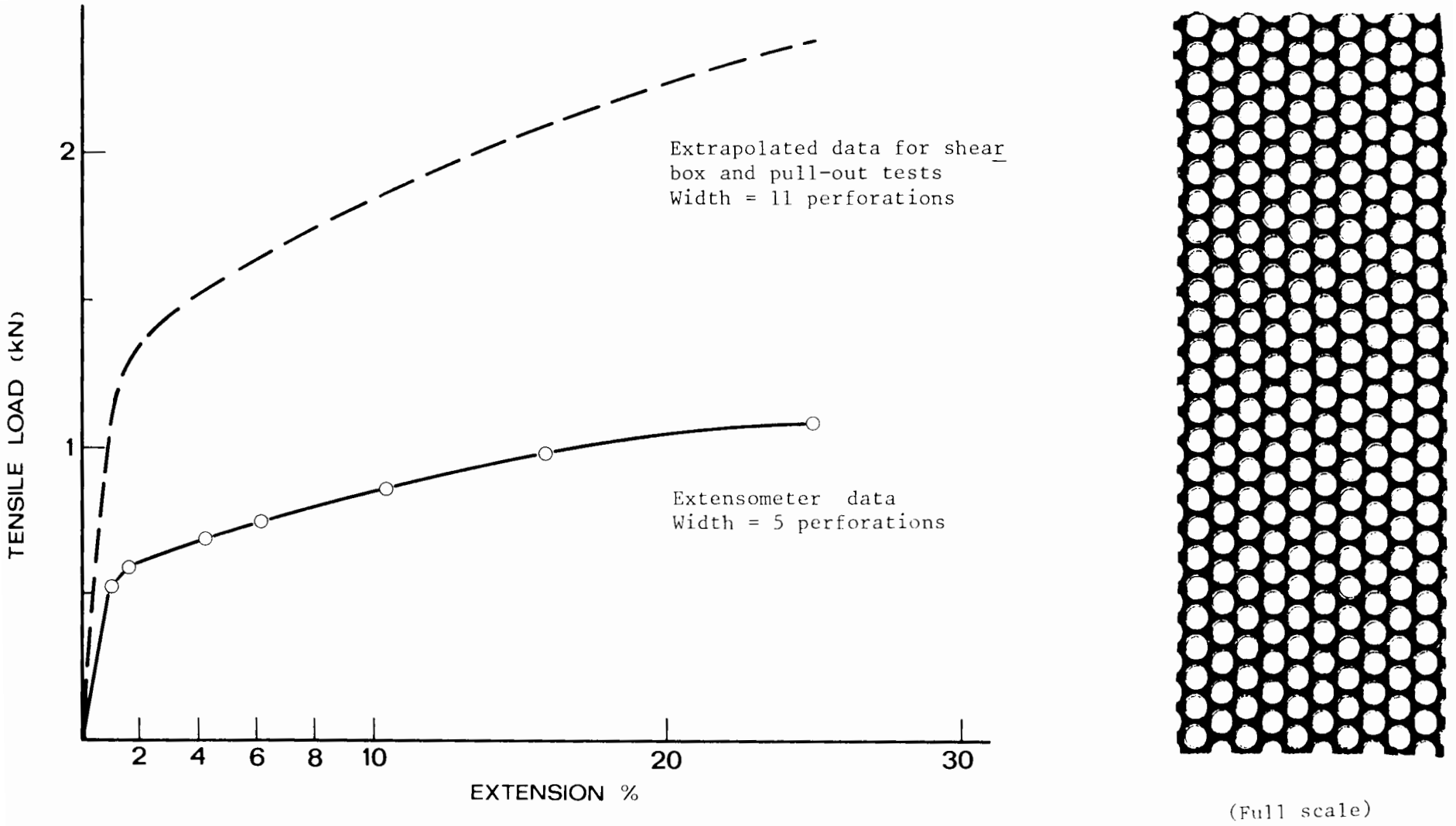


Fig. 3.2 Illustration of perforated brass sheet with load-extension curves

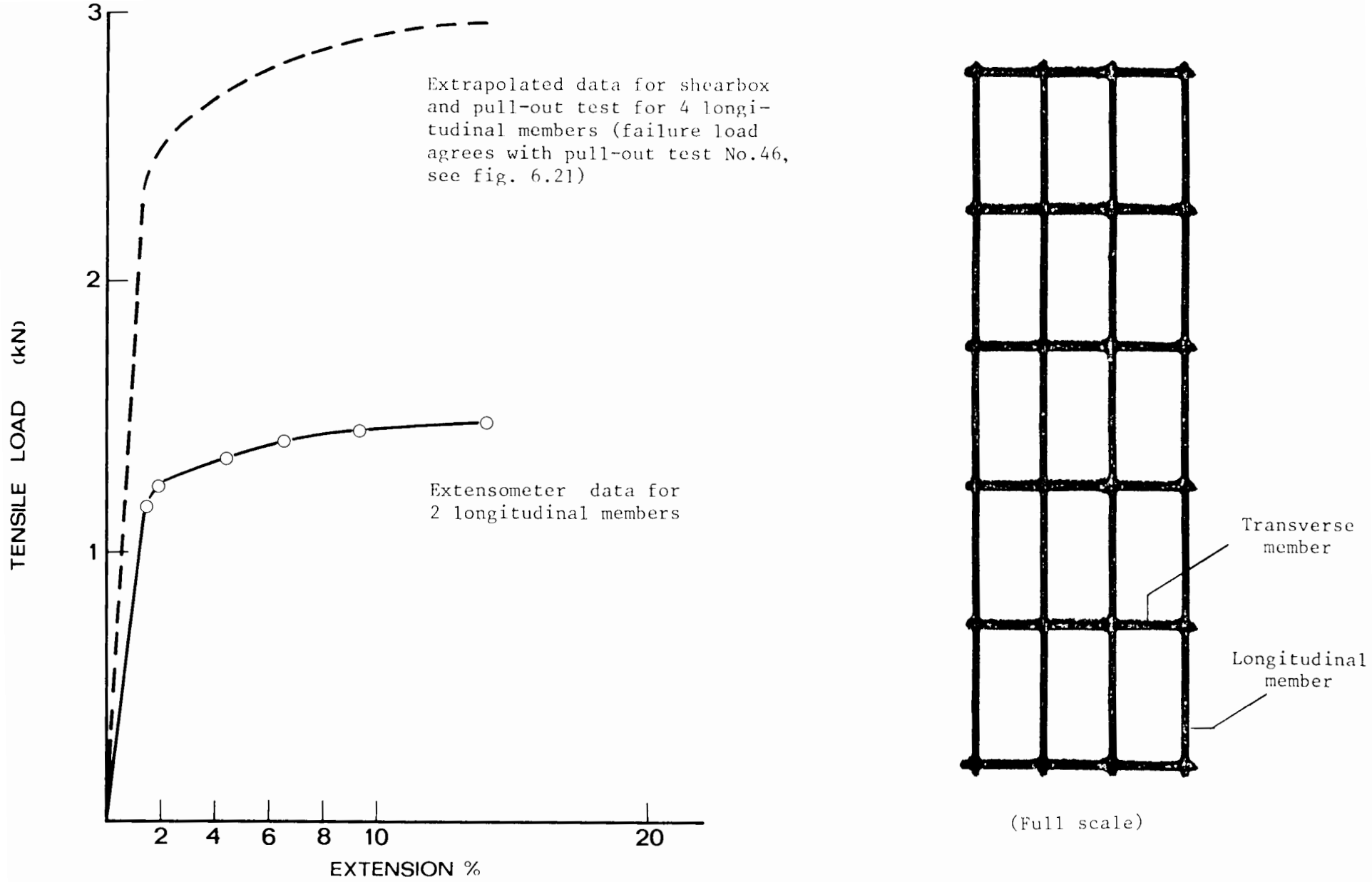


Fig. 3.3 Illustration of steel grid with load-extension curves

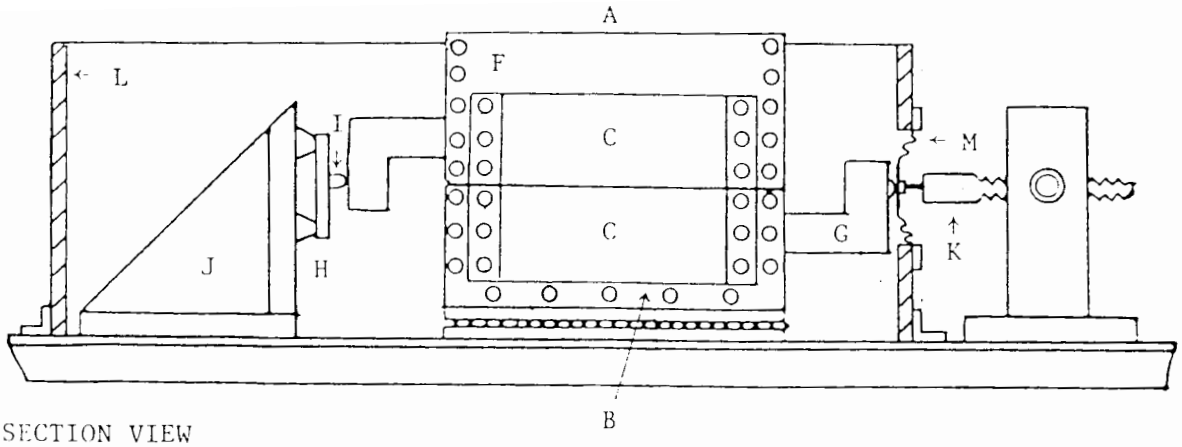


SECTION VIEW

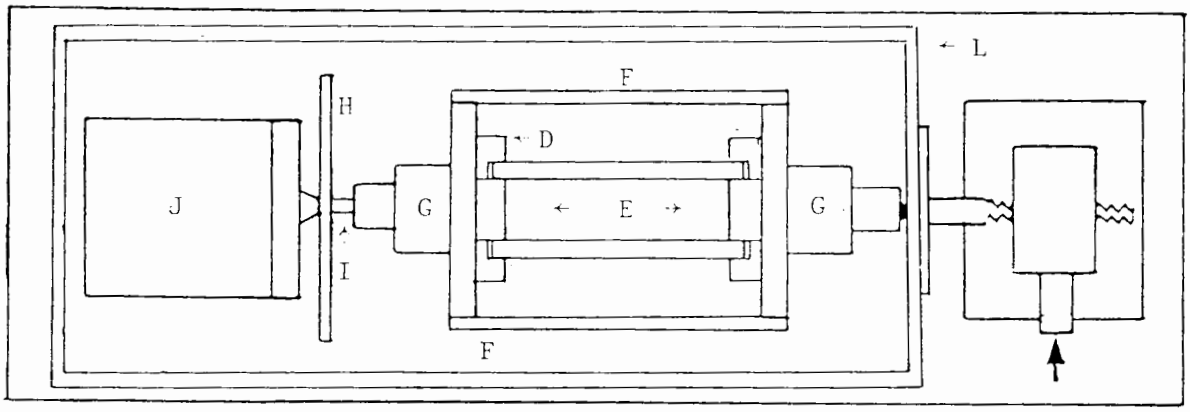


PLAN VIEW

| | |
|---|---|
| ... | Roller bearings |
| → | Drive from an electric motor |
| A | Upper half of the shearbox |
| B | Lower half of the shearbox |
| C | Glass sidewalls of the shearbox |
| D | Metal clamps for the glass sidewalls |
| E | Internal sides of the shearbox |
| F | Dural support frames for the shearbox, originally designed to accomodate a larger sand sample |
| G | Solid connectors for transmitting shear load |
| H | Deflector bar |
| I | Roller bearing attached to the deflector bar |
| J | Stand for the deflector bar |
| K | Loading beam |
| L | Perspex sidewalls surrounding the shearbox and the deflector bar |
| M | Rubber membrane inserted in the perspex endwall to transmit the shear load from the loading beam K |
| O | Countersunk caphead screws |

Fig. 3.4 Schematic diagram of the direct shearbox apparatus

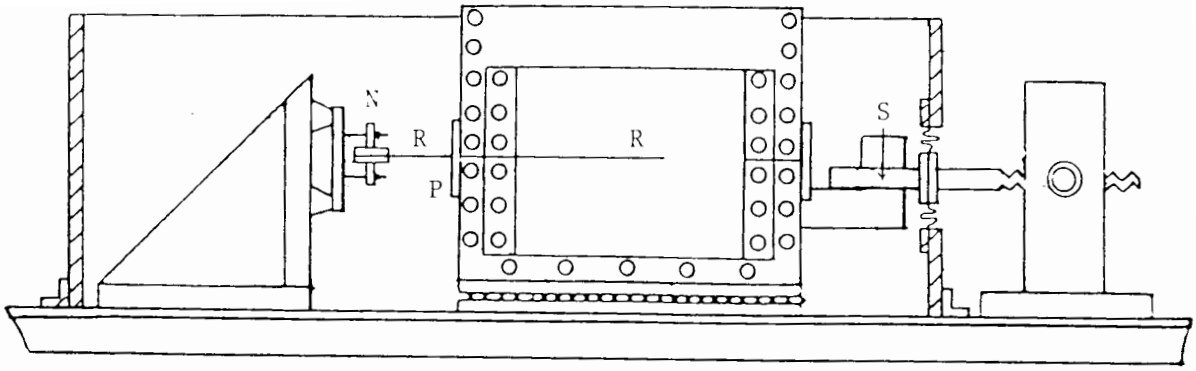


SECTION VIEW

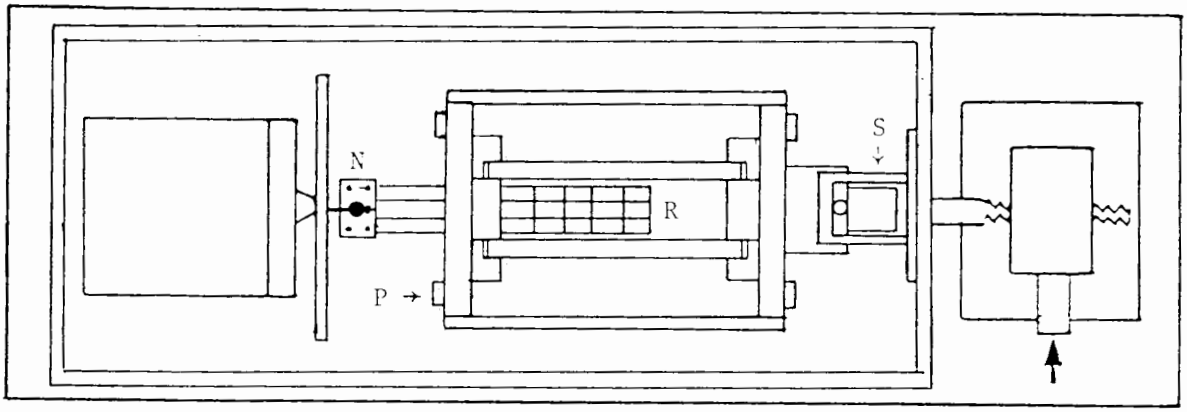


PLAN VIEW

In addition to the key for fig. 3.4

N Attachment of the reinforcement to the deflector bar (see fig. 3.6)

P Clamps for holding the halves of the box together for pull-out tests

R Reinforcement

S Transmitter of pull-out load to the box

Fig. 3.5 Schematic diagram of pull-out apparatus

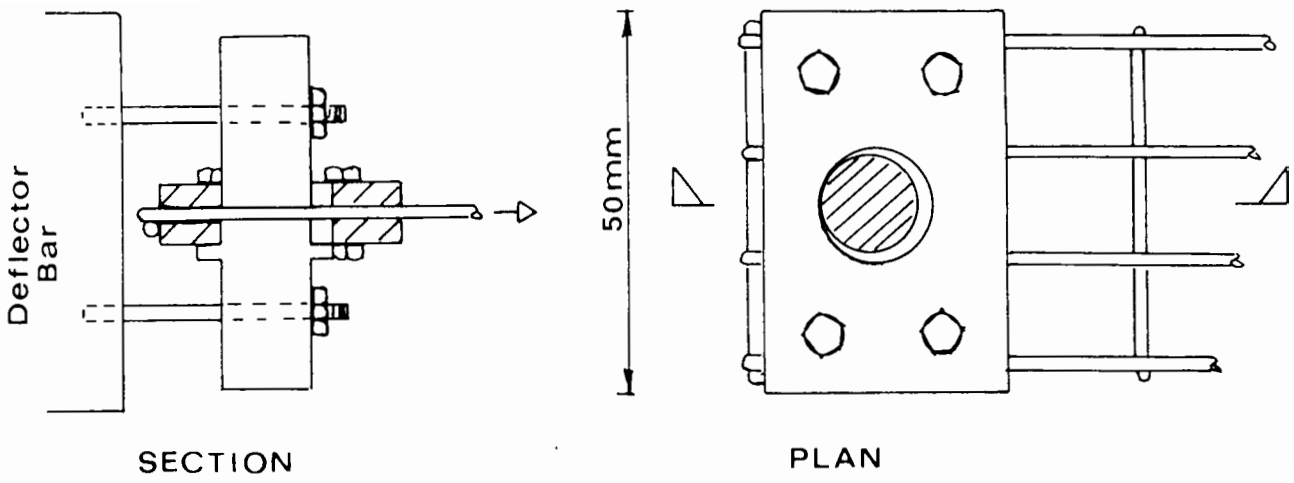


Fig. 3.6 Arrangement for attaching reinforcement to the deflector bar

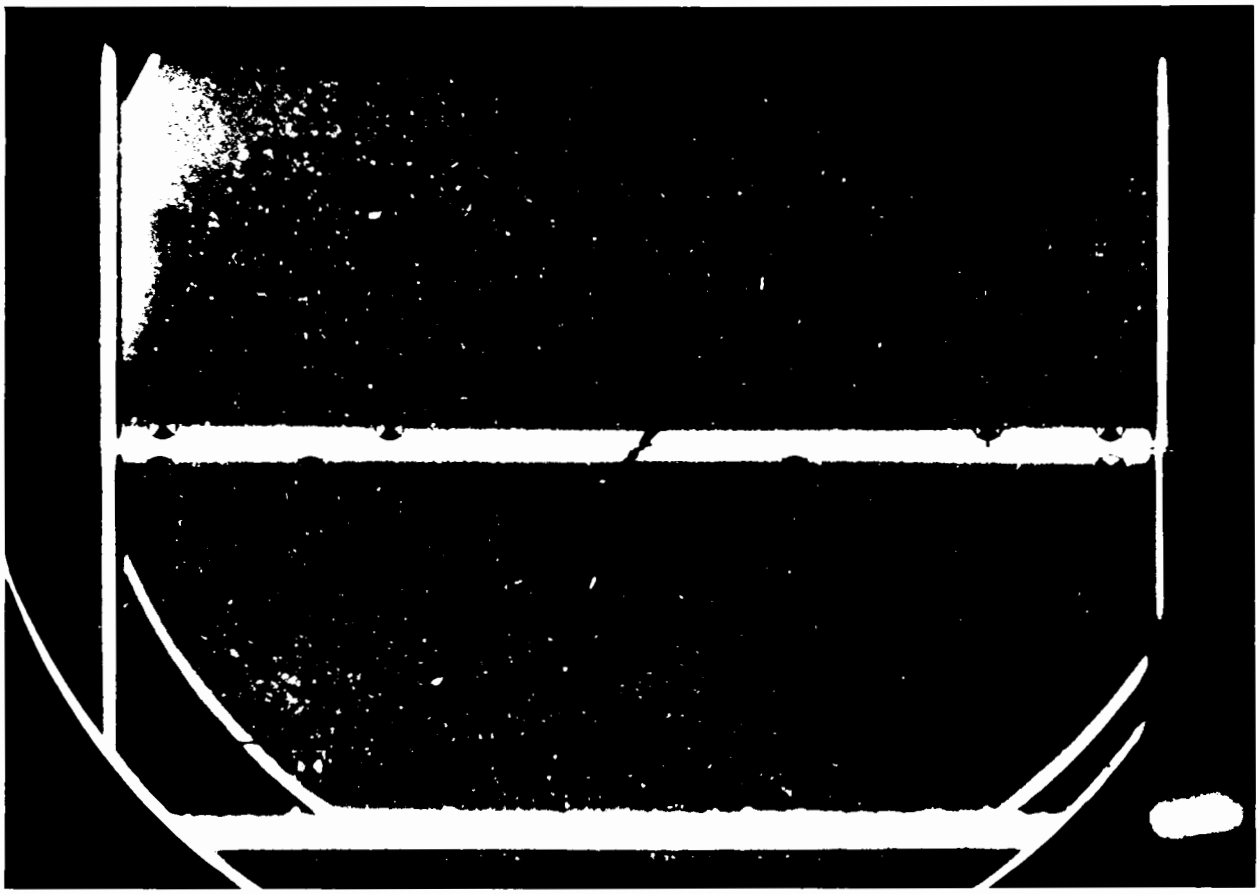

Fig. 3.7 Residual stresses observed in the glass sidewalls of the shearbox through a circular polariscope with a dark field

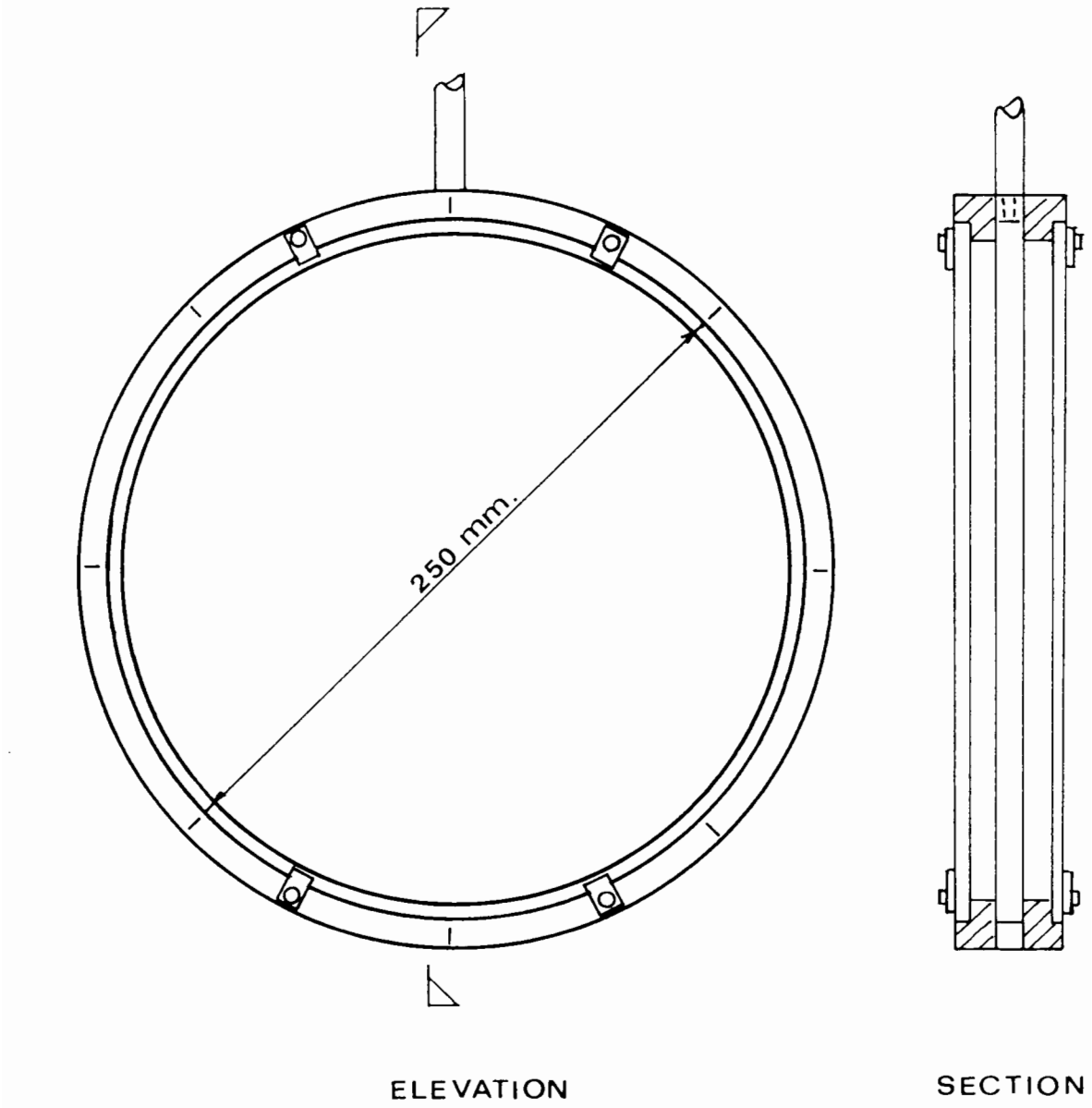


Fig. 3.8 Dural frame for the polariscope

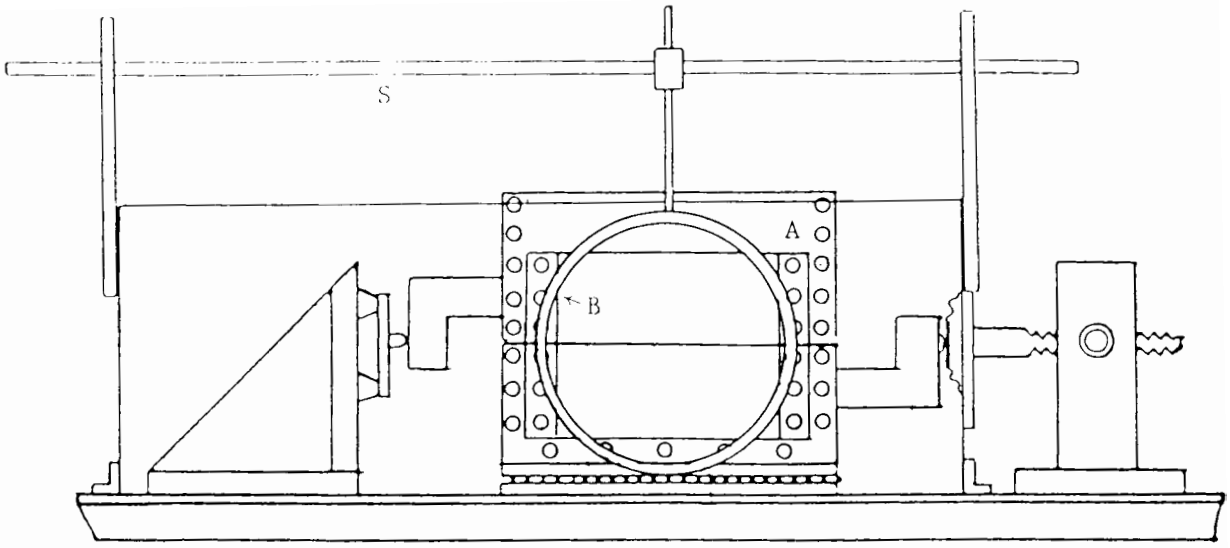


ELEVATION

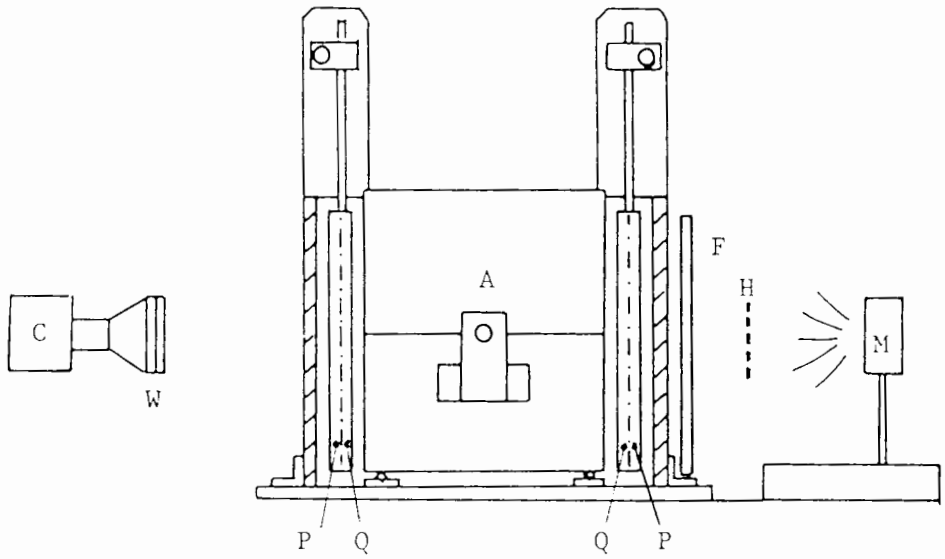


SIDE VIEW

| | |
|---|---|
| A | Shearbox |
| B | Polariscope frame |
| C | Camera |
| F | Flashed opal perspex sheet for diffusing light |
| H | Heat filter inserted when not taking photographs |
| M | Mercury arc lamp |
| P | Linear polariser filter |
| Q | Quarter wave plate |
| S | Horizontal beams for supporting the polariscope frames |
| W | Wratten colour filter nos. 15 and 58 |

Fig. 3.9 Arrangement of circular polariscope either side of the shearbox and clamped to horizontal beams overhead

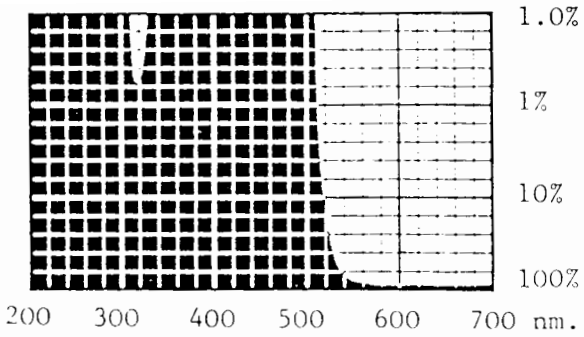


No. 15 Very deep yellow. Absorbs ultra violet, blue and a small amount of green

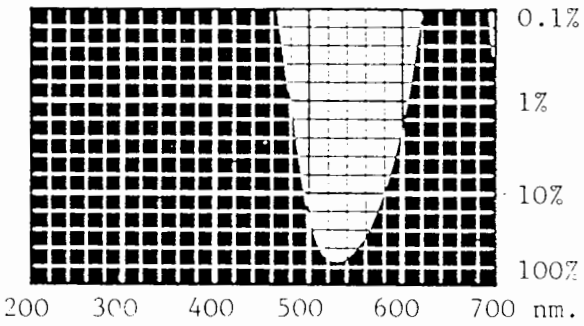


No. 58 Green. Absorbs ultra violet, blue and red

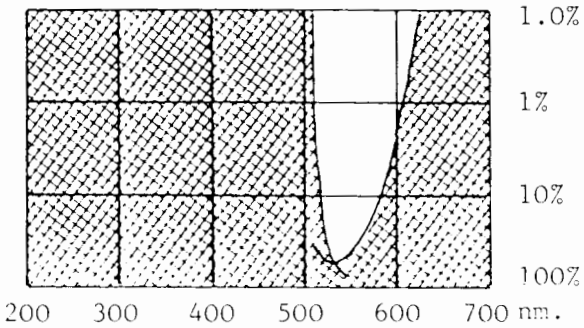


Nos. 15 + 58 Yellowish green

Fig. 3.10 Light transmission charts for wratten filter nos 15 and 58

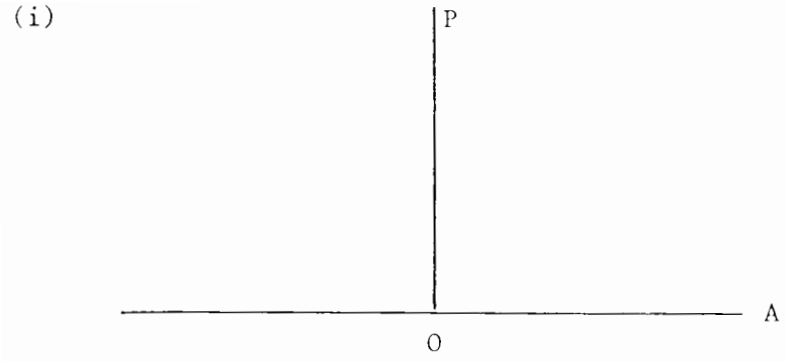


PLANE POLARISCOPE

Crossed polariser (P) and analyser (A) for maximum extinction of light

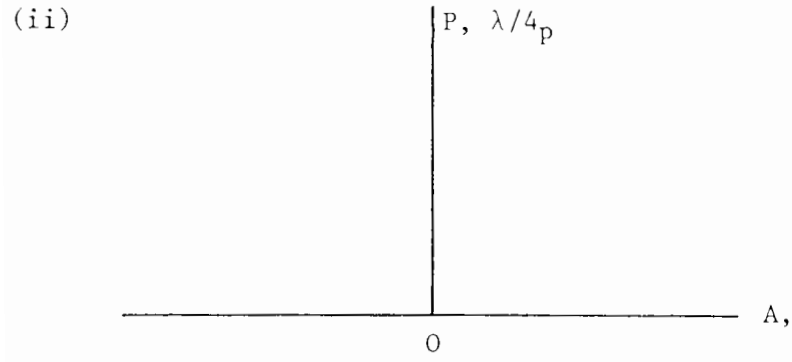


λ/4 Plate adjacent to polariser ($\lambda/4_p$) installed for maximum extinction of light

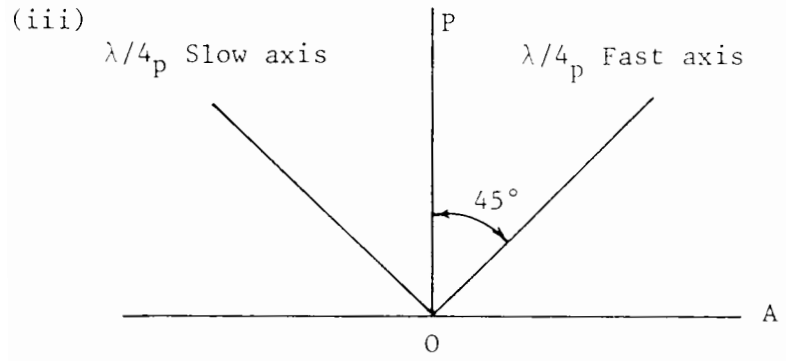


λ/4 Plate rotated by 45° for maximum transmission of light

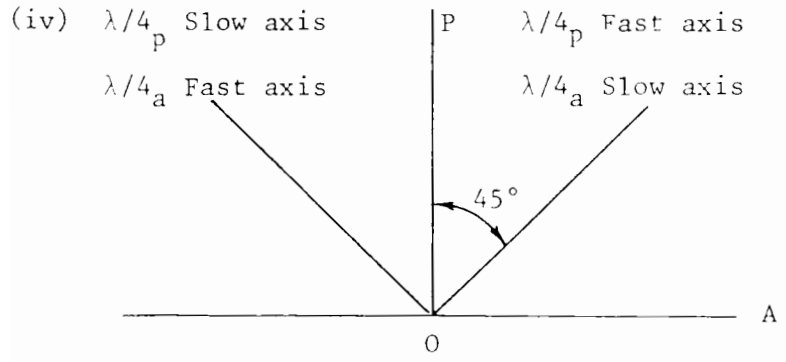


CIRCULAR POLARISCOPE
(DARK FIELD)

2nd λ/4 Plate installed adjacent to analyser ($\lambda/4_a$) for maximum extinction of light

Fig. 3.11 Orientation of the filter axes for assembly of plane and circular polariscopes

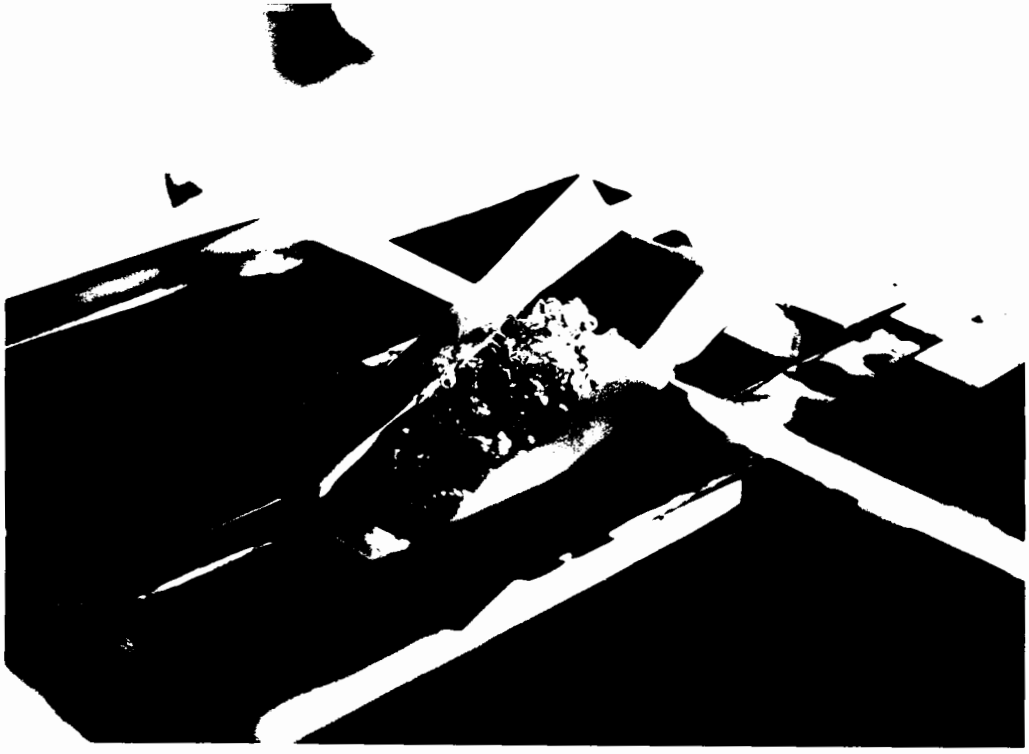

Fig. 3.12 Sliding of paraffin coated crushed glass particles into paraffin filled shearbox

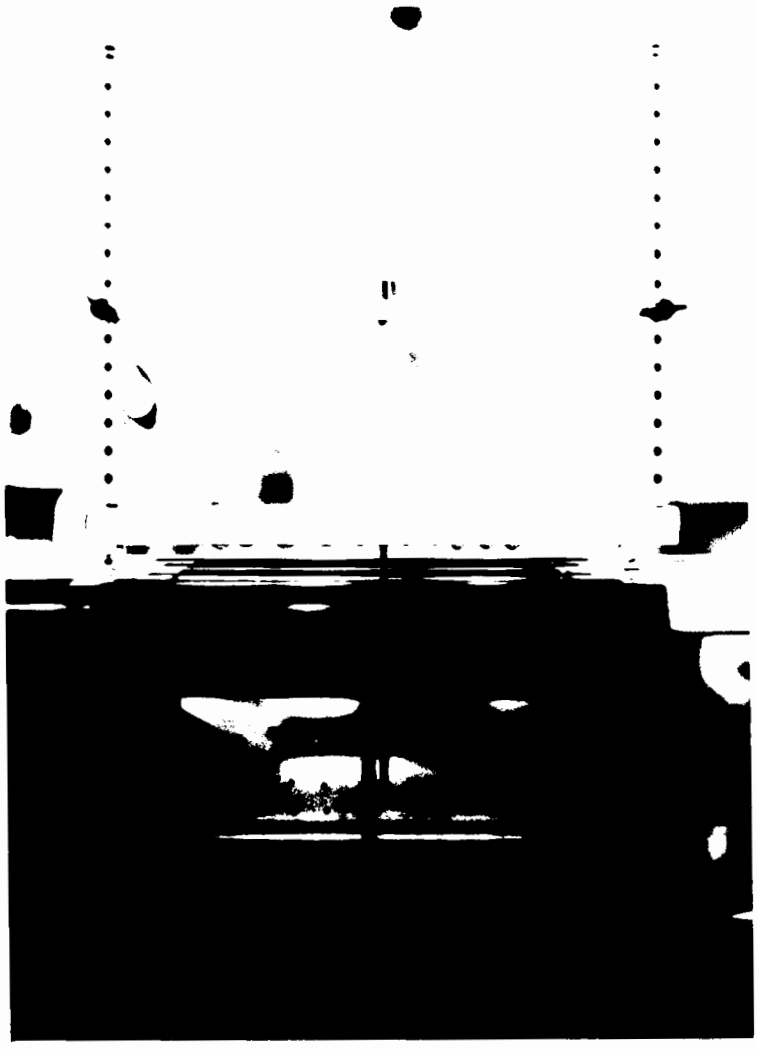

Fig. 3.13 Pair of spacing bars and tube for positioning steel balls in the crushed glass to form a 15 mm x 15 mm vertical grid

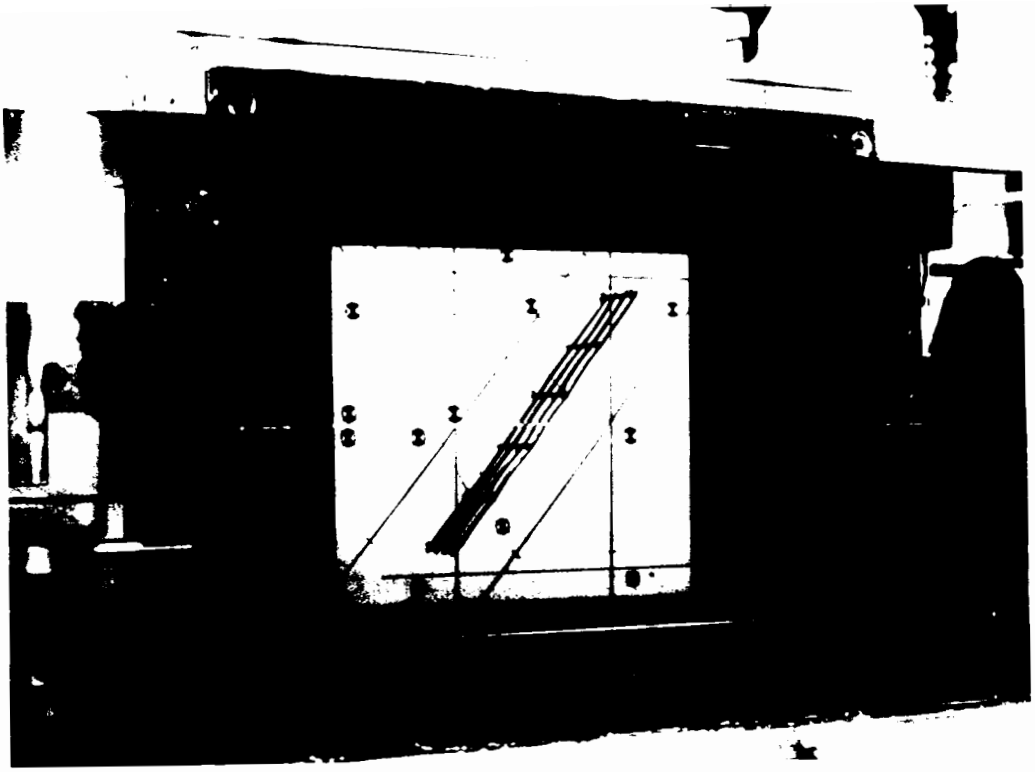

Fig. 3.14 Network of threads for suspending grid reinforcement in the empty shearbox prior to filling with crushed glass - technique taken from Jewell (1980). Black lines parallel to the reinforcement were drawn on perspex sheets to provide a guide for orientating the reinforcement as required

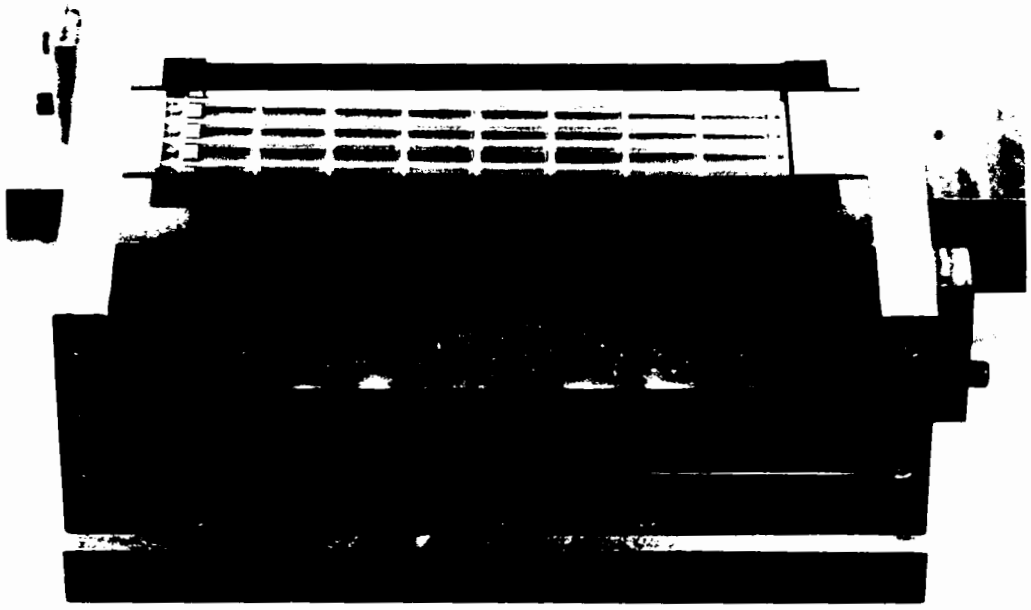

Fig. 3.15 Arrangement for laying the steel grid along the central plane of the shearbox on a polished steel block with transverse members hooked over a set of teeth milled out of the end wall of the box. This is in preparation for measuring direct sliding resistance of crushed glass over the grid

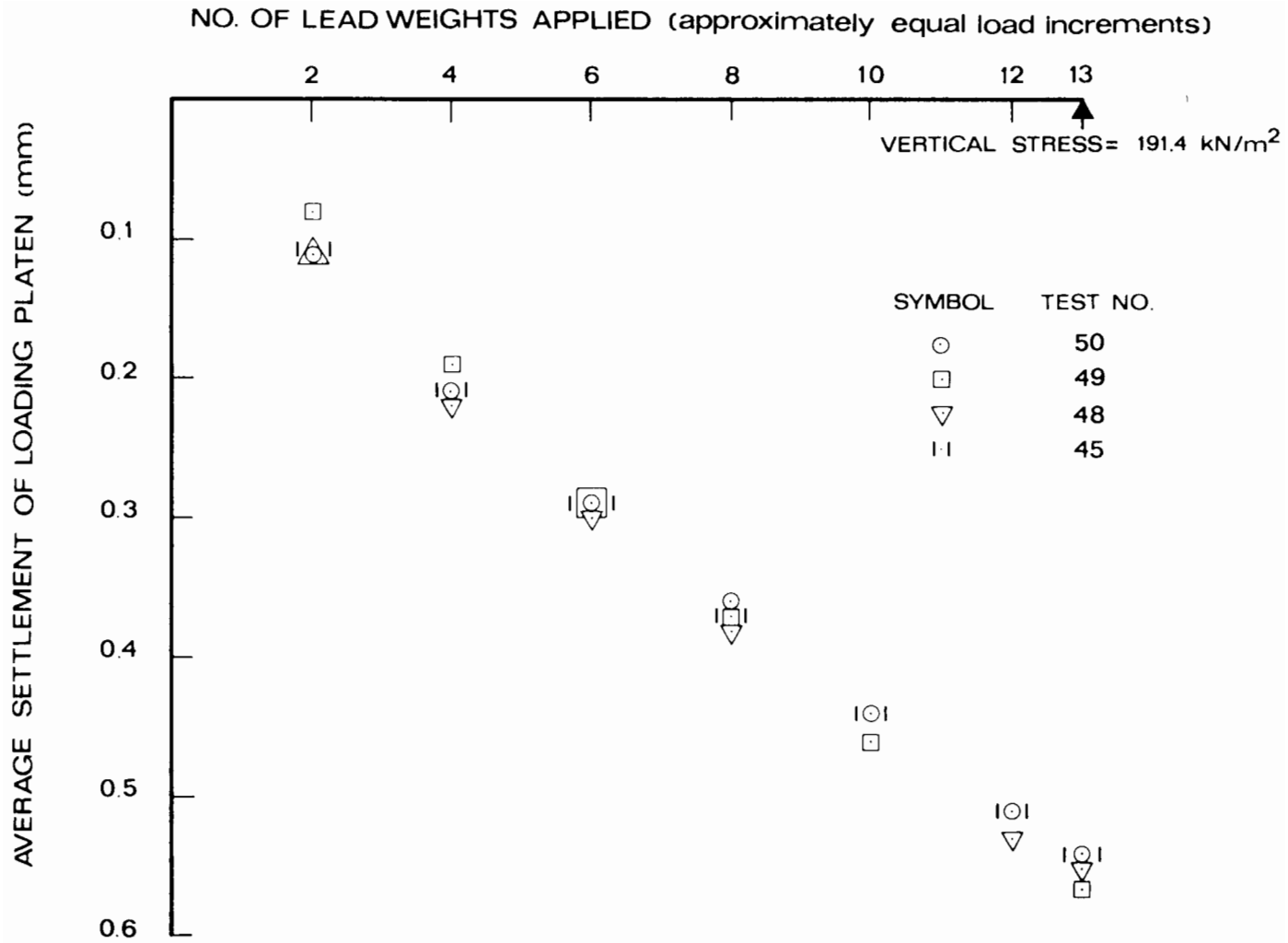


Fig. 3.16 Average settlement of loading platen in the shearbox under vertical load

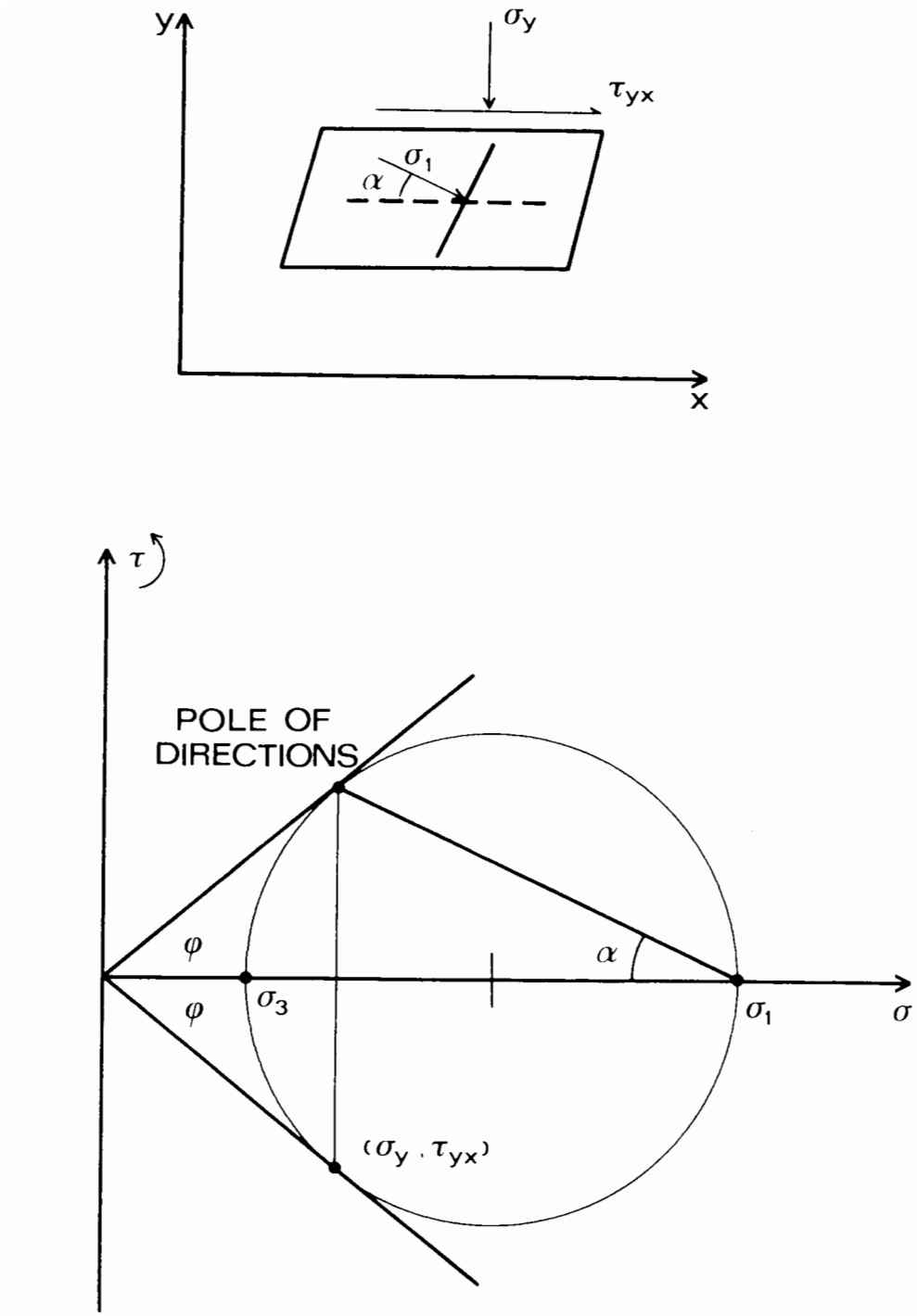


Fig. 4.1 Mohr's circle of stresses : terminology and sign convention

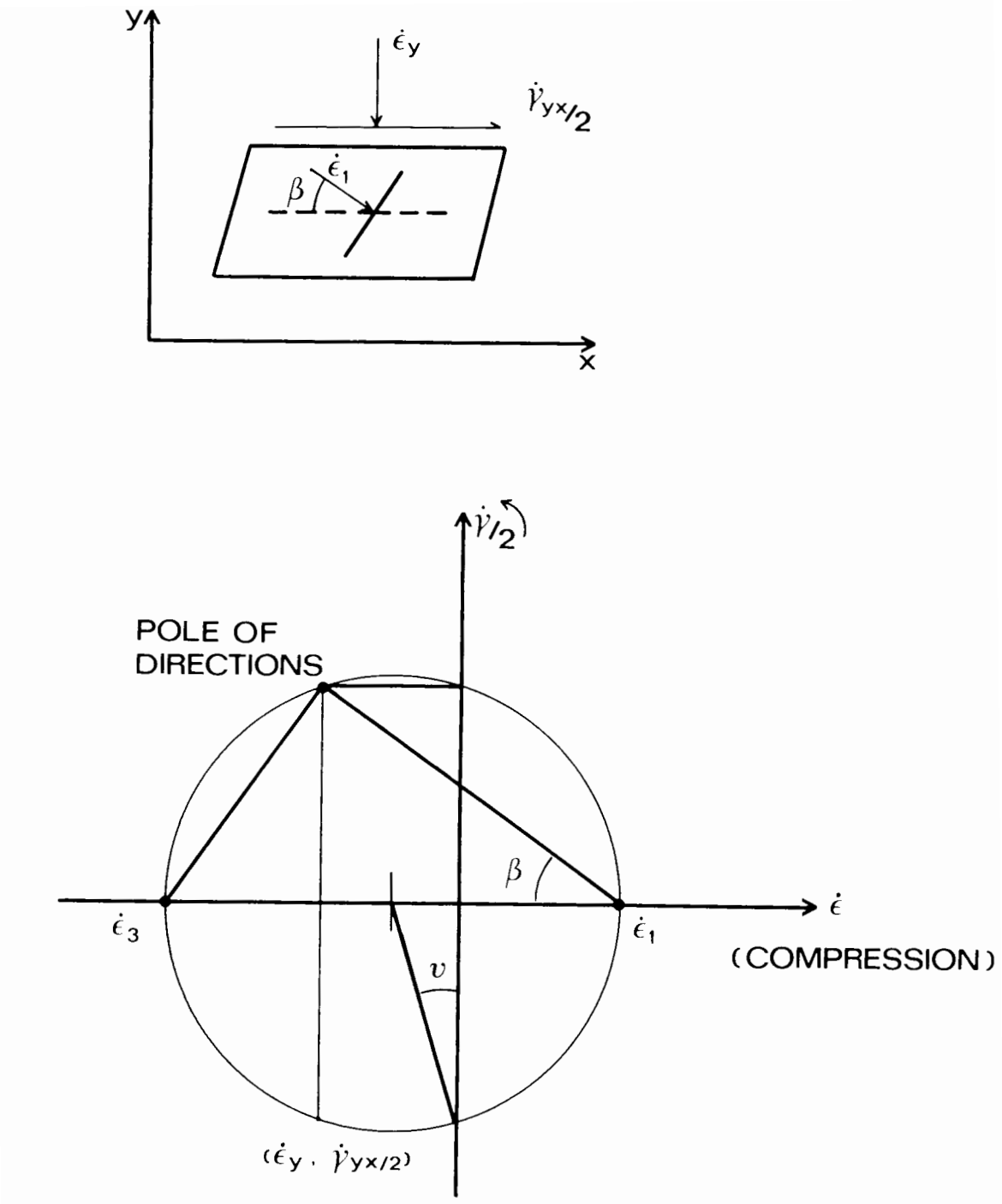


Fig. 4.2 Mohr's circle of strain increment : terminology and sign convention

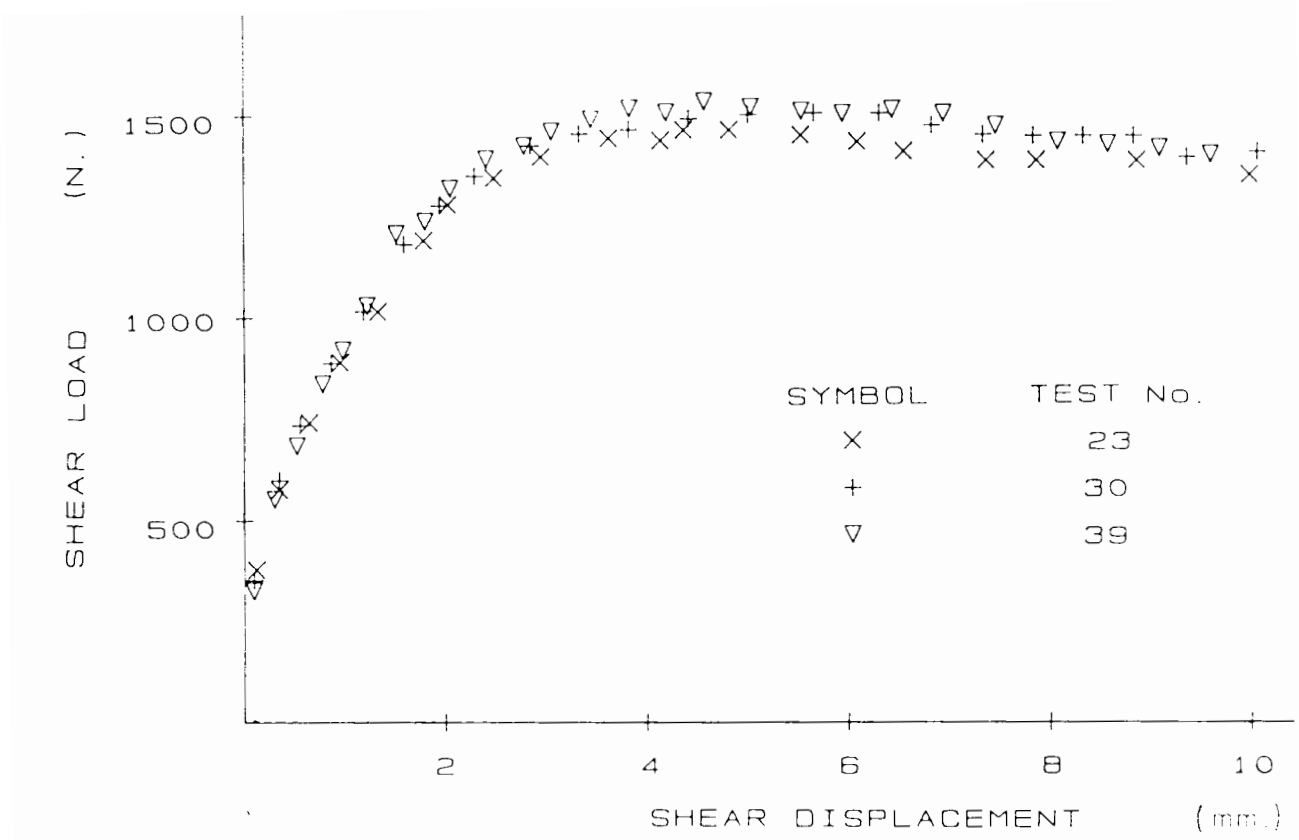


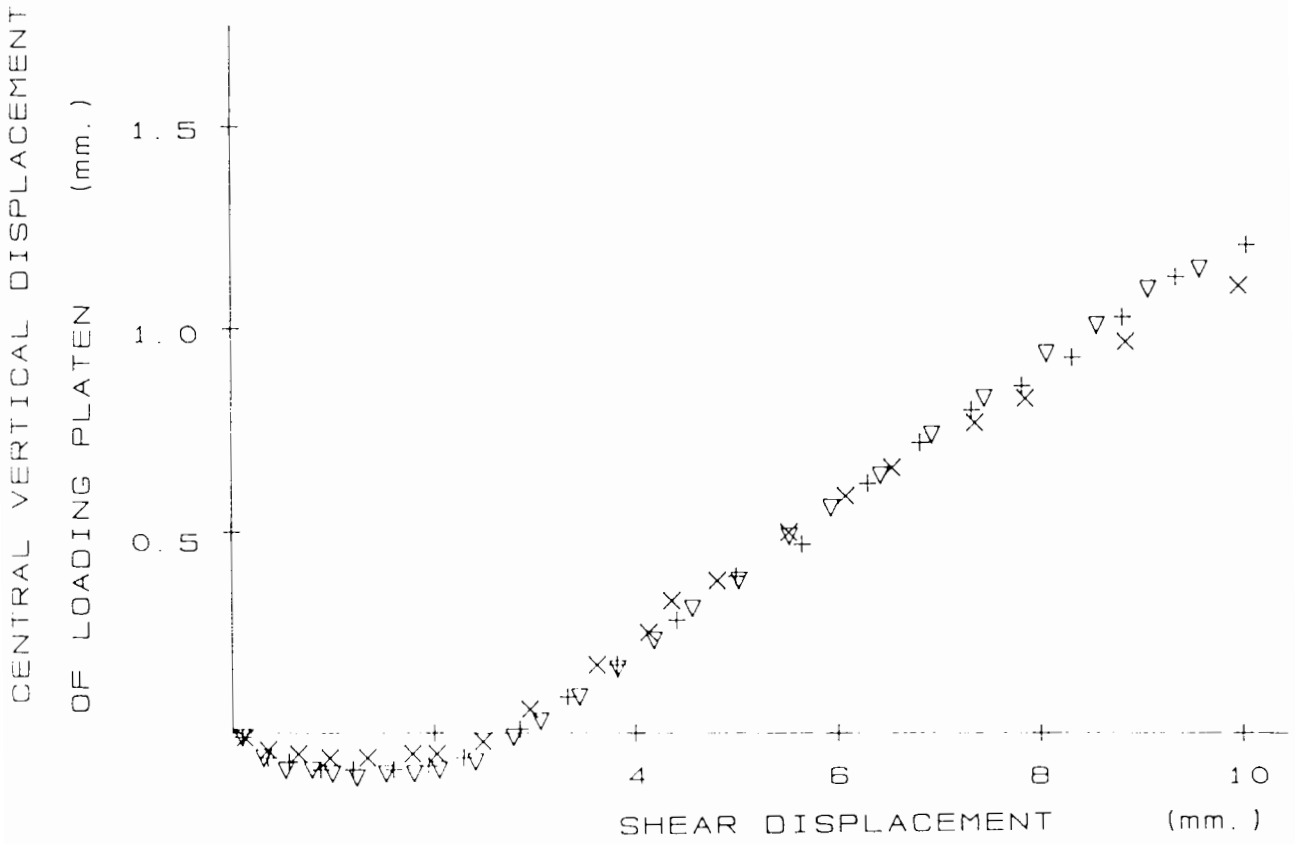


Fig. 4.3 Boundary measurements for direct shear tests on crushed glass

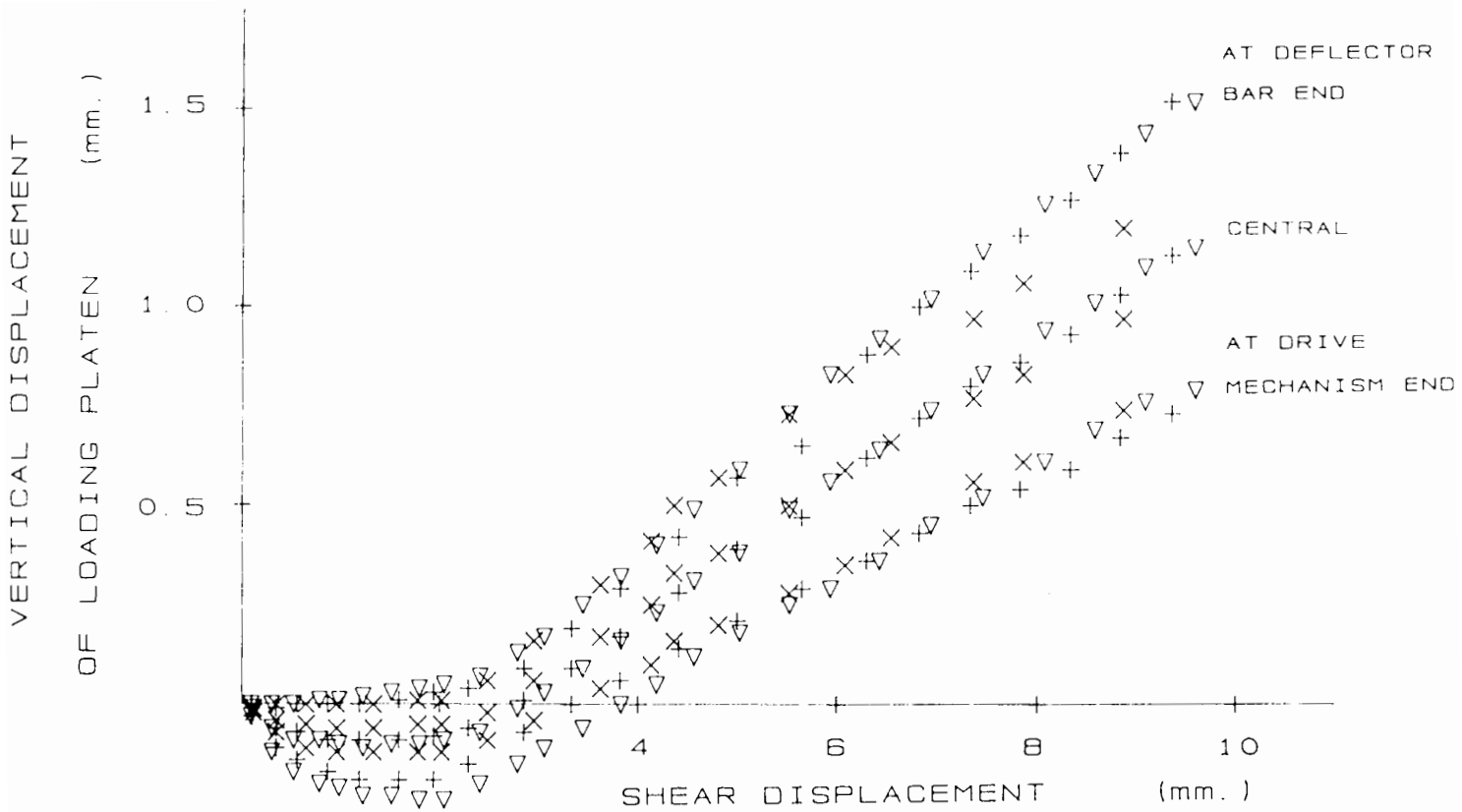


Fig. 4.4 Variation of vertical displacement along the loading platen in direct shear tests on crushed glass

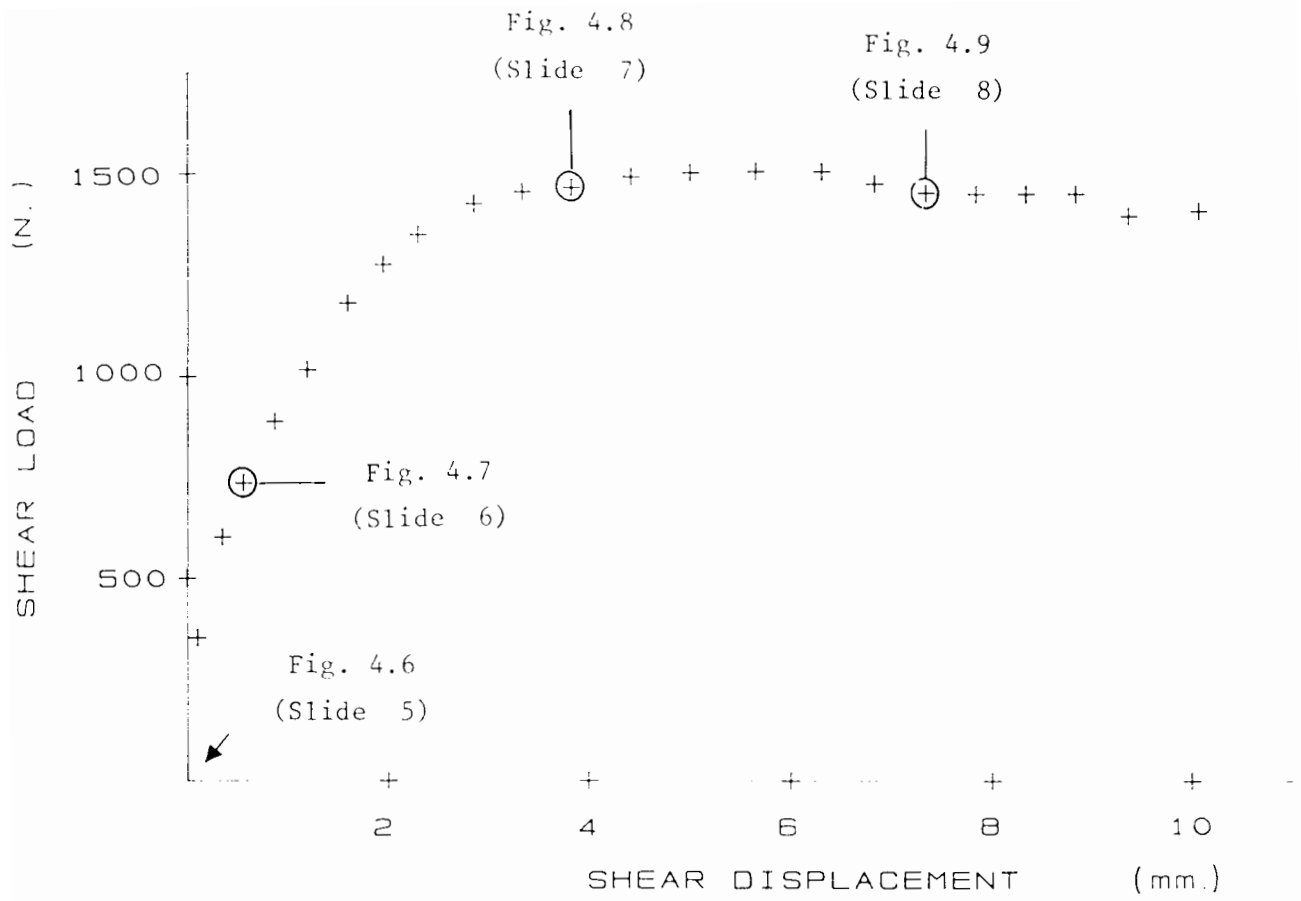


Fig. 4.5 Stages during direct shear test no. 30 on crushed glass corresponding to the light stripes shown in the figures indicated

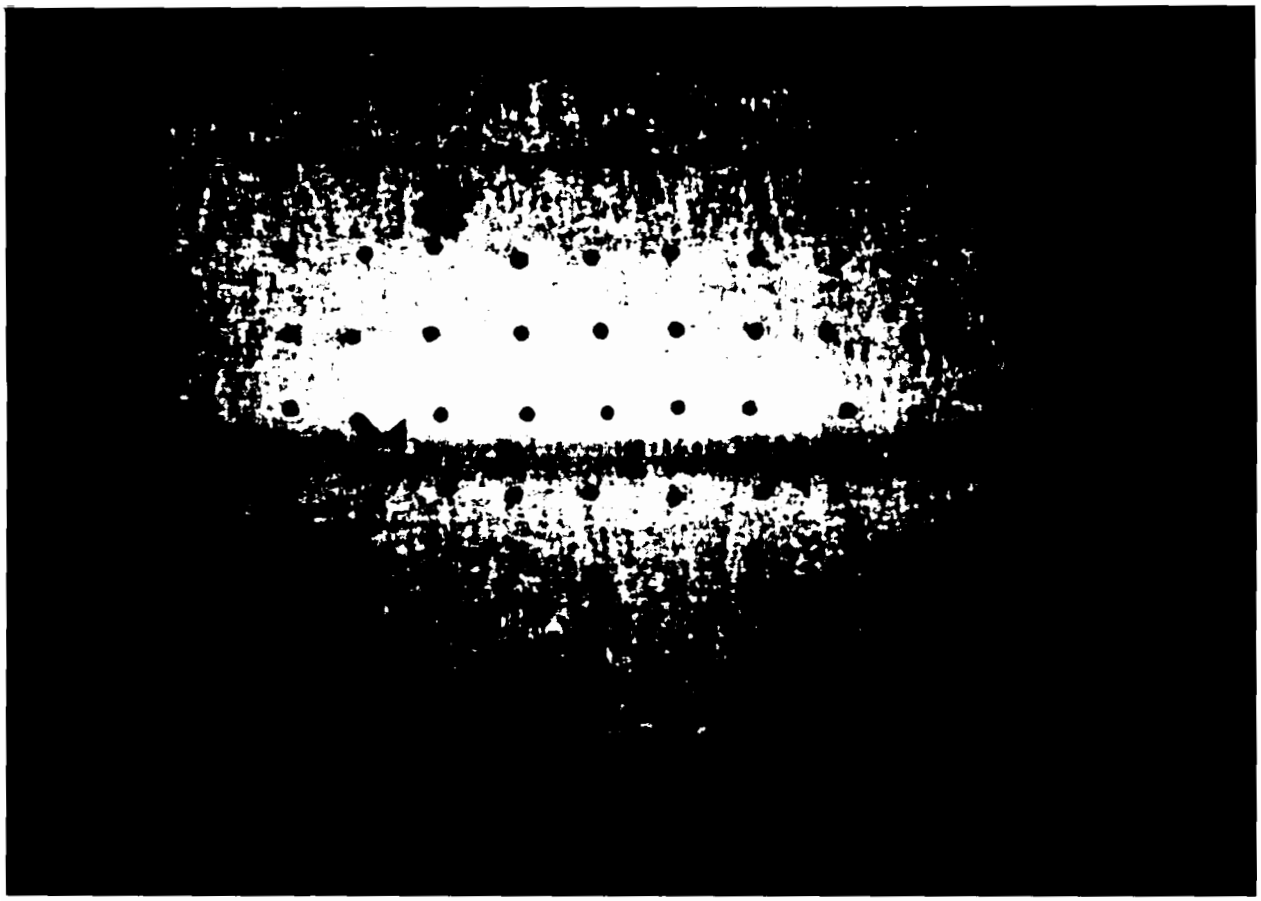

Fig. 4.6 Light stripes observed at the start of direct shear test no. 30 on crushed glass with only vertical load applied

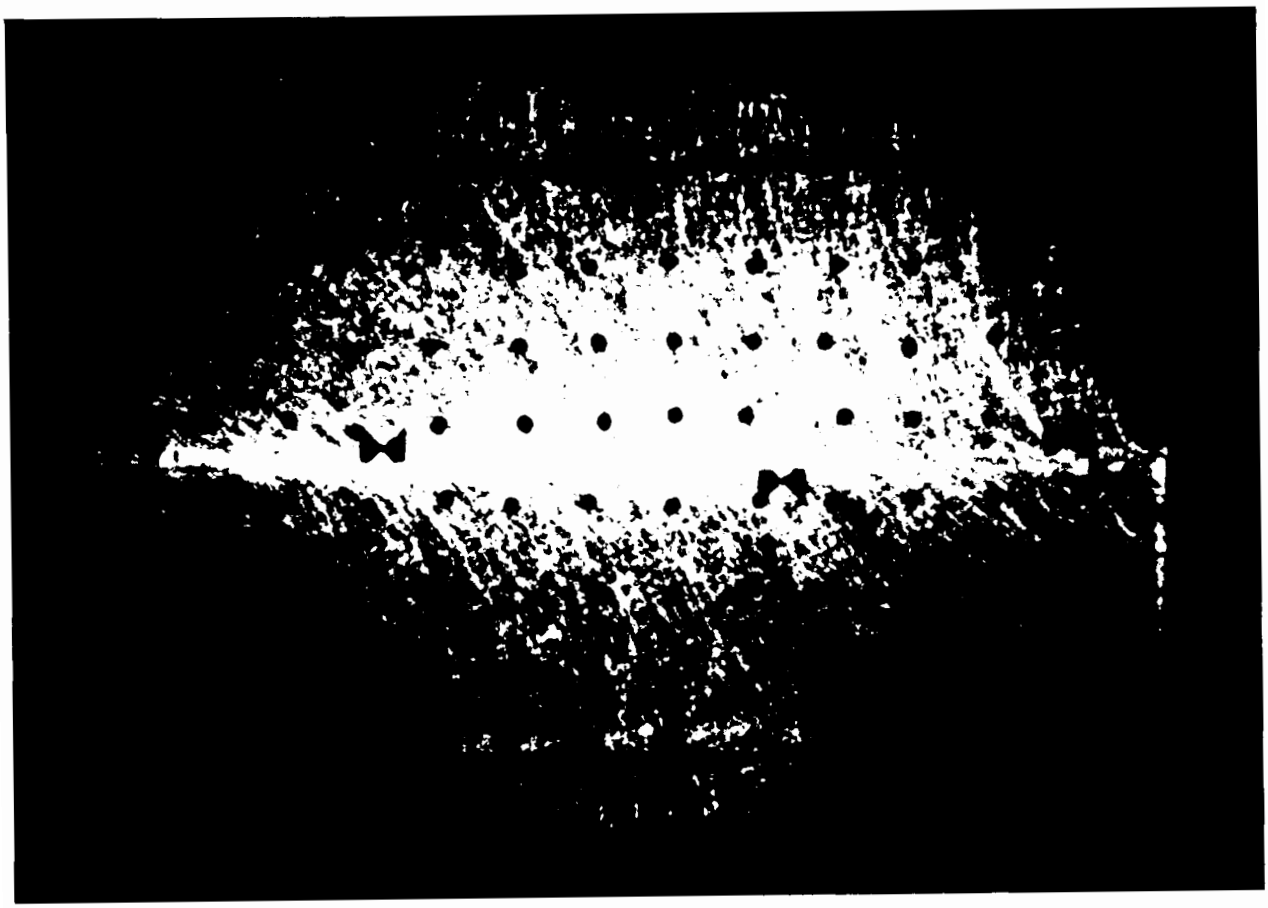

Fig. 4.7 Light stripes observed in direct shear test no. 30 on crushed glass after 0.56 mm shear displacement

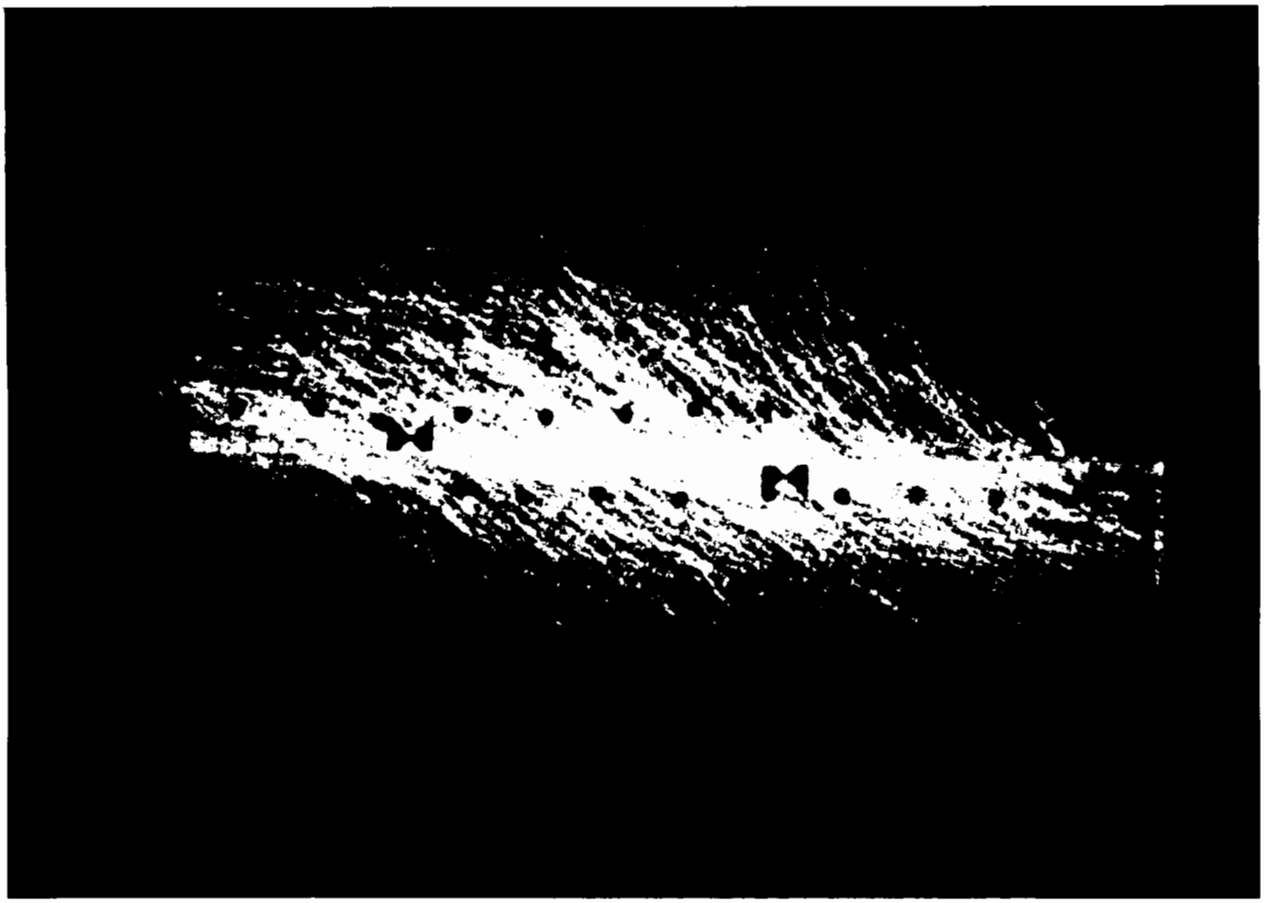

Fig. 4.8 Light stripes observed in direct shear test no. 30 on crushed glass at maximum shear load, 4.41 mm shear displacement

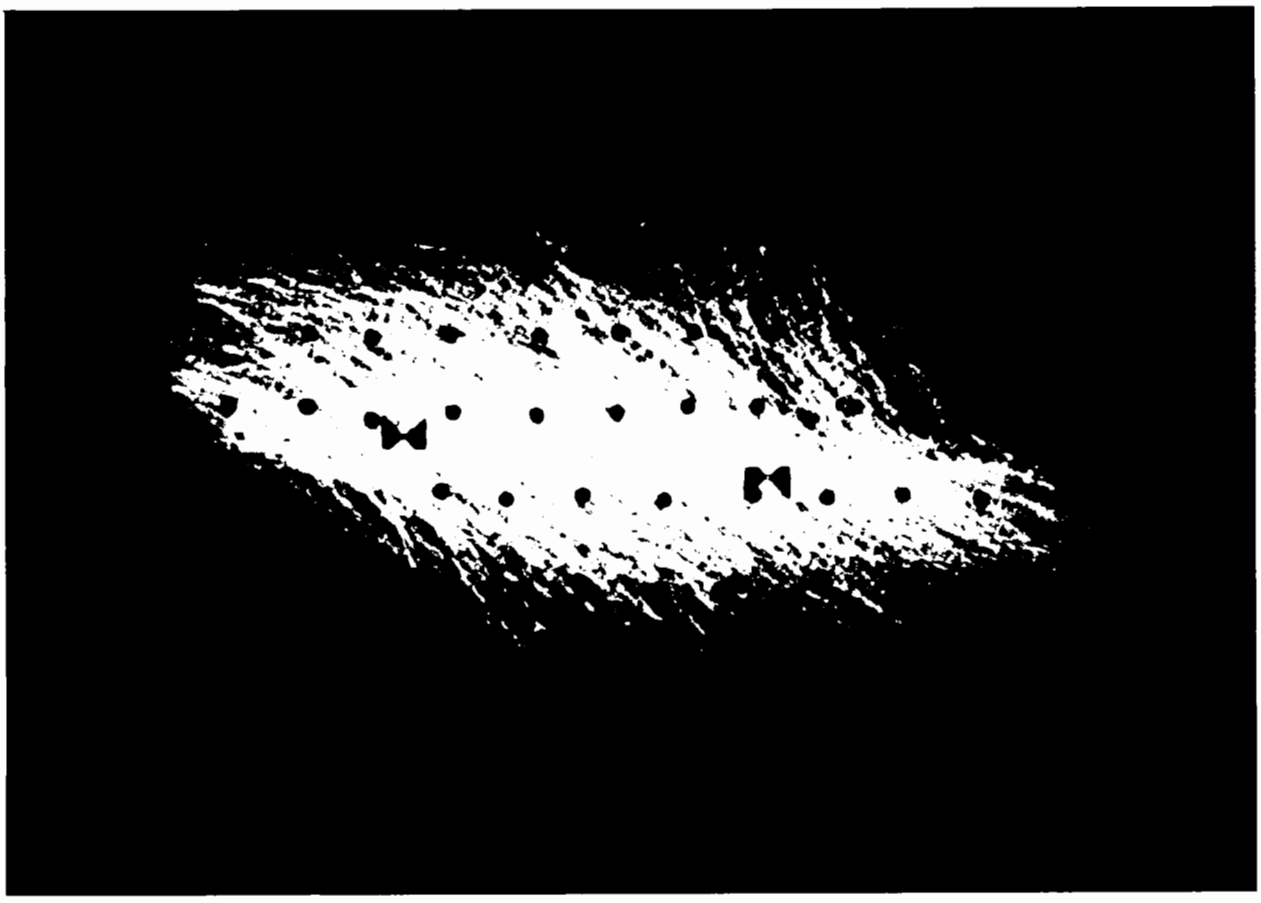

Fig. 4.9 Light stripes observed in direct shear test no. 30 on crushed glass after 7.33 mm shear displacement

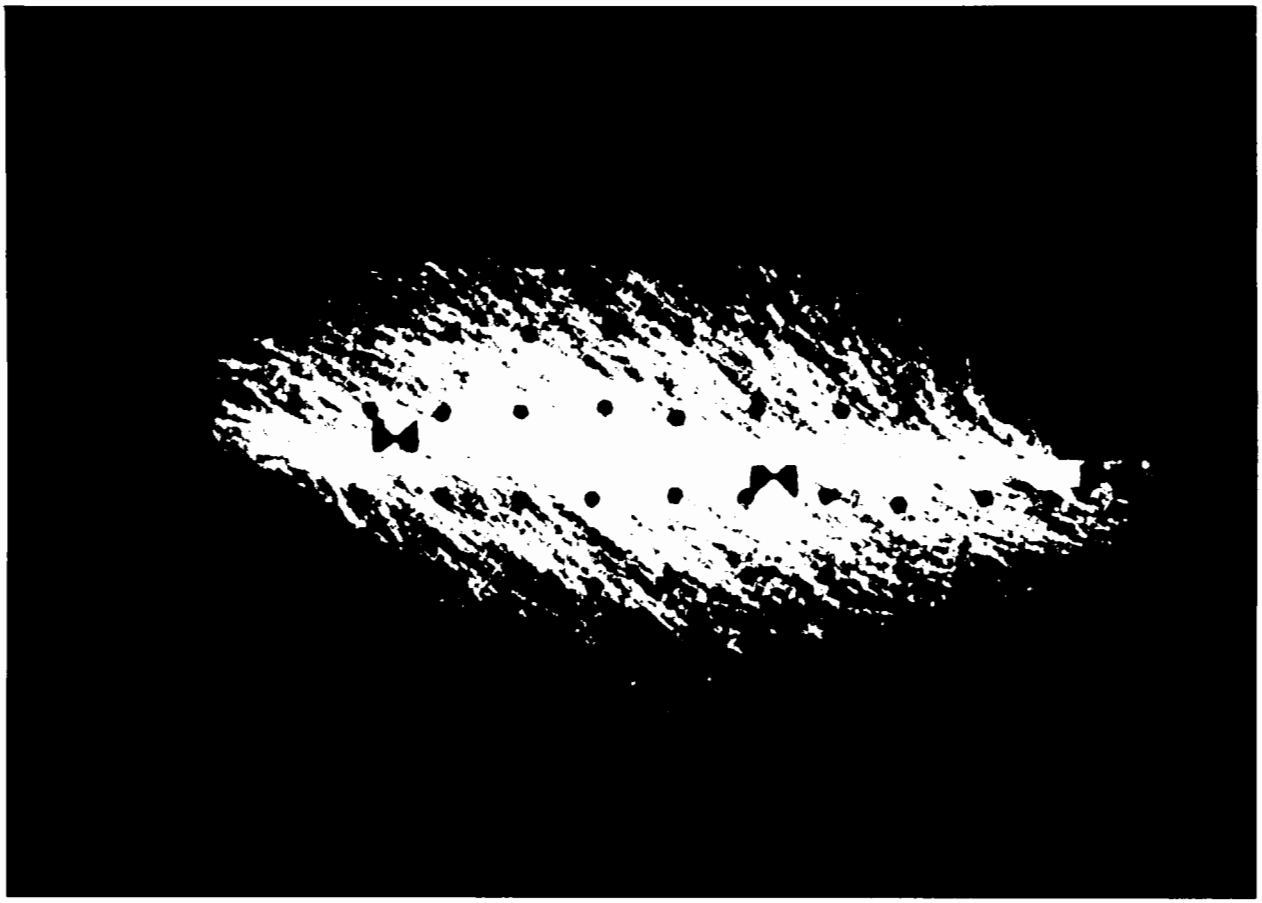

Fig. 4.10 Light stripes observed in direct shear test no. 23 on crushed glass at maximum shear load, 4.13 mm shear displacement

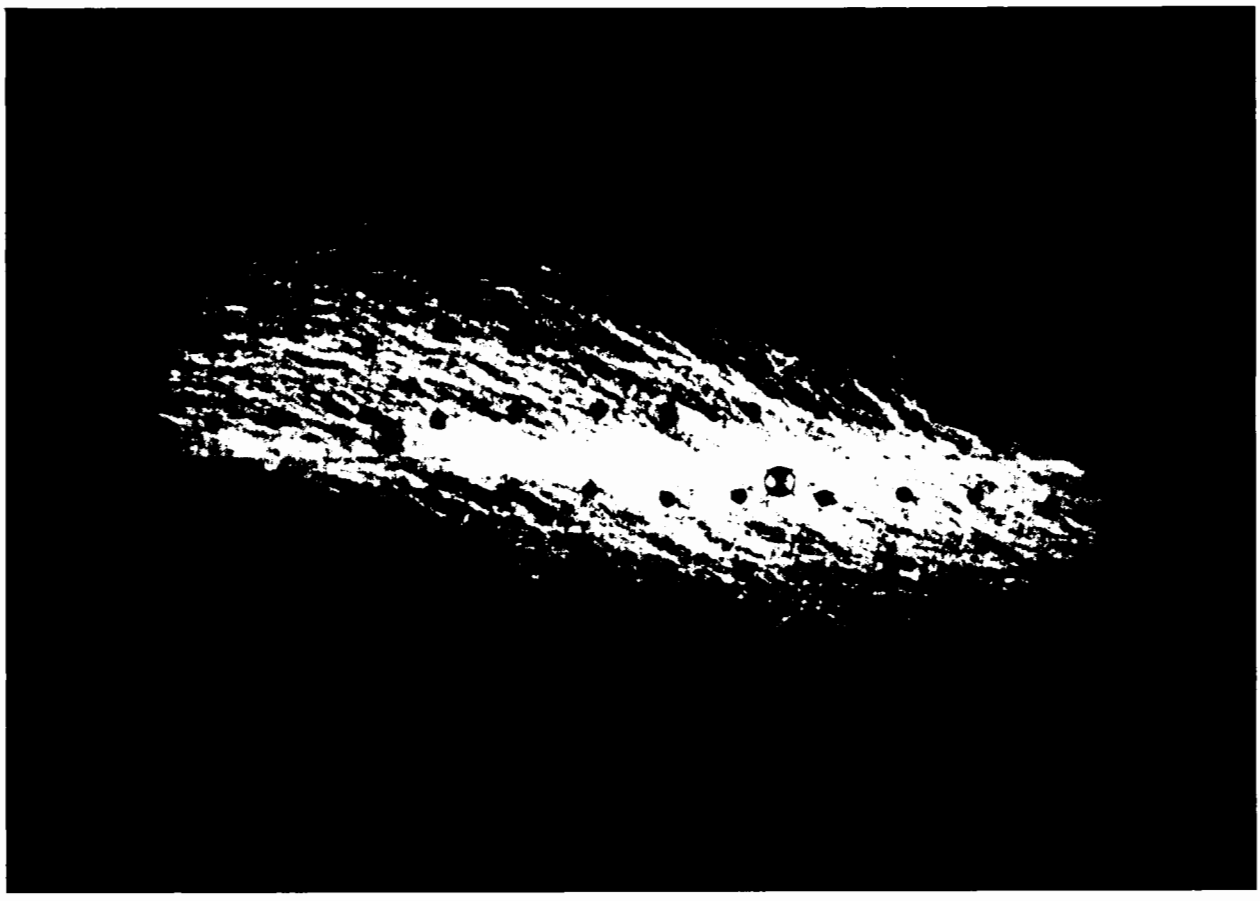

Fig. 4.11 Light stripes observed in direct shear test no. 39 on crushed glass at maximum shear, 4.20 mm shear displacement

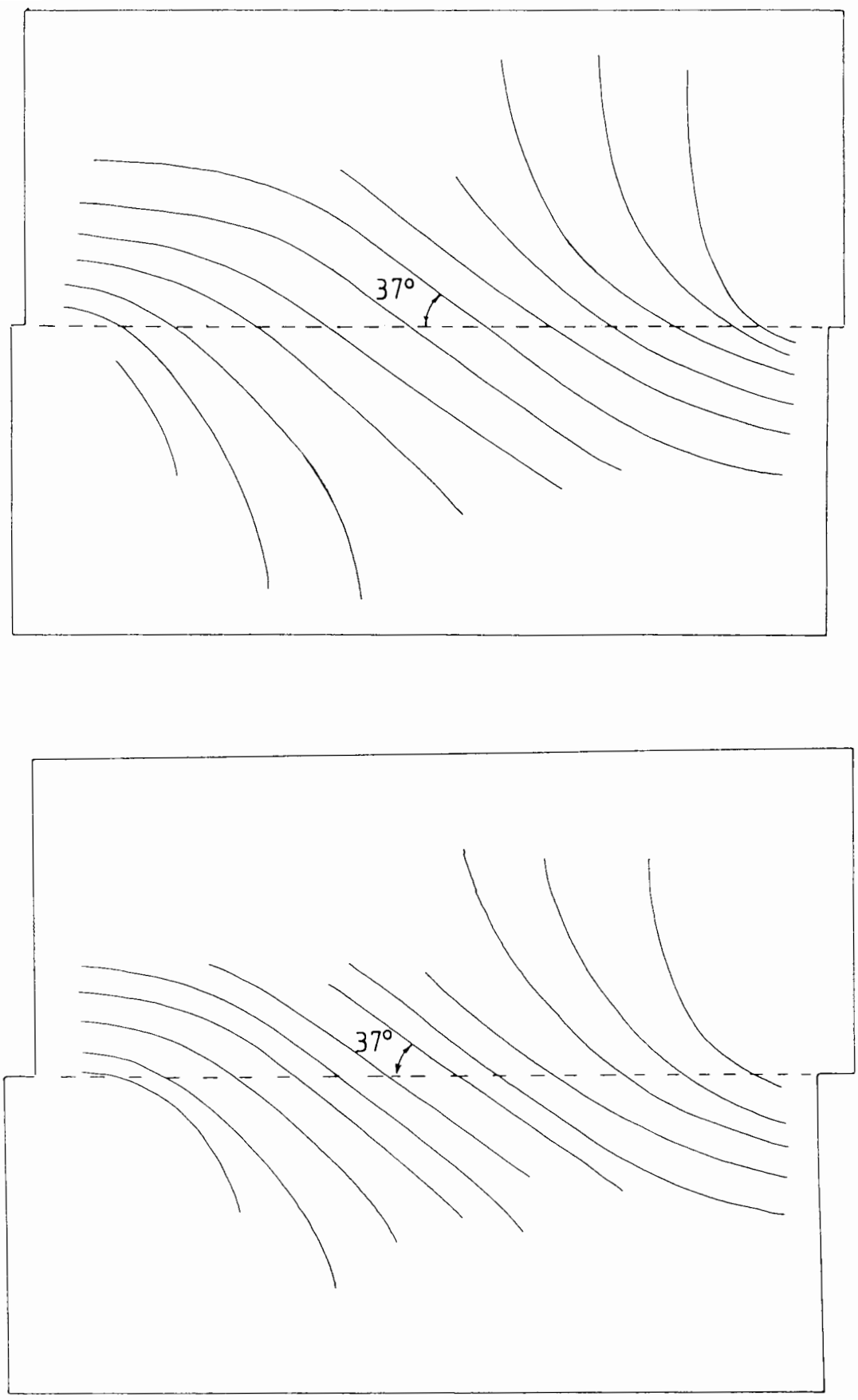


Fig. 4.12 Major principal stress trajectories drawn from light stripes observed in direct shear test no. 30 a) at maximum shear load (fig. 4.8) and b) after 7.33 mm shear displacement (fig.4.9)

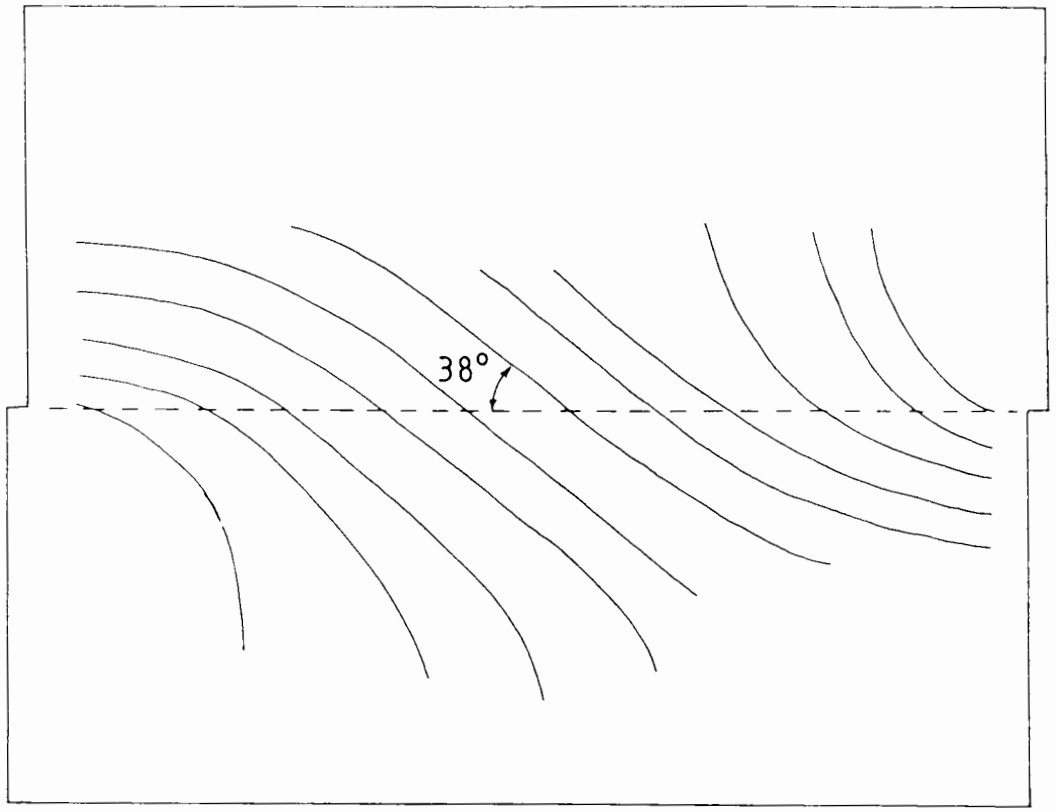


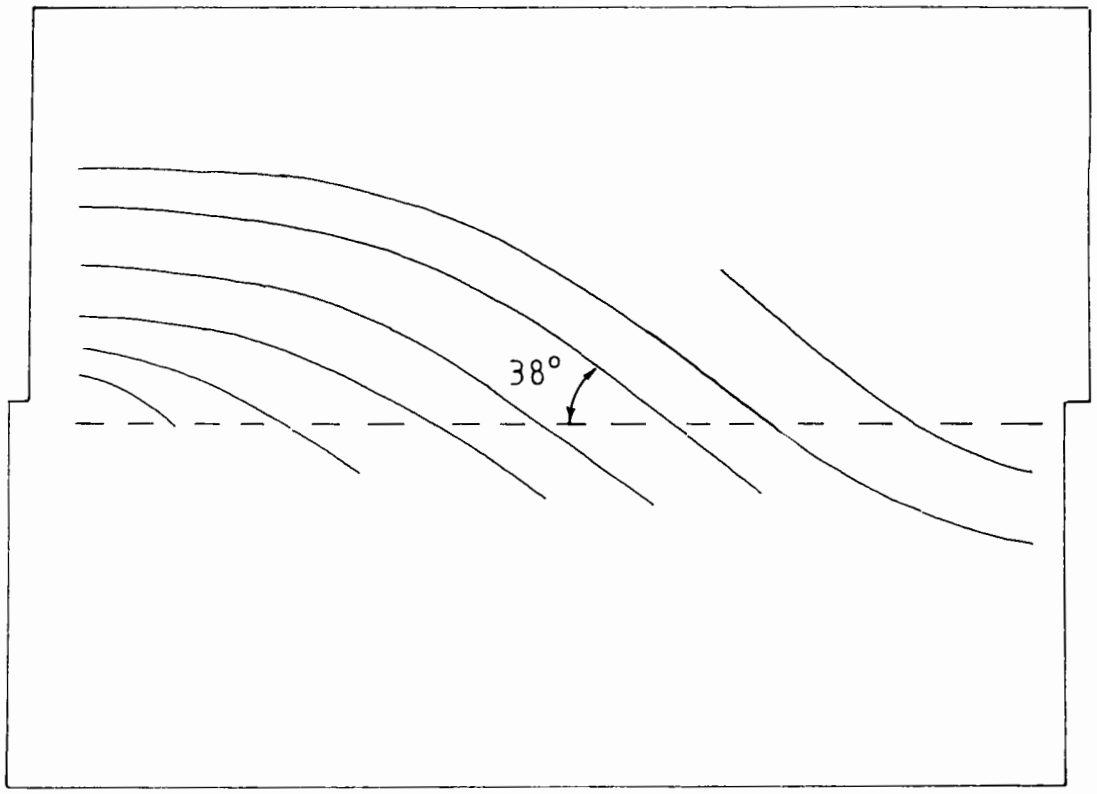


Fig. 4.13 Major principal stress trajectories drawn from light stripes observed at maximum shear load in direct shear test a) no. 23 (fig. 4.10) and b) no. 39 (fig. 4.11)

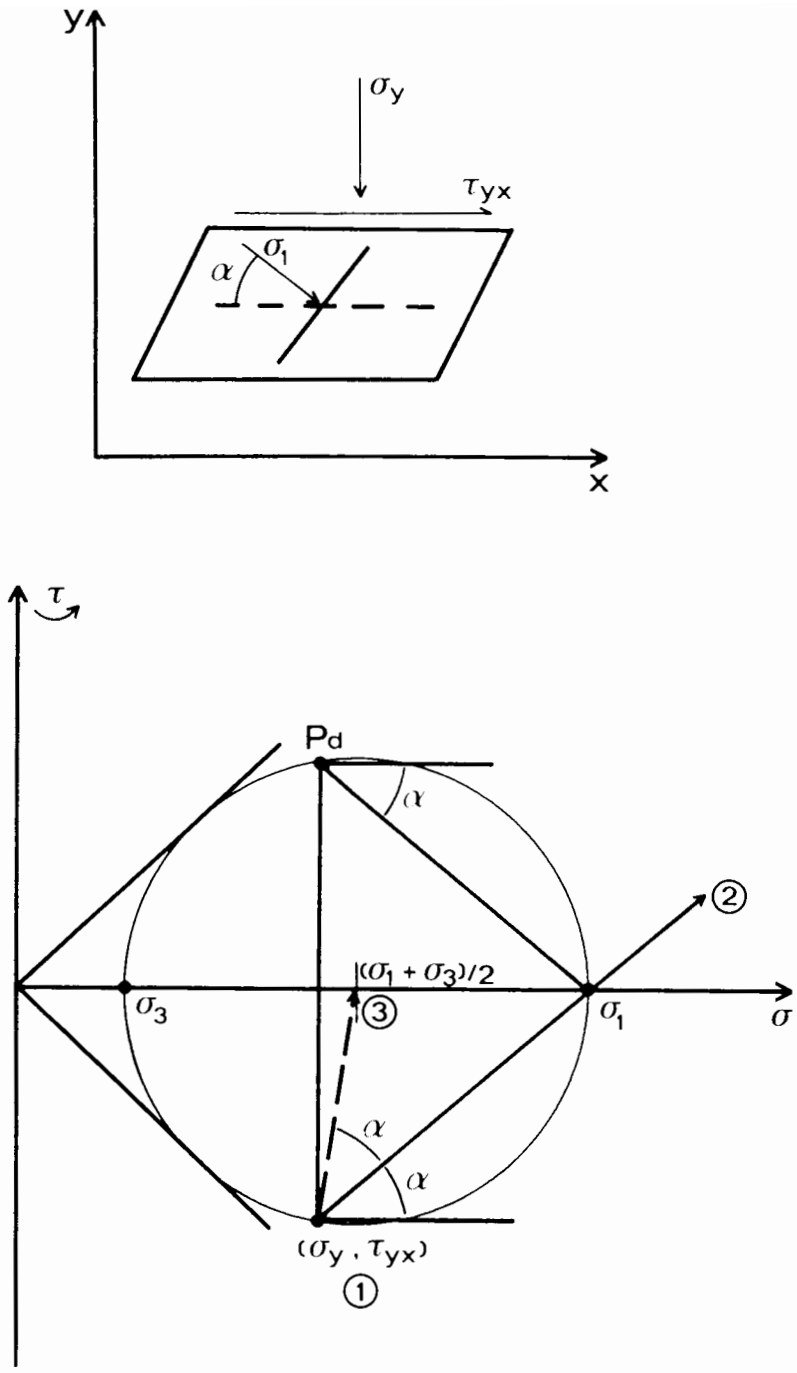


Fig. 4.14 Method for constructing Mohr's circle of stress from average shear and normal stresses along the central plane of the shearbox and the inclination of major principal stress trajectory to the central plane

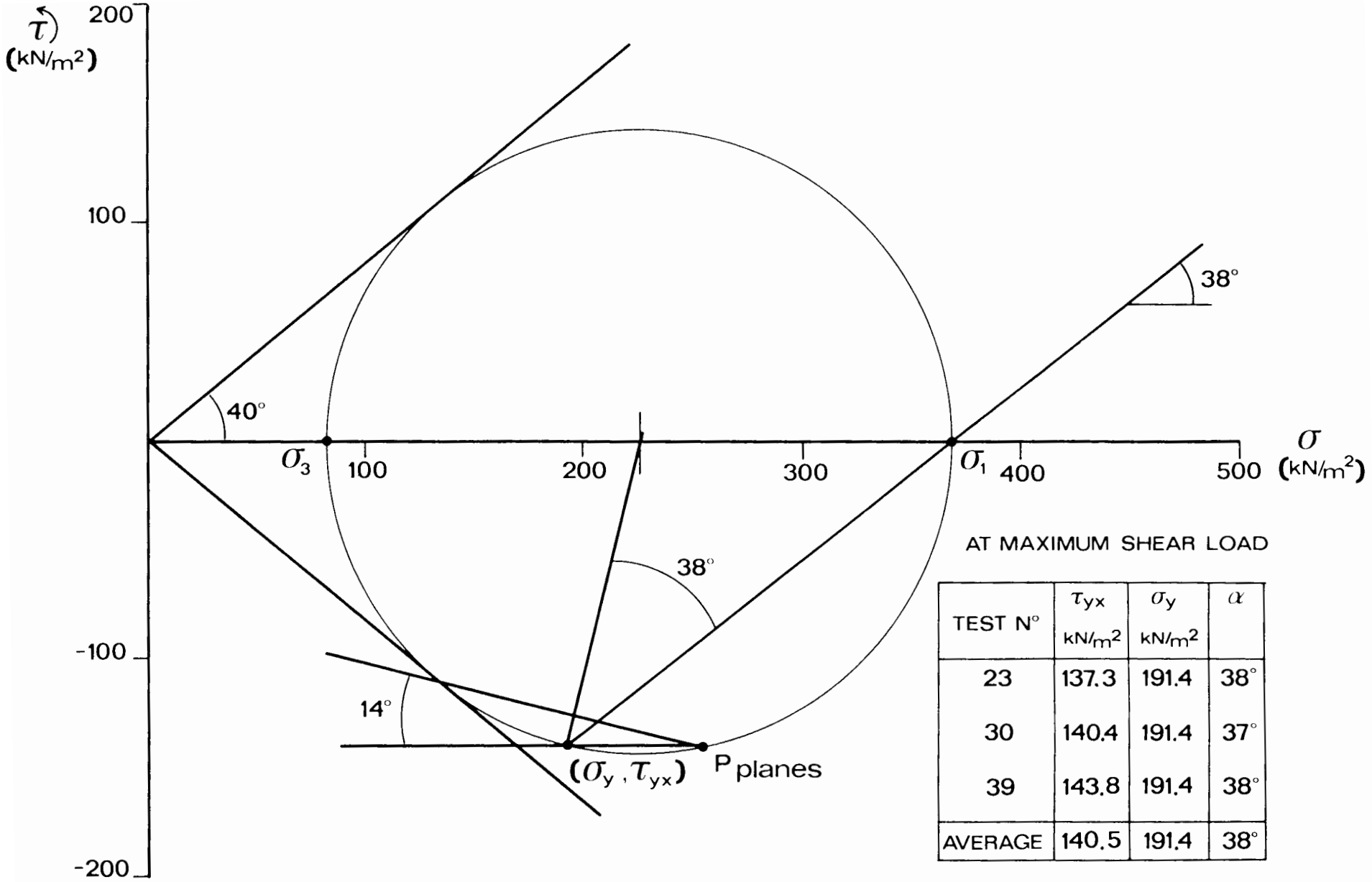


AT MAXIMUM SHEAR LOAD

| TEST N° | $\tau_{yx}$ kN/m² | $\sigma_y$ kN/m² | $\alpha$ |
|---|---|---|---|
| 23 | 137.3 | 191.4 | 38° |
| 30 | 140.4 | 191.4 | 37° |
| 39 | 143.8 | 191.4 | 38° |
| AVERAGE | 140.5 | 191.4 | 38° |

Fig. 4.15 Mohr's circle of stress for average boundary stresses and inclination of major principal stress trajectories at maximum shear load in the three direct shear tests on crushed glass

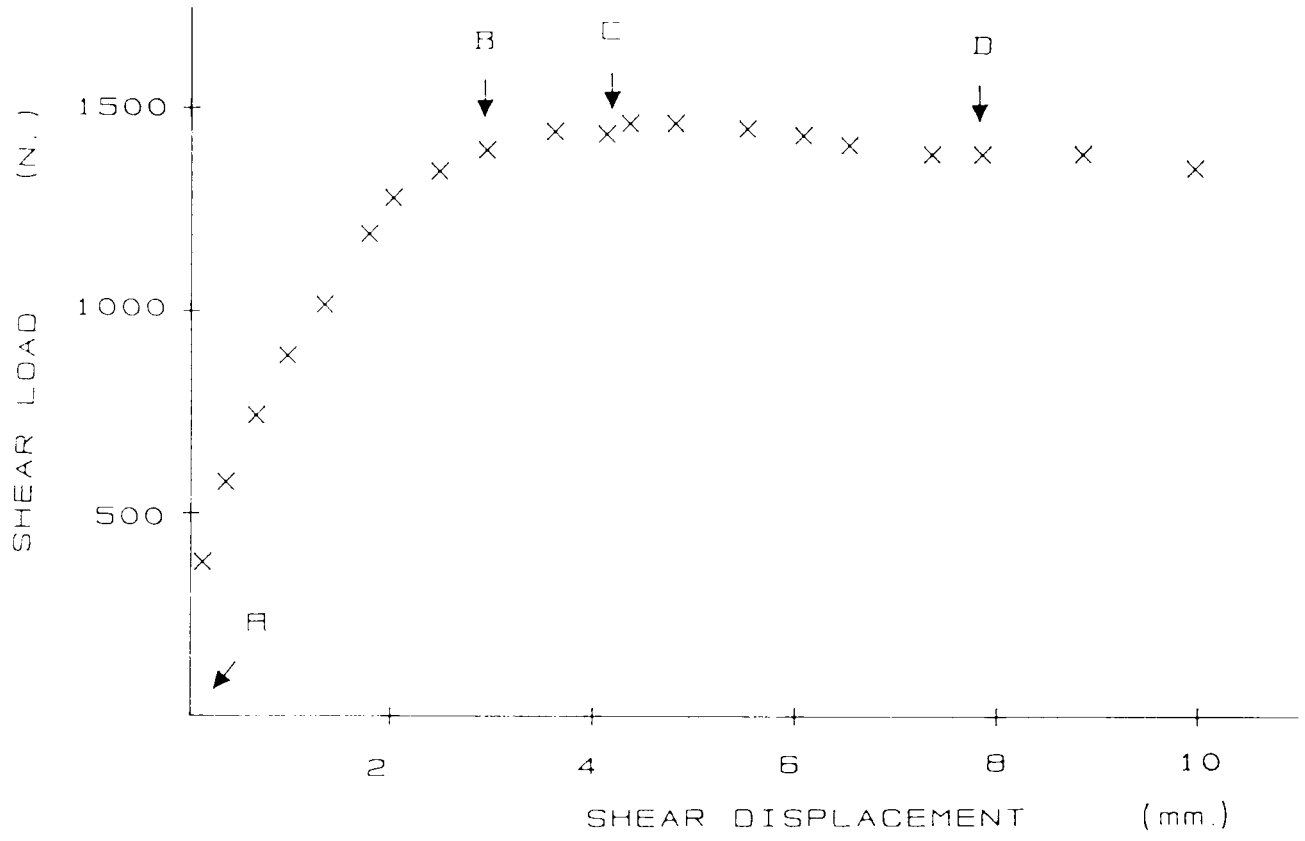


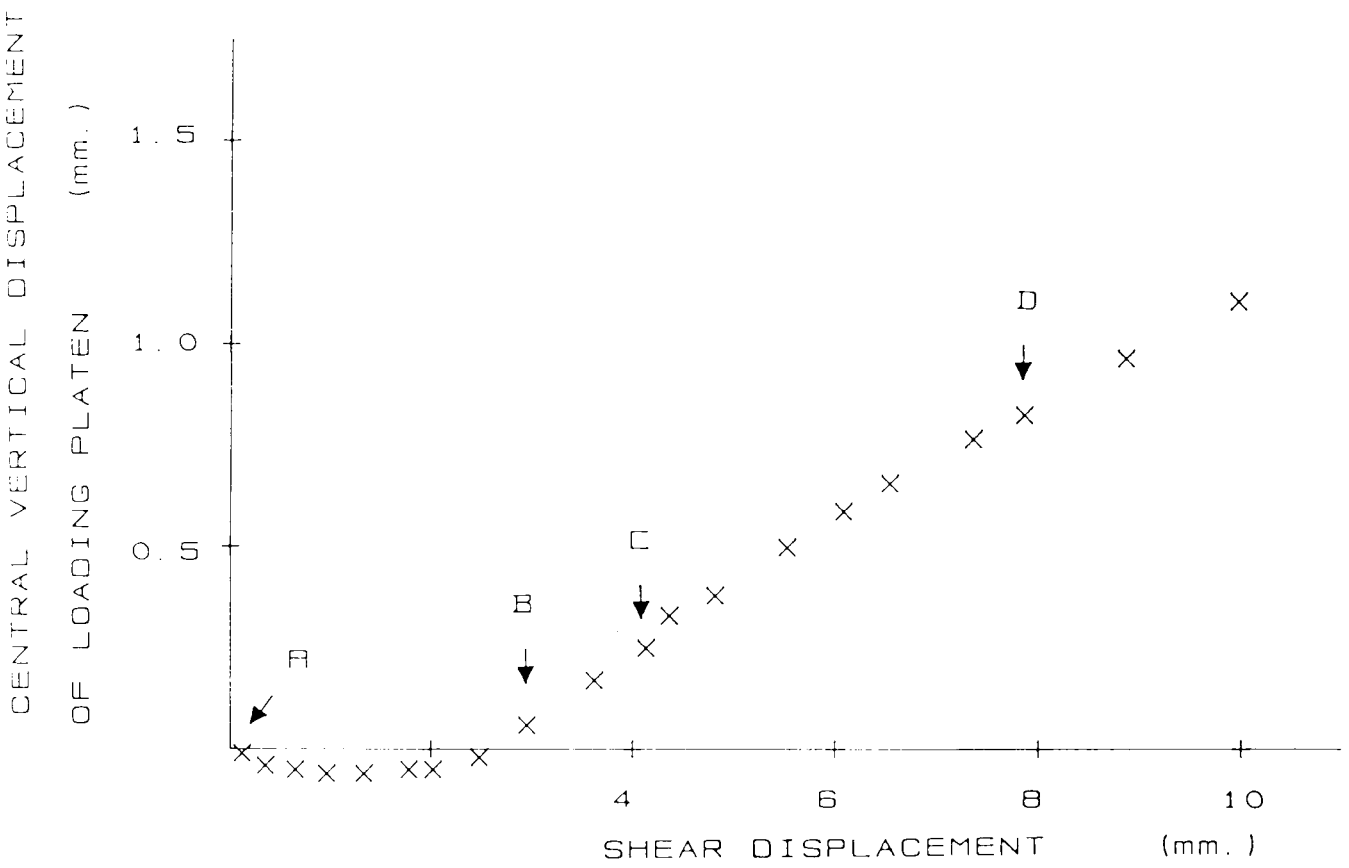


Fig. 4.16 Stages A to B and C to D in direct shear test no. 23 corresponding to the patterns of strains shown in figs. 4.18 and 4.19

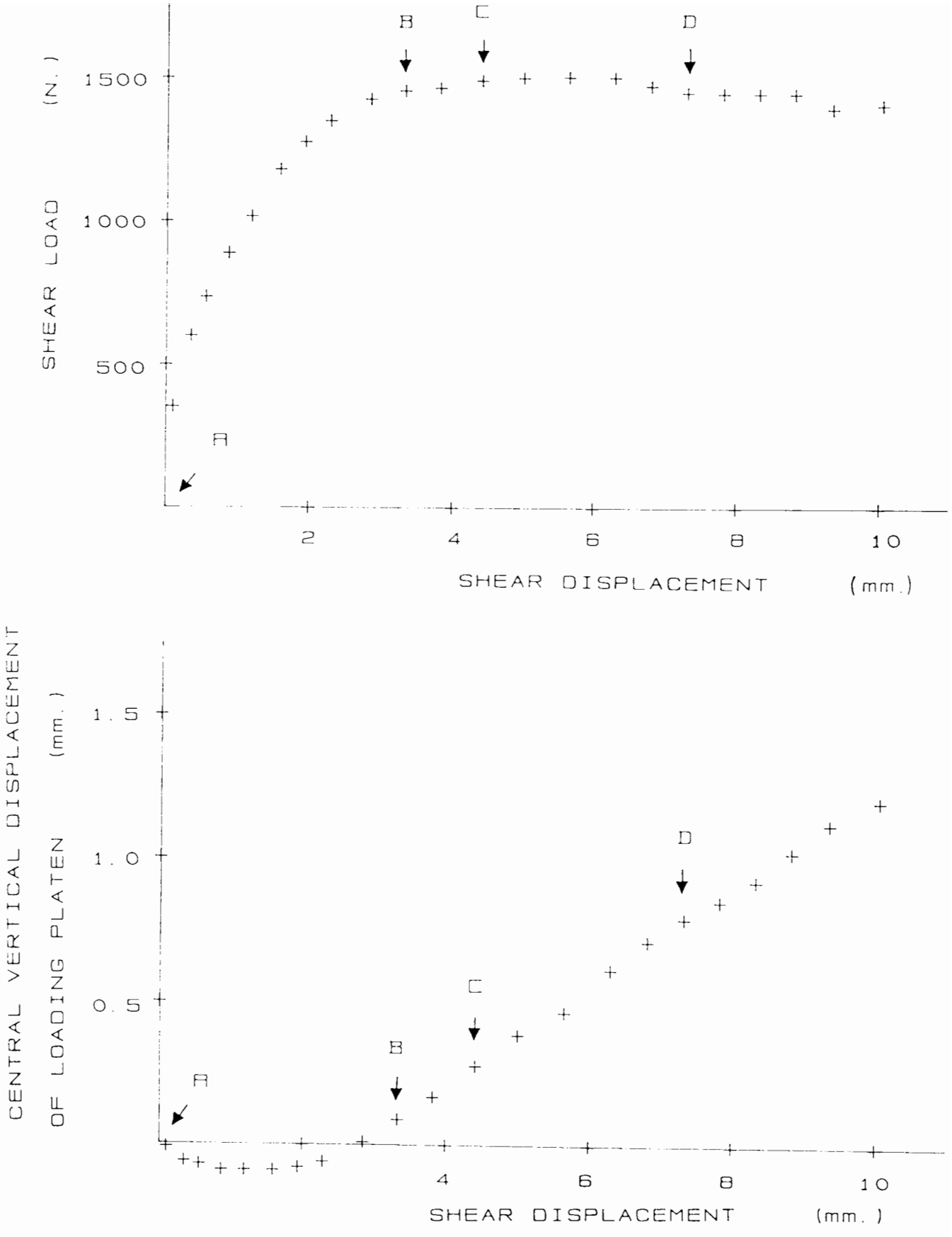


Fig. 4.17 Stages A to B and C to D in direct shear test no. 30 corresponding to the patterns of strains in figs. 4.20 and 4.21

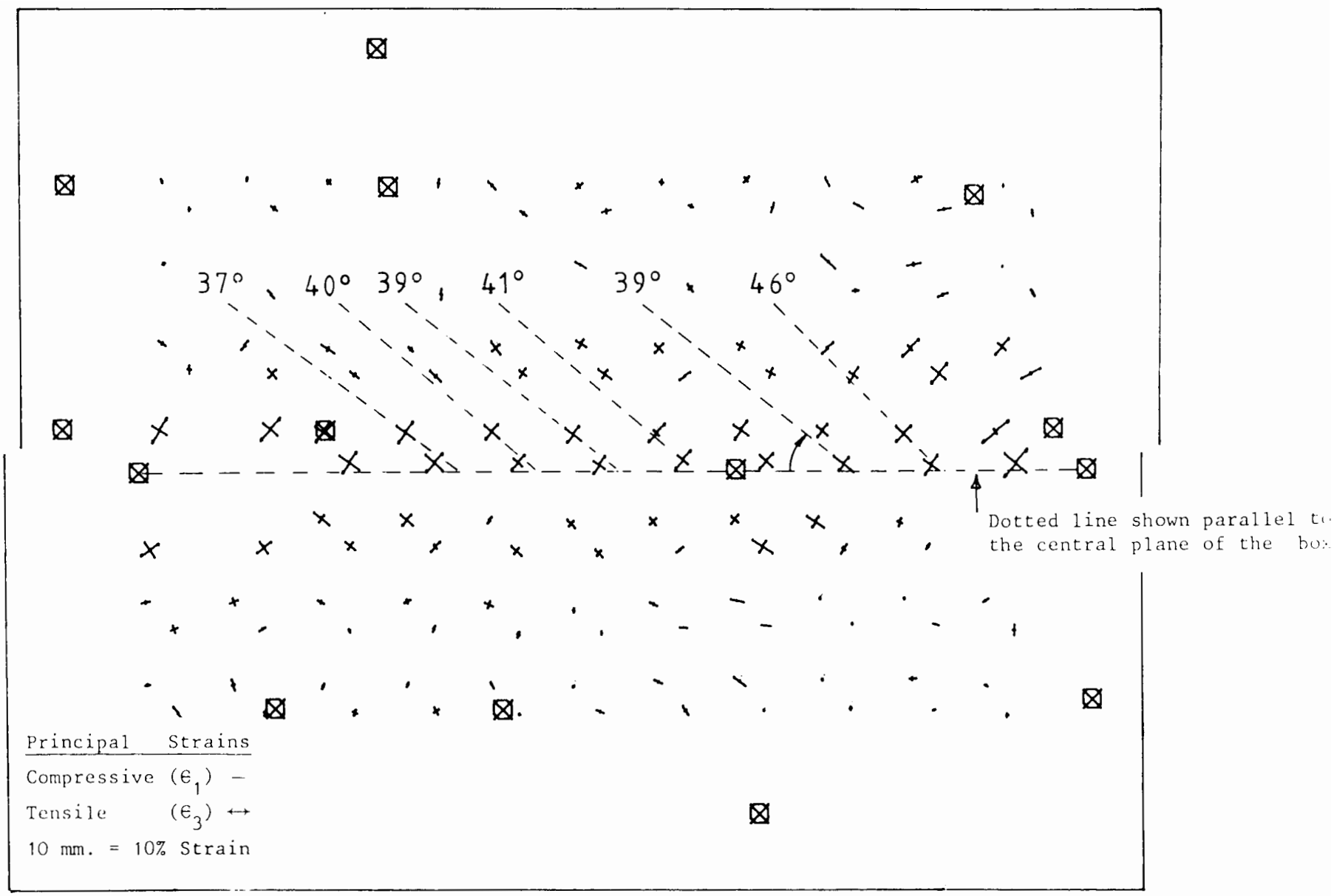


Fig. 4.18 Strains determined in direct shear test no. 23 between stages A to B before maximum shear load — with the inclination of major principal strains to the central plane shown

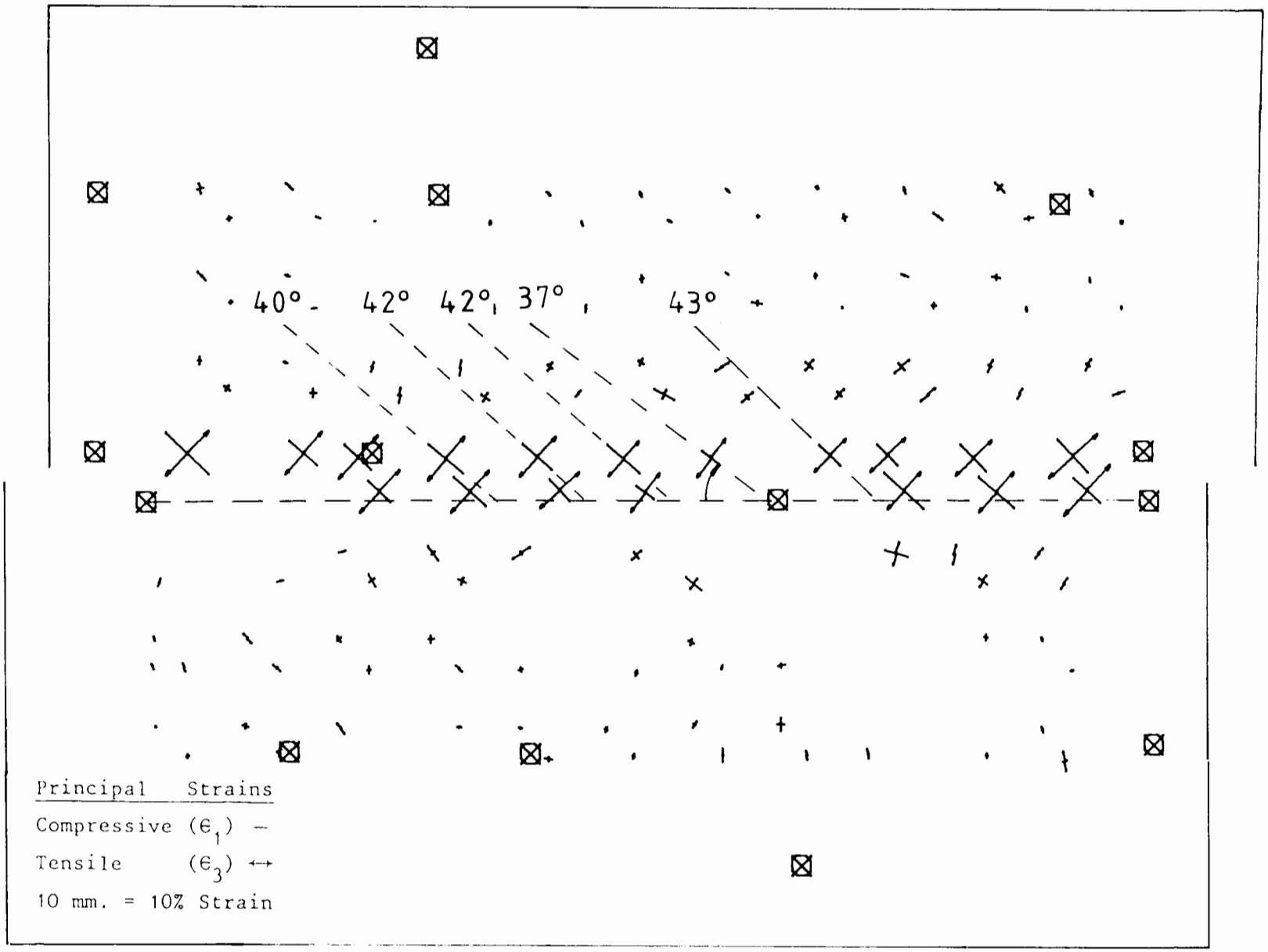


| $\dot{\epsilon}_1$ | $\dot{\epsilon}_3$ |
|---|---|
| 5 | - 8½ |
| 5 | - 8 |
| 4 | - 8 |
| 4 | - 8 |
| 7½ | - 8 |
| 5 | - 9 |
| 7 | - 9½ |
| 7½ | -10 |
| 8 | -10 |
| 5½ | -10 |
| 7 | -10 |
| Average | |
| 6% | - 9% |

Fig. 4.19 Strain increments determined in direct shear test no. 23 between stages C to D after maximum shear load — with the inclination of major principal strains to the central plane shown as well as average magnitudes of principal strains away from the end walls

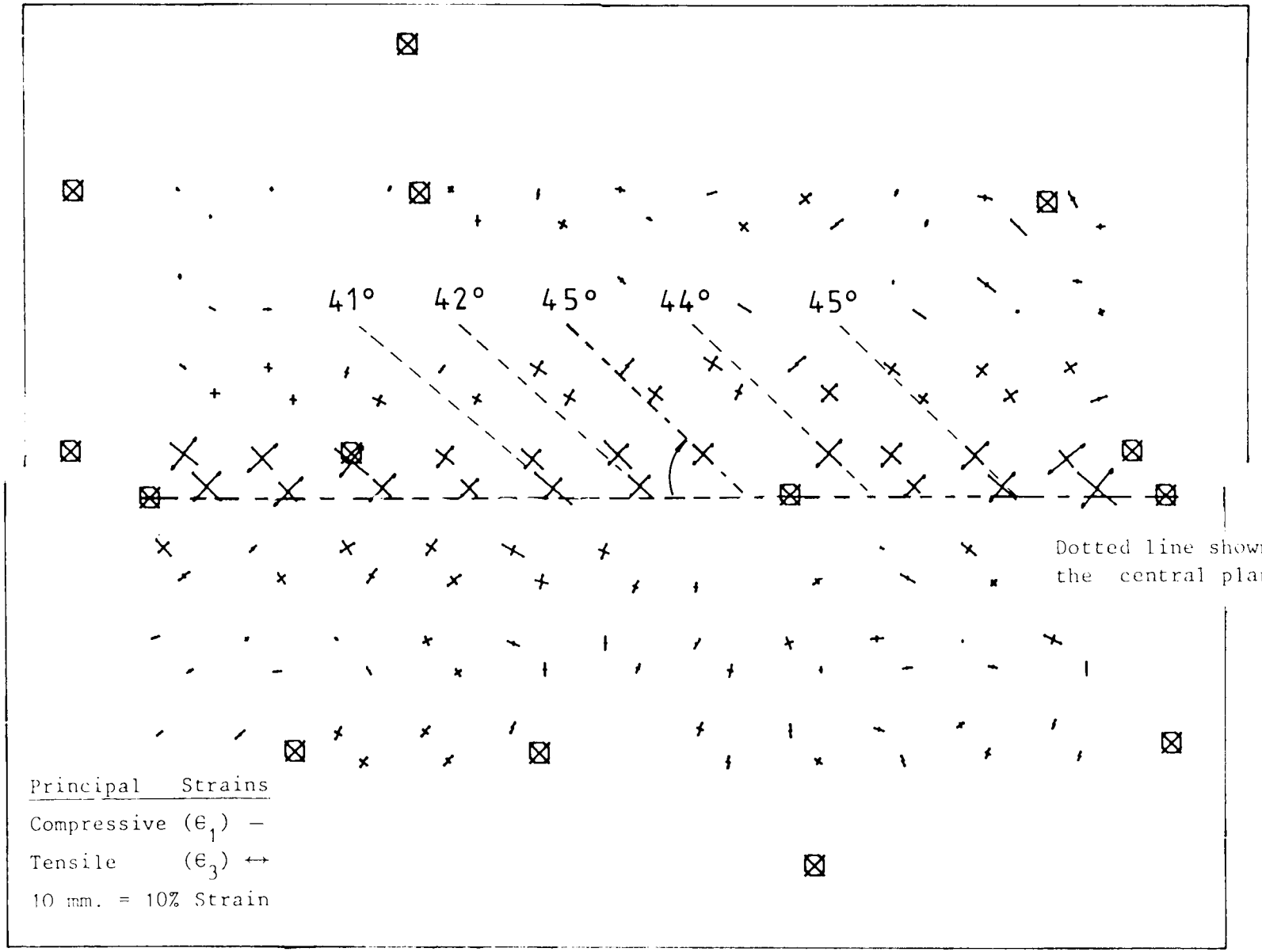


Fig. 4.20 Strains determined in direct shear test no. 30 between stages 0 to 3 before maximum shear load – with the inclination of major principal strains to the central plane shown

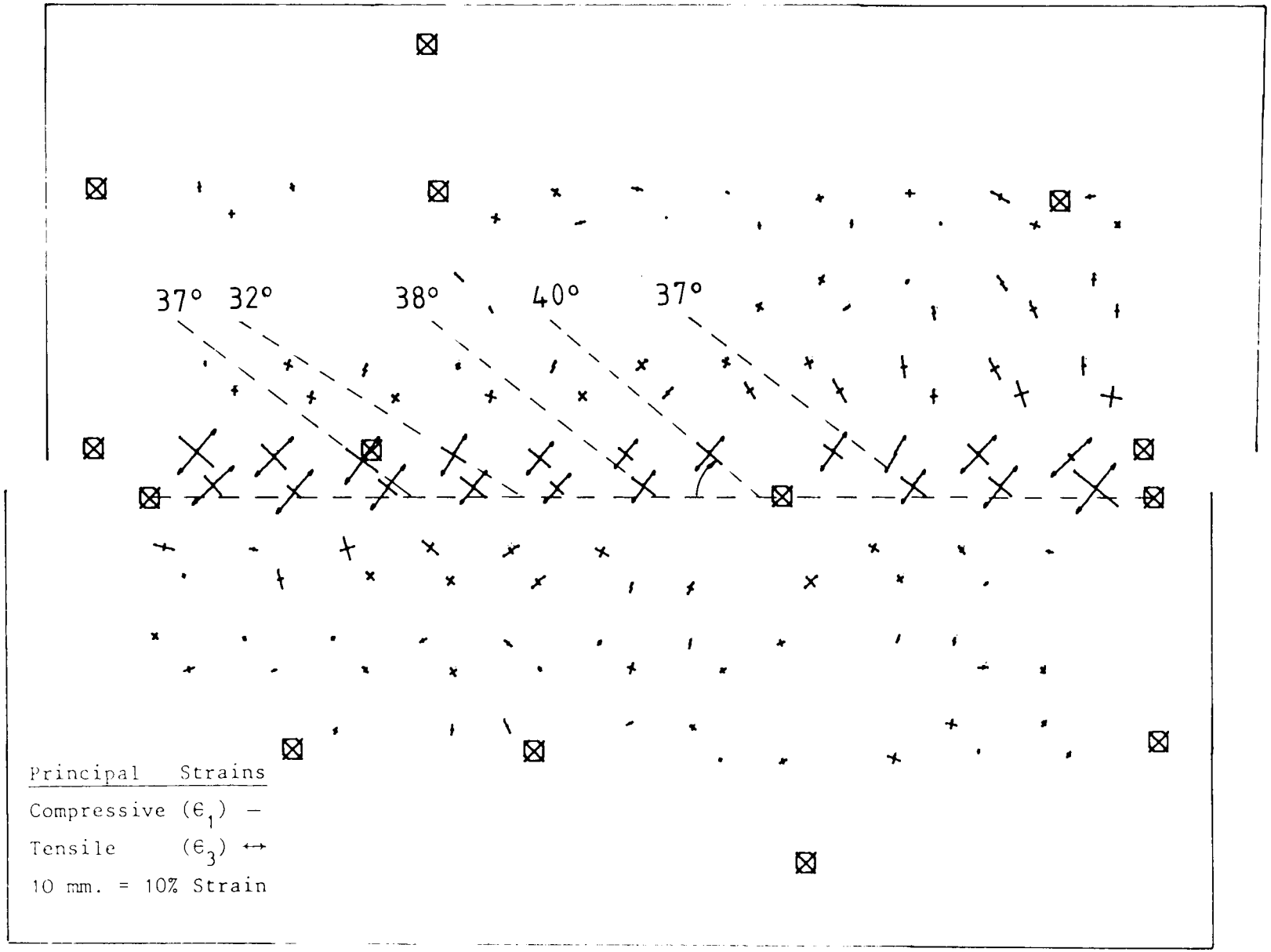


| $\dot{\epsilon}_1$ | $\dot{\epsilon}_3$ |
|---|---|
| 5 | - 7 |
| 4 | - 8 |
| $5\frac{1}{2}$ | - $7\frac{1}{2}$ |
| 5 | - $6\frac{1}{2}$ |
| 3 | - 6 |
| 3 | - 7 |
| 5 | - 7 |
| $5\frac{1}{2}$ | - 7 |
| 5 | - 8 |
| 4 | - $9\frac{1}{2}$ |
| 7 | -10 |
| Average | |
| 4.7% | - 7.6% |

Fig. 4.21 Strain increments determined in direct shear test no. 30 between stages C to D after maximum shear load — with the inclination of major principal strains to the central plane shown as well as average magnitudes of principal strains away from the end walls

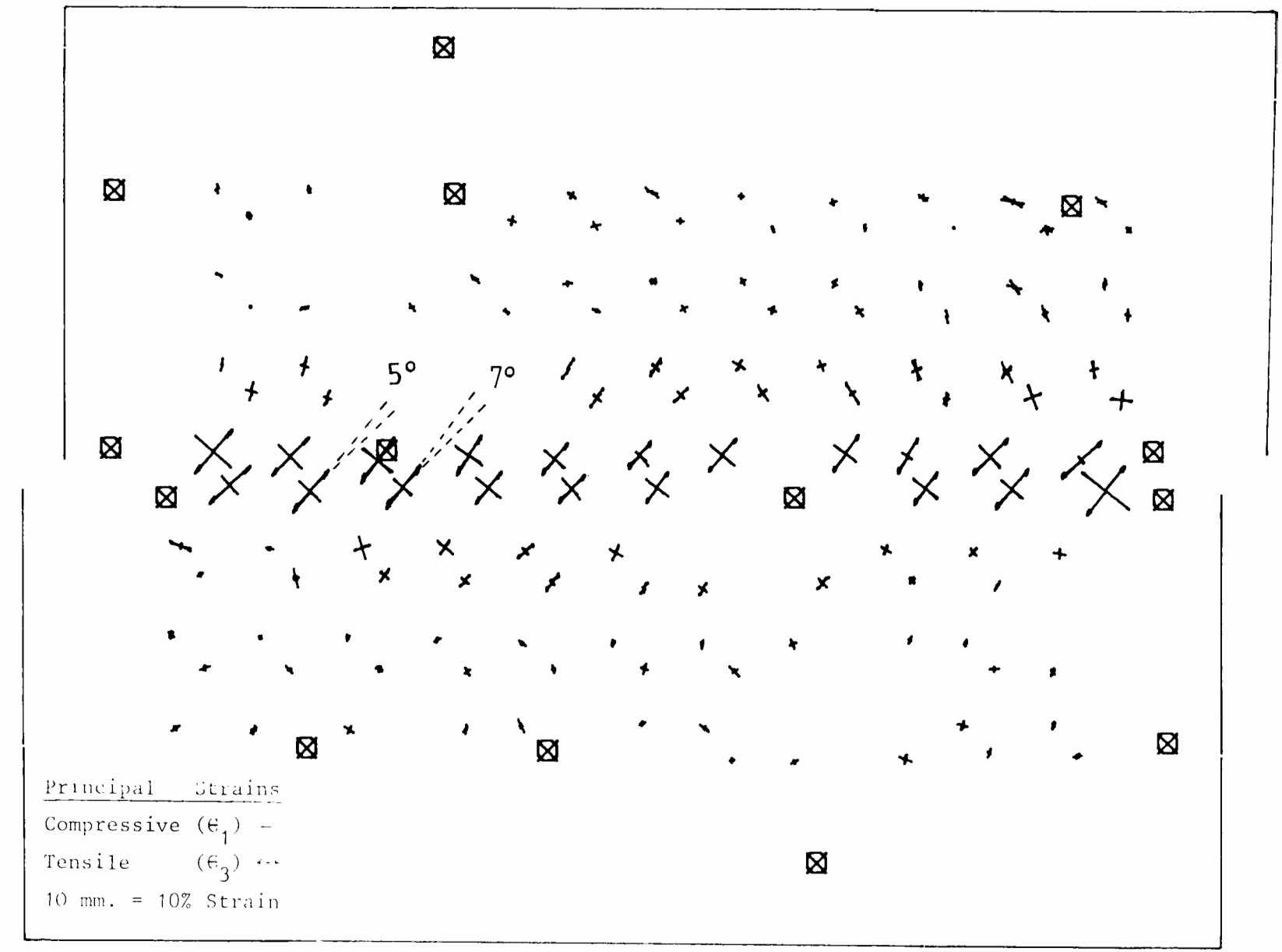


Fig. 4.22 Two plots of strains determined between identical stages of direct shear test no. 30 illustrating the accuracy of the strain analysis

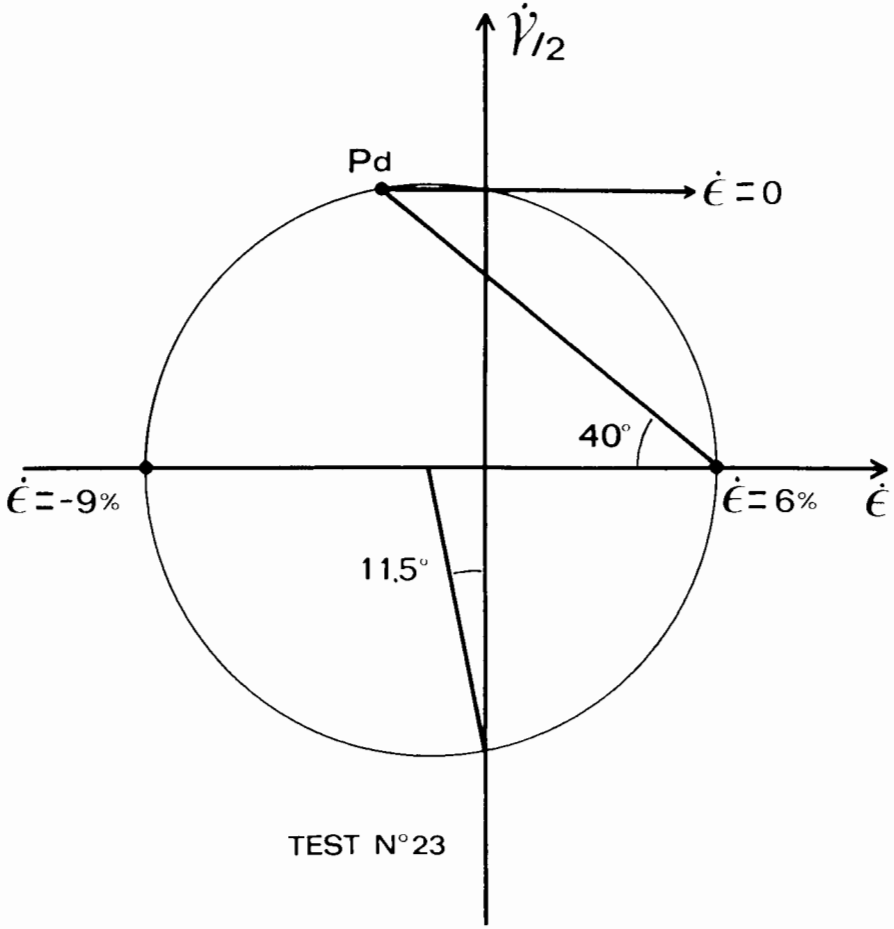


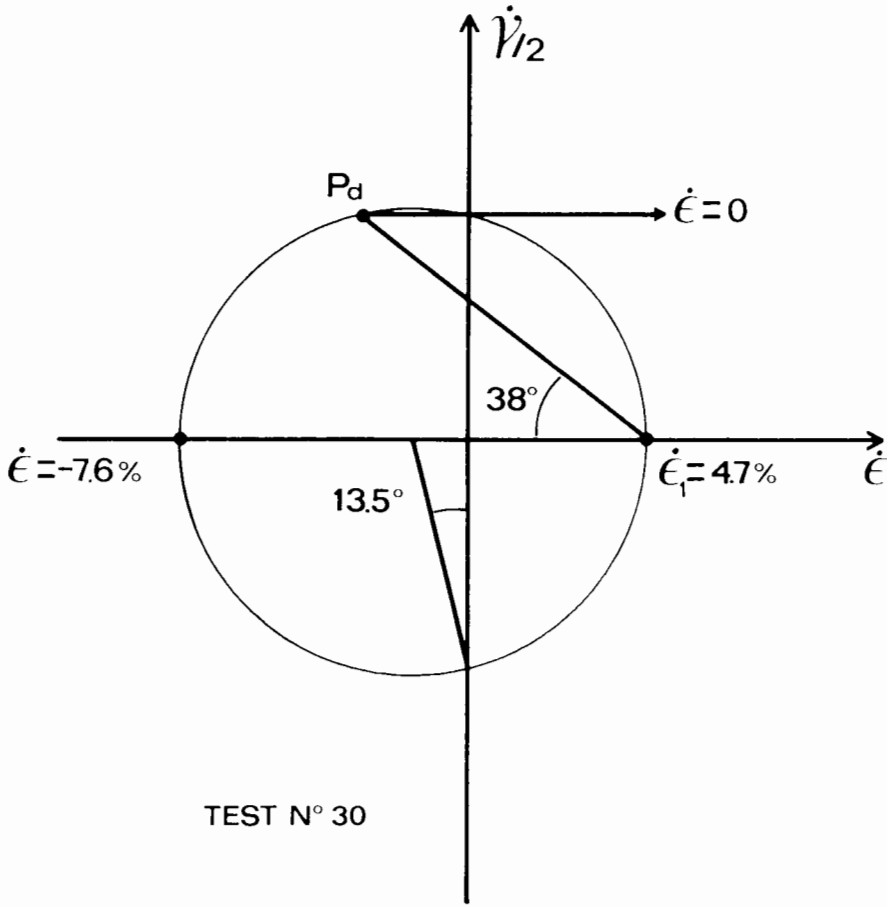


Fig. 4.23 Mohr's circles of strain increment for stages C to D after maximum shear load in direct shear test nos. 23 and 30

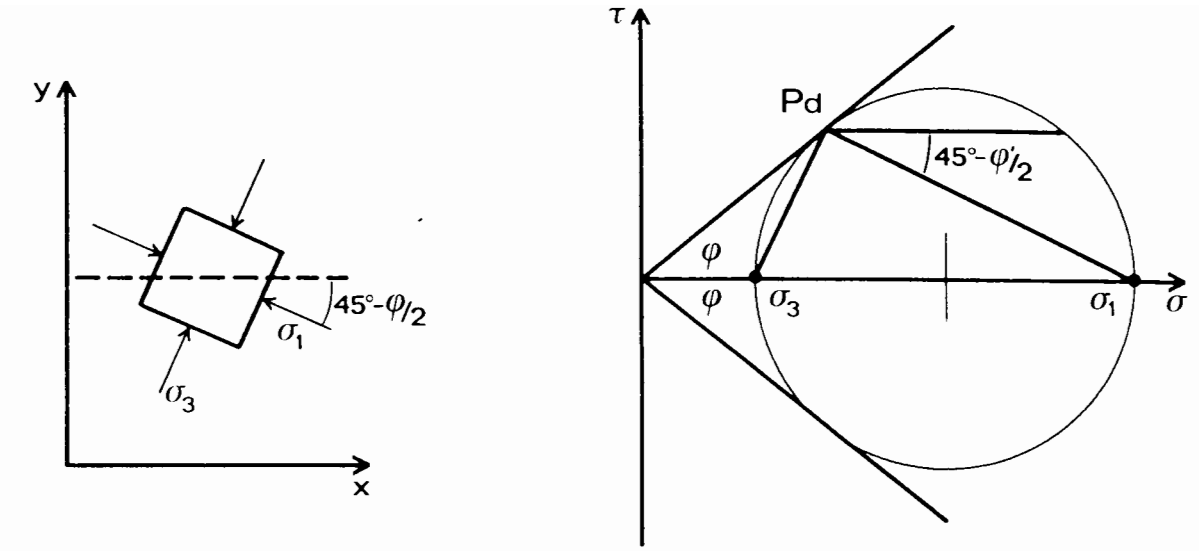


(a) ALIGNMENT OF RUPTURE WITH PLANES OF MAXIMUM STRESS OBLIQUITY.

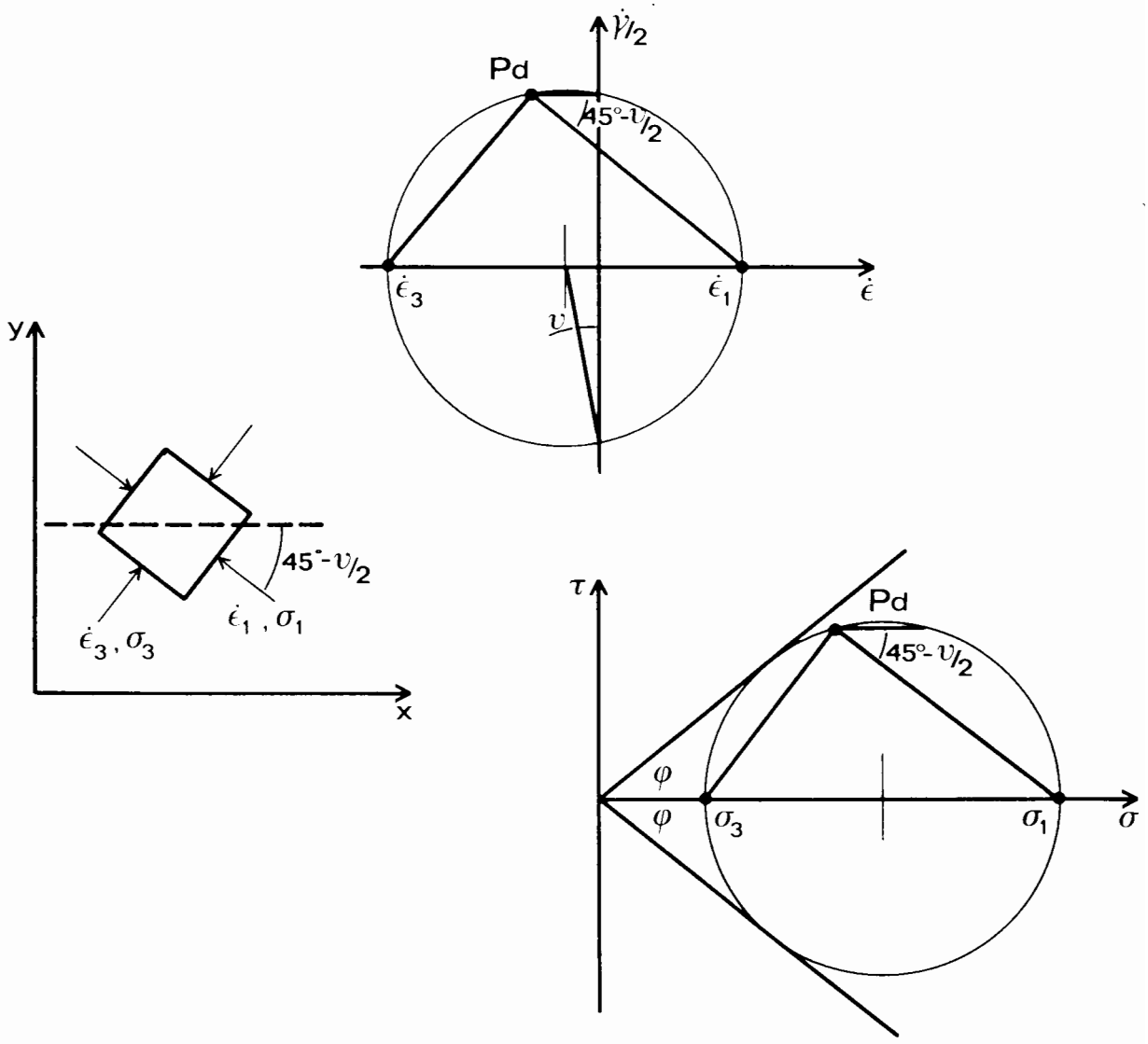


(b) ALIGNMENT OF RUPTURE WITH DIRECTION OF ZERO EXTENSION COMBINED WITH ASSUMPTION OF COAXIALITY.

Fig. 4.24 Two orientations of a rupture band relative to the stress and strain fields in a cohesionless soil (taken from Scarpelli and Wood 1982)

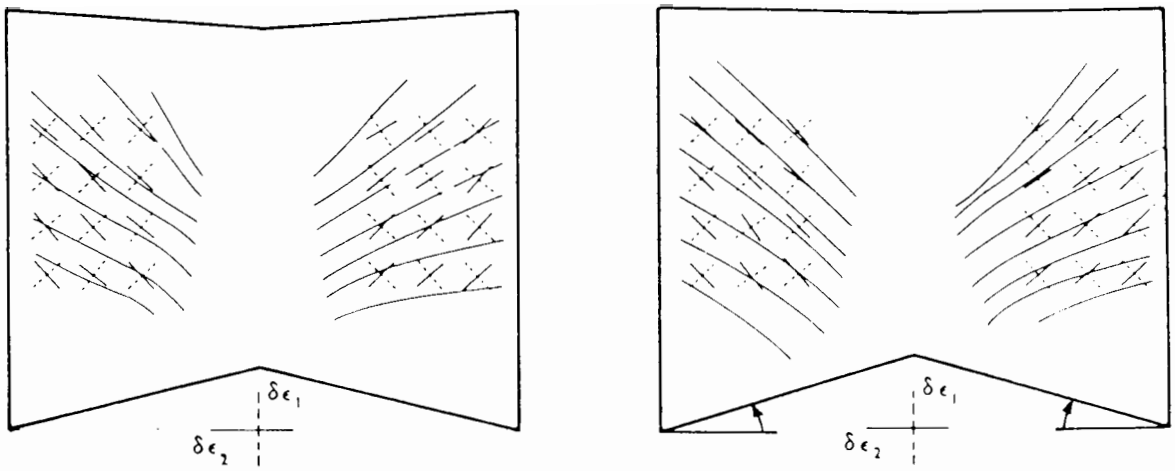


(a) Comparison of principal stress and strain increment directon in crushed glass by Drescher in a double shear apparatus - results for two tests presented

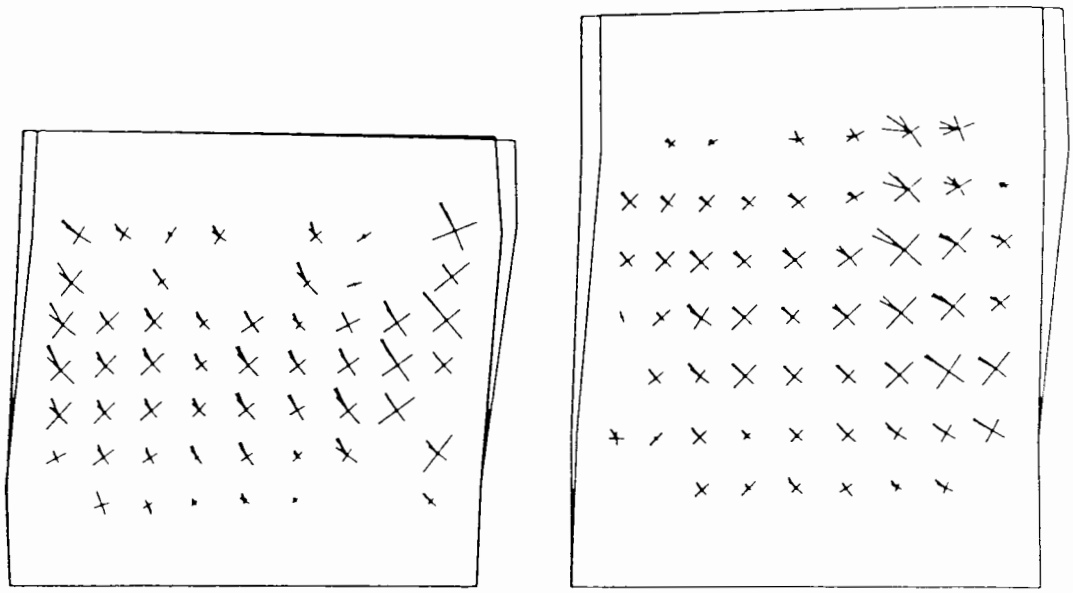

(b) Comparison of principal stress and strain increment directions in crushed glass by Allersma in a simple shear apparatus for i) counter clockwise and ii) clockwise rotation of principal stress trajectories

Fig. 4.25 Comparisons of principal stress and strain increment directions in crushed glass by a) Drescher 1976 and b) Allersma 1982b

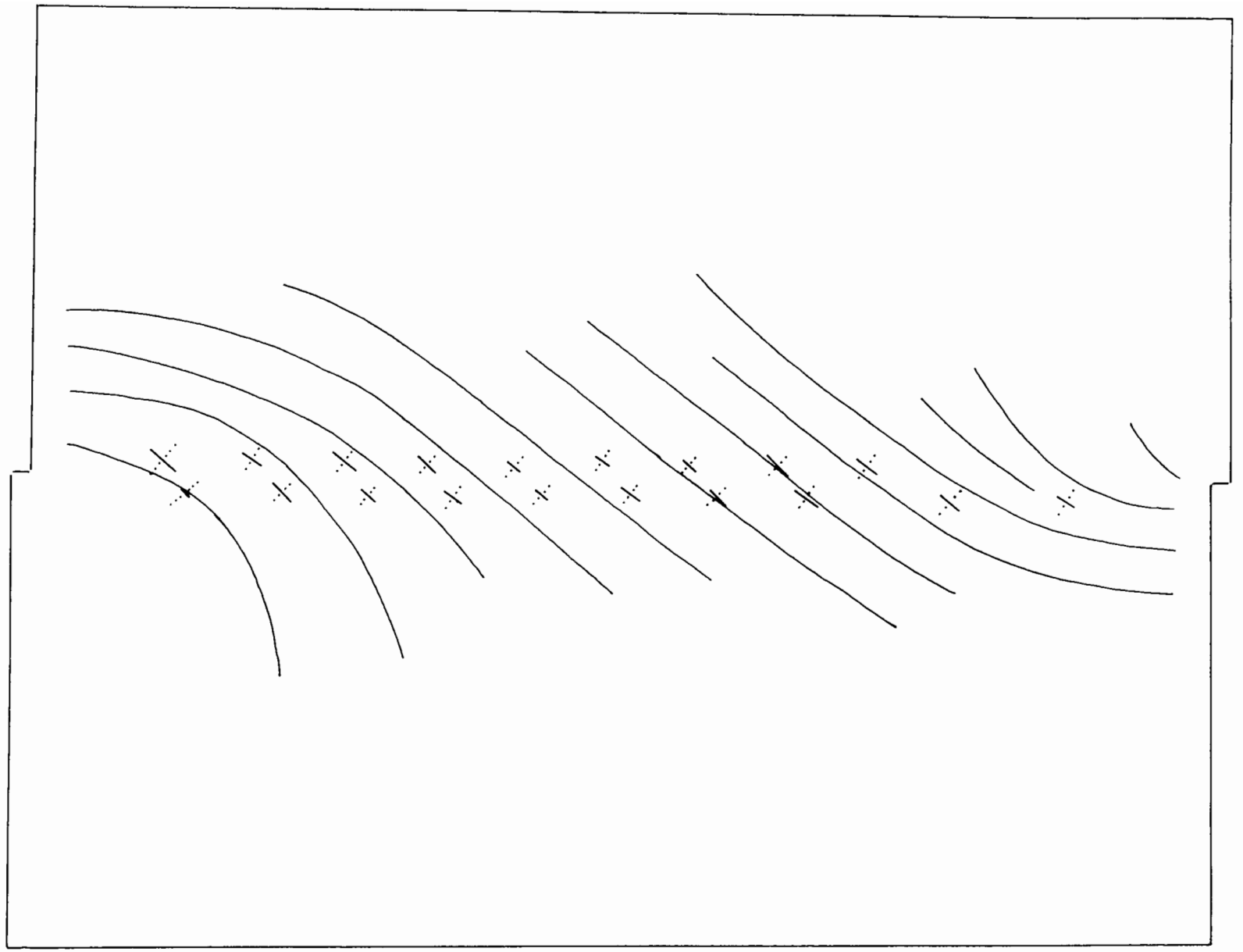

Fig. 4.26 Comparison of principal strain directions determined between stages A to B before maximum shear load in direct shear test no. 23 with the major principal stress trajectories observed at stage B

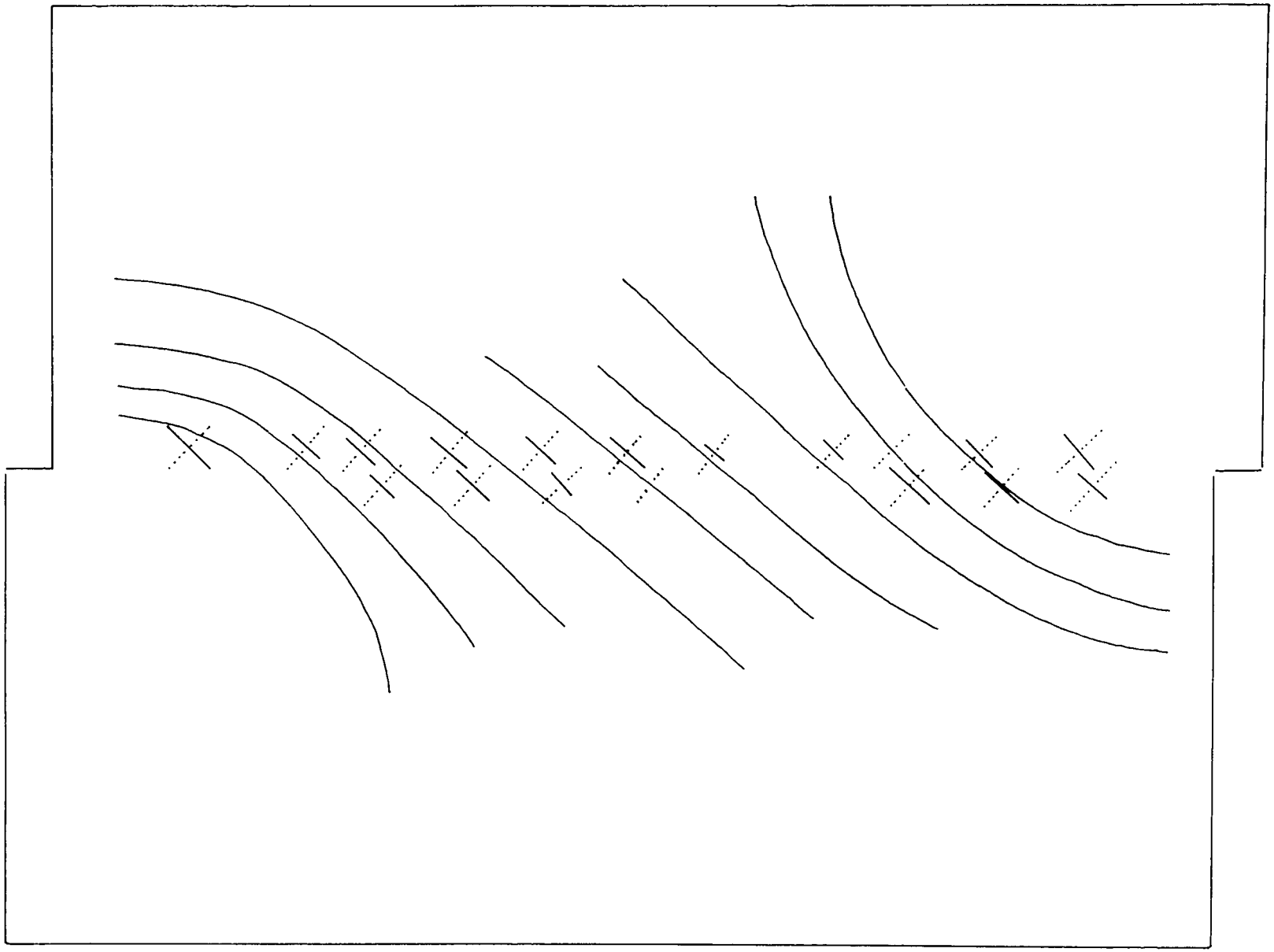

Fig. 4.27 Comparison of principal strain increment directions determined between stages C to D after maximum shear load in direct shear test no. 23 with the major principal stress trajectories observed at stage D

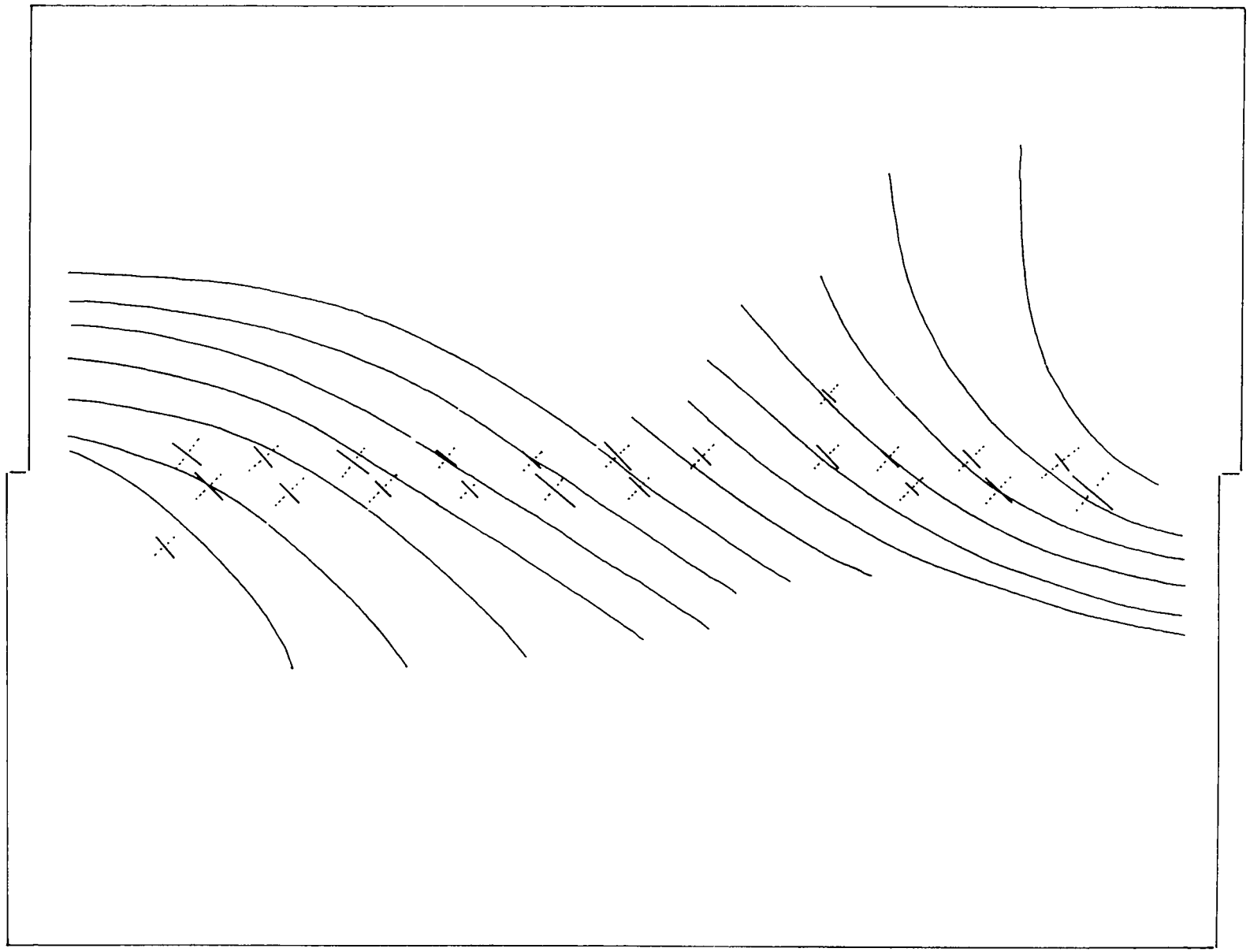

Fig. 4.28 Comparison of principal strain directions determined between stages A to B before maximum shear load in direct shear test no. 23 with the major principal stress trajectories observed at stage B

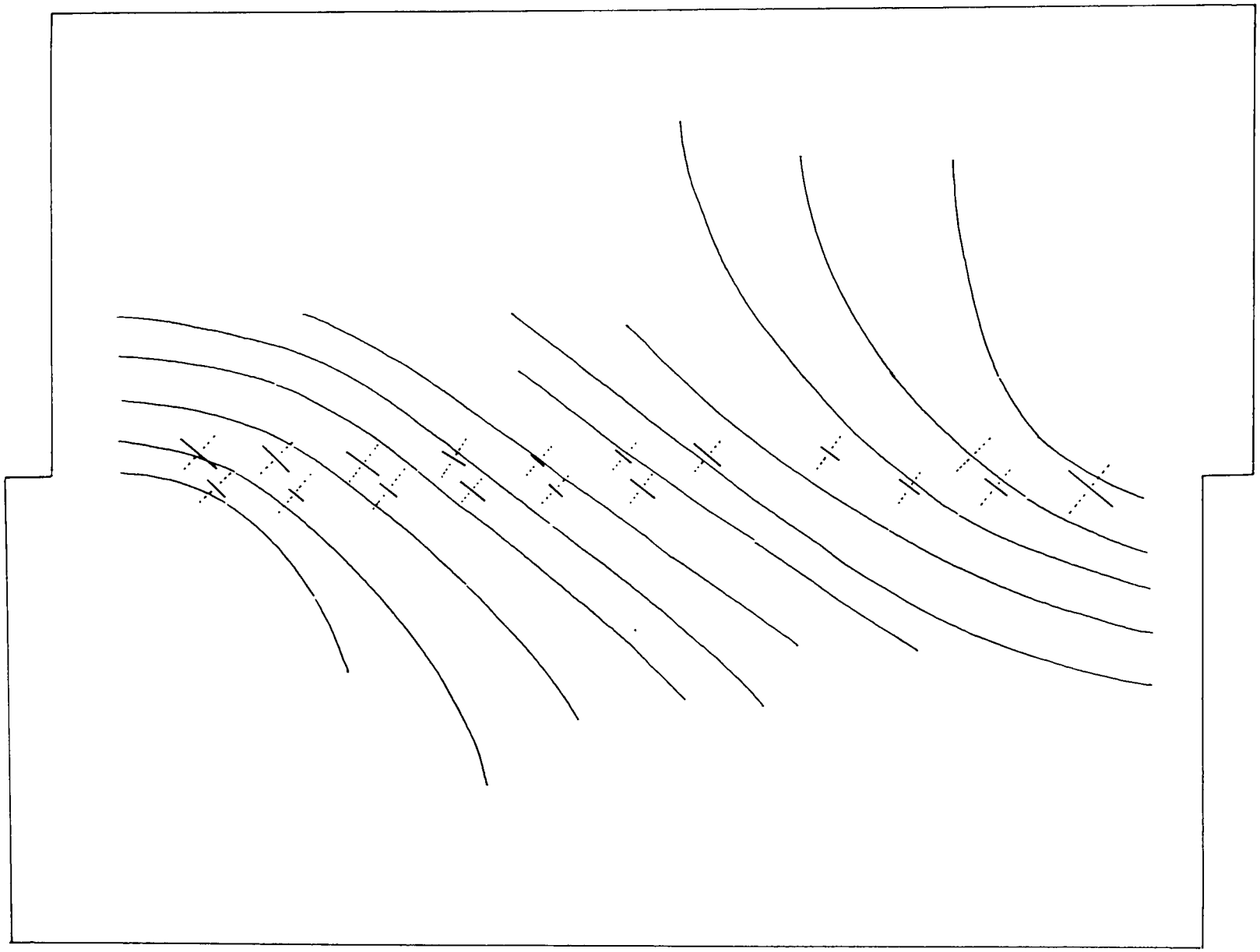

Fig. 4.29 Comparisons of principal strain increment directions determined between stages C to D after maximum shear load in direct shear test no. 30 with the major principal stress trajectories observed at stage D

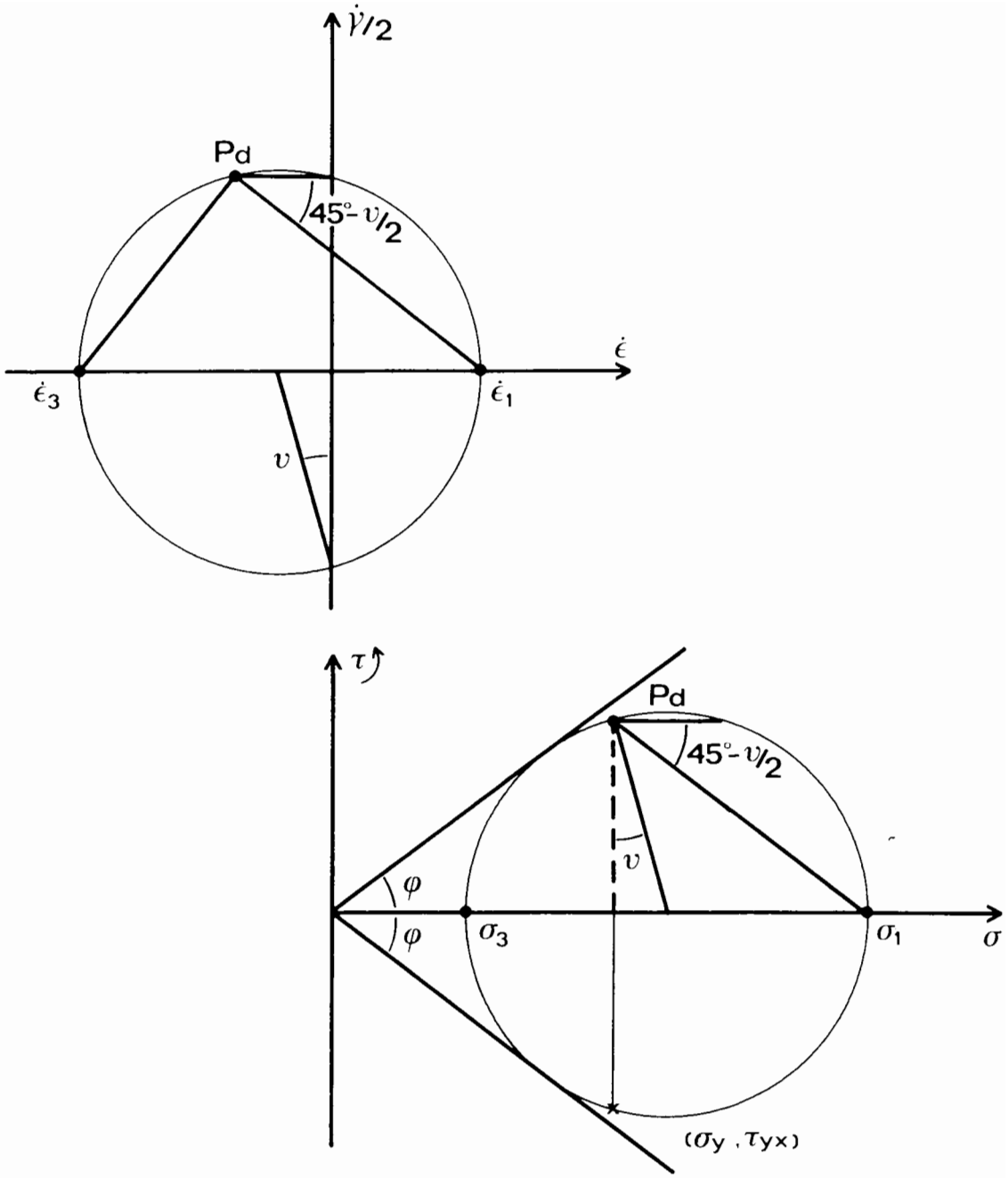


$$\sin\varphi = \frac{\tau_{yx}/\cos\upsilon}{\sigma_y + \tau_{yx}\tan\upsilon}$$

$$\sin\varphi = \frac{\tan\varphi_m}{\cos\upsilon + \tan\varphi_m \sin\upsilon} \qquad \text{where: } \tan\varphi_m = \frac{\tau_{yx}}{\sigma_y}$$

Fig. 4.30 Relationship of the internal angle of friction $\phi$ with mobilised angle of friction $\phi_m$ along the central plane of the shear box and angle of dilation, for rupture along the central plane and coincidence of principal axes

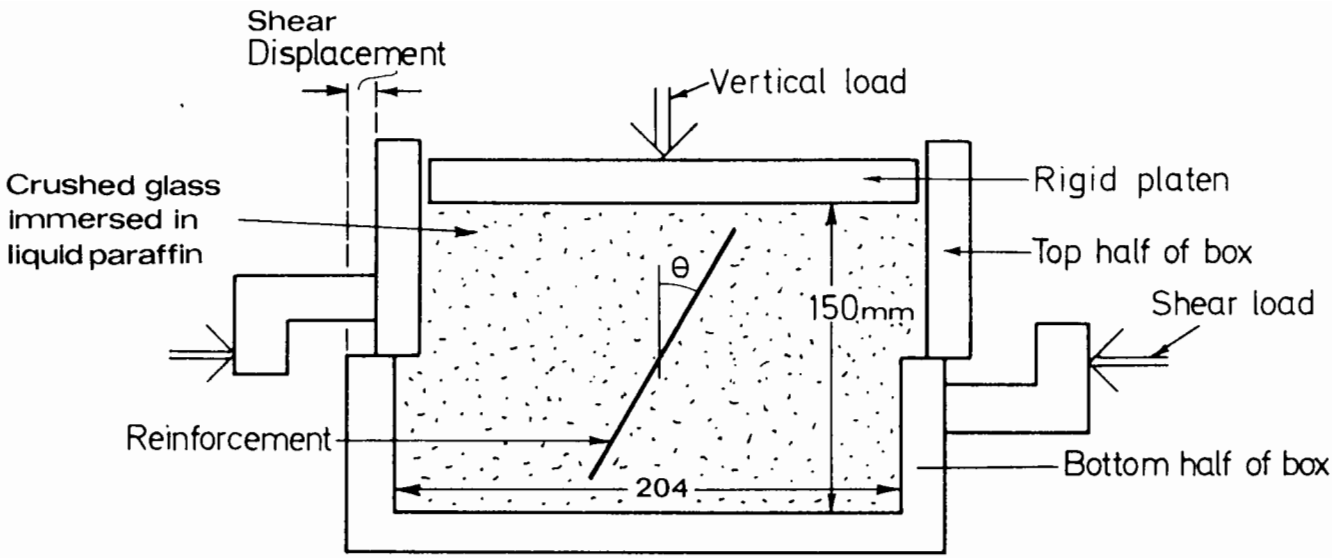


Fig. 5.1 Arrangement of direct shear tests on crushed glass containing a single reinforcing element shown schematically

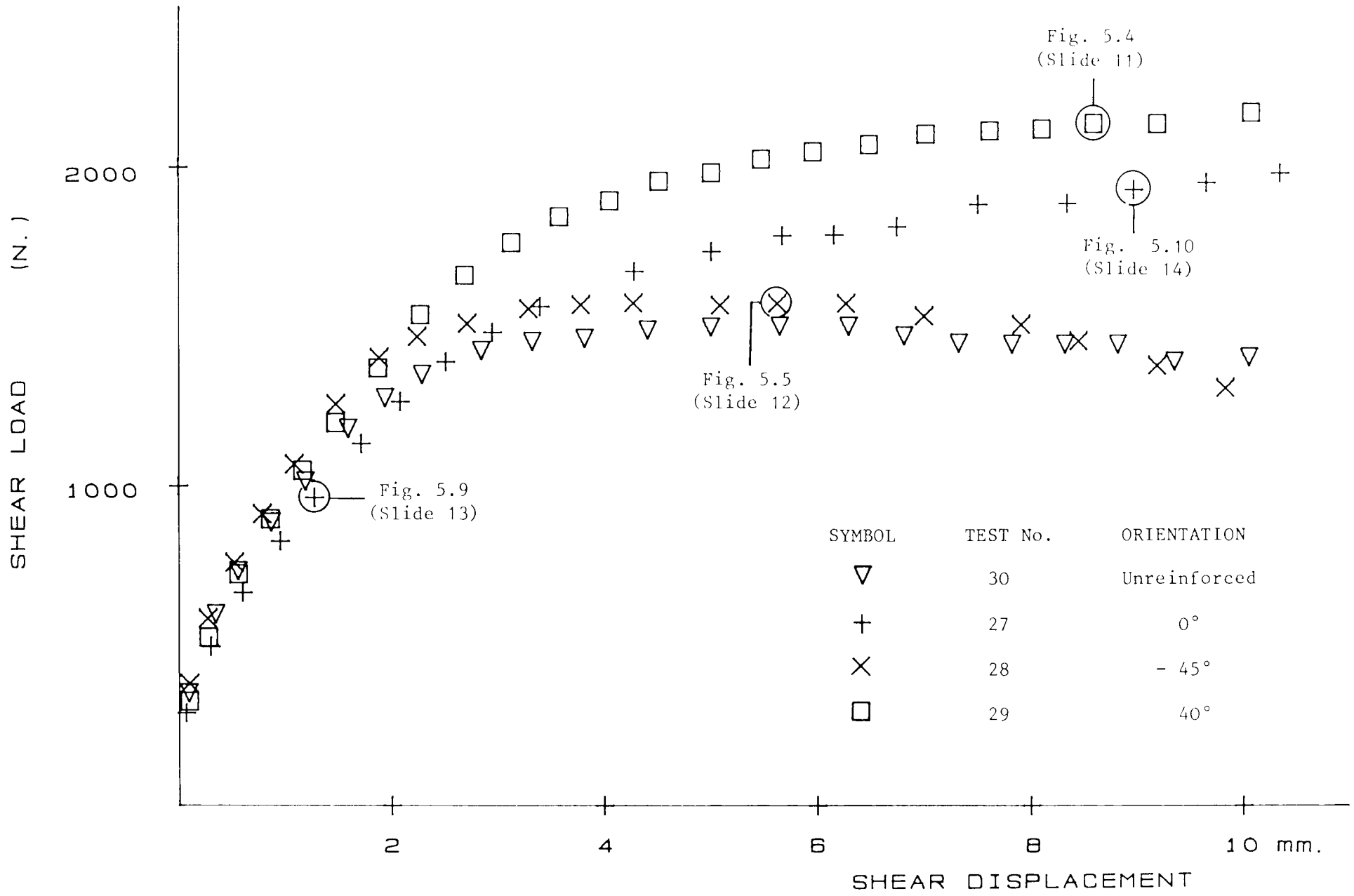


Fig. 5.2 Reinforcing effects produced by the flexible sheet reinforcement at different orientations in the shearbox

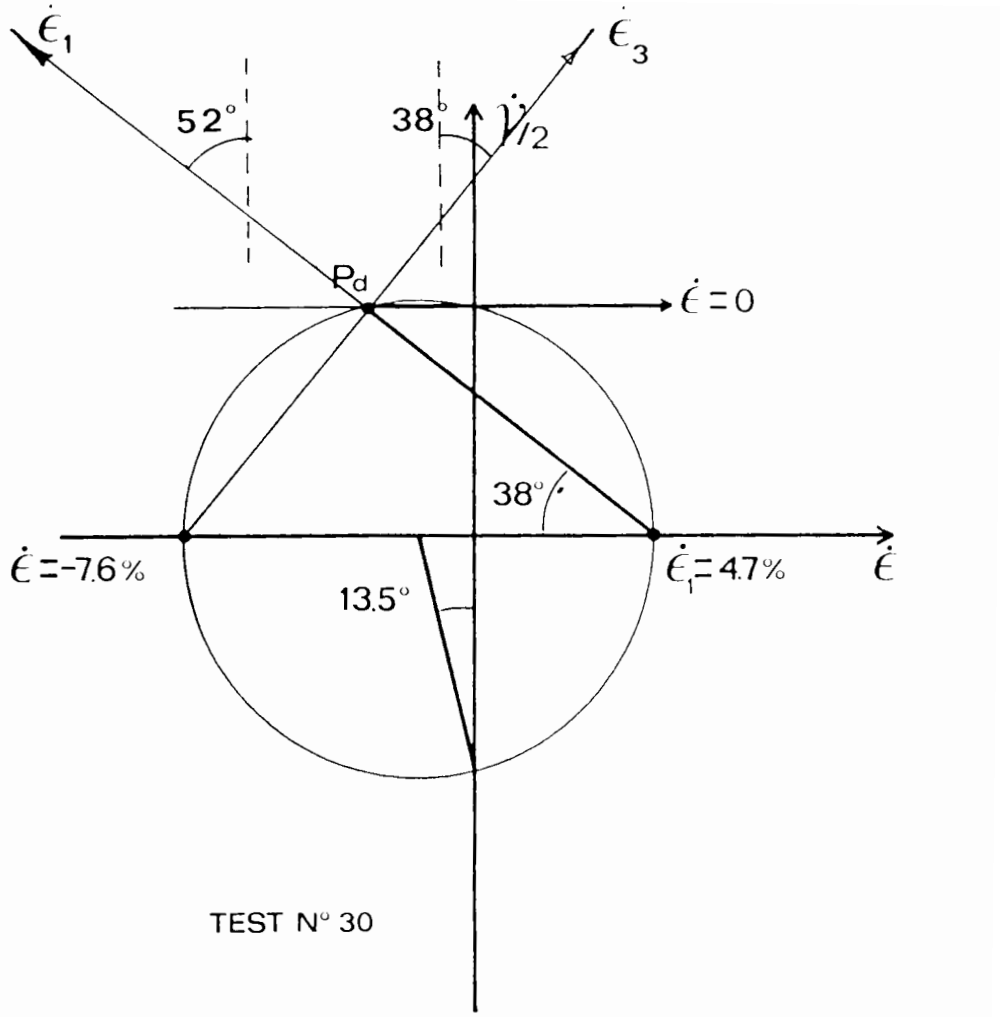


Fig. 5.3 Strain fields determined for unreinforced direct shear test on crushed glass after maximum shear load (stages C to D)

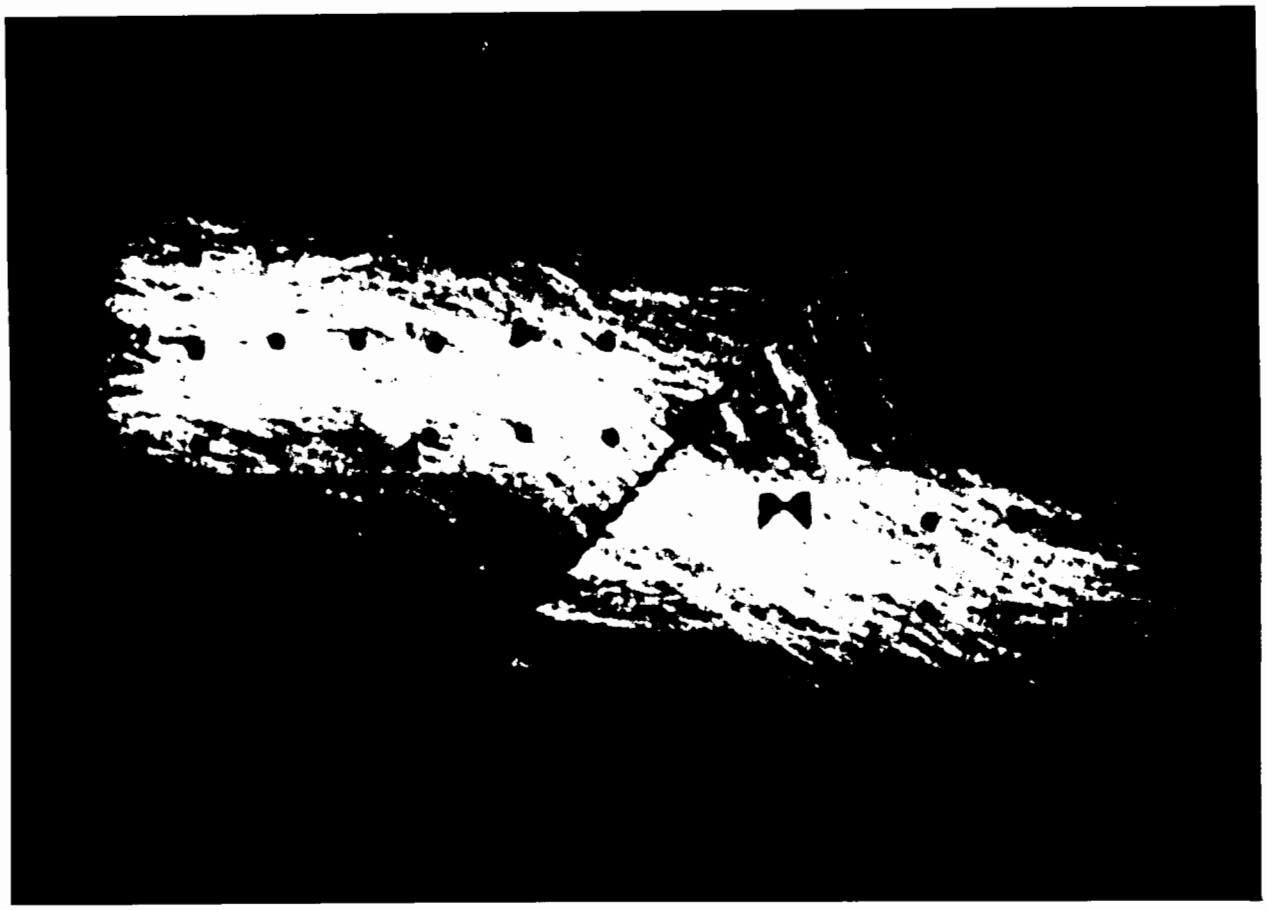

Fig. 5.4 Light stripes observed at 8.60 mm shear displacement for the direct shear test on crushed glass containing the flexible sheet reinforcement orientated at $\psi = 40°$ (test no. 29)

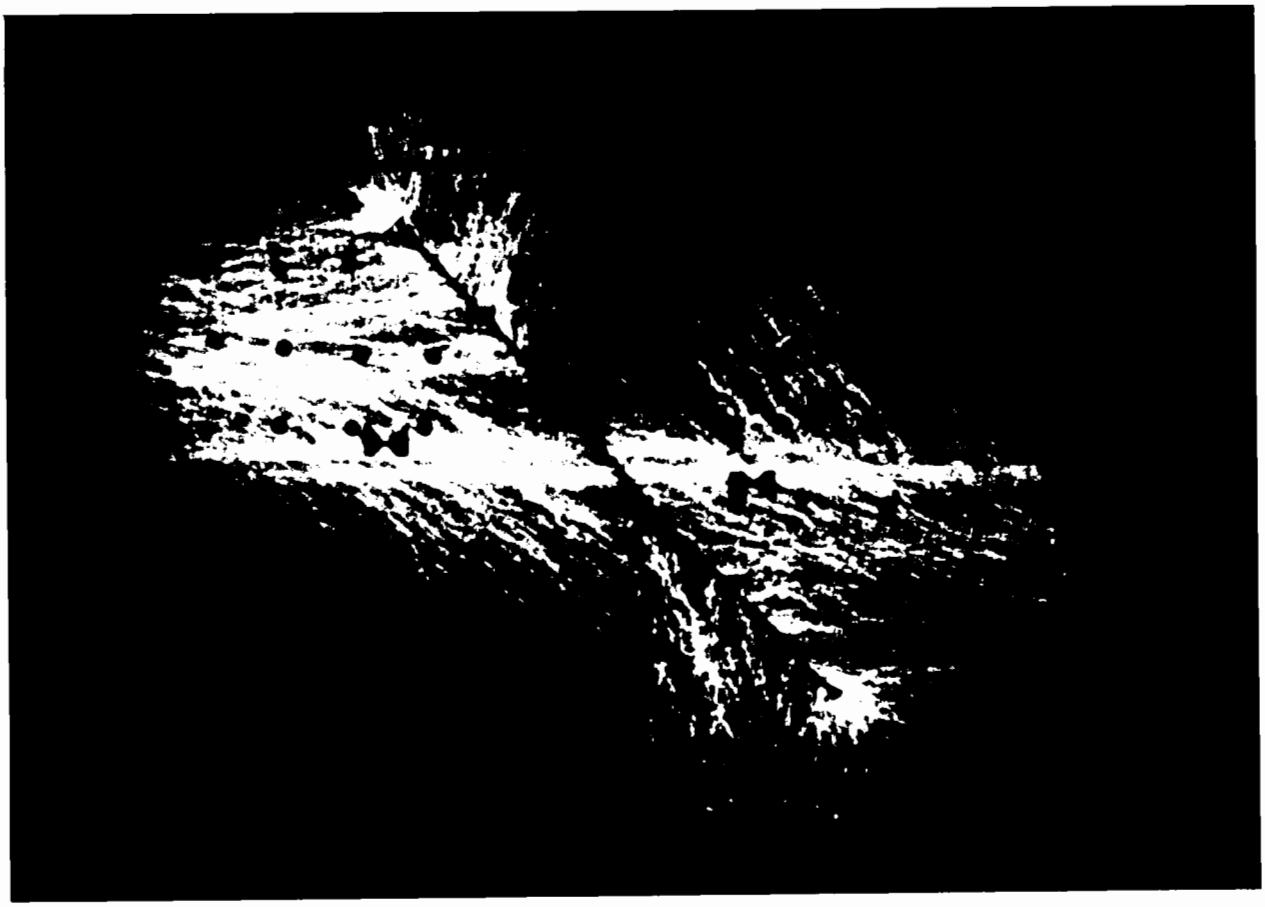

Fig. 5.5 Light stripes observed at 5.62 mm shear displacement for the direct shear test on crushed glass containing the flexible sheet reinforcement orientated at $\psi = -45°$ (test no. 28)

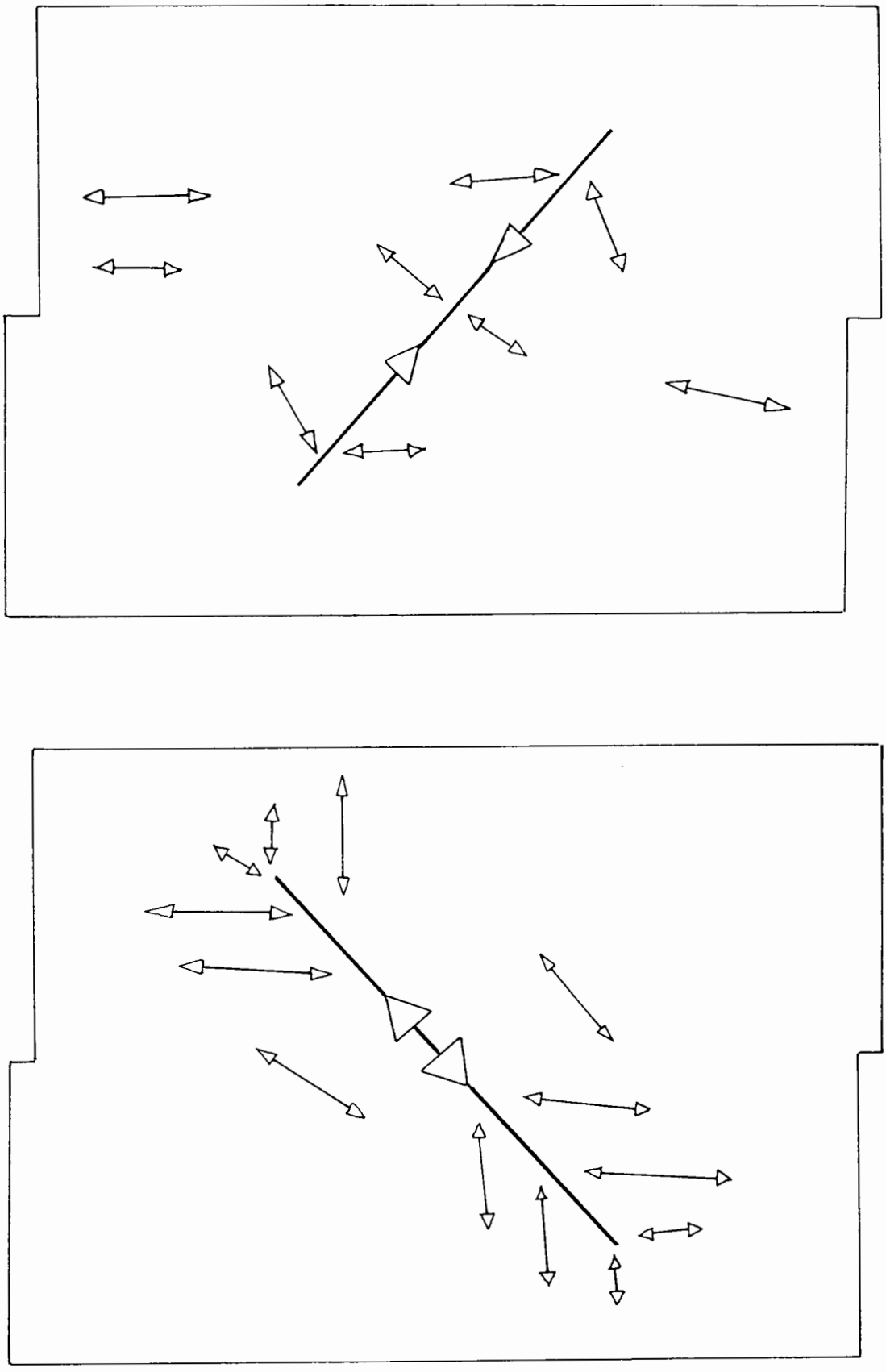

Fig. 5.6 Simple representations of the loading mechanism in the shear box for crushed glass interacting with the flexible sheet reinforcement orientated at a) $\theta = 40°$ and b) $\theta = -45°$

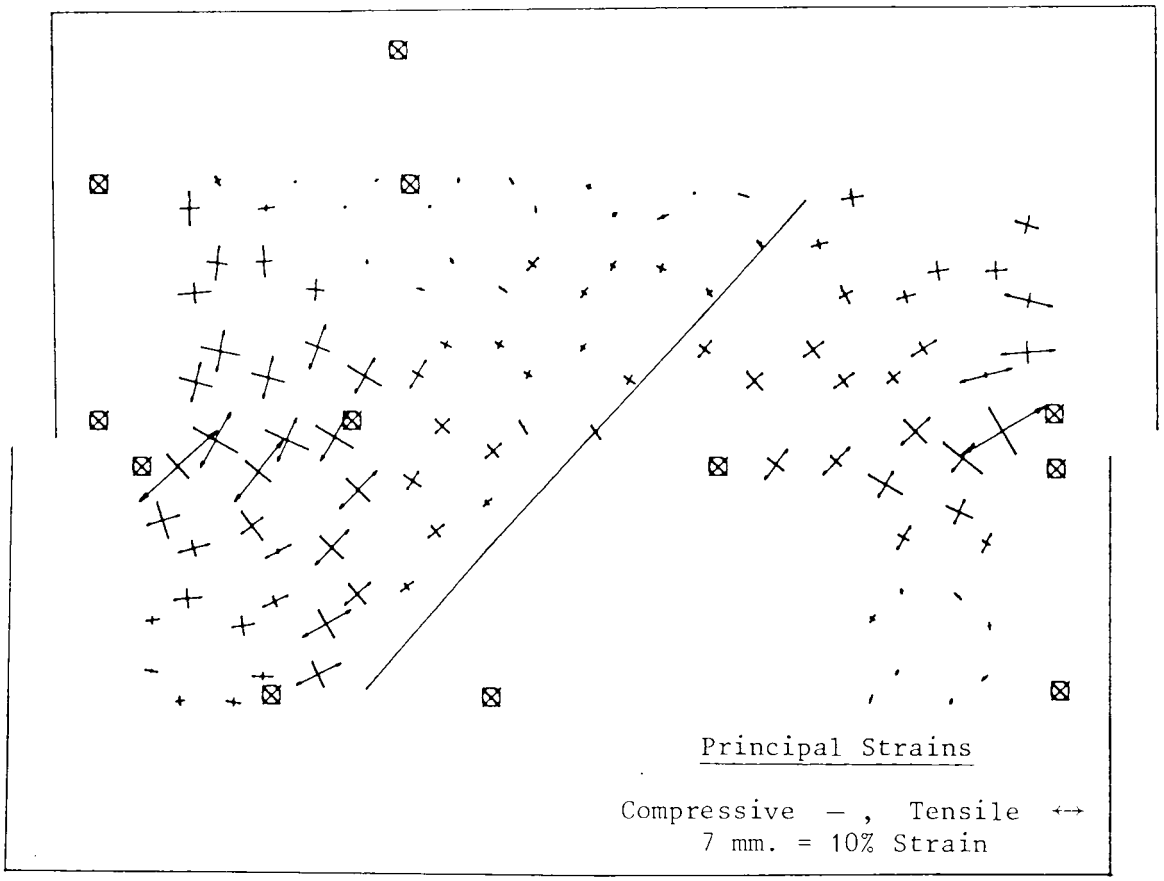


Fig. 5.7 Strains determined between 1.87 and 8.60 mm shear displacement for crushed glass containing the flexible sheet reinforcement orientated at $\theta$ = 40°

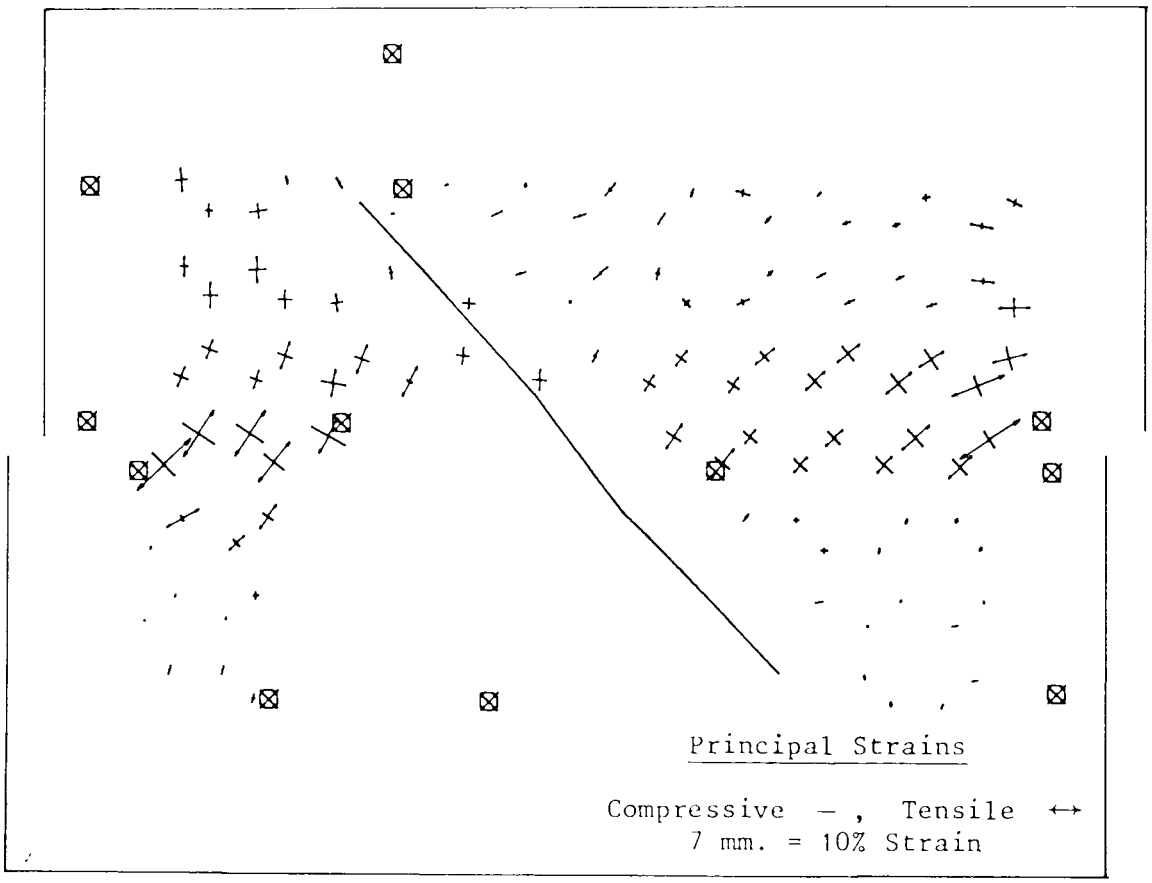


Fig. 5.8 Strains determined between 2.71 and 7.00 mm shear displacement for crushed glass containing the flexible sheet reinforcement orientated at $\theta$ = -45°

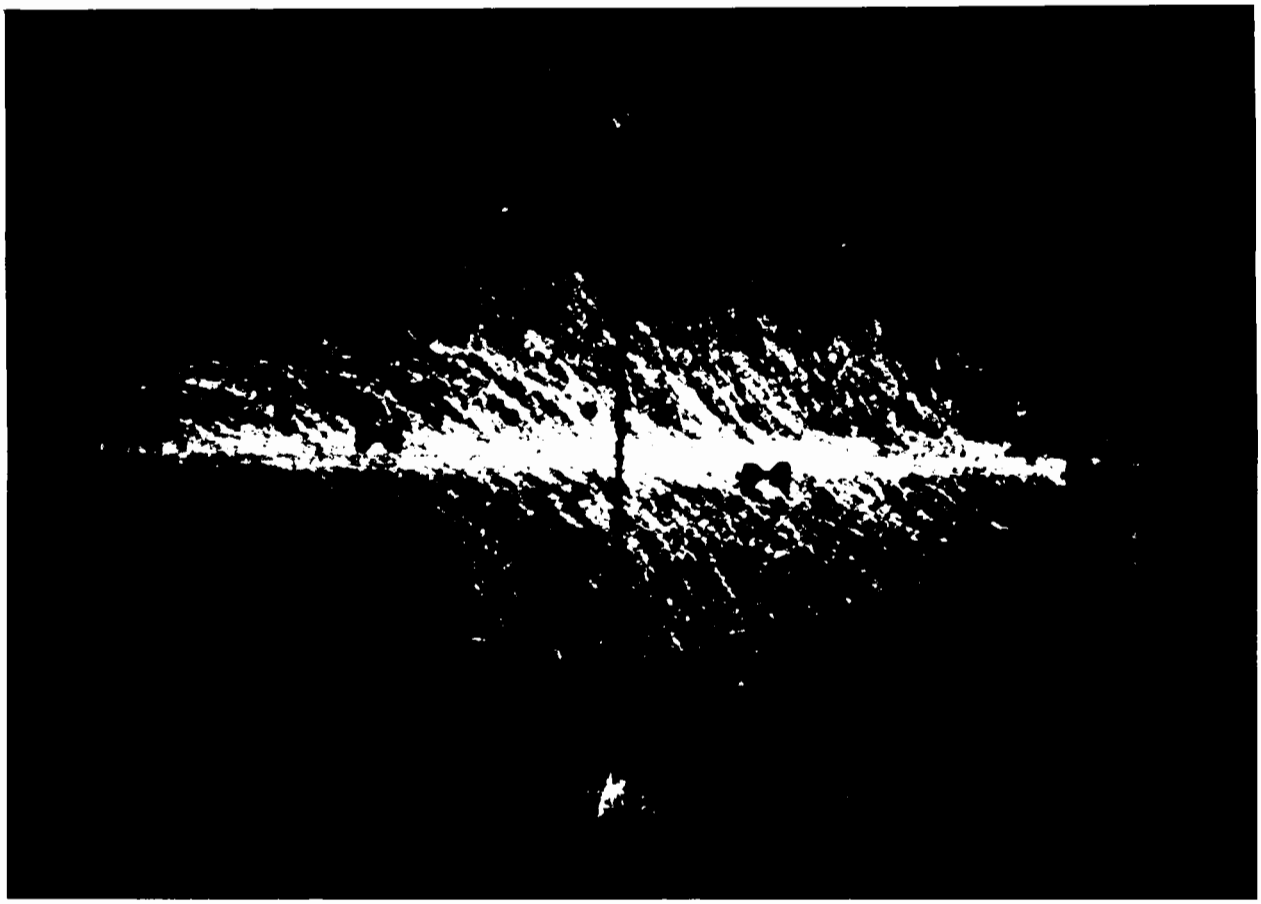

Fig. 5.9 Light stripes observed at 1.27 mm shear displacement for the direct shear test on crushed glass containing the flexible sheet reinforcement orientated at $\psi = 0°$ (test no. 27)

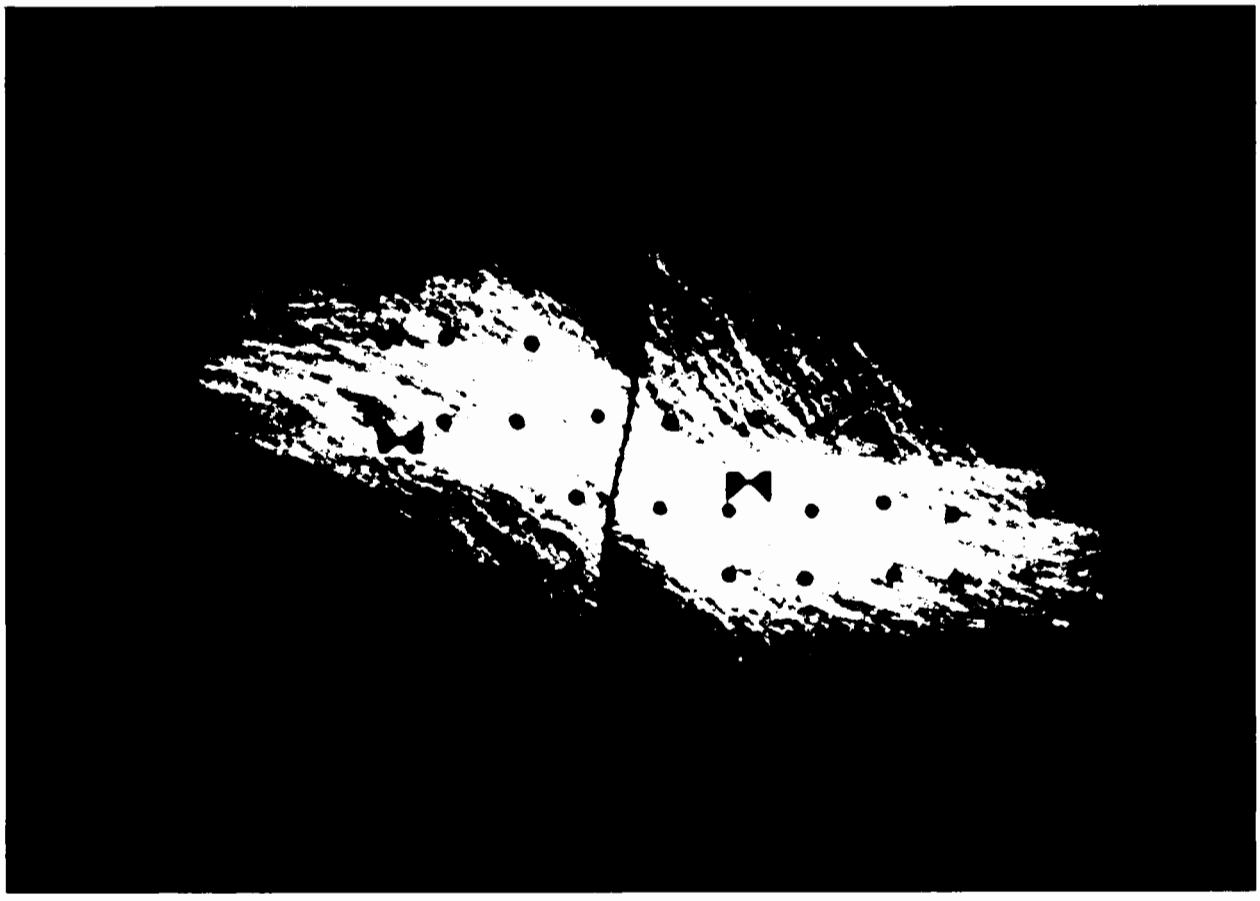

Fig. 5.10 Light stripes observed at 8.98 mm shear displacement for the direct sheat test on crushed glass containing the flexible sheet reinforcement orientated at $\psi = 0°$ (test no. 27)

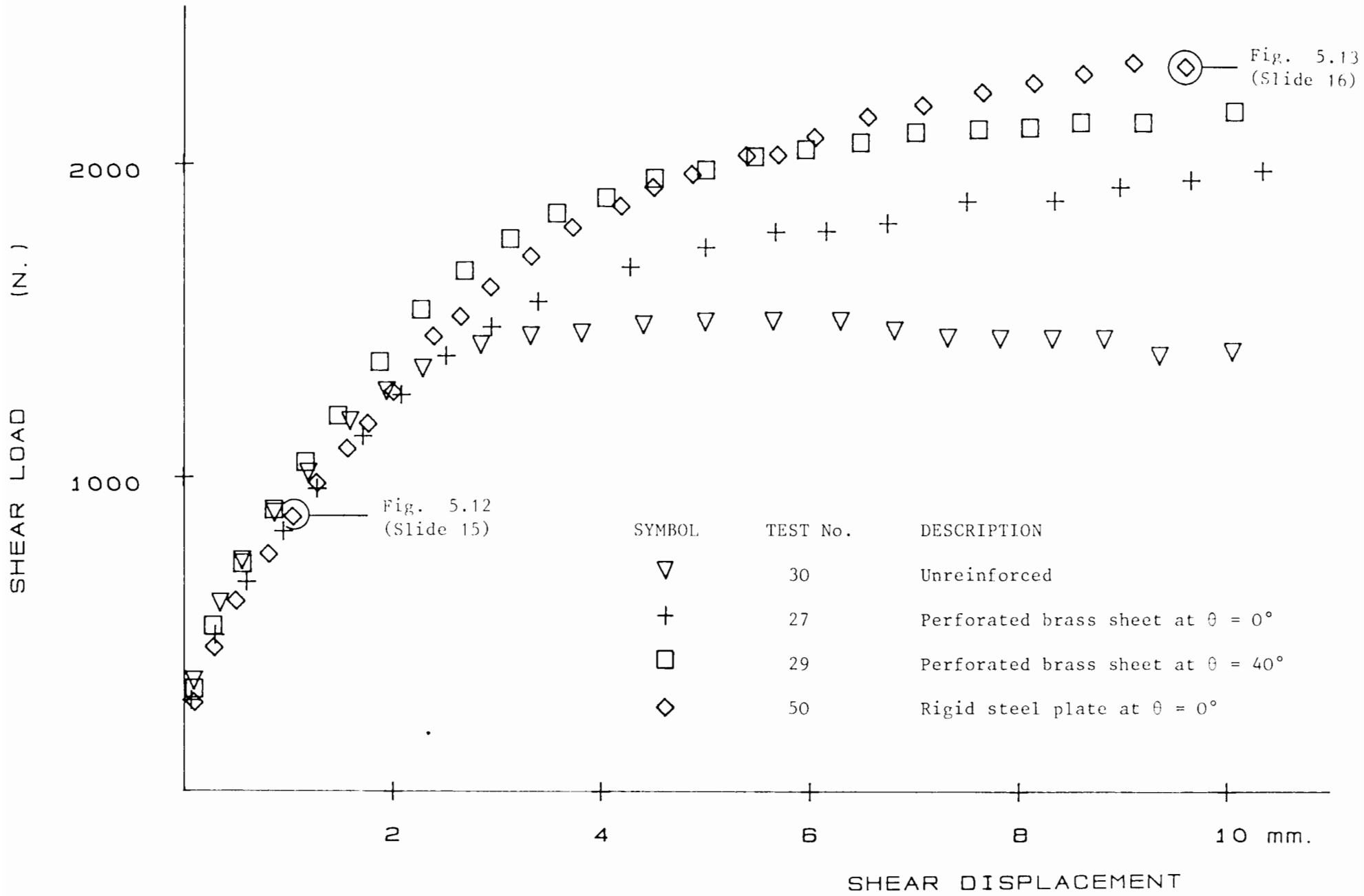


Fig. 5.11 A comparison of the reinforcing effects produced by the flexible sheet reinforcement orientated at $\theta$ = 40 and 0° with the rigid reinforcement orientated at $\theta$ = 0°

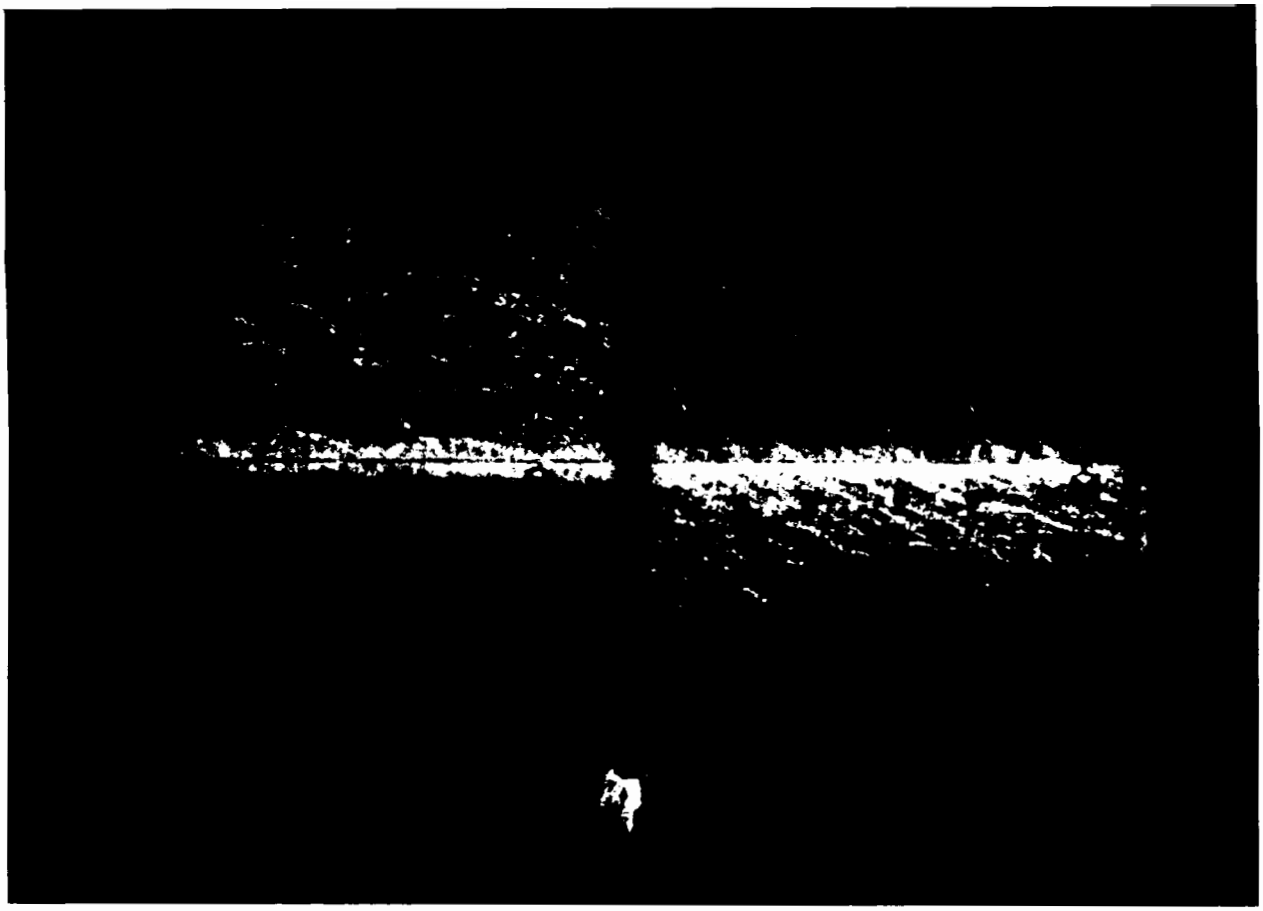

Fig. 5.12 Light stripes observed at 1.04 mm shear displacement for the direct shear test on crushed glass containing the rigid plate reinforcement orientated at $\theta = 0°$ (test no. 50)

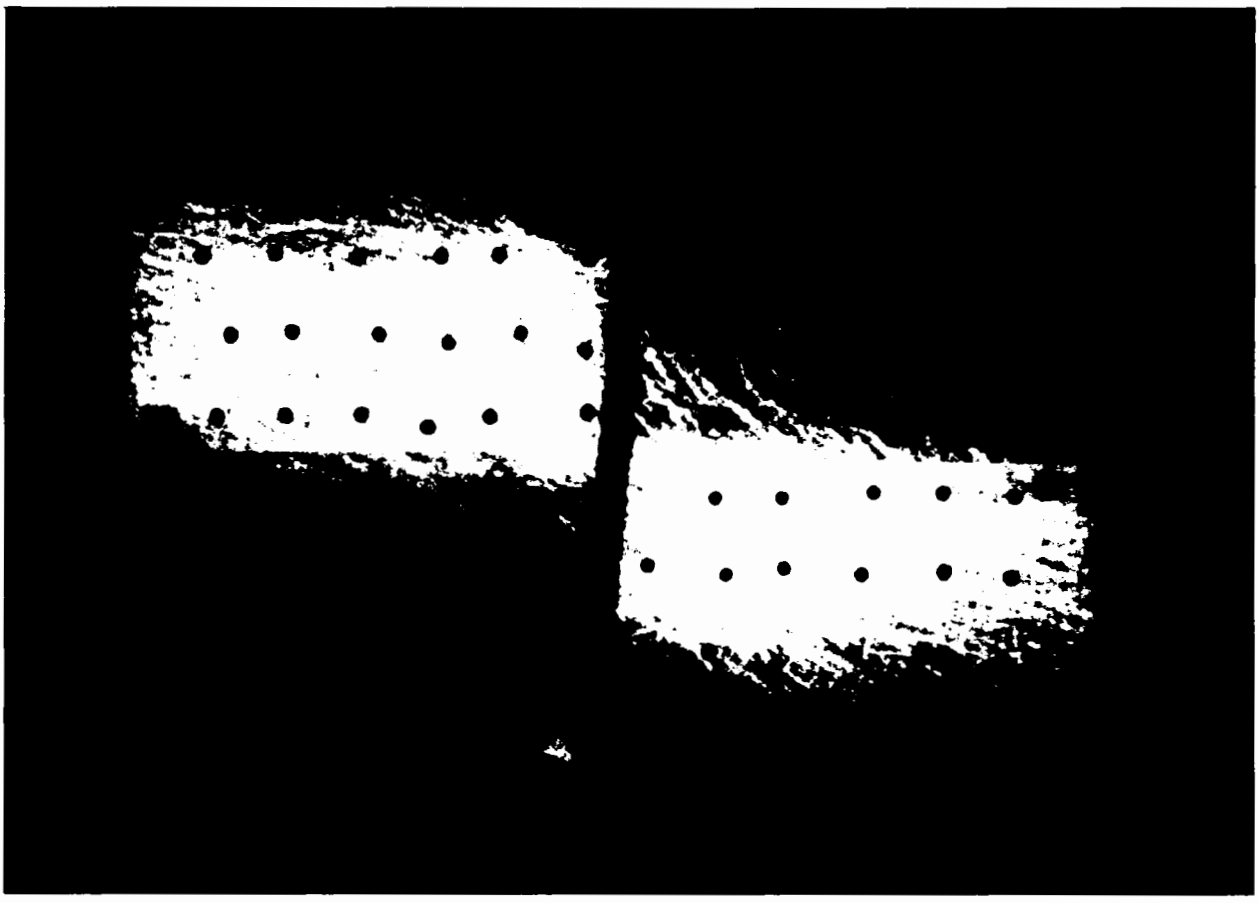

Fig. 5.13 Light stripes observed at 9.61 mm shear displacement for the direct shear test on crushed glass containing the rigid plate reinforcement orientated at $\theta = 0°$ ( test no. 50)

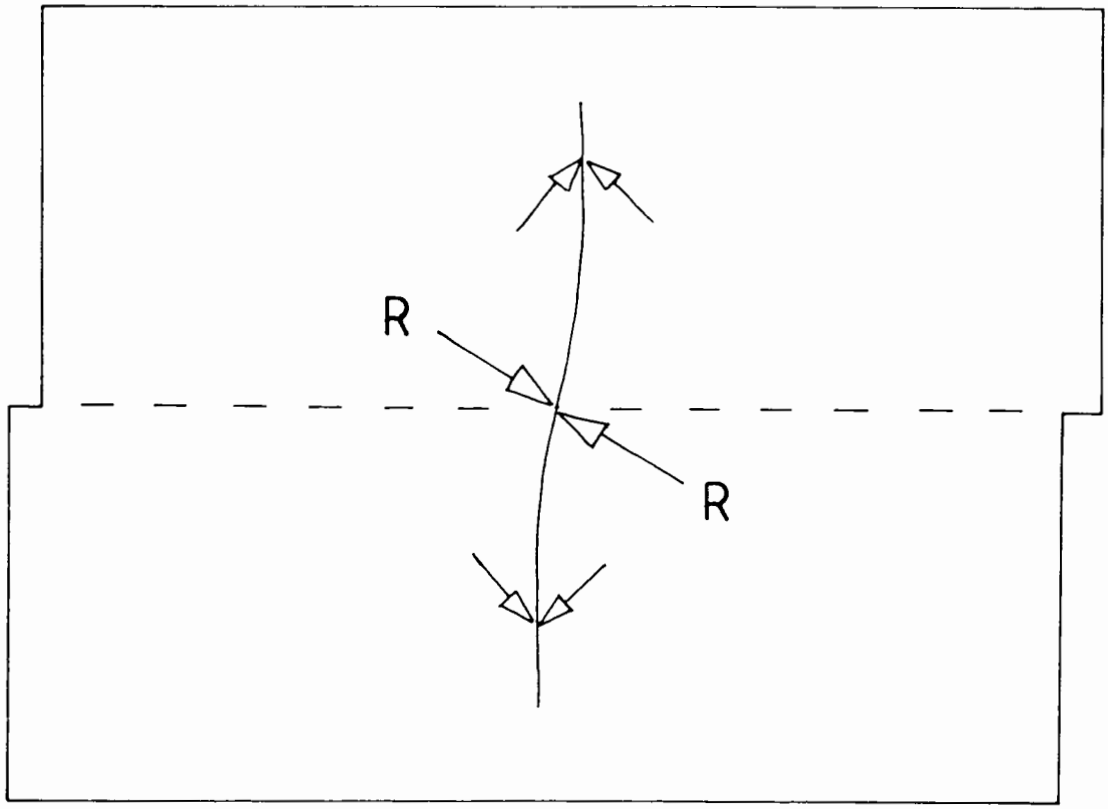


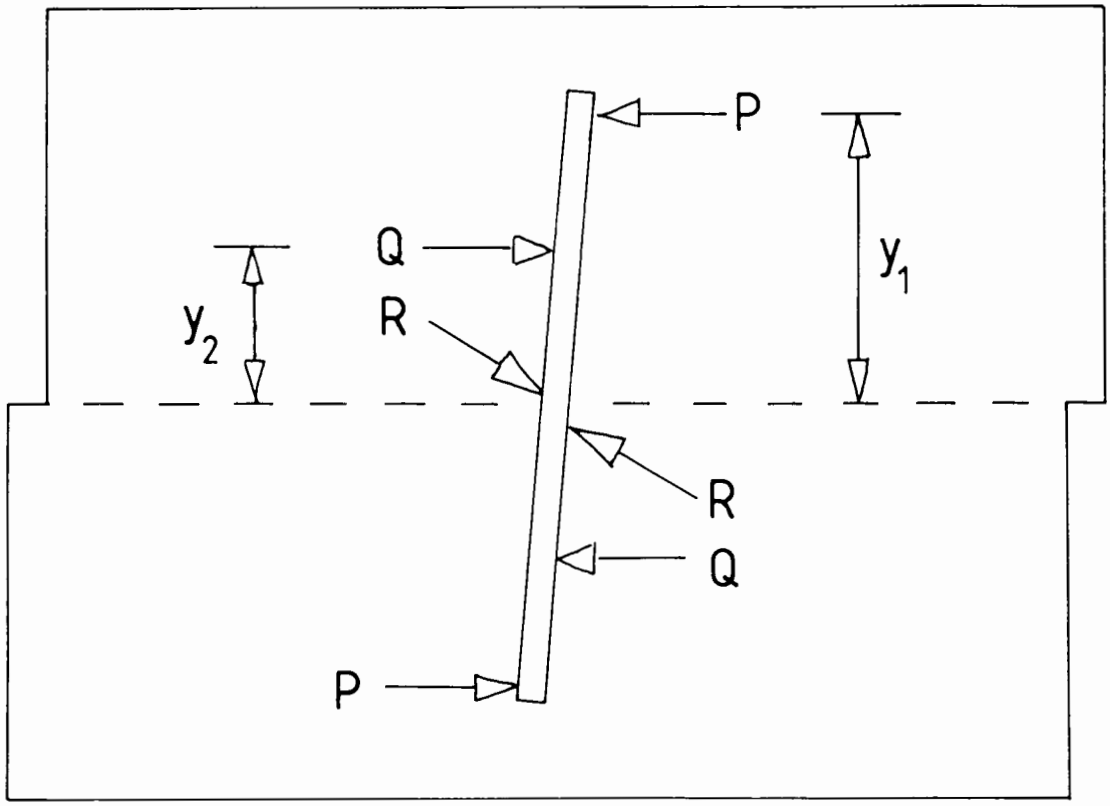


Fig. 5.14 Simple representations of the loading mechanisms in the shearbox for crushed glass interacting with a) flexible sheet and b) rigid reinforcements at $\theta = 0°$

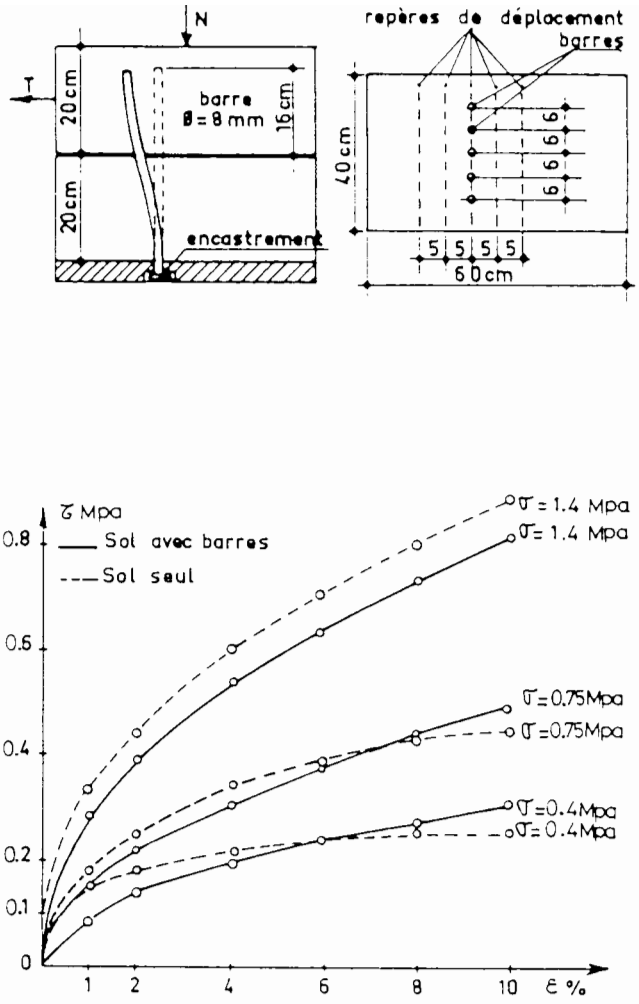


Fig. 5.15 Effects of the vertical steel bars rigidly encased into the base of a direct shearbox on the shear strength of clayey silt by Juran et al (1981)

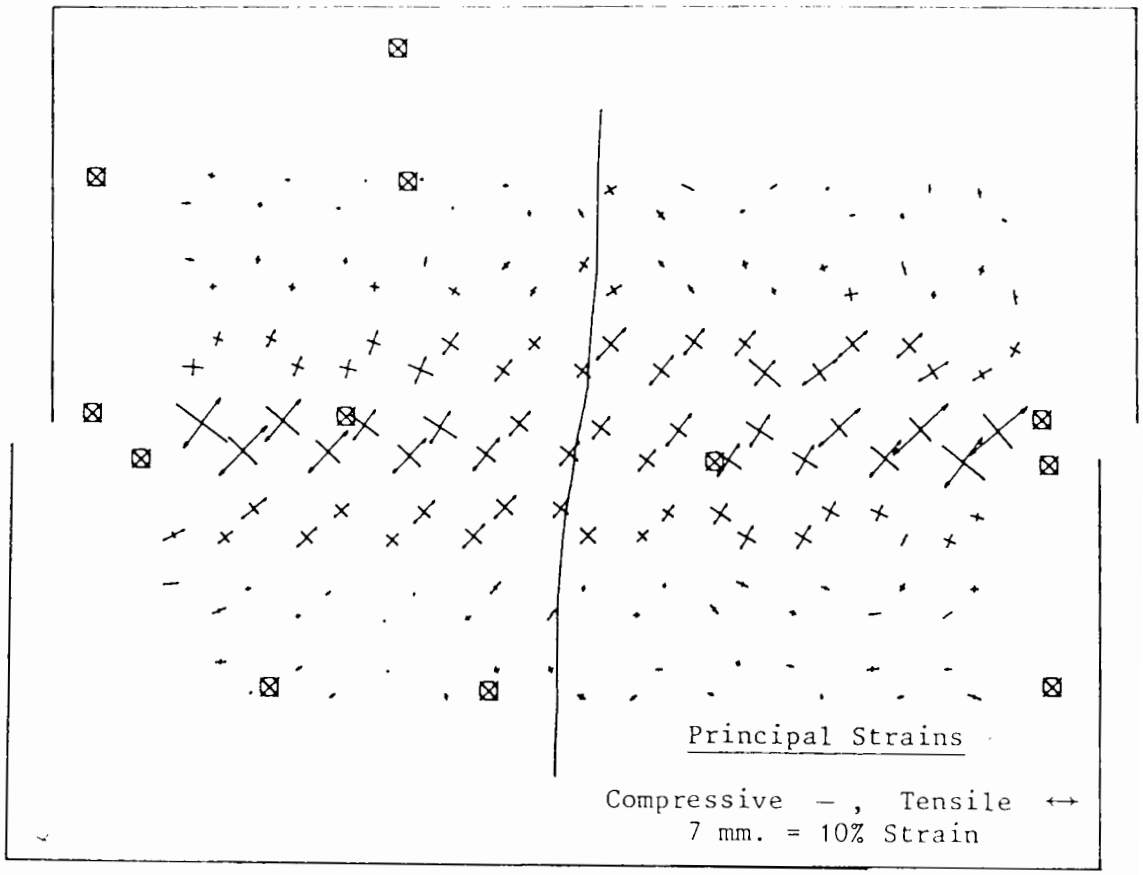


Fig. 5.16 Strains determined between 2.09 mm and 7.51 mm shear displacement for crushed glass containing flexible sheet reinforcement orientated at $\theta = 0°$

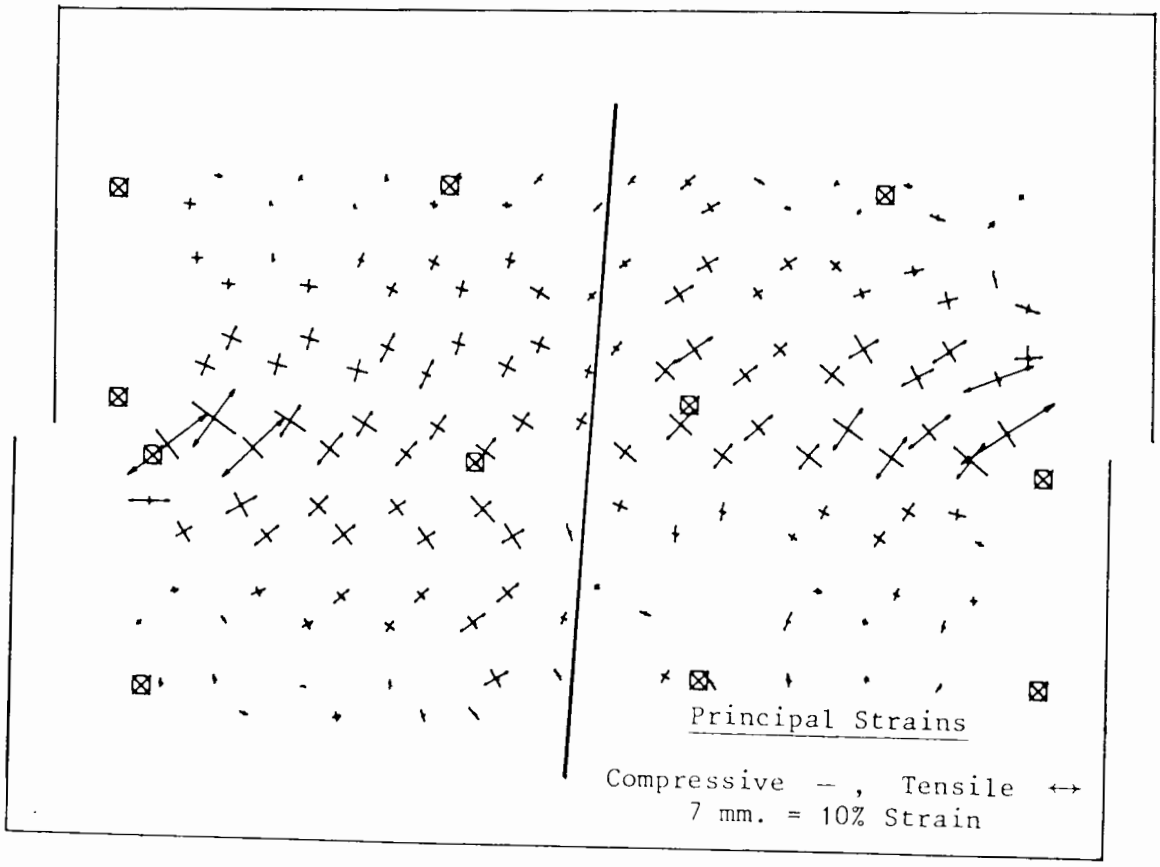


Fig. 5.17 Strains determined between 2.00 mm and 7.66 mm shear displacement for crushed glass containing the rigid reinforcement orientated at $\theta = 0°$

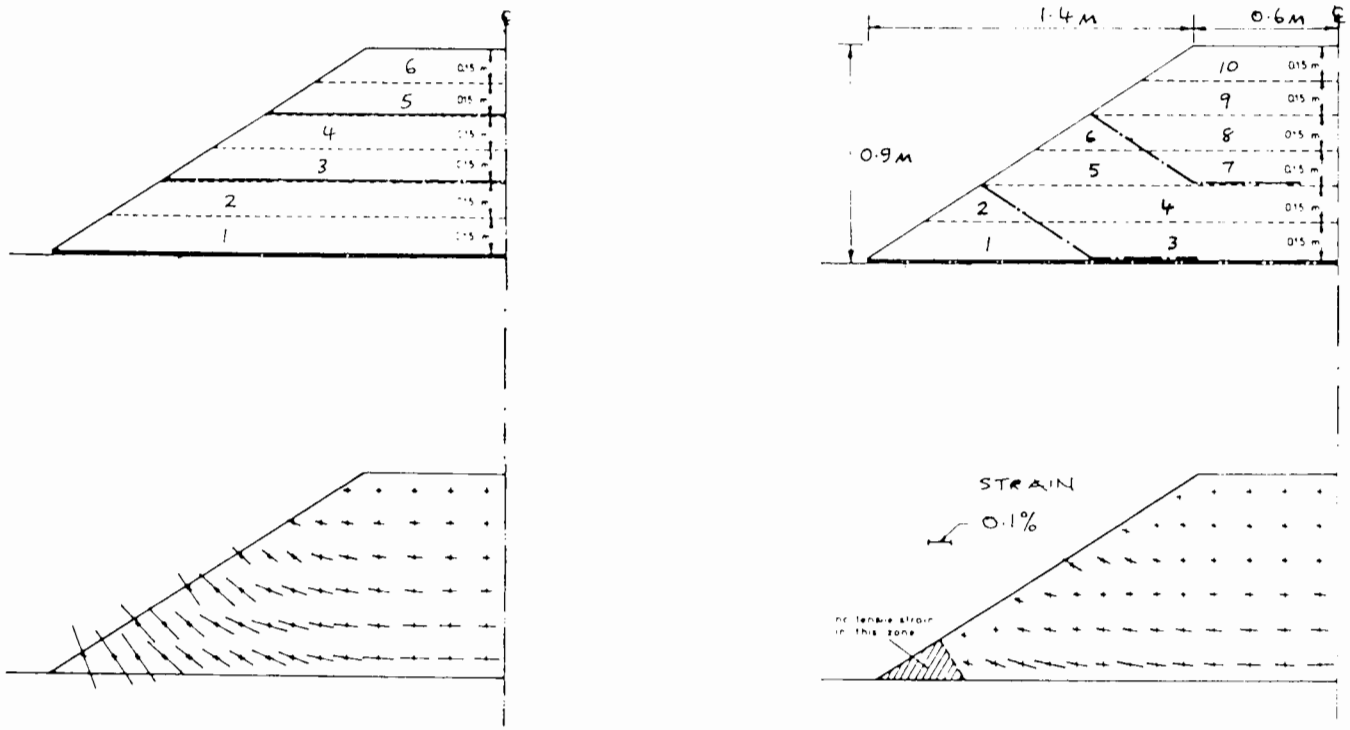


Fig. 5.18 Strain fields determined by McGown et al (1981) for two construction sequences of model sand embankments

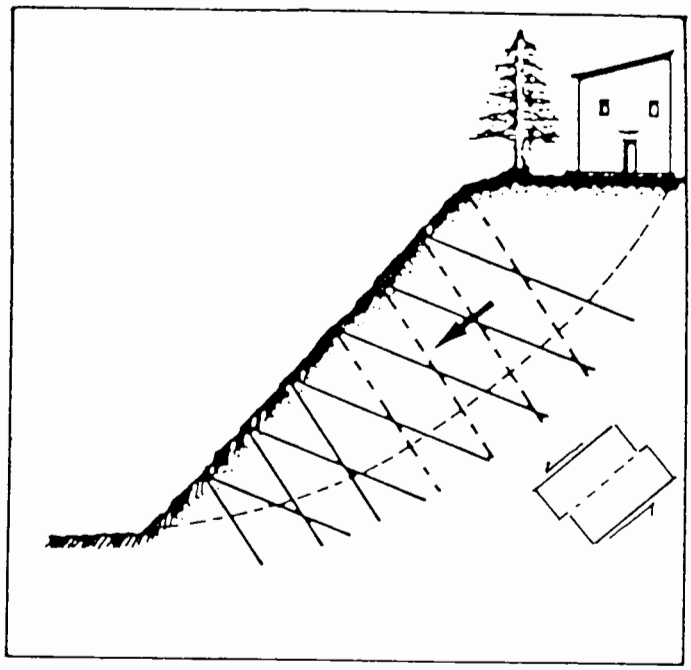

Micropiles loaded in compression — — — —

Fig. 5.19 Indication of micropiles loaded in compression in a network for slope stabilisation (adapted from Lizzi 1983)

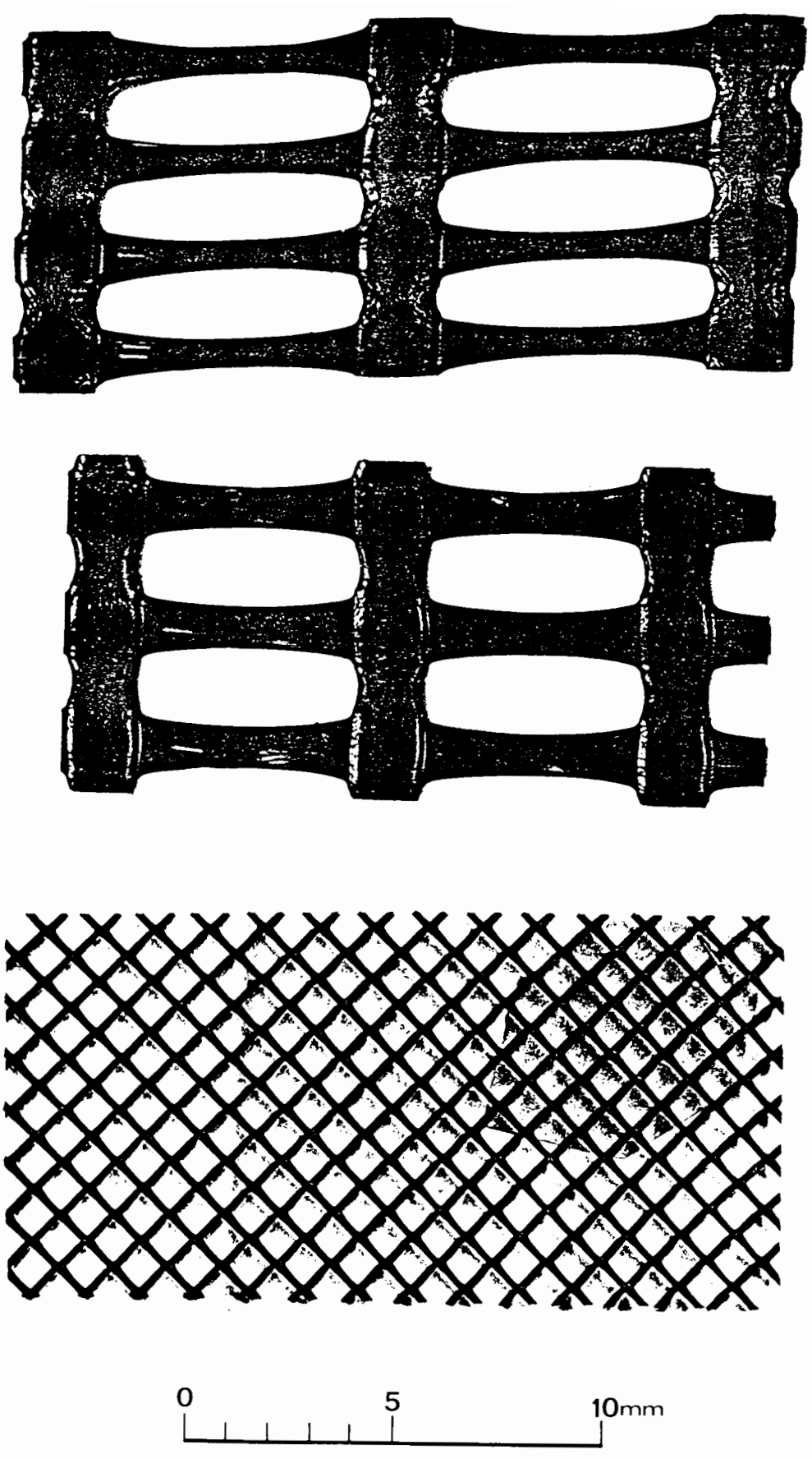


Fig. 6.1 Examples of commercially available polymer grids and net for soil reinforcement

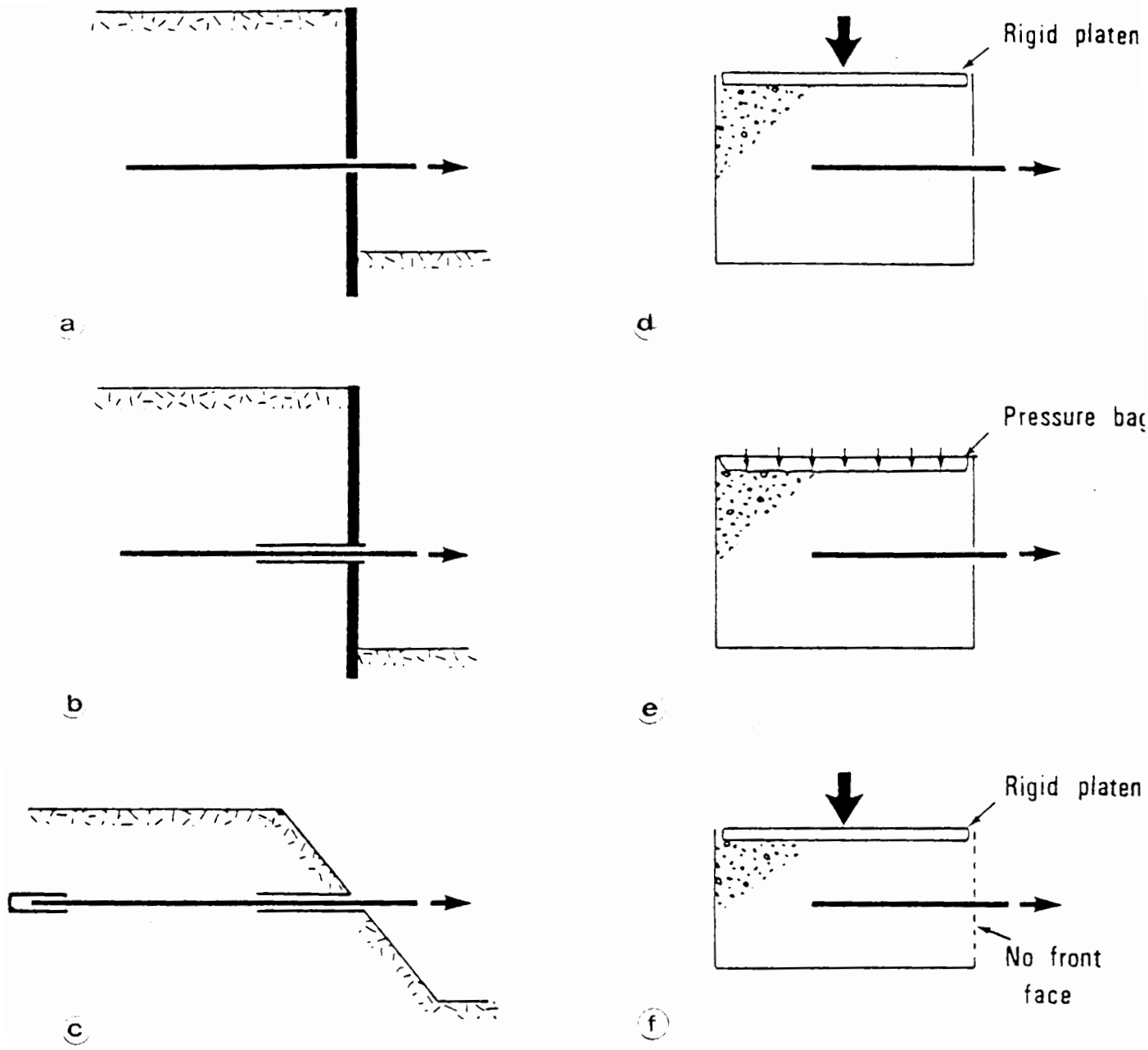


| | |
|---|---|
| Chang, Hannon and Forsyth (1977) | a, f |
| Schlosser and Elias (1978) | c, d |
| Murray, Carder and Krawczyk (1979) | a |
| Schlosser and Guilloux (1979) | b |
| Jewell (1980) | e |
| Ingold (1984) | e |

Fig. 6.2 Some of the typical configurations and boundary conditions which have been used for pull-out tests (adapted from Jewell 1980)

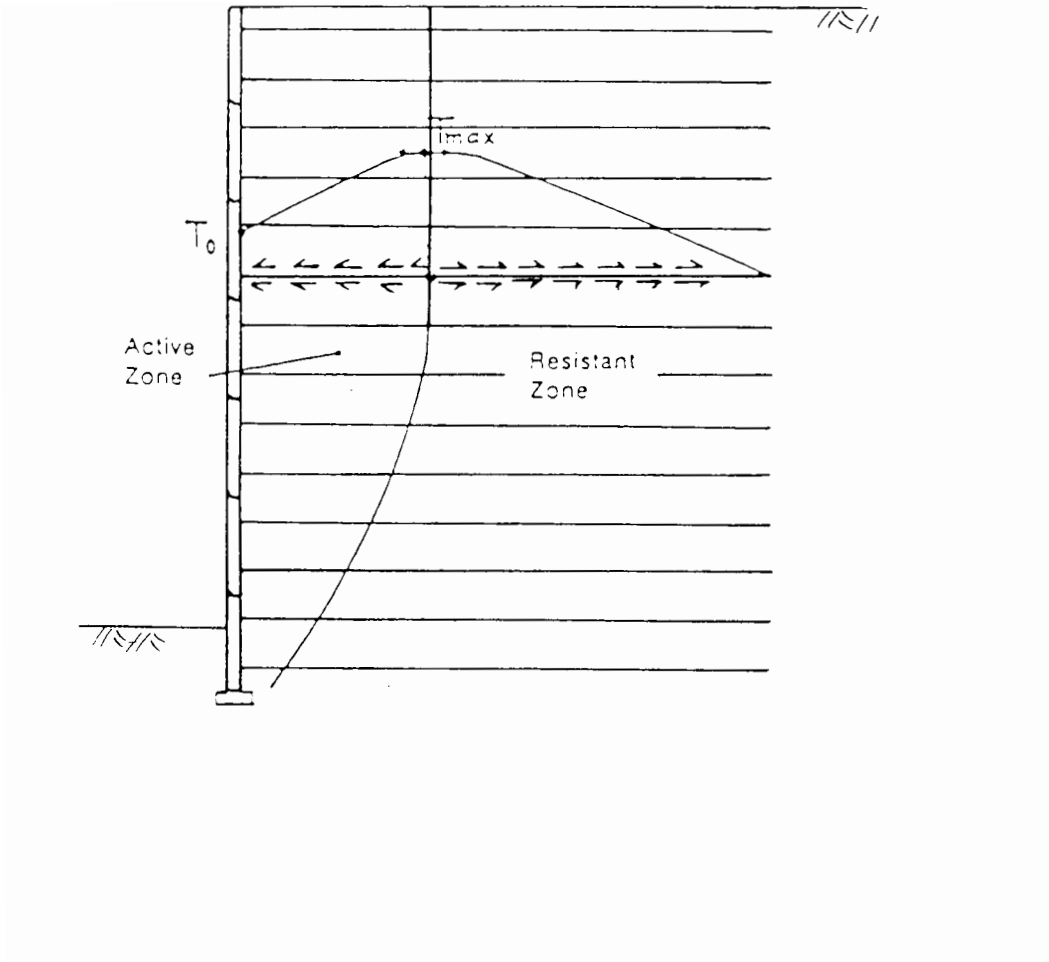


Fig. 6.3 Schematic illustration of pull-out mechanism in a reinforced earth retaining wall (from Schlosser and Elias 1978)

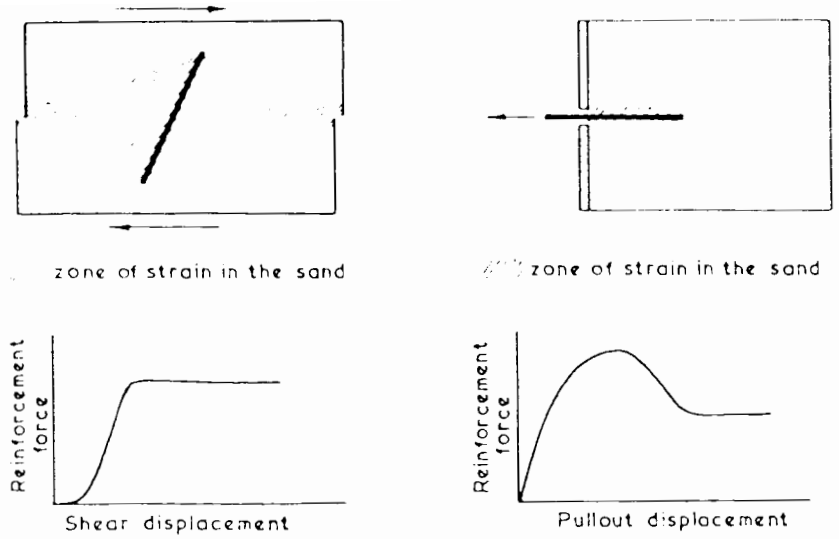


Fig. 6.4 Comparisons of patterns of strain in sand and mobilisation of reinforcement force for a) sand strengthened by tensile reinforcement in a shearbox, and b) pull-out tests on the tensile reinforcement from sand by Jewell (1979)

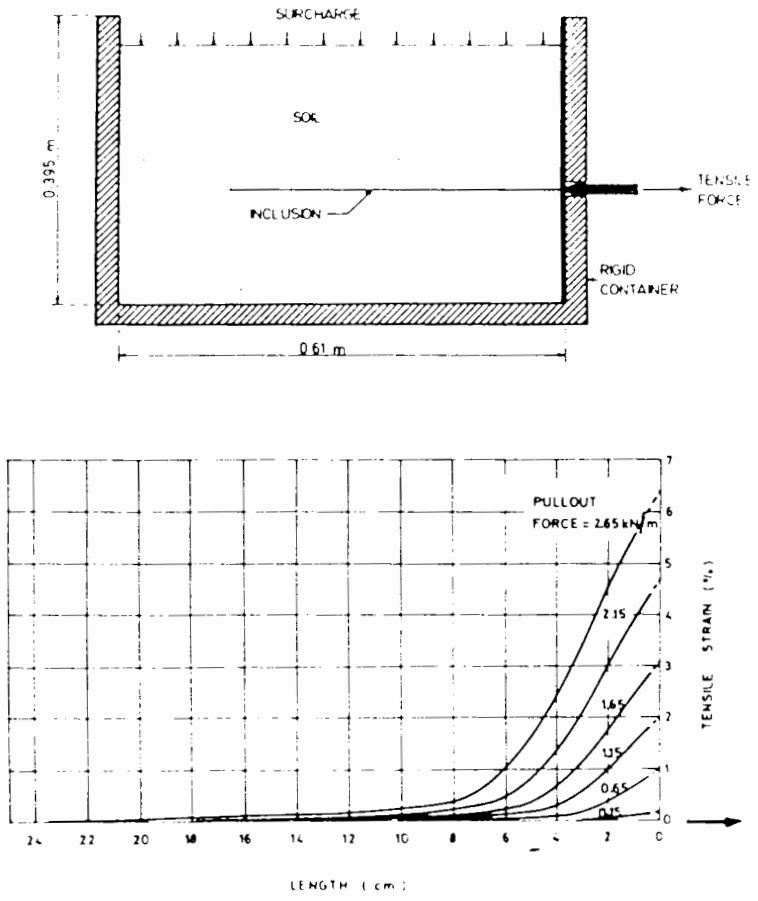


Fig. 6.5 Strain distribution in a geotextile during pull-out at different increments of pull-out force by McGown (1979)

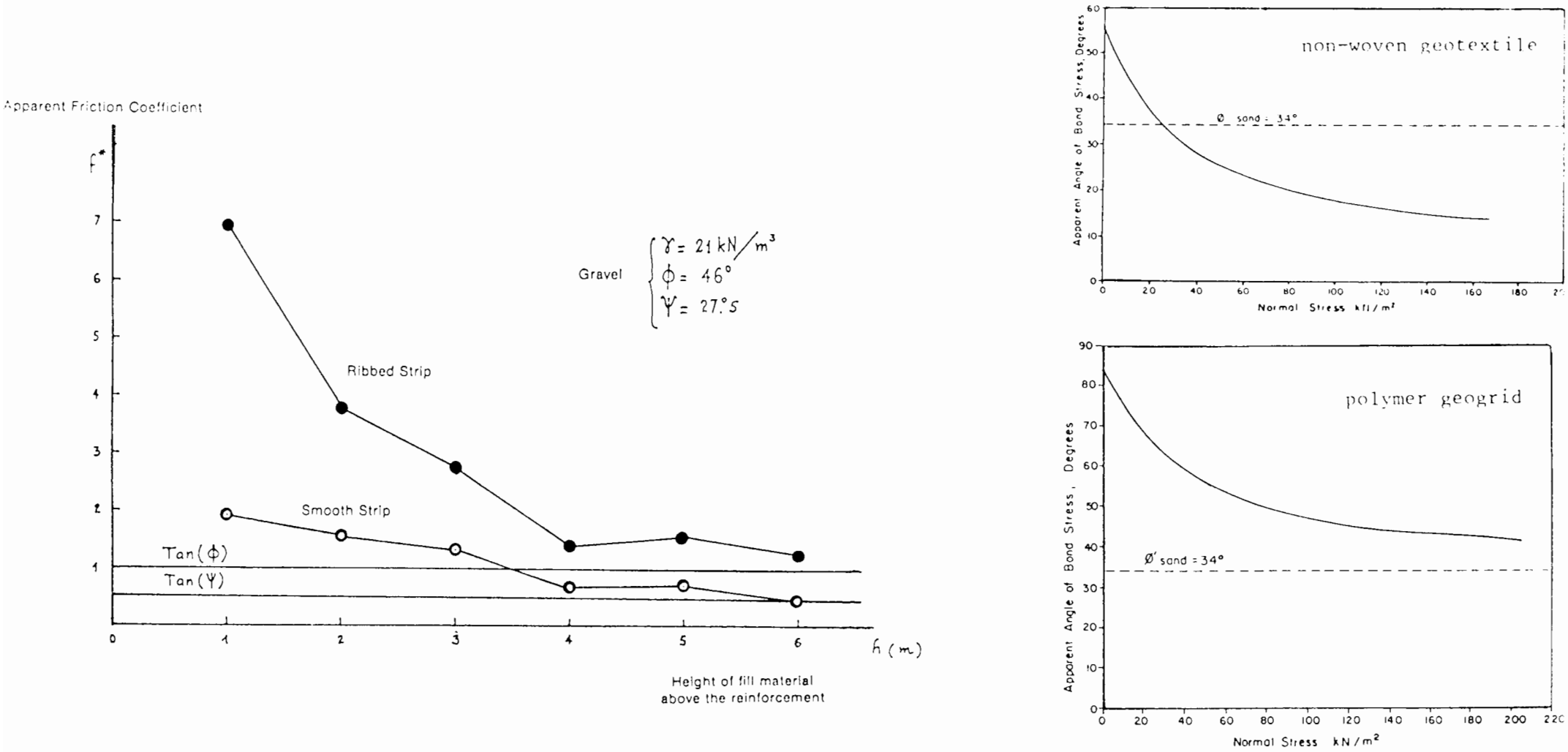


Fig. 6.6 Apparent coefficient of friction and angle of bond for pull-out tests on a) smooth and ribbed steel strips (from Schlosser and Elias 1978) and b) polymer geogrid and non-woven geotextile (from Ingold 1984), for different values of vertical stress

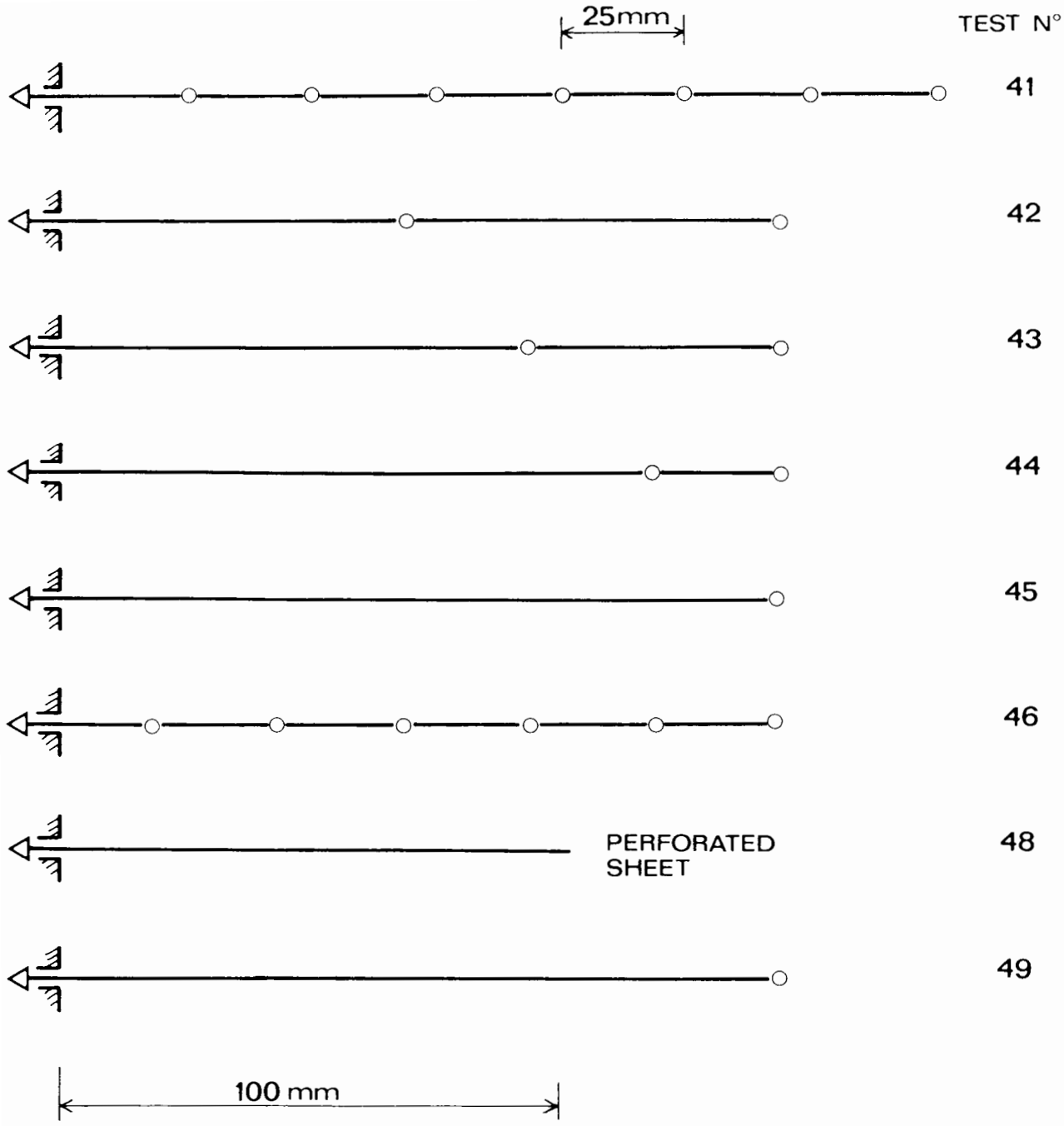


Fig. 6.7 Schematic illustration of pull-out tests performed from crushed glass on lengths of grid, perforated sheet, and single and pairs of transverse members of the grid

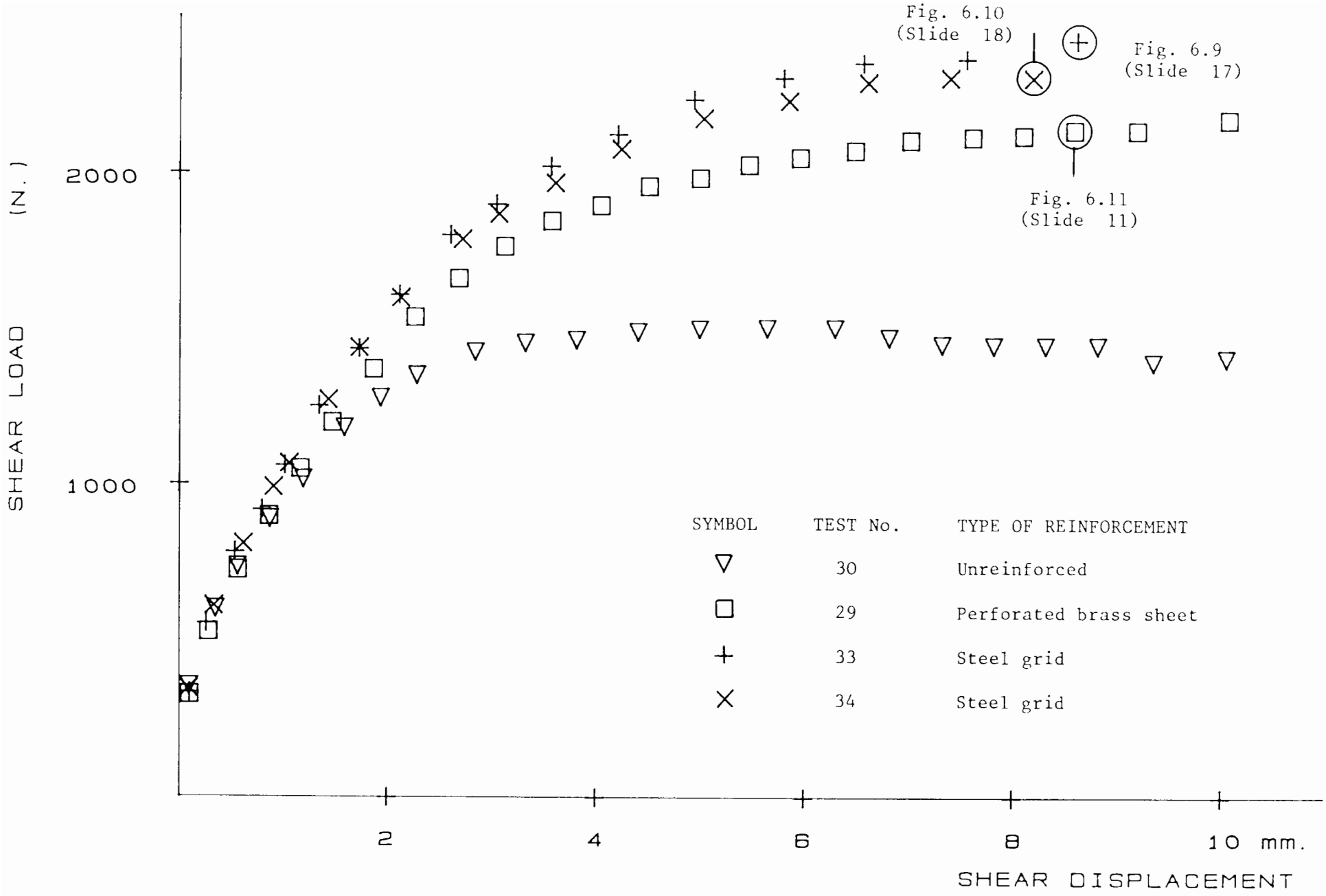


Fig. 6.8 Comparison of the reinforcing effects produced by the perforated sheet and grid acting as tensile reinforcement in the shearbox orientated at $\theta = 40°$

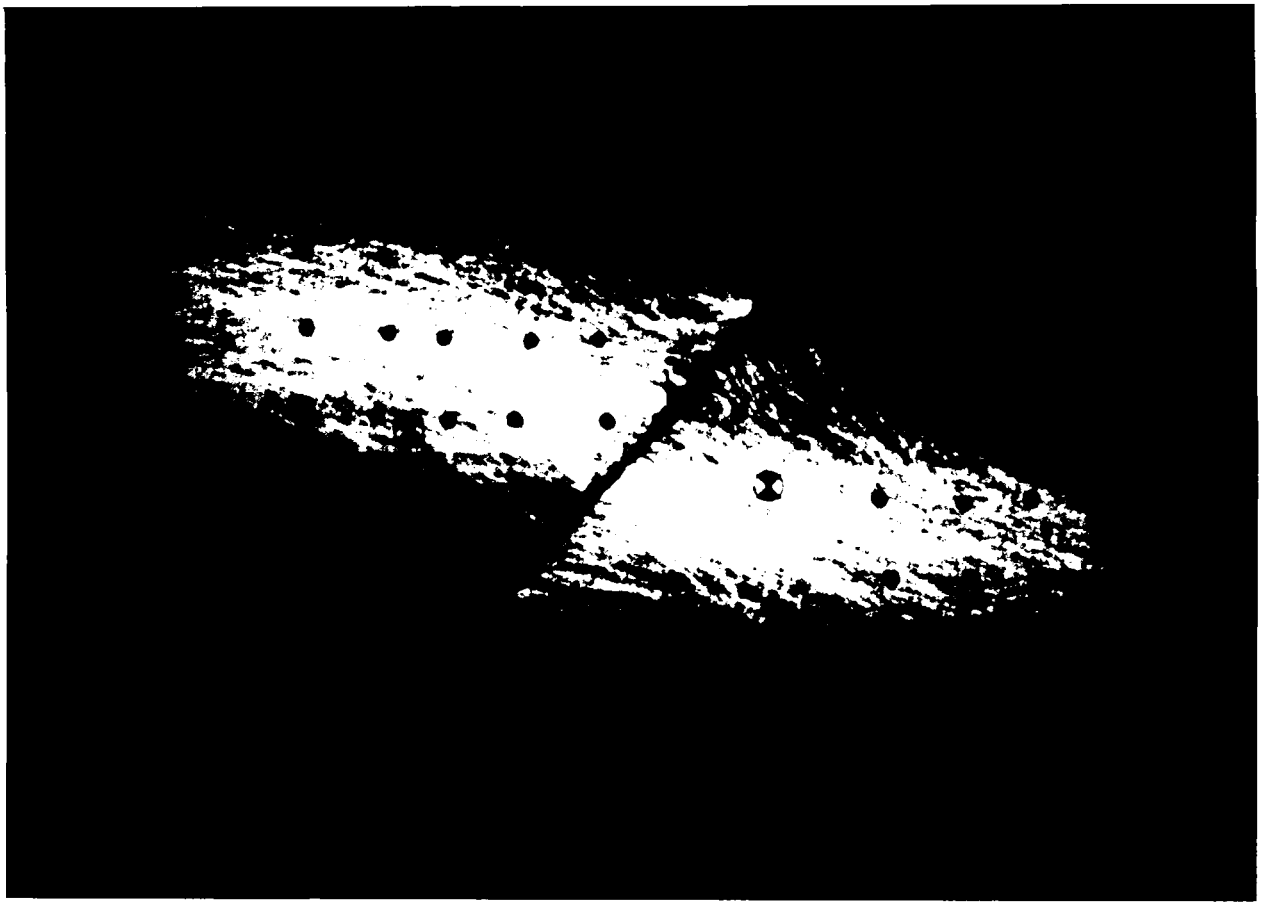

Fig. 6.9 Light stripes observed at 8.63 mm shear displacement in a direct shear test on crushed glass containing the steel grid orientated at $\theta$ = 40° (test no. 33)

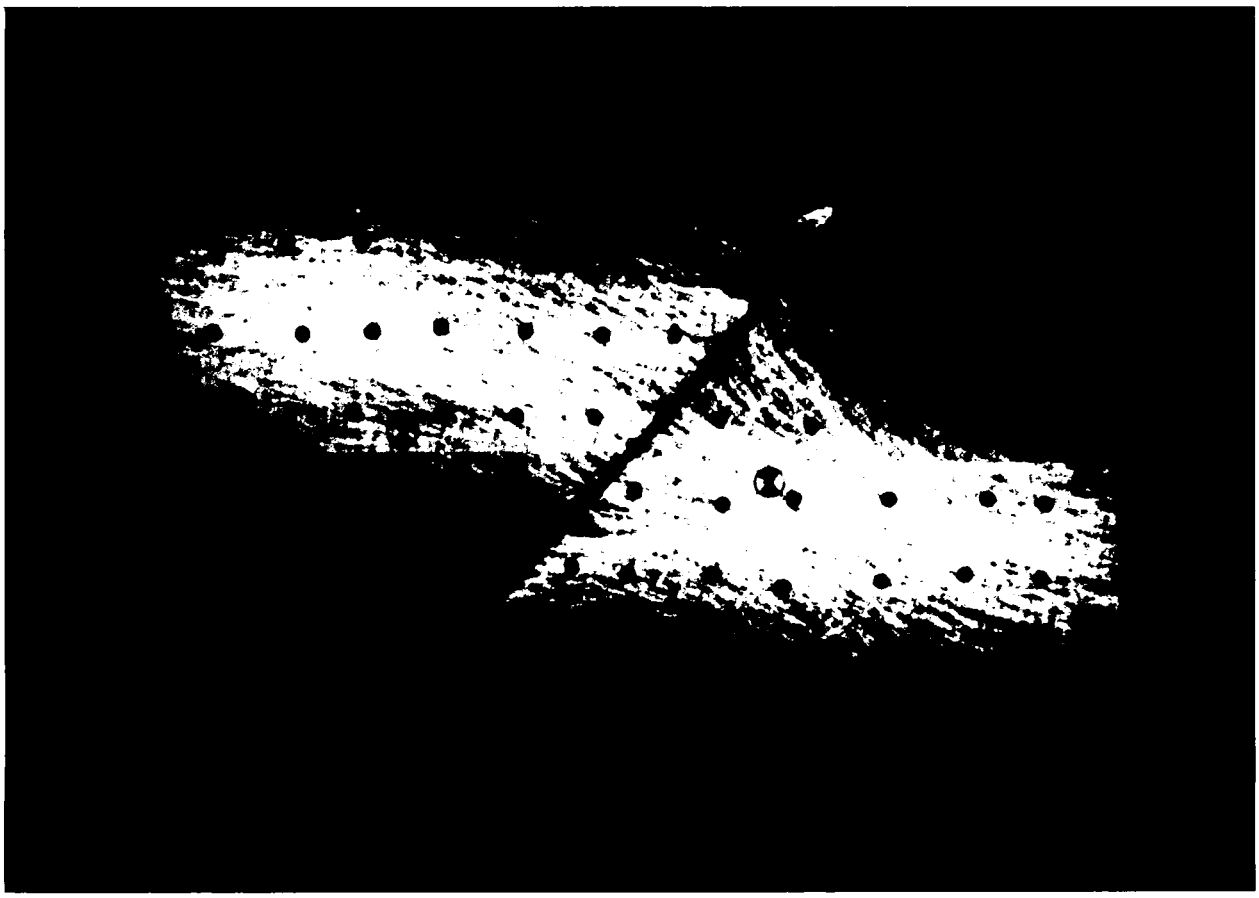

Fig. 6.10 Light stripes observed at 8.20 mm shear displacement in a direct shear test on crushed glass containing the steel grid orientated at $\theta$ = 40° (test no. 34)

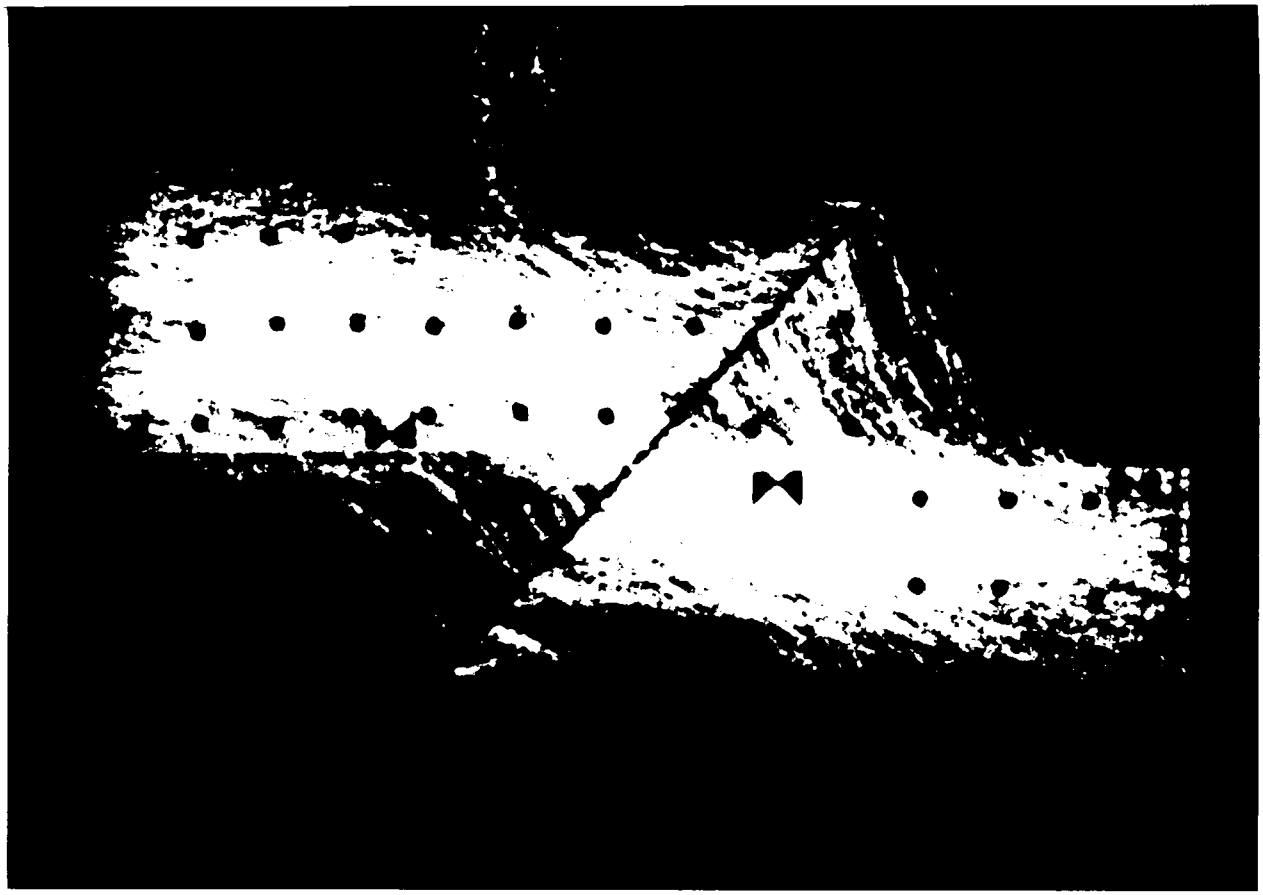

Fig. 6.11 Light stripes observed at 8.60 mm shear displacement in a direct shear test on crushed glass containing the perforated sheet orientated at $\theta = 40°$ (test no. 29)

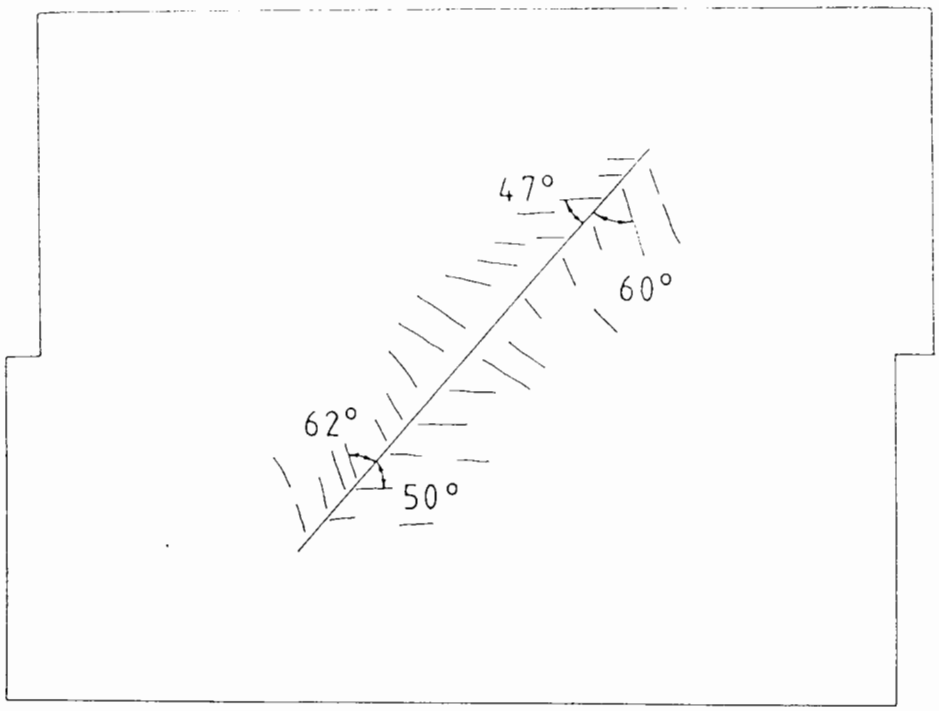


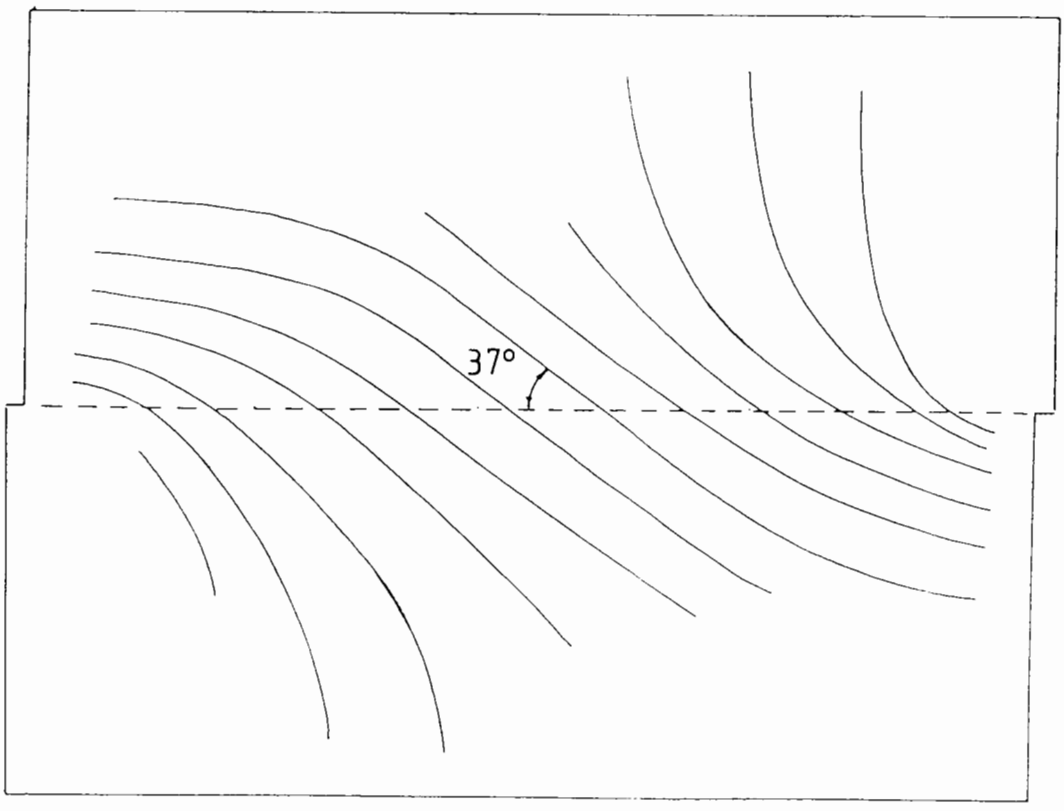


Fig. 6.12 Comparison of the inclination of light stripes to a) perforated sheet acting as tensile reinforcement in the shearbox (from fig. 6.11), and b) central plane of the box for maximum direct shear resistance of crushed glass (from fig. 4.8)

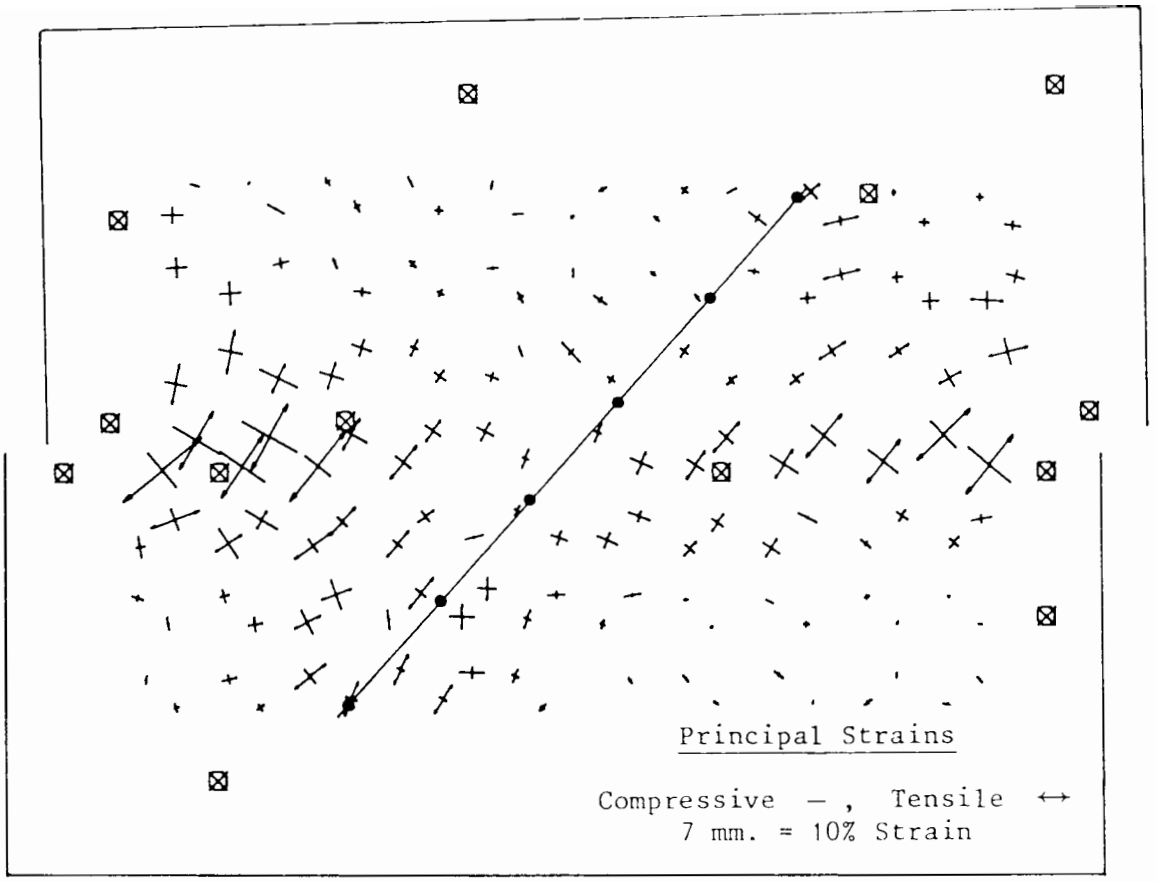


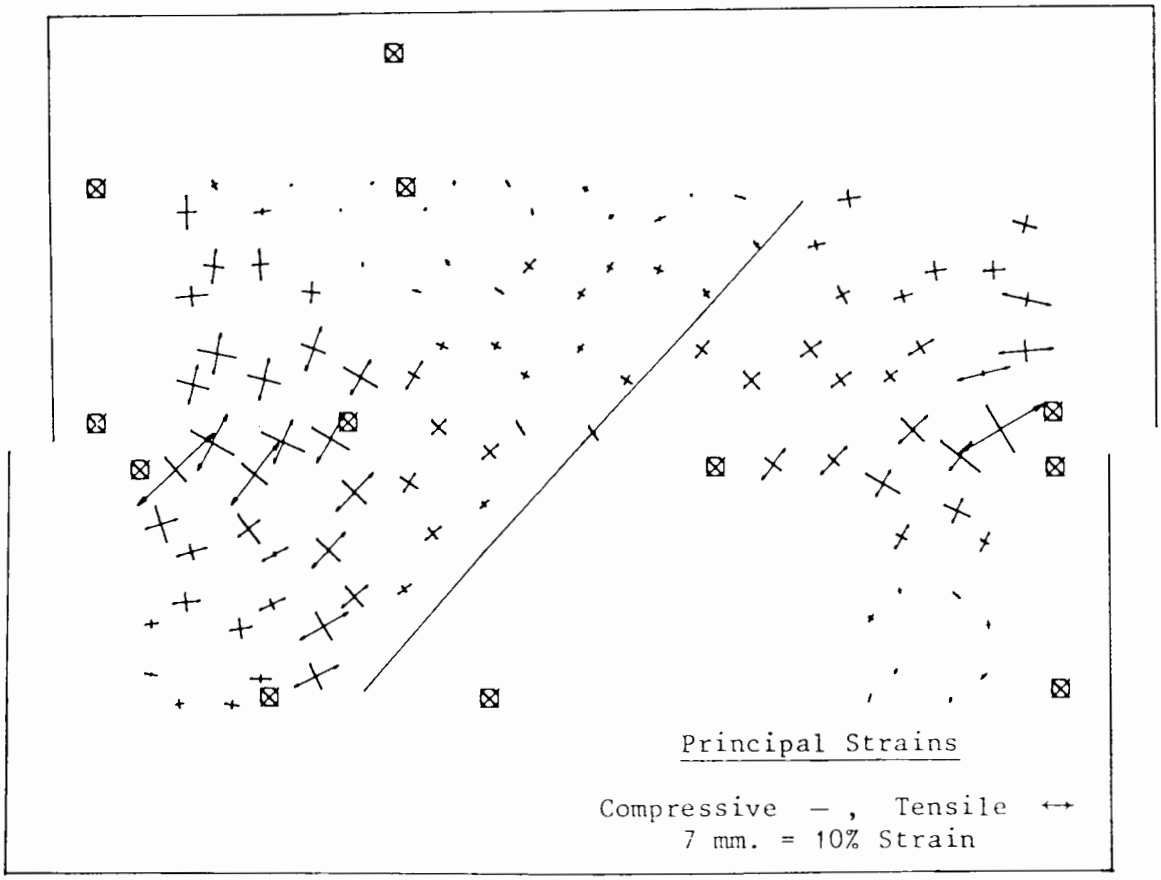


Fig. 6.13 Patterns of strains developed in crushed glass for a) grid and b) perforated sheet acting as tensile reinforcement

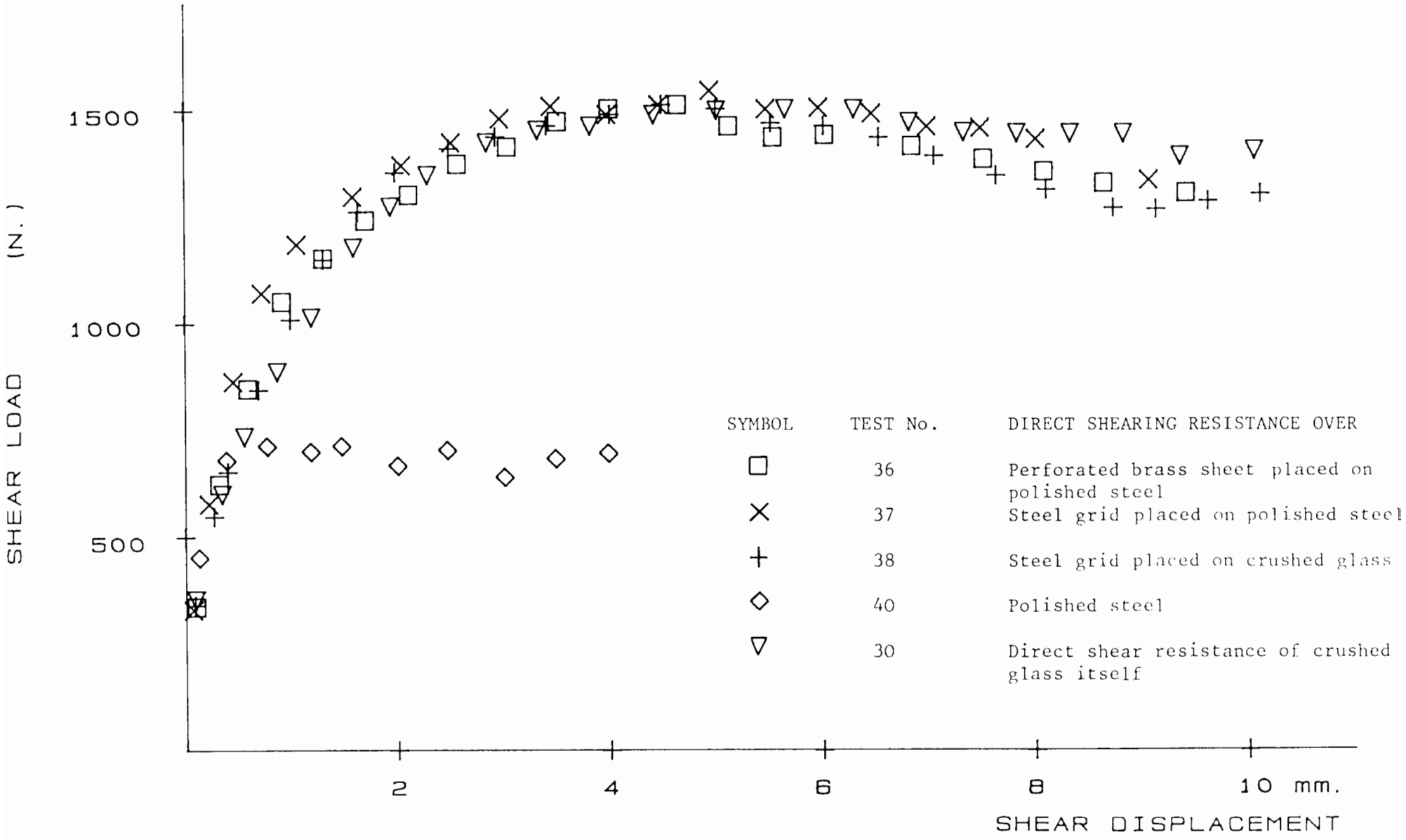


Fig. 6.14 Direct sliding resistance of crushed glass over steel grid, perforated brass sheet and polished steel compared with direct shear resistance of crushed glass itself

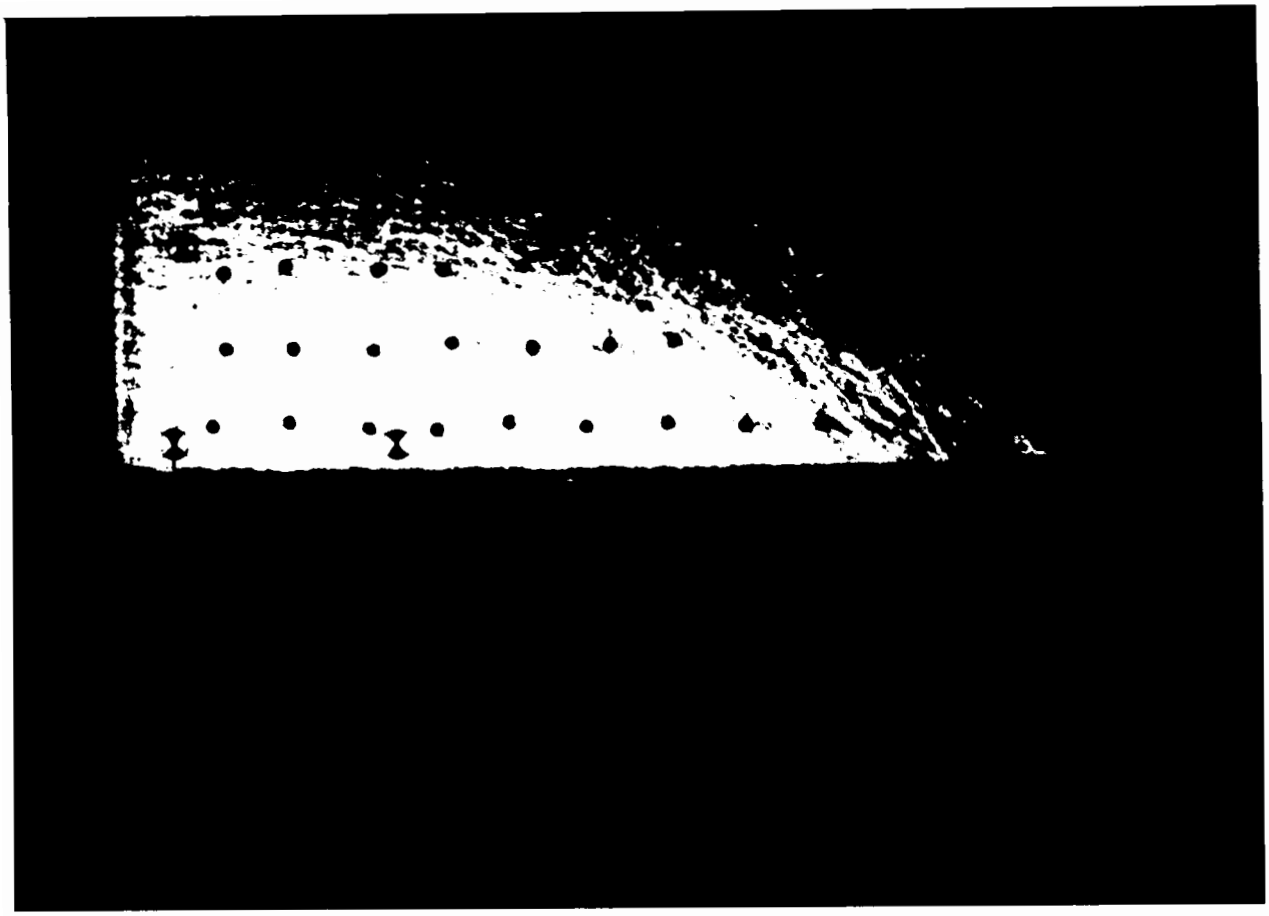

Fig. 6.15 Light stripes observed at 3.96 mm shear displacement for direct sliding of crushed glass over the steel grid placed along the central plane of the box on a polished steel block (test no. 37)

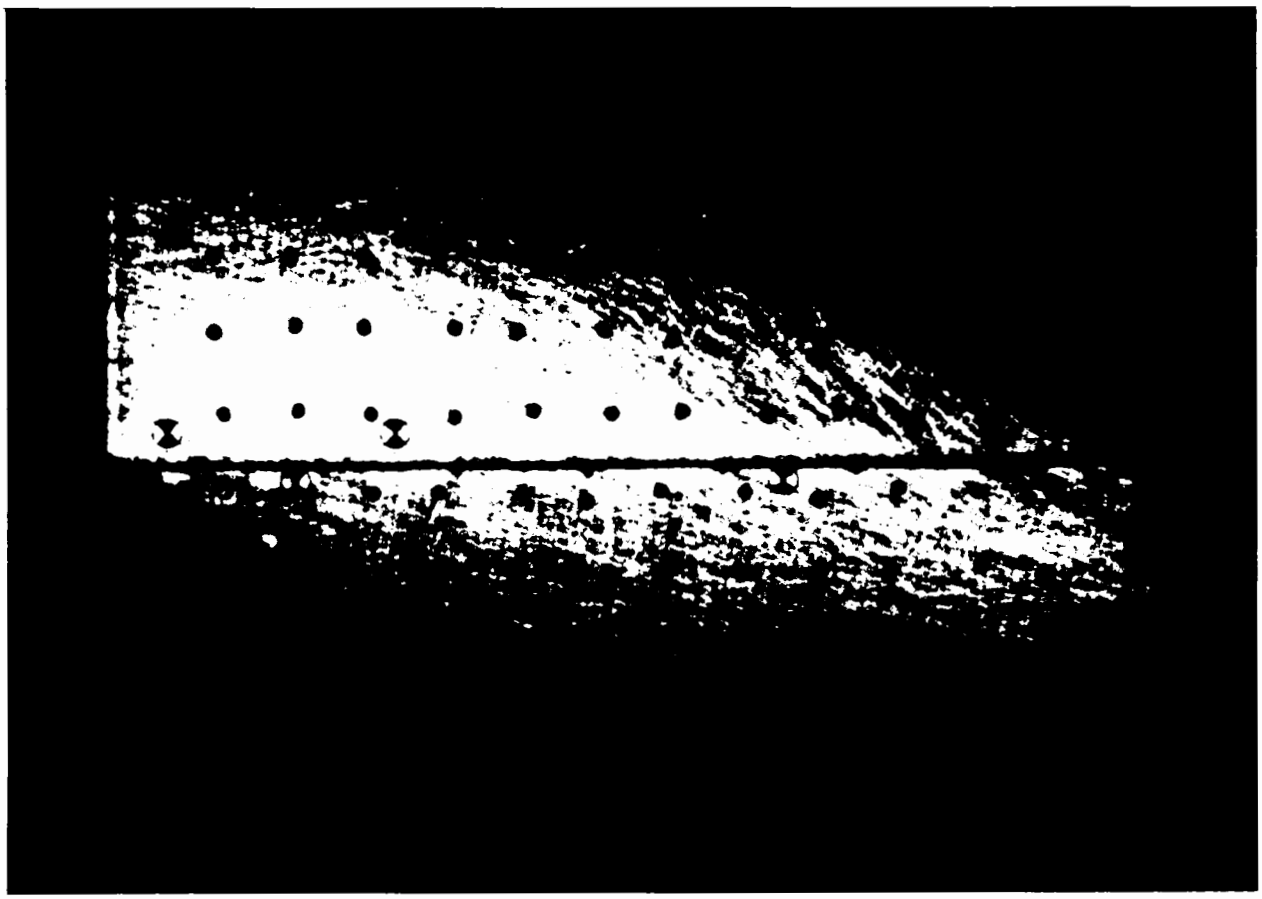

Fig. 6.16 Light stripes observed at 3.96 mm shear displacement for direct sliding of crushed glass over the steel grid placed along the central plane of the box directly on crushed glass (Test no. 38)

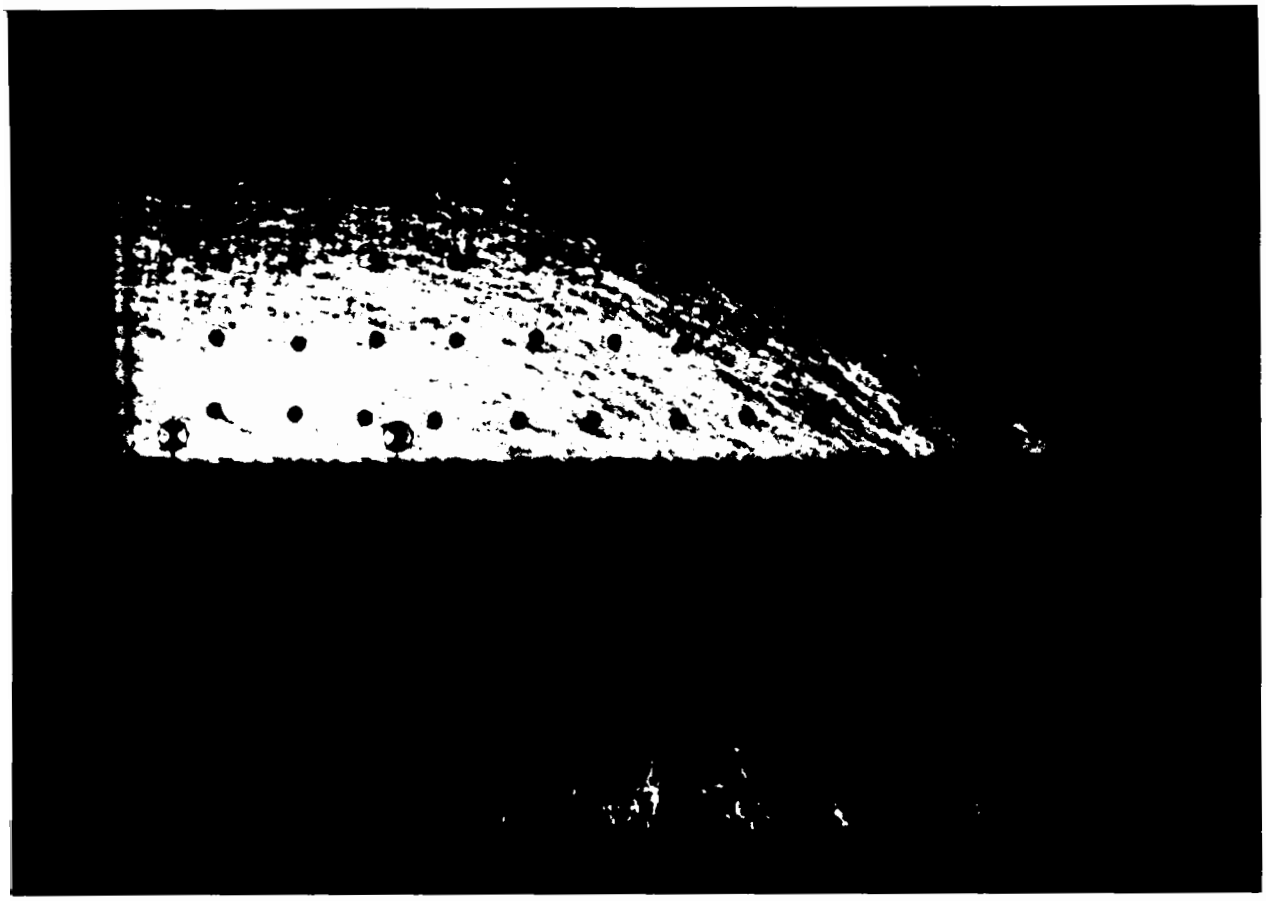

Fig. 6.17 Light stripes observed at 4.00 mm shear displacement for direct sliding of crushed glass over the perforated brass sheet placed along the central plane of the box on a polished steel block

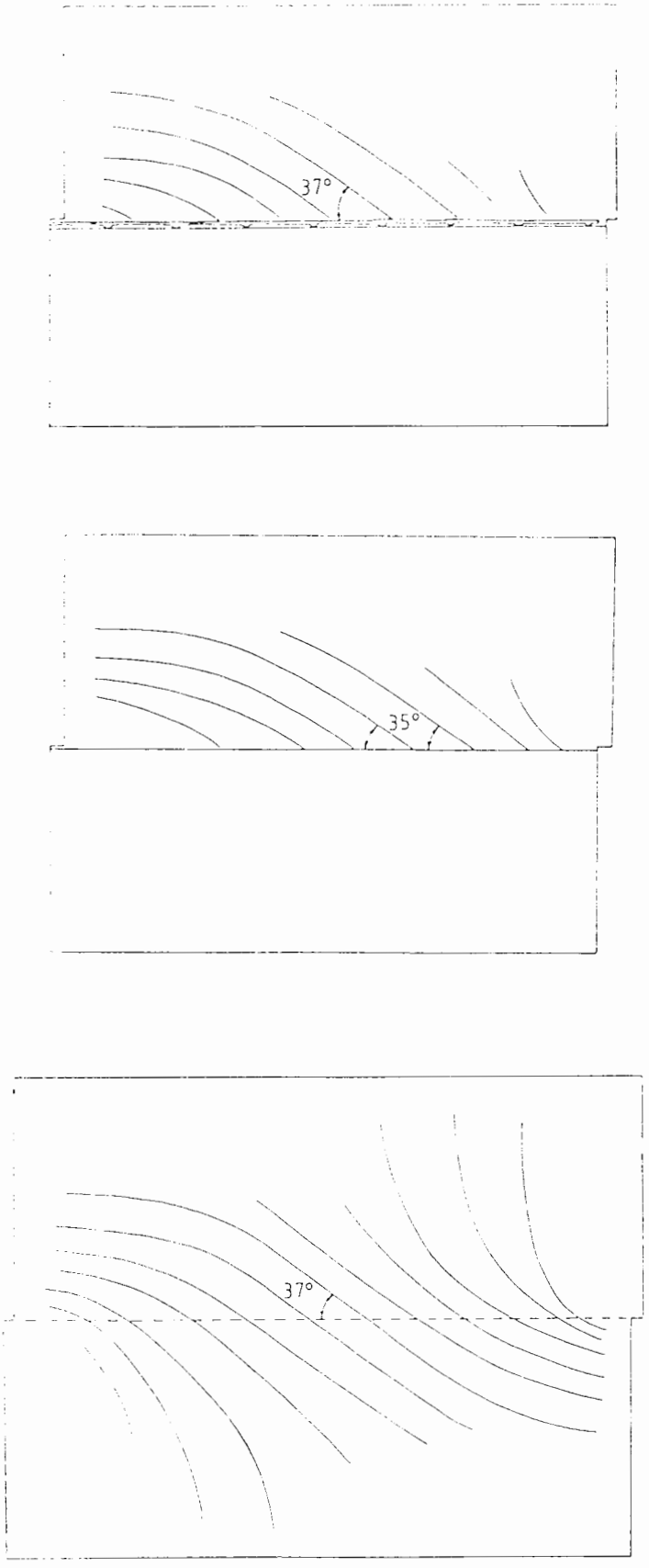


Fig. 6.18 Comparison of the inclination of light stripes for a) direct sliding resistance over steel grid (from fig. 6.15), b) direct sliding resistance over perforated sheet (from fig. 6.17) and c) direct shear resistance of crushed glass itself (from fig. 4.8), all at maximum resistance

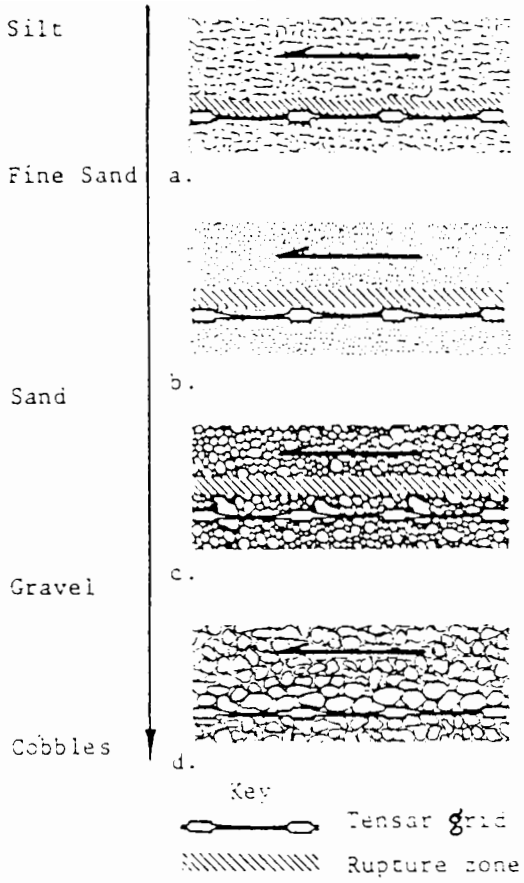


(i) Four main mechanisms for direct sliding resistance over a polymer grid. View in cross section across direction of sliding

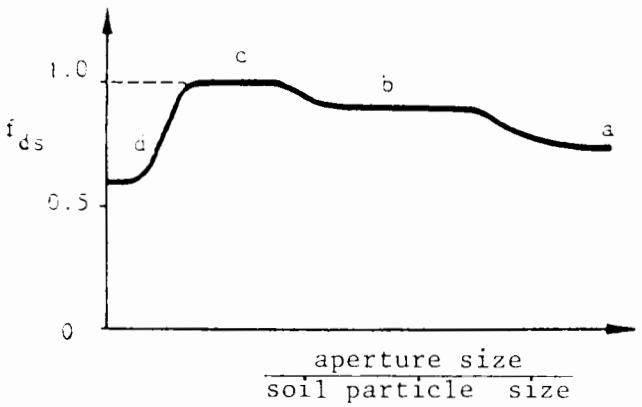


(ii) Variation of direct sliding resistance as a multiple of tan $\phi'$ for the mechanisms illustrated above

Fig. 6.19 Schematic illustrations given by Jewell et al. (1984) for the influence of soil porfide size on direct sliding resistance over a polymer grid

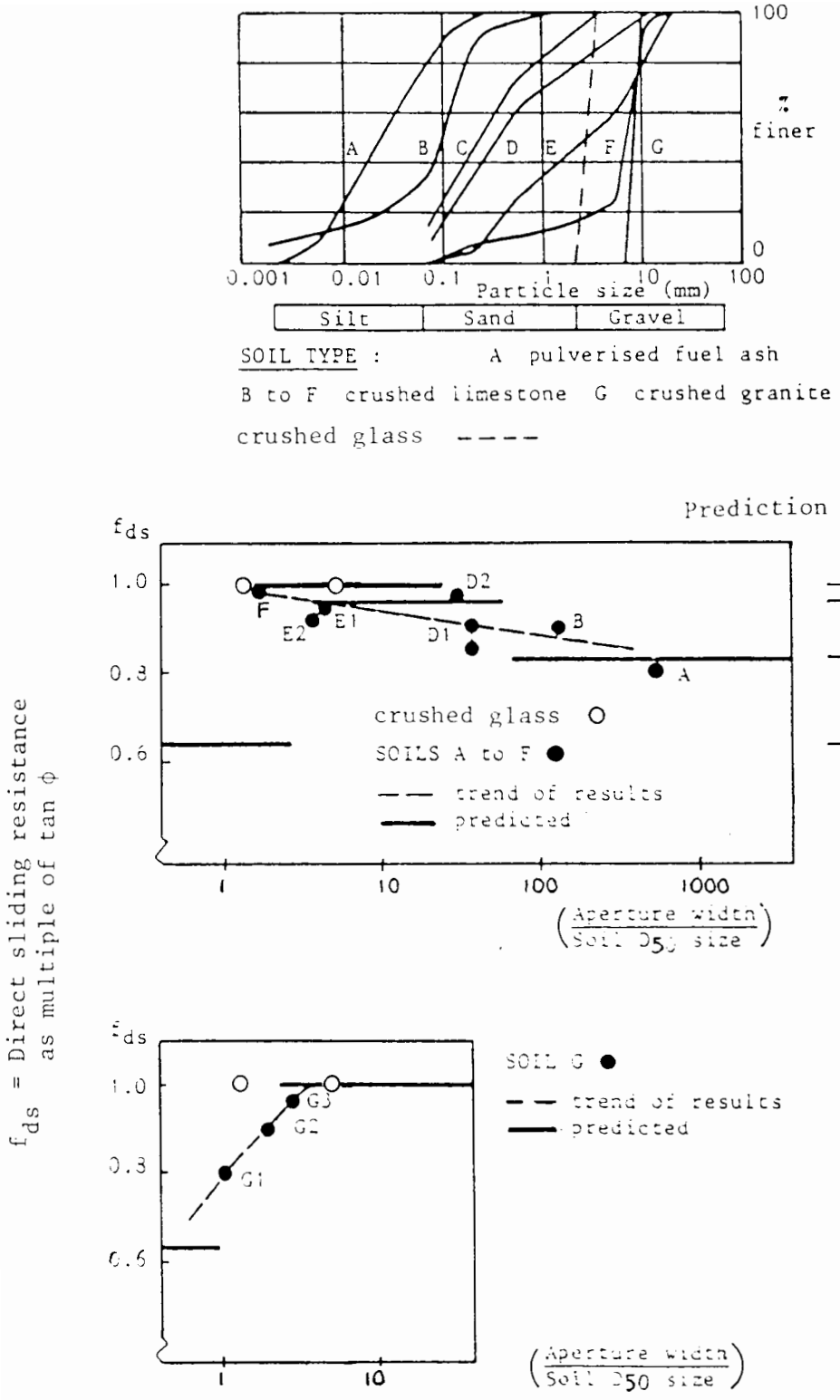


Fig. 6.20 Measured peak direct sliding resistance for granular soils over polymer grids by Jewell et al. (1984) compared with direct sliding resistance of crushed glass over the steel grid and perforated sheet

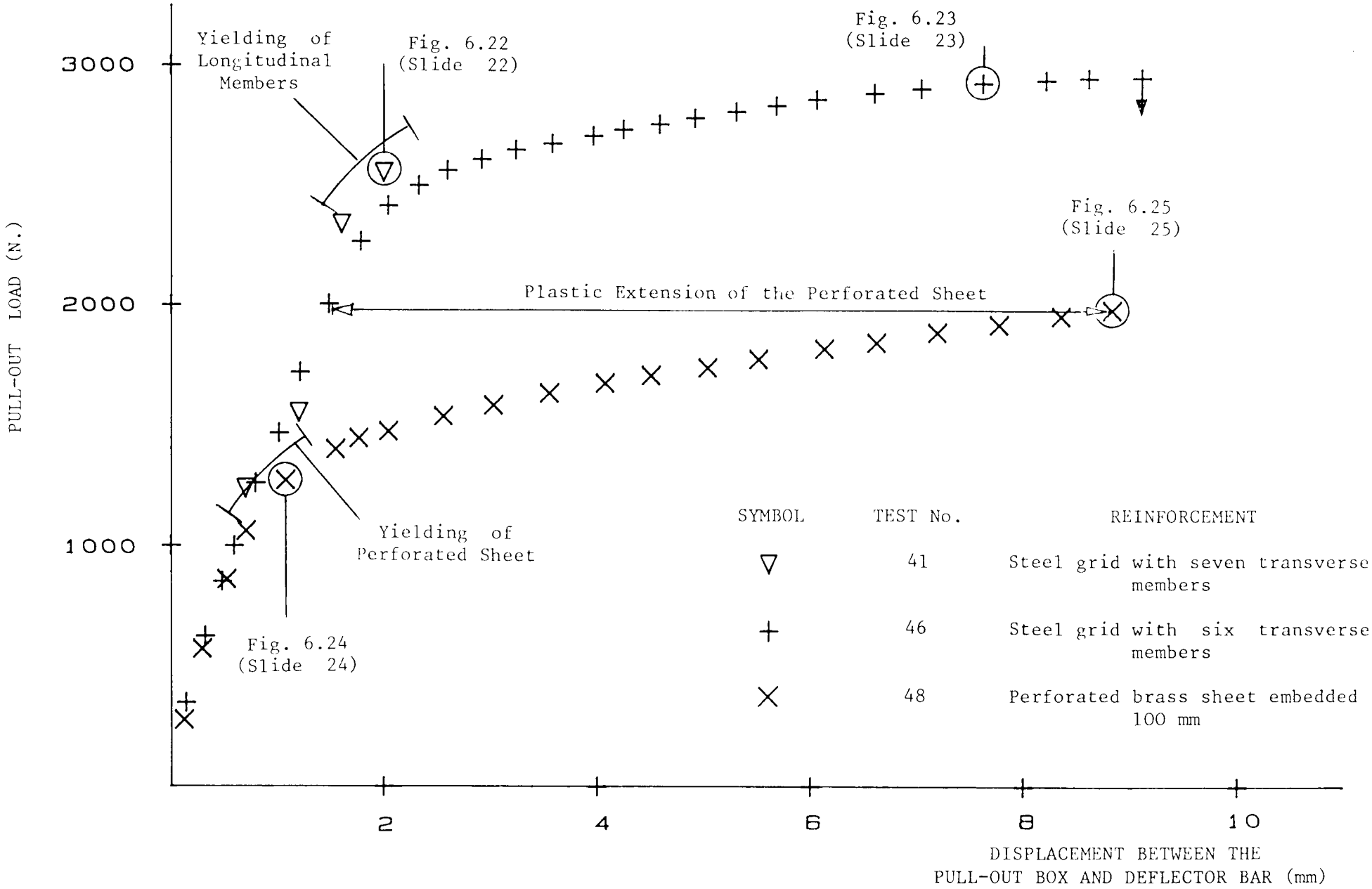


Fig. 6.21 Pull-out tests on lengths of steel grid and perforated brass sheet

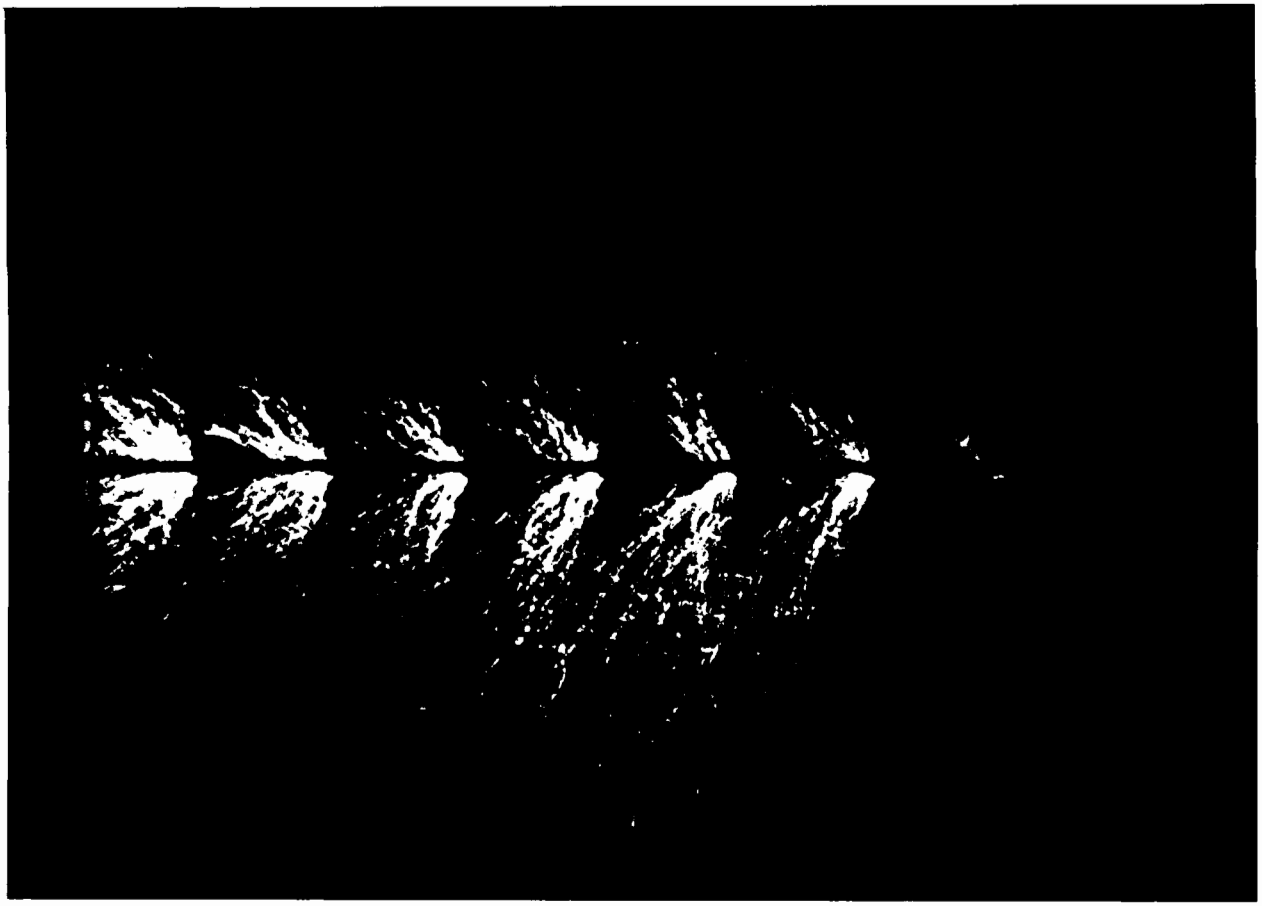

Fig. 6.22 Light stripes observed for a pull-out test on a length of steel grid after approximately 2.0 mm pull-out displacement (test no. 41)

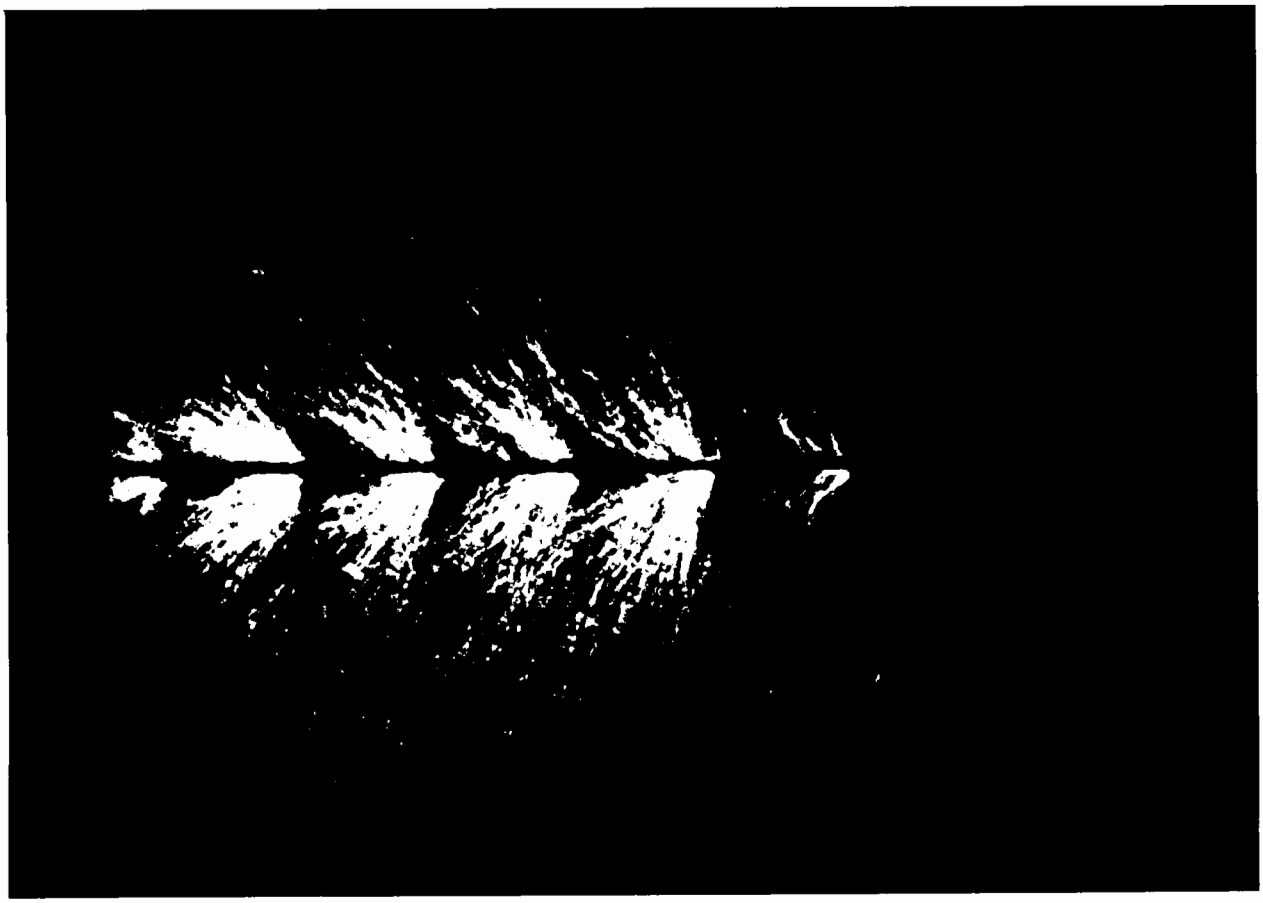

Fig. 6.23 Light stripes observed for a pull-out test on a length of steel grid after 7.62 mm displacement between the pull-out box and deflector bar (test no. 46)

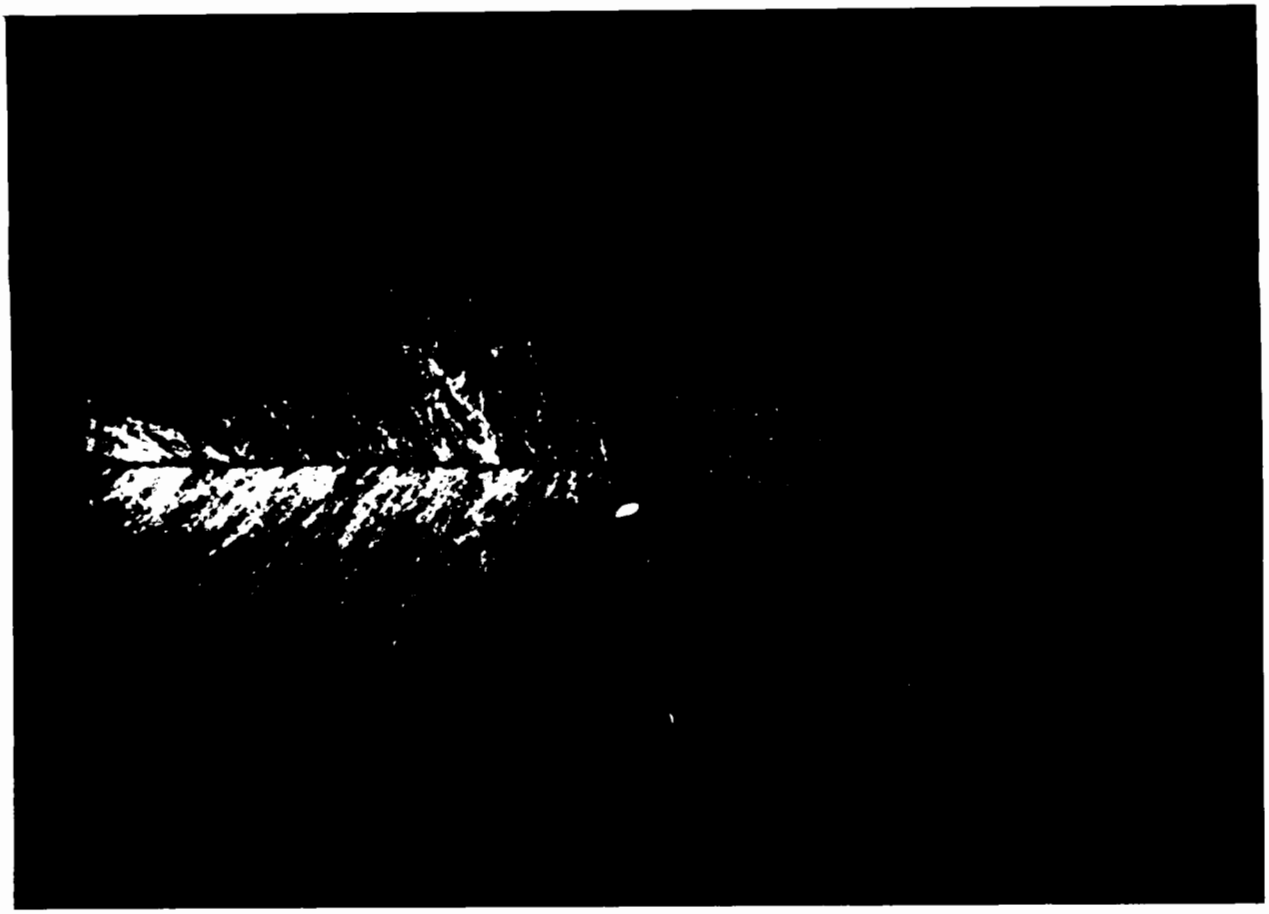

Fig. 6.24 Light stripes observed for a pull-out test on a length of perforated brass sheet after 1.07 mm displacement between the pull-out box and deflector bar (test no. 48)

Fig. 6.25 Light stripes observed for a pull-out test on a length of perforated brass sheet after 8.83 mm displacement between the pull-out box and deflector bar

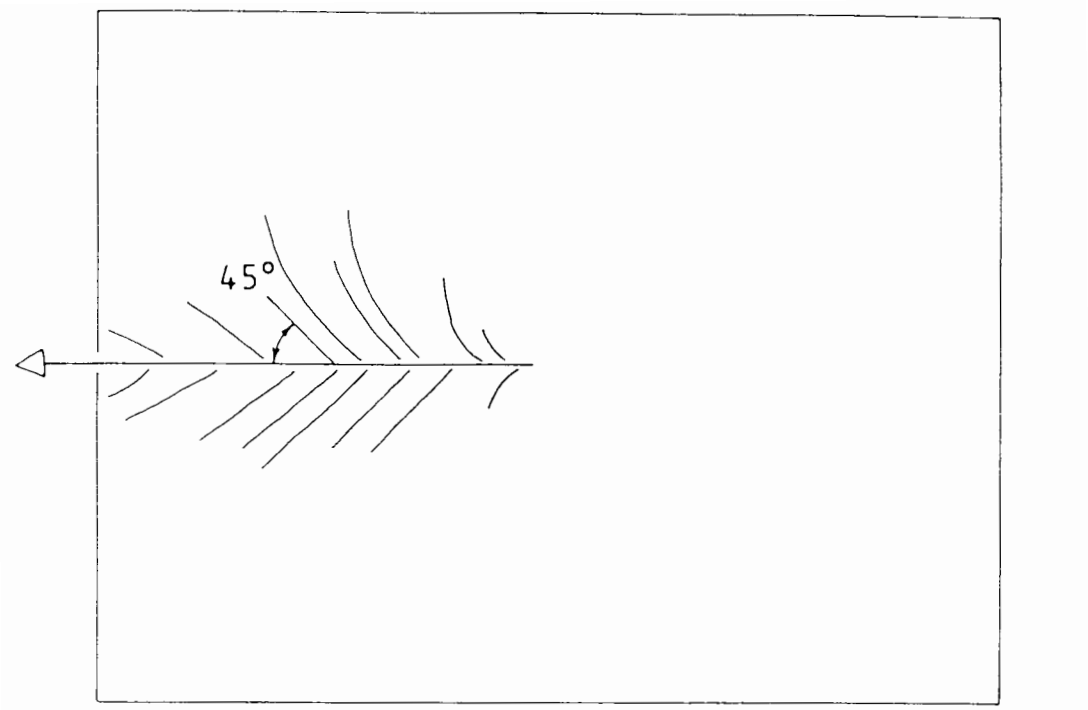


Fig. 6.26 Inclination of the light stripes to the perforated sheet during pull-out as shown in fig. 6.25

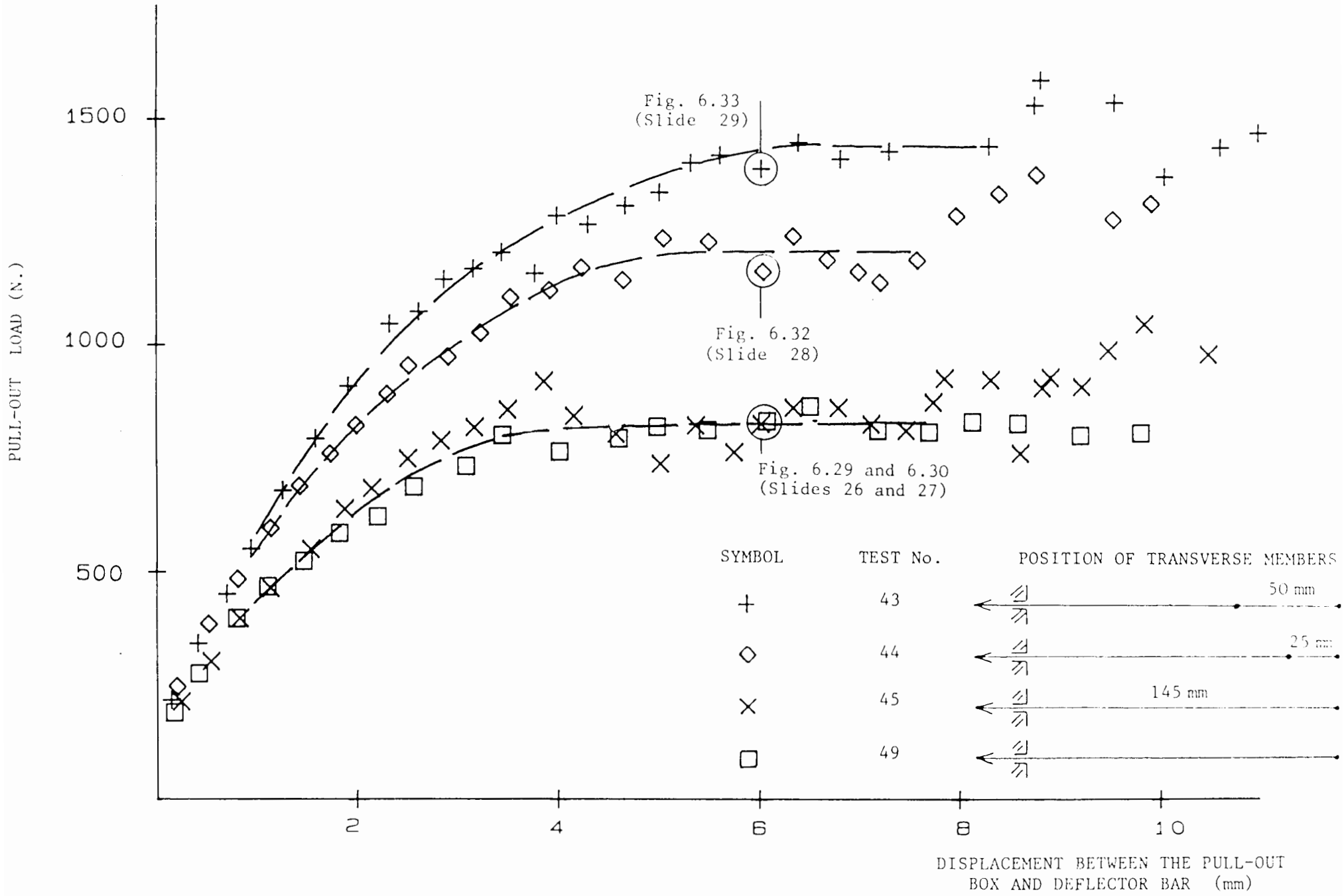


Fig. 6.27 Pull out of single and pairs of transverse members of the steel grid

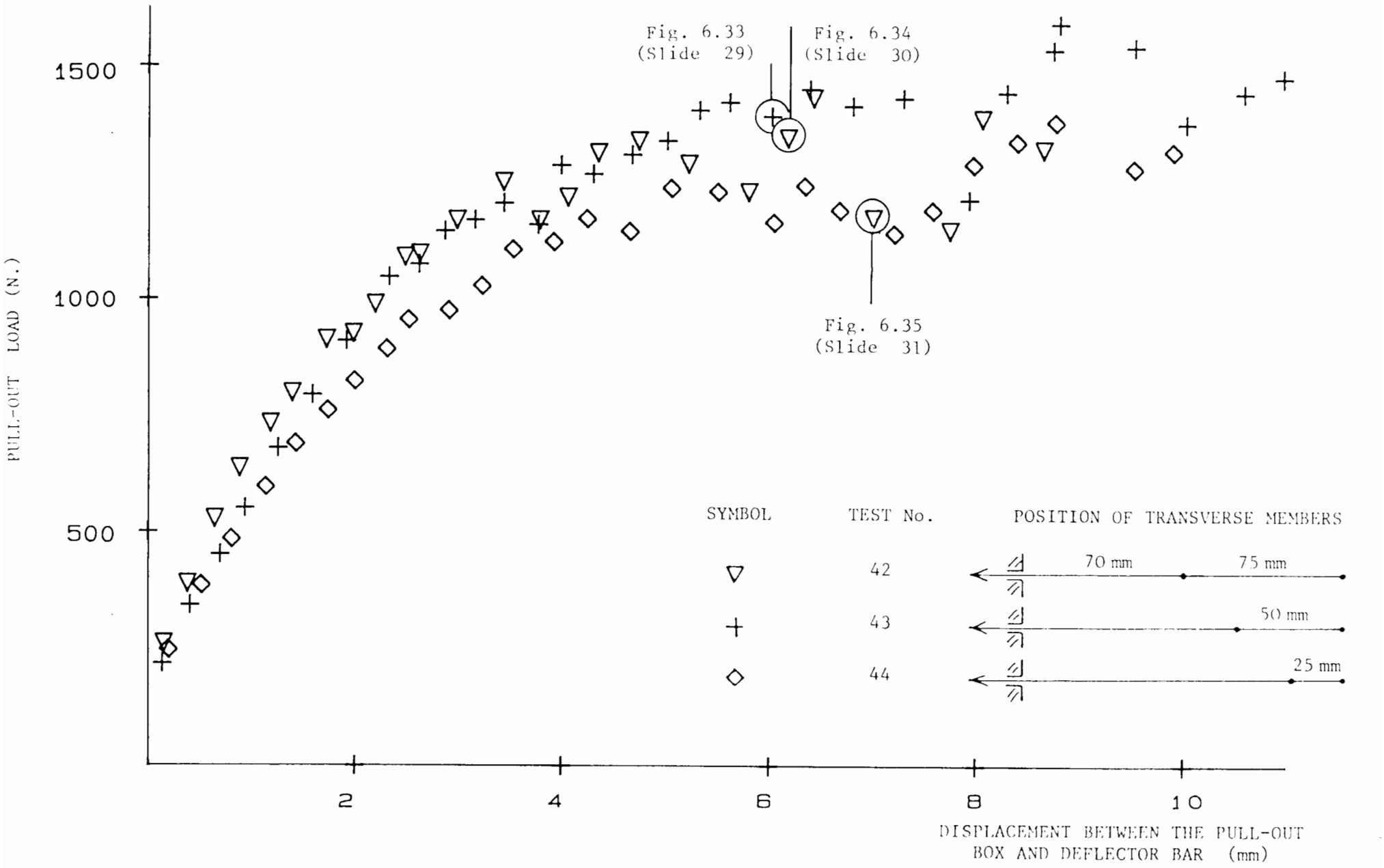


Fig. 6.28 Pull-out of pairs of transverse members of the steel grid

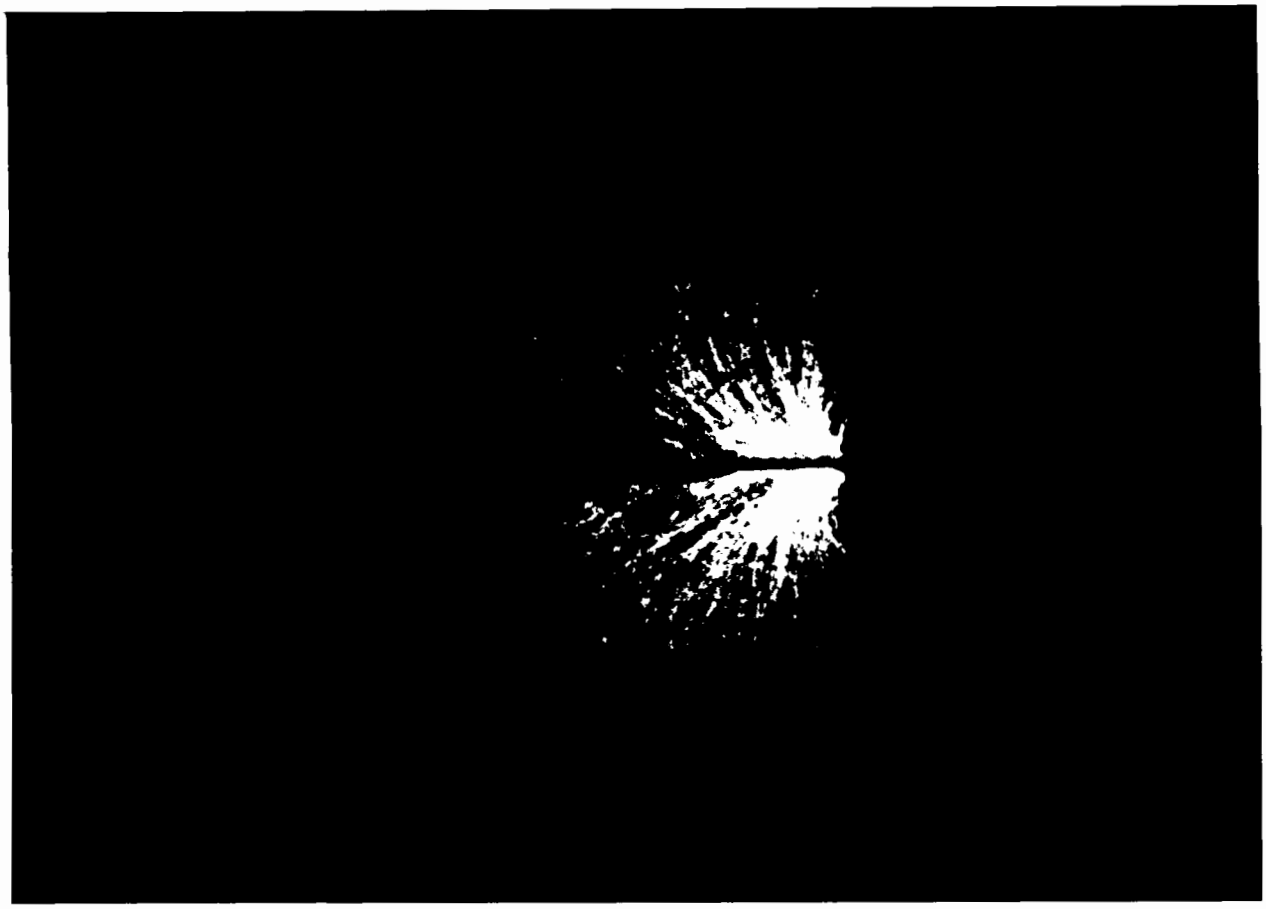

Fig. 6.29 Light stripes observed for a pull-out test on a single transverse member after 6.09 mm displacement between the pull-out box and deflector bar (test no. 45)

Fig. 6.30 Light stripes observed for a pull-out test on another single transverse member after 6.08 mm displacement between the pull-out box and deflector bar (Test no. 49)

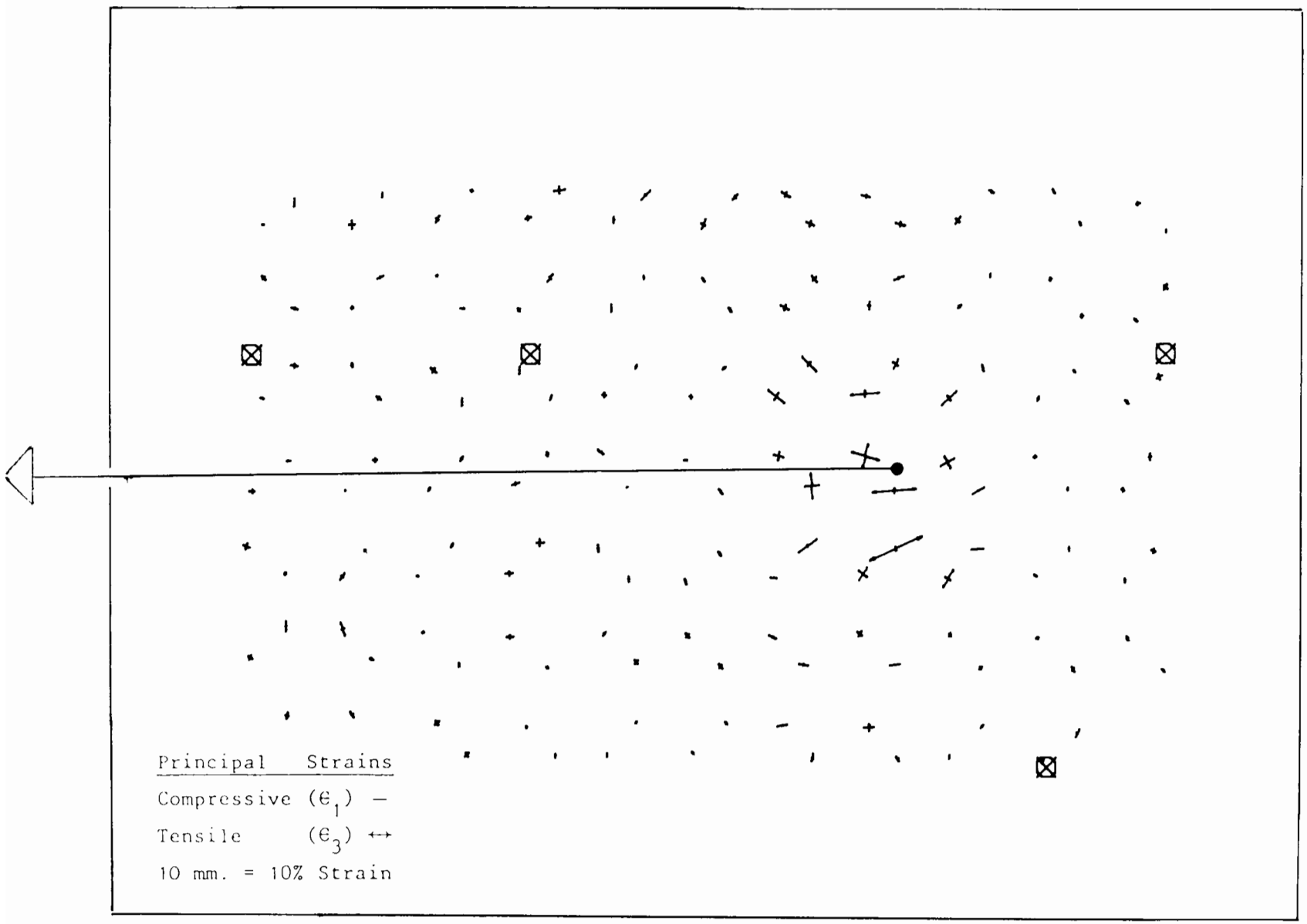


Fig. 6.31 Pattern of strains determined for pull-out of a single transverse member in crushed glass between 0.00 and 9.20 mm pull-out displacement between the pull-out box and deflector bar (test no. 49)

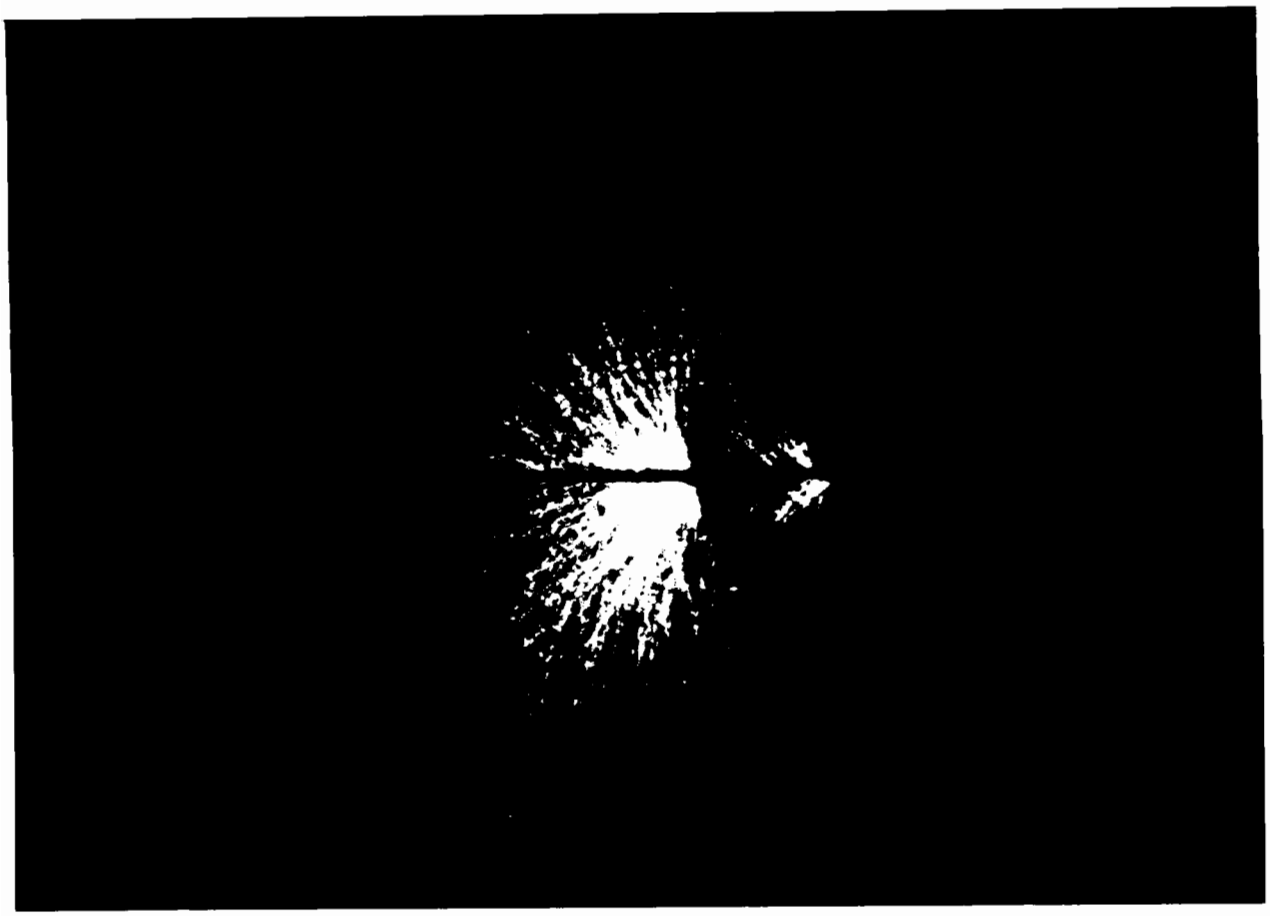

Fig. 6.32 Light stripes observed for a pull-out test on a pair of transverse members spaced 25 mm apart (test no. 44), after 6.04 mm displacement between the pull-out box and deflector bar

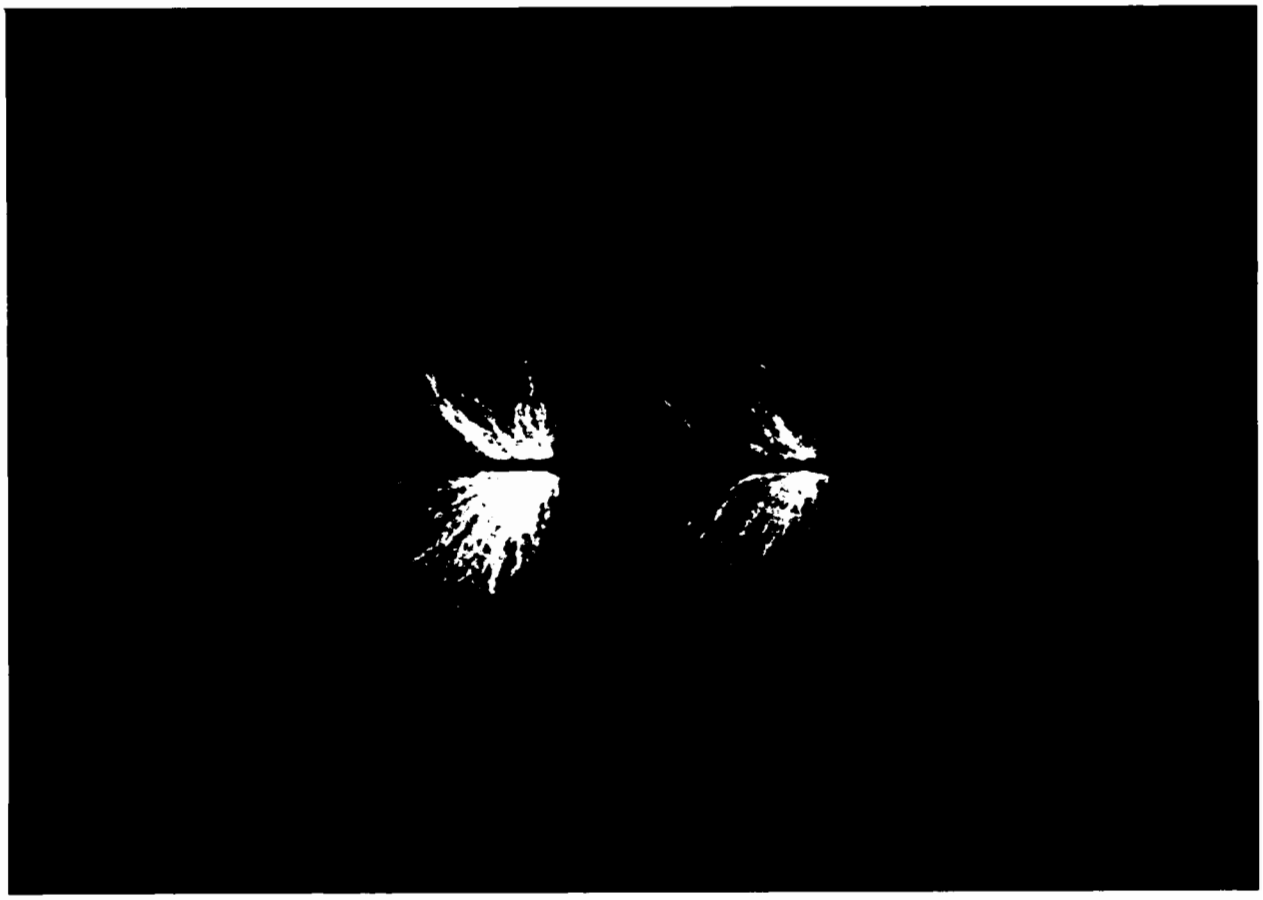

Fig. 6.33 Light stripes observed for a pull-out test on a pair of transverse members spaced 50 mm apart (test no. 43), after 6.02 mm displacement between the pull-out box and deflector bar

Fig. 6.34 Light stripes observed for a pull-out test on a pair of transverse members spaced 75 mm apart (test no. 42), after 6.18 mm displacement between the pull-out box and deflector bar

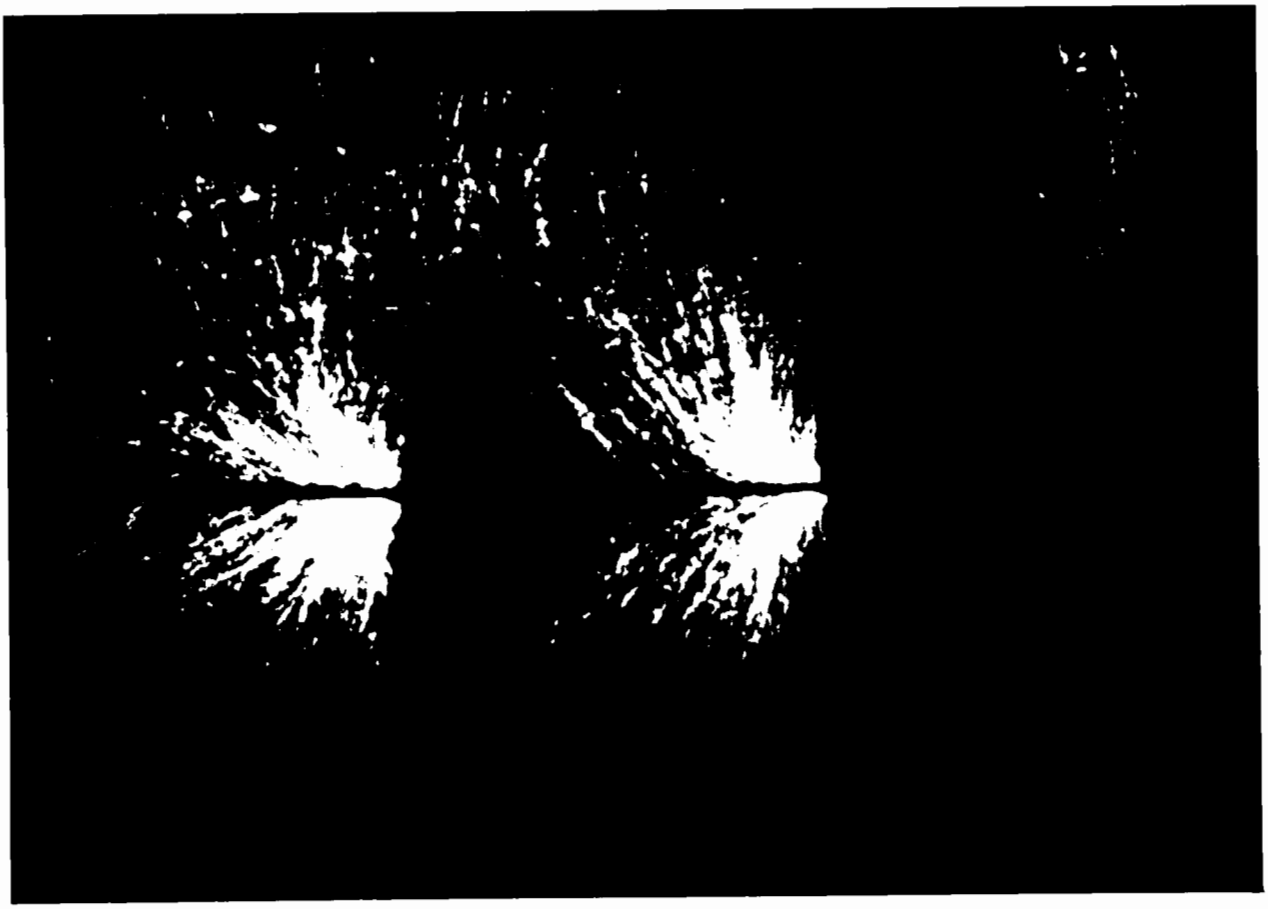

Fig. 6.35 Light stripes observed for a pull-out test on a pair of transverse members spaced 75 mm apart (test no. 42), after 7.01 mm displacement between the pull-out box and deflector bar

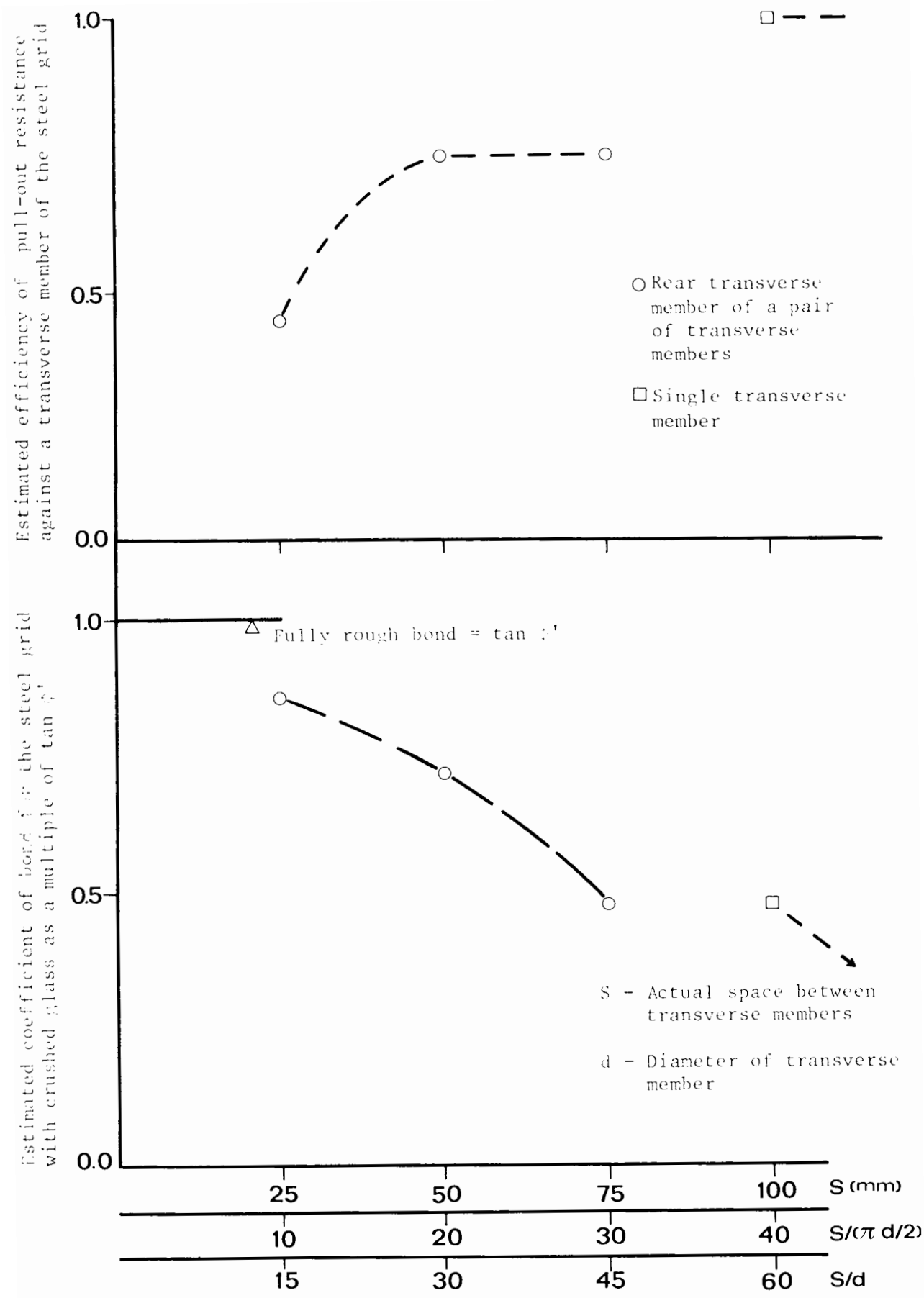


Actual and normalised spacing for transverse members of the grid

Fig. 6.36 a) Relative efficiency of pull-out resistance against individual transverse members of the grid for different spacings determined from experiment results compared with b) predicted coefficient of bond for the grid corresponding to the same spacings of transverse members

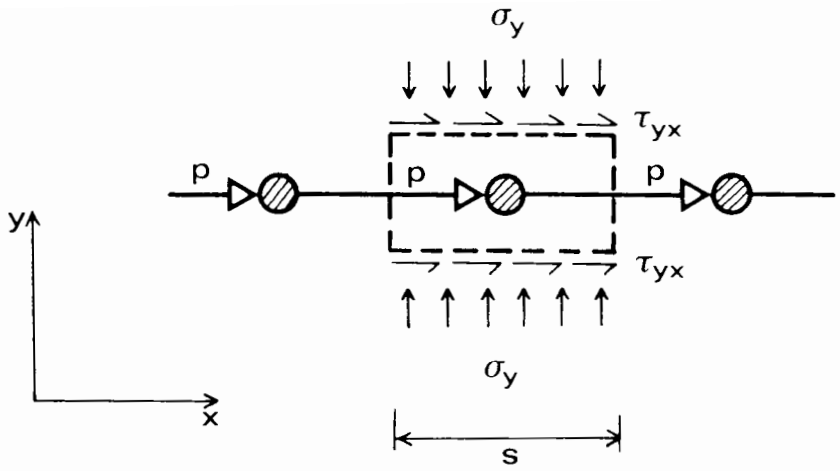


$$\tan \phi_b = \frac{\tau_{yx}}{\sigma_y} = f_b \tan \phi$$

$$= \frac{P}{2\ S\ W_t} \times \frac{W_s\ L_s}{P_y}$$

In the pull-out box,

$$= \frac{P}{2\ S\ W_t} \times \frac{W_s\ 204\ (mm.)}{2030\ (N)}$$

$$= \frac{P\ (N)}{S(mm.)} \times 0.05$$

$\phi_b$ = Equivalent angle of bond between grid and crushed glass

$f_b$ = Coefficient of bond between grid and crushed glass as a multiple of the angle of friction for crushed glass

$P$ = Pull-out resistance against a rear or single transverse member, taken from fig. 6.27

$S$ = Spacing between transverse members

$W_s$, $L_s$ = Sample width and length of crushed glass in the pull-out box

$W_t$ = Width of transverse member $\approx W_s$

$P_y$ = Normal load acting on sample

| S (mm) | P (N) | P/S (N/mm) | $\tan \phi_b$ | $f_b = \frac{\tan \phi_b}{\tan \phi}$ |
|---|---|---|---|---|
| 25 | 375* | 15.0 | 0.75 | 0.86 |
| 50 | 625* | 12.5 | 0.63 | 0.72 |
| 75 | 625* | 8.3 | 0.42 | 0.48 |
| 100 | 835≠ | 8.3 | 0.42 | 0.48 |

(*) For rear transverse member (≠) For single transverse member

Fig. 6.37 Method for determining a coefficient of bond between grid and crushed glass from pull-out tests (adapted from Jewell et al. 1984)

## APPENDIX A

### Suppliers of Equipment and Materials for the Photoelastic Tests

LINEAR POLARISERS AND QUARTER WAVE PLATES Polarizer Technical Products, Lincoln Road, Cressex Estate, High Wycombe, Bucks.

KODAK WRATTEN FILTERS Kodak Ltd., Station Road, Hemel Hempstead, Herts.

LIQUID PARAFFIN BDH Chemicals Ltd., Fairways, Atherstone, Warwickshire.

PYREX GLASS Corning Ltd., Consumer Division, Wear Glass Works, Sunderland, SR4 6EJ.

FLOAT GLASS SIDE WALLS T. and W. Ide Ltd., Glasshouse Fields, London, E1 9JA.

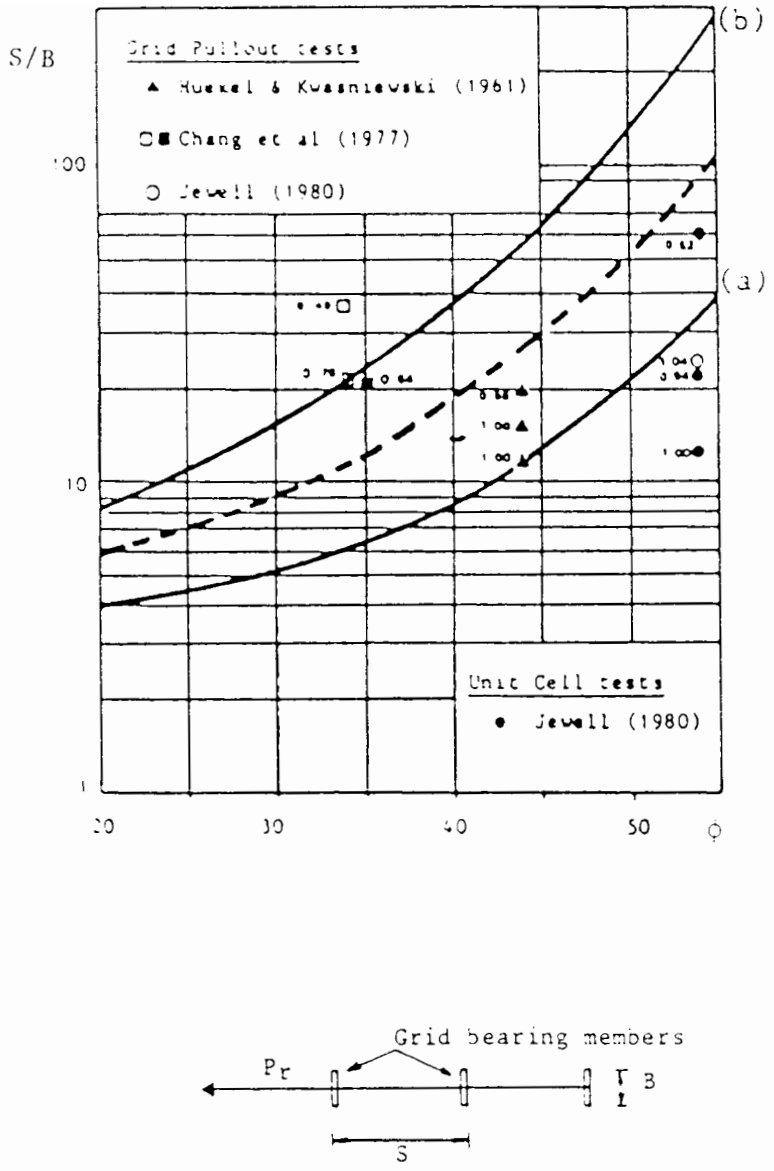


Fig. 6.38 Lower (a) and upper (b) estimates of grid reinforcement geometry (S/B) for a fully rough bond in cohesionless soil ($\tan\phi'$) by Jewell et al. (1984)

## APPENDIX B

### Captions for Slides

No. 1 Light stripes observed in a dark field of circularly polarised light for a direct shear test on crushed glass containing a flexible sheet reinforcement orientated at $\theta = -45°$.

No. 2 Light stripes observed in the same direct shear test as for slide 1 but in plane polarised light with the polariscope's crossed axes inclined at 45° either side of the vertical.

No. 3 Light stripes observed in the same direct shear test as for slide 1 but in plane polarised light with the polariscope's crossed axes vertical and horizontal.

No. 4 Residual stresses observed in the glass sidewalls of the shearbox in a dark field of circularly polarised light.

No. 5 Light stripes observed at the start of a direct shear test on crushed glass with only vertical load applied (test no. 30).

No. 6 Light stripes observed in a direct shear test on crushed glass (test no. 30) after 0.56 mm shear displacement.

No. 7 Light stripes observed in a direct shear test on crushed glass (test no. 30) at maximum shear load, 4.41 mm. shear displacement.

No. 8 Light stripes observed in a direct shear test on crushed glass (test no. 30) after 7.33 mm. shear displacement.

No. 9 Light stripes observed in a direct shear test on crushed glass (test no. 23) at maximum shear load, 4.13 mm. shear displacement.

No. 10 Light stripes observed in a direct shear test on crushed glass (test no. 39) at maximum shear load, 4.20 mm. shear displacement.

No. 11 Light stripes observed in the direct shear test containing the flexible sheet reinforcement orientated at $\theta = 40°$ (test no. 29) after 8.60 mm. shear displacement.

No. 12 Light stripes observed in the direct shear test containing the flexible sheet reinforcement orientated at $\theta = -45°$ (test no. 28) after 5.62 mm. shear displacement.

No. 13 Light stripes observed in the direct shear test containing the flexible sheet reinforcement orientated at $\theta = 0°$ (test no. 27) after 1.27 mm. shear displacement.

No. 14 Light stripes observed in the direct shear test containing the flexible sheet reinforcement orientated at $\theta = 0°$ (test no. 27) after 8.98 mm. shear displacement.

No. 15 Light stripes observed in the direct shear test containing the rigid reinforcement orientated at $\theta = 0°$ (test no. 50) after 1.04 mm. shear displacement.

No. 16 Light stripes observed in the direct shear test containing the rigid reinforcement orientated at $\theta = 0°$ (test no. 50) after 9.61 mm. shear displacement.

No. 17 Light stripes observed in the direct shear test containing the grid reinforcement orientated at $\theta = 40°$ (test no. 33) after 8.63 mm. shear displacement.

No. 18 Light stripes observed in the direct shear test containing the grid reinforcement orientated at $\theta = 40°$ (test no. 34) after 8.20 mm. shear displacement.

No. 19 Light stripes observed for direct sliding of crushed glass in the upper half of the shearbox over the perforated sheet placed on a steel block along the central plane of the box (test no. 36) after 4.00 mm. shear displacement.

No. 20 Light stripes observed for direct sliding of crushed glass in the upper half of the shearbox over the grid placed on a highly polished steel block along the central plane of the box (test no. 37) after 3.96 mm. shear displacement.

No. 21 Light stripes observed for direct sliding of crushed glass in the upper half of the shearbox over the grid mounted on crushed glass placed in the lower half of the box (test no. 38) after 3.96 mm shear displacement.

No. 22 Light stripes observed in the pull-out test on a length of grid (test no. 41) after 2.00 mm. pull-out displacement.

No. 23 Light stripes observed in the pull-out test on a length of grid (test no. 46) after 7.62 mm. displacement between the pull-out box and deflector bar.

No. 24 Light stripes observed in the pull-out test on a length of perforated sheet (test no. 48) after 1.07 mm. displacement between the pull-out box and deflector bar.

No. 25 Light stripes observed in the pull-out test on a length of perforated sheet (test no. 48) after 8.83 mm. displacement between the pull-out box and deflector bar.

No. 26 Light stripes observed in the pull-out test on a single transverse member of the grid (test no. 45) after 6.09 mm. displacement between the pull-out box and deflector bar.

No. 27 Light stripes observed in the pull-out test on a single transverse member of the grid (test no. 49) after 6.08 mm. displacement between the pull-out box and deflector bar.

No. 28 Light stripes observed in the pull-out test on a pair of transverse members spaced 25 mm. apart (test no. 44) after 6.04 mm. displacement between the pull-out box and deflector bar.

No. 29 Light stripes observed in the pull-out test on a pair of transverse members spaced 50 mm. apart (test no. 43) after 6.02 mm. displacement between the pull-out box and deflector bar.

No. 30 Light stripes observed in the pull-out test on a pair of transverse members spaced 75 mm. apart (test no. 42) after 6.18 mm. displacement between the pull-out box and deflector bar.